PARAGLACIAL ROCKSLOPE STABILITY

A thesis submitted in partial fulfilment of the requirements

for the Degree of

Doctor of Philosophy in Geology

in the Department of Geological Sciences,

University of Canterbury

by Samuel Thomas McColl

2012

ABSTRACT

The aim of this research was to study the relationship between rock slope stability and glacial processes. An in-depth analysis of our current understanding of how glaciated rock slopes develop instability and movement during deglaciation is presented; this shows that understanding is incomplete without an appreciation of the variable mechanical behaviour of glacier ice. In this thesis, I argue that:

(1) The ductile behaviour of ice at low strain rates allows movement of rock slopes buttressed by ice. Field evidence and simple force models are used to explore rate of movement of ice-contact slopes and the conditions under which they evolve. The results indicate that large rockslides can move and deform glacial ice at rates of 10^{-2} to 10^{2} m^{-yr}. This implies that ice-contact slope movement may be important for slope evolution and the erosion and entrainment processes of glaciers; and

(2) the elastic strength of glacier ice at the high strain rates associated with seismic shaking enables ice to modify the response of the surrounding rock to seismic shaking. To explore this, numerical analyses of the interaction between glacial erosion, glacier mass, topography, and earthquake shaking intensity are undertaken. Shaking of mountains of variable shape and with different levels of ice inundation is simulated using FLAC 6.0. The results suggest that complete inundation by ice can significantly reduce shaking intensity. This, in combination with glacial steepening of slopes, may make recently deglaciated slopes more prone to coseismic failure.

In the final chapter of the thesis, I present a conceptual model of the evolution of slope stability during stages of glaciation and deglaciation. The model incorporates the ideas presented in the thesis. I then offer recommendations for how our understanding of these processes can be further advanced.

Deputy Vice-Chancellor's Office
Postgraduate Office

UNIVERSITY OF CANTERBURY
Te Whare Wānanga o Waitaha
CHRISTCHURCH NEW ZEALAND

Co-Authorship Form

This form is to accompany the submission of any PhD thesis that contains research reported in co-authored work that has been published, accepted for publication, or submitted for publication. A copy of this form should be included for each co-authored work that is included in the PhD thesis.

Please indicate the chapter/section/pages of this thesis that are extracted from co-authored work and provide details of the publication or submission from the extract comes:
Section 2.2: McColl, S.T., Davies, T.R.H., McSaveney, M.J., 2010. Glacier retreat and rock-slope stability: debunking debuttressing. Geologically active: delegate papers 11th Congress of the International Association for Engineering Geology and the Environment, Auckland, Aotearoa, 5-10 September 2010. Auckland, New Zealand. pp. 467-474

Please detail the nature and extent (%) of contribution by the PhD candidate:
This publication was initiated and written by the PhD candidate, and the figures were designed and drafted by the candidate. Some of the ideas presented were suggested by the co-authors, but subsequently modified by the PhD candidate. The contribution by the candidate was over 80%.

Please list the co-authors and the nature and extent of the contribution by each below:

Name: *Timothy Davies.* Contribution: *Tim provided edits and comments on two versions of the manuscript, and some of the ideas were suggested by Tim.*
Name: *Mauri McSaveney.* Contribution: *Mauri provided edits and comments on one version of the manuscript. Mauri suggested including the force diagrams (Figures 2.2.2 – 2.2.3) but these were designed and drafted by the PhD candidate.*

Certification by Co-authors:
The undersigned certify that:

- The above statement correctly reflects the nature and extent of the PhD candidate's contribution to this work and the nature and contribution of each of the co-authors
- In cases where the PhD candidate was the lead author of the co-authored work he or she wrote the text

Name: *Timothy Davies.* Signature: Date: *4 July 2012*

Name: *Mauri McSaveney.* Signature: Date: *25 June 2012*

Deputy Vice-Chancellor's Office
Postgraduate Office

UNIVERSITY OF CANTERBURY
Te Whare Wānanga o Waitaha
CHRISTCHURCH NEW ZEALAND

Co-Authorship Form

This form is to accompany the submission of any PhD thesis that contains research reported in co-authored work that has been published, accepted for publication, or submitted for publication. A copy of this form should be included for each co-authored work that is included in the PhD thesis.

Please indicate the chapter/section/pages of this thesis that are extracted from co-authored work and provide details of the publication or submission from the extract comes:
Section 4.2: McColl ST.; Davies TRH. Large ice-contact slope movements and glacial buttressing, deformation and erosion. First submitted in May 2012 to the journal Earth Surface Processes and Landforms; revised manuscript submitted June 2012.

Please detail the nature and extent (%) of contribution by the PhD candidate:
The manuscript was conceived and written by the PhD Candidate. All of the figures were conceived, designed, and drafted by the PhD candidate. All of the data collected, analysis, and interpretation was by the PhD candidate. The equations were developed by the candidate but received minor modifications from the co-author. The main idea presented in the manuscript, that the ductile behaviour of ice cannot support slopes, was suggested by Tim but the approach for describing and modelling the process, and refinements to the idea were a result of discussion between both authors. The contribution by the PhD candidate was over 80%.

Please list the co-authors and the nature and extent of the contribution by each below:

Name: *Timothy Davies.* Contribution: *Tim provided edits and comments on 4 versions of the manuscript, and suggested modification to some of the equations.*

Certification by Co-authors:
The undersigned certify that:

- The above statement correctly reflects the nature and extent of the PhD candidate's contribution to this work and the nature and contribution of each of the co-authors
- In cases where the PhD candidate was the lead author of the co-authored work he or she wrote the text

Name: *Timothy Davies.* Signature:  Date: *4 July 2012*

Deputy Vice-Chancellor's Office
Postgraduate Office

UNIVERSITY OF CANTERBURY
Te Whare Wānanga o Waitaha
CHRISTCHURCH NEW ZEALAND

Co-Authorship Form

This form is to accompany the submission of any PhD thesis that contains research reported in co-authored work that has been published, accepted for publication, or submitted for publication. A copy of this form should be included for each co-authored work that is included in the PhD thesis.

Please indicate the chapter/section/pages of this thesis that are extracted from co-authored work and provide details of the publication or submission from the extract comes:
Section 4.3: McColl ST; Davies TRH; McSaveney MJ (in press) The effect of glaciation on the intensity of seismic ground motion, Earth Surface Processes and Landforms.

Please detail the nature and extent (%) of contribution by the PhD candidate:
The publication was initiated and written by the PhD candidate. All of the modelling, analysis and most of the interpretation was by the PhD candidate, as was the design and drafting of the figures. The main idea, that glaciers modify the co-seismic shaking of mountains, was suggested to the candidate by Timothy Davies but refinement of the idea, the approach for modelling it, and the development of the idea into a conceptual model for understanding slope processes, was that of the PhD candidate. The candidate contributed to over 80% of the publication.

Please list the co-authors and the nature and extent of the contribution by each below:

Name: *Timothy Davies.* Contribution: *Tim provided edits and comments on 2 versions of the manuscript and discussed the ideas with the candidate on several occasions. Tim helped with some of the interpretations of the results.*
Name: *Mauri McSaveney.* Contribution: *Mauri provided edits and comments on 2 versions of the manuscript, in particular making suggestions to the terminology used. Mauri had discussions with the candidate about some of the results and interpretation.*

Certification by Co-authors:
The undersigned certify that:

- The above statement correctly reflects the nature and extent of the PhD candidate's contribution to this work and the nature and contribution of each of the co-authors
- In cases where the PhD candidate was the lead author of the co-authored work he or she wrote the text

Name: *Timothy Davies.* Signature:  Date: *4 July 2012*

Name: *Mauri McSaveney.* Signature: 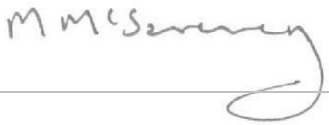 Date: *25 June 2012*

Deputy Vice-Chancellor's Office
Postgraduate Office

UNIVERSITY OF CANTERBURY
Te Whare Wānanga o Waitaha
CHRISTCHURCH NEW ZEALAND

Co-Authorship Form

This form is to accompany the submission of any PhD thesis that contains research reported in co-authored work that has been published, accepted for publication, or submitted for publication. A copy of this form should be included for each co-authored work that is included in the PhD thesis.

Please indicate the chapter/section/pages of this thesis that are extracted from co-authored work and provide details of the publication or submission from the extract comes:
Appendix A: McColl ST; Davies, T.R. 2011. Evidence for a rock-avalanche origin for `The Hillocks' "moraine", Otago, New Zealand. Geomorphology 127: 216-224

Please detail the nature and extent (%) of contribution by the PhD candidate:
This publication was written by the PhD candidate. The co-author developed the hypothesis but the candidate collected the data, made his own interpretations, and designed and drafted the figures. The contribution by the candidate was over 80%.

Please list the co-authors and the nature and extent of the contribution by each below:

Name: *Timothy Davies.* Contribution: *Tim developed the hypothesis and provided edits and comments on two versions of the manuscript.*

Certification by Co-authors:
The undersigned certify that:

- The above statement correctly reflects the nature and extent of the PhD candidate's contribution to this work and the nature and contribution of each of the co-authors
- In cases where the PhD candidate was the lead author of the co-authored work he or she wrote the text

Name: *Timothy Davies.* Signature:  Date: *4 July 2012*

One of the vistas that encouraged me to reach the top of the Sealy Range, Aoraki/Mount Cook National Park, over and over again.

As Glaciers Move by Henry Rawle

Look back in pity from a place
Where time is measured by another's hand
Green bush cathedrals hear his prayers
Swift rivers wash away his hurts
And in the whispering of the hills
He learns the secret they have always known
Change comes imperceptibly as glaciers move
The truth deep-frozen for a thousand years

Published in the 1976 edition of Massif, the Massey University Alpine Club journal.

ACKNOWLEDGMENTS

First, I would like to acknowledge the support given to me by my partner, family, friends, flatmates, office mates, and colleagues during this research; for without such support, the undertaking would have been far less enjoyable.

Thanks go to those who assisted with fieldwork and the technical aspects of the project. For that, I would like to make particular mention of Patrick Kailey, Lorraine Cook, Natasha Reznichenko, Tim Stahl, Ali Bazgard, Simon Stewart, Michael Cronin, Louise Vick and Anna Sintenie. To the fantastic technical, computing, and administrative staff of the Department of Geological Sciences, I wish to express my gratitude to your unconditional support and assistance. GNS Science staff Chris Massey, Stuart Read, Neville Palmer, John Young, Garth Archibald, Graham Hancox, and Grant Dellow are all thanked for providing advice, help, and making resources available – even though much of this was not used in the final thesis.

I express my sincere appreciation to Tim Davies for his supervision of the project and mentoring. In particular, his open and critical mind has helped shape my thinking (for the better I hope!). Both he and Mauri McSaveney have been instrumental in exposing me to some of the problems in the paraglacial literature and in leading me astray from conventional wisdom. Patrick Kailey, Natasha Reznichenko, David Alexander, and Timothy Stahl were hugely desirable peers to have during the project, spending hours arguing with me and thus helping me to develop as a scientist. Tim, Mauri, Pat, David, and Rob McColl generously proofread and discussed sections of the thesis and in doing so guided me in writing a considerably shorter, and more informed and readable thesis. The project and my development have also gained from the early co-supervision by Jamie Shulmeister and later by Mark Quigley. I'm grateful to have benefited from the resources made available by University of Canterbury's College of Science and Department of Geological Sciences, and by GNS Science. Finally, the constructive comments, suggestions and effort given by external examiners Colin Ballantyne and Simon Nelis are deeply appreciated; the thoughtful comments by Colin, and the detailed improvements to the text by Simon are especially appreciated.

TABLE OF CONTENTS

LIST OF FIGURES

LIST OF TABLES

CHAPTER 1: INTRODUCTION

Global climate is changing; glaciers and ice sheets are in general retreat. Landslides**,** glacier-lake outburst floods, and other natural events in glaciated mountain systems around the globe have resulted in over 30,000 deaths and billions of dollars of damage over the last 150 years (Evans and Clague, 1992). These events are related to changes in climate and the withdrawal of glaciers, and are a natural part of the process of deglaciation, which began over 15,000 years ago. The transition from full-glaciation to inter-glacial conditions is a long-drawn-out process and it continues today. Evidence of its continuation includes the ongoing retreat and loss of glaciers and ice sheets around the world, but also the vertical retreat of permafrost (permanently frozen ground) and snow lines. The transition also affects non-climatic processes, such as seismicity; this is revealed most vividly by geodetic and seismic studies that show continental crust is still 'bouncing' back from loads imposed by kilometre-thick ice sheets that have long since vanished (Muir-Wood, 2000; Stewart et al., 2000). The rebound can produce brittle faulting, which can cause earthquakes (Adams, 1989). Deglaciation also influences the distribution of vast amounts of sediments on the earth's surface; rivers draining the mountains still continue to rework and relocate the sediments produced during glaciation (Church and Ryder, 1972). Harrison (2009) suggested that as the existing global ice masses complete deglaciation, the Earth will undergo the last major sediment movement for perhaps tens of thousands of years until the next glaciation. Furthermore, the warming of alpine areas and the retreat of glaciers during the glacial-interglacial transition can reduce the stability of slopes and can lead to slope failure (McColl, 2012). The hazards associated with this reduction in slope stability will continue to be the most threatening of all responses to climate change in populated mountainous regions. Rockfalls, rockslides, and rock avalanches can cause direct and substantial damage and loss but some events, such as those that form landslide-dams or generate glacier-lake outburst floods, can affect entire catchments and have long-lasting impact on the geomorphic stability and safety of those catchments.

The natural hazards associated with this ongoing transition are likely to continue and possibly increase over the coming centuries as the projected climate changes occur (McGuire, 2010). Understanding how these hazards develop and how they may manifest themselves in the future will provide a sound basis for making decisions to help to reduce their impacts on society.

1.1 Rock slope stability in a changing climate

Increased landslide activity in several regions around the world coincided with a period in the early-Holocene when those regions were undergoing deglaciation (Ballantyne, 2002). Many of those landslides were large catastrophic slope failures, and if similar events were to happen in the populated mountainous regions of today, the consequences would be devastating. For example, the giant (27 km^3) Green Lake Landslide in Fiordland, New Zealand – one of the largest of its type in the world – formed soon after a glacier retreated beyond its slopes (Hancox and Perrin, 2009). An event such as this in a more populated mountain range has potential to impact severely over a large area. As our remaining glaciers continue to recede and climates continue to adjust, further landsliding – perhaps large-scale – appears likely to result.

Mitigation of landslide hazards may be achieved only by first identifying the hazard, which involves knowing the types of locations in which they can occur, quantifying the hazards (which requires estimation of frequency, size, extent, velocity, and potential impacts) and then understanding their *causes*. One difficulty in identifying these hazards by using the commonly used precedence approach, in which hazard assessment is based on information gained about past landslide activity, is that evidence of past landslide activity is limited. There are two main reasons for this: 1) many landslide deposits are morphologically similar to glacial deposits and may be unrecognised (e.g., Hewitt, 1999); and 2) the evidence for these events is rapidly destroyed or buried during deglaciation, particularly when large amounts of sediment infill valleys after glacier retreat.

These constraints on landslide identification are being gradually overcome as better awareness and techniques are made available. For example, McColl and Davies (2011) (appendix A) demonstrated that an understanding of landslide run-out

behaviour (e.g. Dufresne and Davies, 2009), as well as sedimentological evidence, can be used to distinguish between landslide deposits and moraine. Reznichenko et al. (2012) have shown that traces of rock avalanche debris in moraines can be identified by the presence of agglomerations of extremely fine particles produced during rock avalanche motion. Their technique has increased our ability to identify rock avalanches that have been emplaced onto glaciers in the past and would otherwise be indistinguishable from other debris types within the moraine. These developments in landslide recognition, as well as increasing application of age-dating techniques to ancient landslide deposits, are improving our records of landslides in glaciated terrain.

Understanding the *causes* of slope failure associated with deglaciation is more difficult than identifying the landslide *hazard*, and it remains a scientific challenge. One of the major problems in previous attempts to do so is that some of the important physical and mechanical properties of glacier ice appear to have been overlooked. For example, the tendency for ice to flow at low rates of strain but to behave in an elastic/brittle fashion at higher strain rates, have been recognised in disciplines such as glaciology and engineering, but have hitherto been largely absent from landslide studies. In this thesis, it is argued that the stress-strain properties of ice are critical in understanding the initiation and development of slope failures in glaciated terrain and that they need to be considered in order to accurately understand and model post-glacial landslide patterns. Recognising that the stress-strain properties of ice play a role in slope stability was therefore a key part in directing the aim's and objectives of this thesis:

1.2 Research aims and objectives

The primary aim of this research is to study the relationship between rock slope stability and glacial processes. The major objectives of this research are:

Objective 1: Identify and evaluate the various factors and processes influencing rockslope instability during glacial cycles;

Objective 2: Re-evaluate the mechanism of glacial debuttressing and its role in promoting and triggering rock slope failure;

Objective 3: Observe, evaluate and model the movement of ice-buttressed rock slopes.

Objective 4: Quantify the changes to seismic shaking intensity in mountainous terrain brought about by glacial erosion and changes in extent of glacial-ice cover.

Objective 5: Develop a conceptual model of rockslope instability during glacial cycles.

1.3 Thesis organisation and summary

The thesis combines several published journal articles and manuscripts (in preparation) which have been prepared and written for the thesis, with each covering a different aspect of rock slope stability in glaciated terrain. The work is presented in four sections, which are briefly outlined and summarised below.

CHAPTER 2: LITERATURE REVIEW: In Chapter 2, a review of the literature relevant to paraglacial rock-slope stability is presented in the form of a published peer-reviewed journal article (McColl, 2012) (Literature Review Part A). This serves to introduce the thesis topic and define terminology, describe the current state of understanding and approaches used in studying rock slope failure in glaciated terrain, and to identify and discuss research gaps and outstanding issues that need further attention. In the second part of Chapter 2 some of these issues are questioned more openly and criticism is given to the concept and applicability of glacial-debuttressing; this is presented as a published conference paper (McColl et al., 2010) (Literature Review Part B). The key points of Chapter 2 are:

i) Interpretation of post-glacial slope-failure patterns must adequately consider the poor preservation of landslides that occur during glaciation and the early stages of deglaciation; landslide activity during glaciation and early deglaciation may be more significant and widespread than previously thought.
ii) Notwithstanding point i), recent landslide age data support a globally consistent pattern of peak landslide activity lagging several thousands of years behind the main retreat of glaciers; as more data are collected, this pattern and the timing of it can be better constrained.
iii) The causes of post-glacial slope instability are many and the often cited ‘glacier retreat’ and ‘glacial debuttressing’ (the removal of slope support) mechanisms

appear inadequate to explain this landslide pattern on their own, as supported by the lag-time mentioned in point ii) above and increasing evidence of other processes being involved.

iv) Temperate glaciers are unlikely to rigidly support unstable rock slopes because of the ductile behaviour of ice at low strain rates and the tendency for basal water pressures to limit the ice loads imposed on rock slopes. There needs to be a re-think on how and when landslides are initiated and develop in periods of glaciation and early deglaciation. This requires the development of models that realistically represent the ductile behaviour of ice, and the collection of field evidence for contemporary slope response to glacier thinning.

v) The deterioration in rock mass strength – through physical weathering processes and thawing of permafrost, stress-release fractures induced by erosional or ice unloading, and stress-corrosion – is likely to be a major factor affecting patterns of post-glacial slope instability; research should focus being able to better define the time-scales over which these processes operate.

vi) It may be possible that seismically induced rock slopes failures are more common following deglaciation because of increased localised earthquake shaking intensity in mountainous terrain. Enhanced seismic shaking intensities may result from the effects of glacial erosion and changes in ice mass, both of which modify the resonant response of rock to seismic shaking; at the strain rates imposed by coseismic shaking, ice behaves as an elastic solid.

CHAPTER 3: THE NEW ZEALAND SOUTHERN ALPS: Before attempting in Chapter 4 to resolve some of these issues, a brief introduction to the geology, geomorphology, and glacial and paraglacial history of the New Zealand Southern Alps is given; this introduction is provided because several New Zealand case-studies and examples are used in the thesis.

CHAPTER 4: RESEARCH CONTRIBUTIONS: Chapter 4 is presented in three parts. These parts, which largely address points iii), iv), and vi) above, are all related to the interaction of glacier ice and rock slopes:

Part A – Investigation of a large ice-contact rockslide *(GNS Science Report in preparation)**:*** The development and potential for catastrophic collapse of a glaciated rock slope is investigated. The Mueller Rockslide is a large (~200 M m^3) active rockslide situated in a glaciated valley of Aoraki/Mount Cook National Park, New Zealand. The Mueller Glacier covers the lower 100-200 metres of the rockslide toe. Movement of the slope threatens an alpine hut, and the runout in the event of a catastrophic failure potentially threatens communities down-valley. The description and analysis provided here is one of the only documented examples of rock slope collapse/deformation during contemporary glacier withdrawal. Thus, it provides a unique opportunity to increase our understanding of the initiation, development, and potential catastrophic failure of a slope that has been influenced by glacial erosion and thinning.

The movement rate and the factors influencing instability were assessed using data collected by geological and geomorphological mapping, engineering geological appraisal, and movement monitoring. These data show that the main failure mechanism is translational sliding along steeply dipping bedding planes, with relaxation and gradual collapse of the upper part of the slope. The morphology suggests that movement has developed recently – in the last 1000-2000 thousand years – but that it may have become more active in the last few decades. Movement data indicate a variable movement rate of 1-4 metres along bedding per year in the most active part of the slope, but the processes controlling the rockslide movement rate remain poorly understood.

Part B – Large ice-contact slope movements and glacial buttressing, deformation and erosion *(published journal article: McColl and Davies, 2012)**:*** I describe, for the first time, a mass movement process involving the deformation of glacial ice. A simple mathematical model adapted from Stokes law, which predicts the settling velocities of particles in fluids, is used to show that stresses exerted on ice by movement of rock slopes is sufficient to allow a significant amount of permanent deformation of a glacial buttress. The movement rates predicted would result in significant displacement of large rock slope failures over as little as hundreds of years. The model is then supported with examples, from the New

Zealand Southern Alps, of large rock slope deformations that have caused glaciers to bulge or narrow in the valley, but over an unknown period of time. A better constraint on how fast these features move is then provided with an analysis of landslide monitoring data collected at a site in Aoraki/Mount Cook National Park, New Zealand, where a large and active rock slide is deforming into a glacier (described in full in Chapter 4 Part B). The movement data shows that the landslide is moving into the glacier at several metres per year.

This research provides the first evidence that glaciers can accommodate the movement of large landslides, a finding that has implications for both slope stability and glacial erosion processes. It suggests that if slopes become unstable during glaciation, because of glacial erosion or some other destabilising factor, they can begin moving. This may also mean that the glacier erodes, or entrains, failed rock debris much sooner than it otherwise would. It seems likely that this process could have contributed significantly to erosion and the generation of sediment in glaciated valleys.

Part C – The effect of glaciation on the intensity of seismic ground motion *(published journal article, McColl et al., 2012)**:*** A different interaction between rock slopes and glacier ice is explored in Part C. The extent to which glacial erosion and changes to glacier ice cover may increase the intensity of seismic shaking of glaciated mountains, and therefore influence the probability of coseismic rock slope failures and rock damage, is considered. It is hypothesised that modification of alpine topography due to erosion by glaciers enhances the seismic shaking response of mountains, but that the inundation of the landscape by glacier ice also damps seismic ground motions until deglaciation has progressed sufficiently.

The idea is tested by numerically simulating the effect of different topographic shapes and various levels of ice inundation on the response to shaking. The results suggest that total inundation of ice may reduce the shaking intensity (peak ground acceleration or velocity) at mountain crests to about 20-50% of that experienced when no ice is present. This effect diminished to about 80-95% if glacier ice level is reduced to half of the mountain slope height. In

general, ice cover reduced shaking most (i) for the steepest-sided edifices and for seismic wave frequencies higher than 3 Hz, and (ii) when ice is thickest and the rock has shear stiffness well in excess of the stiffness of ice. It is possible that the effect investigated is sufficient to have influenced the distribution of large post-glacial slope failures in seismically-active and mountainous glaciated regions of the world. Other implications and further discussion are provided in the manuscript.

CHAPTER 5: SYNOPSIS AND RECOMMENDATIONS FOR FUTURE WORK: In the last chapter of the thesis, I summarise the research and discuss it in reference to a conceptual model of the evolution of slope stability during glacial cycles. Finally, I suggest some directions for further research on this topic.

CHAPTER 2: LITERATURE REVIEW

2.1 PART A: PARAGLACIAL ROCK-SLOPE STABILITY

Paraglacial rock-slope stability, McColl ST; *Geomorphology* 153-154: 1-16, Copyright © 2012 Elsevier B.V.

http://www.sciencedirect.com/science/article/pii/S0169555X12000979

Only formatting and pagination has been modified for production in the thesis

Abstract: Glaciation and deglaciation, along with their associated climatic and non-climatic processes, modify slope stresses and influence slope stability. Paraglacial slope failures are those that are a part of, or influenced by, the transition from glacial conditions to non-glacial conditions. Gravitational failure of rock slopes is a primary and dominant process of slope evolution in mountainous terrain and is the subject of this chapter, which: (1) reviews the approaches taken for researching paraglacial rock slope failure patterns and processes; (2) summarises the spatial and temporal patterns of post-glacial failures; (3) assesses the factors influencing slope stability during glaciation and deglaciation; (4) explores some of the applications of paraglacial research; and (5) highlights some of the outstanding issues to be resolved and provides recommendations for terminology relating to paraglacial slope processes.

2.1.1 Paraglacial slope failure

Slope stability is a condition that varies with time, especially in the long term in landscapes affected by glaciations. As glacial cycles evolve, the factors influencing slope stability change. These factors include ice mass distribution, vegetation assemblages and cover, hydrological conditions, glacial erosion and seismicity. As a consequence, the distributions, magnitudes and frequencies of slope failures change throughout glacial cycles. Landslides dominate erosion processes and overwhelm sediment distributions in mountainous areas (Hovius et al., 1997; Korup and Clague, 2009) so understanding the non-uniformity and unsteadiness of landslide activity is

important for Quaternary landscape evolution and sediment flux models, as well as for managing landslide hazard risks in glaciated areas. Most models of post-glacial sediment flux have an initial period of enhanced landslide activity and sediment production, diminishing as deglaciation proceeds. For example, Ballantyne (2003) conceptualises the sediment contributions from four different mass-movement types, all of which show initially high sediment contributions but then diminish at different rates (see Figure 2B of Ballantyne 2003). Where human populations and resources are affected by landslide hazards and sediment flux, understanding the change of landslide activity through glacial cycles is an important endeavour (Holm et al., 2004).

Over the last few decades there have been substantial advances in awareness of the many factors influencing post-glacial slope stability, and there has in particular been a sustained effort to document and understand the locations and timing of post-glacial slope failures. However, most rock slope failure studies reported in the literature have been conducted in valleys no longer occupied by glaciers. Fewer studies have focussed on valleys undergoing deglacierization, and fewest on glaciations prior to the most recent one. Thus the information available remains limited and the theories explaining the patterns are seldom subject to rigorous testing. Consequently, causes of post-glacial slope failure are often inferred without substantive evidence, and failure mechanisms are postulated without adequate scientific investigation. For example, terms like glacial oversteepening and debuttressing, used to explain the failure of a rock slope in a glaciated valley, are often found in the literature but these terms are seldom justified in any detail. Researchers have found disagreements about the relative roles of factors that influence slope stability, for example: glacier retreat compared with climatic change; whether frost weathering can cause a large-scale rock slope failure (Matsuoka and Murton, 2008); and how important the debuttressing mechanism is for triggering slope failures in temperate glacier settings (McColl et al., 2010).

This chapter updates and extends the information on post-glacial rock slope failure presented as part of a paraglacial geomorphology review paper by Ballantyne (2002). The purpose is to summarise what the main approaches have revealed about paraglacial rock slope stability, and to assess the failure mechanisms and explanations proposed to explain failure patterns. In addition, it highlights some of the outstanding issues and research gaps, and makes suggestions on nomenclature.

2.1.1.1 Paraglacial framework

Changes in slope stability during deglaciation can be considered in the framework of paraglacial geomorphology. Ballantyne (2002, pp. 1937–1938) defined the term paraglacial as "non-glacial earth surface processes, sediment accumulations, landforms, land-systems and landscapes that are directly conditioned by glaciation and deglaciation". Slaymaker (2009) suggested that this term was too broad, and that it should be restricted to geomorphic transition, or adjustment, to non-glacial conditions. In the present review the term paraglacial describes rock slope failures that are a part of, or influenced by, the transition from glacial conditions to non-glacial conditions — in other words, it combines the elements of both definitions.

While the term 'paraglacial' and its application to slope failure are relatively new (Ryder, 1971; Cruden and Hu, 1993), geomorphologists have long been aware that slope form and process are influenced by glaciation and deglaciation, with specific reference appearing in the literature at the beginning of the 1900s. In 1911 for example, geologists noted that destabilisation of slopes in a 'U-shaped' valley in the Tararua Ranges, New Zealand, evident as prominent anti-scarps (uphill facing scarps), indicated a former glaciation (Brook, 2008).

2.1.1.2 Focus on rock slope failure

This chapter deals specifically with slope failures that directly modify the bedrock topography and are the primary drivers of landscape change. Regolith failures (shallow soil, drift/debris, or moraine collapses), and their consequent debris flows, have been excluded because they are secondary phenomena. Regolith accumulates on bedrock through weathering or sedimentation and is critically important for understanding changes in paraglacial sediment fluxes, but it is essentially a surficial process. Readers wishing to learn more about the role of such paraglacial sediments and sediment failures are directed to Ballantyne's (2002) detailed synthesis of paraglacial changes to sediment-mantled slopes. Rock slope failures described herein follow classification based on terminology from Cruden and Varnes (1996) and International Union of Geological Science Working Group on Landslides (1995), and include three main types:

vii) catastrophic rock slides — these are rapid to extremely rapid failures of the rock mass and can include translational and rotational rock slides that may develop into rock avalanches;

viii) deep-seated gravitational slope deformations (DSGSD) — these are slow to extremely slow flows (creep or sagging) or displacements of bedrock that often have geomorphic expression as sackungen, anti-scarps and toe bulging; and

ix) rock topples or rock falls — these are very rapid to extremely rapid dislodgements of loose bedrock.

2.1.2 Research tools and approaches

2.1.2.1 Spatial distribution of slope failures

One way to investigate the influence of glacial cycles on slope failure has been to document where failures have occurred relative to a glacier's changing perimeter and physical manifestations. This has been done at mountain scale and for individual slopes.

2.1.2.1.1 Mountain scale

Several researchers (e.g. Thorarinsson et al., 1959; Rapp, 1960; Caine, 1982; Cruden and Eaton, 1987) have recognised that rock slope failures are abundant in valleys that have been deeply eroded by glacier action (Figure 2.1.1). Caine (1982) for example, found this association in Tasmania, Australia, where extensive cliff toppling only occurred in places where glacial action had produced steep slopes, and was mostly absent in places unaffected by glacial erosion. In an extensive literature review of anti-scarp features, Pere (2009) concluded that almost all non-tectonic anti-scarps are found in glaciated terrain. This most basic link between glacially-modified terrain and the spatial clustering of landslides and slope deformation is a strong argument for the influence of glaciation/deglaciation on slope instability, but on its own it does not provide sufficient information about failure mechanisms or triggers because other processes, such as fluvial erosion, can produce similarly steep slopes, and not all steep slopes have failed.

Figure 2.1.1. Rock slumping of a glacially modified slope in Mount Cook National Park, New Zealand. The Mueller and Hooker glaciers are out of sight to the right but would once have eroded the toe of the slump; the Little Ice Age and Holocene moraine from these glaciers can be seen in the mid and foreground. The glacial trim-line, indicated by a break in slope and shown here by the dashed line, appears to have been shifted down-slope by slumping. Numerous other landslides have been identified in this glaciated region. Like this case, rock slope failure is common where glaciers have eroded and steepened slopes.

A correlation between failure distribution and localised stresses or stress-changes has been observed in several studies. Panizza (1973) found concentrated slope failures at glacier confluences in the Italian Dolomites, leading to the suggestion that at confluences, where glaciers merge, stresses exerted on the slopes are greater. This, he suggested, causes more "glacio pressure deformation" (i.e. more damage) in the rock mass, especially along existing structural weaknesses, which in turn predisposes the slope to failure. The strength of this interpretation suffers from not being able to distinguish rock damage caused by glacial processes from the tectonic controls on the development of such confluences. More convincingly, Cossart et al. (2008) compared the distribution of slope failures in the Southern Alps of France to the calculated regional distribution of ice-loading stresses. They found that more instability occurred where calculated normal and longitudinal ice loading stresses were higher. Unlike

Panizza (1973), who argued that loading damages the rock during glaciation, Cossart et al. (2008) considered that the relief of stresses after the unloading of the ice damages the rock — a process called stress-release (Section 2.1.3.2.3).

In a study of rock slope failures in the Scottish Highlands, Jarman (2006) noted that although glaciation affected the entire mountainous area in the last glacial cycle, the failures are unevenly distributed (65% are in seven main clusters, with the rest non-randomly scattered), and glaciological, lithological and seismotectonics did not adequately explain these distributions. Areas with similar relief and lithology could display either very few or abundant failures. Jarman (2006) found that landslide clustering occurred where slopes had undergone intense erosion because they were glaciated for the first time in the last glacial cycle. For example, where a glacier or ice cap had breached a watershed for the first time, landslides were more abundant. He suggested that the intense erosion of rock would have augmented stress-release with localised unloading, and caused exposure of additional failure planes or creep zones at the base of the eroded slopes. In older glacial terrain where failures were sparse, he suggests that the slopes had already adjusted to previous stress-redistributions (a concept which he has named stress-hardening), and were therefore less likely to suffer further stress-release due to erosion.

2.1.2.1.2 Slope scale

Previous investigations of paraglacial failure distributions on the slope scale have involved measuring the proximity to ice margins, slope form, and the localisation of stresses. Cossart et al. (2008) extended their mountain-scale approach by comparing the distributions of failures on slopes, and damage on roche-moutonnées, to the distribution of localised glacier loading stress at those sites. In addition to lithological and slope gradient controls, they identified a pattern of rock-slope failure and rock damage concentration at the lower parts of slopes and stoss-faces of roche-moutonnées where glacial loading stresses were inferred to be high. This confirmed that localised stresses affect the rock mass, adding support to the stress-release mechanism.

Other studies indicate a different stress mechanism. In deglaciated terrain in Canada, it is evident that most failures occur at convex slope breaks (i.e. in places where the slope angle increases towards the valley floor) situated immediately above

glacial trim-lines. The failure surfaces intersect with lower slopes that have been steepened by glacial action (Holm et al., 2004; Dadson and Church, 2005). This is a strong indication that glacial erosion changes stresses within the slope simply by changing slope form, and may be a sufficient cause of slope failure without invoking stress-release.

Field investigations and numerical modelling by Leith et al. (2010a; 2010b) make a strong case that the distribution of post-glacial rock slope failures can be driven by different mechanisms in different places along a slope profile, and that different parts of a slope can be activated at different times through retrogressive behaviour. They found a process of 'bottom–up erosion', in which glacially-modified valley walls are destabilised by progressive rock falls occurring near the base of the slope, which is presumably where stress redistributions and increases in slope angles have been greatest because of concentrated erosion. This process then leads to the development of larger-scale bedrock instabilities that appear to be continuing today.

Allen et al. (2011) argued that the close proximity of rock slope failures to glacial ice indicates that glacier retreat or permafrost degradation is an important factor. They note that 19 of the 20 rock avalanches recorded in New Zealand's central Southern Alps over the last 100 years have been initiated from sites situated less than 300 vertical metres from glacier ice. Thirteen of these were within 300 vertical metres of the estimated lower permafrost boundary.

All of the observations substantiate the influence of glacially-modified terrain as a preparatory factor but do not elucidate the triggering mechanisms — glacial erosion, stress-release, permafrost retreat and freeze–thaw mechanisms are just some of the factors that may have influenced these failures.

2.1.2.2 Temporal distribution of slope failures

Analysis of temporal patterns of slope failures has been another means of evaluating the influence of deglaciation on rock-slope stability and has been made possible largely due to the application of absolute dating techniques, mostly over the last 15 years. In particular, terrestrial cosmogenic nuclide concentrations (originating from cosmic ray bombardment) have been used to date landslide debris (Ballantyne et al., 1998; Ballantyne and Stone, 2004; Bigot-Cormier et al., 2005; Hippolyte et al.,

2006; Mitchell et al., 2007; Cossart et al., 2008; Hormes et al., 2008; El Bedoui et al., 2009; Hippolyte et al., 2009; Ivy-Ochs et al., 2009; Prager et al., 2009; Sanchez et al., 2009; Shroder et al., 2010). Radiocarbon as well as tephrachronology and optically stimulated luminescence methods have also been applied (Beget, 1985; André, 1986; André, 1997; Watanabe et al., 1998; Smith, 2001; Soldati et al., 2004; Ballantyne, 2008; Agliardi et al., 2009a; Pánek et al., 2009; Borgatti and Soldati, 2010; Pánek et al., 2011). The same dating techniques have been applied to paleoclimate reconstructions, which has helped to constrain the timing of glaciation and deglaciation in many parts of the world.

Landslide inventories enable assessment of the random or clustered nature of the landslide distributions (Cossart et al., 2008). Comparing these clusters with the timing of other events, for example, glacier retreat, climatic events, or seismicity, has been crucial in developing an understanding of cause. This type of analysis has mostly been carried out at three time-scales of interest: the late-glacial to late Holocene glacial transition; short-lived climatic events, particularly the Little Ice Age in Europe; and contemporary glacier retreat or climate warming. Few studies have examined paraglacial rock slope failures over multiple glacial cycles; in a study of the Kawarau Valley, New Zealand, Bell (1976) suggested that glacial over-steepening and withdrawal of ice over several Pleistocene glaciations, each time initiated landslides from slopes weakened by unfavourably oriented schist foliation and joints; and Tibaldi et al. (2004) studied a deep-seated gravitational deformation that has been active since at least since 120 ka.

2.1.2.2.1 Late-glacial–late-Holocene

A common pattern in glaciated catchments is that many major landslides are of the order of 10–8 ka in age, with another cluster around the mid-late Holocene at about 3–2 ka (Table 2.1.1; Figure 2.1.2). This finding was both a surprise and a concern to researchers in the European Alps, who had previously assumed that the ancient large landslides were a relic of deglaciation and not a phenomenon that had occurred under climatic conditions similar to present (Abele, 1997).

Table 2.1.1 Major (>10 M m^3) global rock slope failures and estimated lag-time following glacier retreat. Only events with reliable radiometric dates within the late Glacial to mid-Holocene (c. 16–1 ka) are included. Type abbreviations are as follows: RS = rock slide; DSGSD = deep-seated gravitational slope deformation; RA = rock avalanche.

ID	Reference	Name	Place	Type	Vol. (10^6 m^3)	Age (ka)	Method	Lag (kyr)
A	(van Husen et al., 2007)	Almtal	Austria	RS	>100	15.6±1.1	^{36}Cl	?
B	(Hancox and Perrin, 2009)	Green Lake	New Zealand	RS	27,000	12.0–13.0 BP	14_C	1.0–2.0
C	(Bigot-Cormier et al., 2005)	La Clapière	France	DSGSD	60	10.3±0.5	^{10}Be	>3.0
D	(Soldati et al., 2004)	Col Maladat	Italy	?	>10?	10.4–10.1 BP	^{14}C cal.	>1.0?
E		Garden Pass	Italy	?	>10?	8.5–11.8 BP	^{36}Cl	>1.0?
F	(Agliardi et al., 2009a)	Mt. Watles	Italy	DSGSD	>1000?	>10 BP	^{14}C cal.	>1.0?
G	(Kubik et al., 1998)	Köfels	Austria	RA	2500	9.8±0.1 BP	^{26}Al and ^{10}Be	>3.0
H	(Mathews and McTaggart, 1978)	Hope	Canada	RS	~50	~9.7	14_C	?
I	(Tinner et al., 2005)	Kandertal	Switzerland	RS	800	9.6±0.16	14_C	?
J	(Soldati et al., 2004)	Corvara	Italy	RS	>50	10.0–9.0 BP	^{14}C cal.	>1.0?
K		Sottocianin	Italy	?	>10?	8.8–9.4 BP	^{14}C cal.	>1.0?
L	(Ivy-Ochs et al., 2009)	Flims	Switzerland	RA	8000–12,000	8.9±0.7	^{36}Cl and ^{10}Be	>3.0
M	(Dortch et al., 2009)	Sichling	Himalaya	?	1400	7.6–9.7	14_C	?
N		Chilam	Himalaya	?	240	8.5±0.5	10_{Be}	?
O		Dear	Himalaya	?	>10	7.9–8.6	^{10}Be	?
P		Ghoro Choh	Himalaya	?	60	7.95	14_C	?
Q		Patseo	Himalaya	?	128	7.9±0.8	10_{Be}	?
R		Darcha	Himalaya	?	10	7.7±1.0	^{10}Be	?
S		Keylong Serai	Himalaya	?	900	7.5±0.1	10_{Be}	?
T		Kuppa	Himalaya	?	600	6.1–8.4	14_C	?
U	(Ballantyne et al., 1998)	Storr	Scotland	RS	>50?	6.5±0.5 BP	^{14}C cal.	4.0–6.0
V	(Prager et al., 2008)	Lavini di Marco 1	Italy	RS	>100	6.5±0.2 BP	^{14}C cal.	?
W		Wildalpen	Austria	RS	>100	5.8±0.3 BP	^{1}C cal.	?
X	(Orwin et al., 2004)	Cheam	Canada	RA	175	5.4±0.7 BP	^{14}C cal.	5.0–7.0
Y	(Prager et al., 2009)	Fern Pass	Austria	RS/RA	1000	4.1–4.2	^{14}C, ^{36}Cl, Th-/U-	>8.0
Z	(Prager et al., 2008)	Tschirgant	Austria	RS	>100	3.75±0.2 BP	^{14}C cal.	?
aa		Tschirgant 2	Austria	RS	>100	3.15±0.4 BP	^{14}C cal.	?
bb		Molveno	Italy	RS	>100	3.08±0.4 BP	^{14}C cal.	?
cc	(Dortch et al., 2009)	Kaza	Himalaya	?	500	3.0±0.1	14_C	?
dd	(Prager et al., 2008)	Marocche di Dro	Italy	RS	>100	2.25±0.1 BP	^{14}C cal.	?
ee	(Adams, 1981)	Chalice	New Zealand	RS	>10	2.16 BP	^{14}C cal.	?
ff	(Prager et al., 2008)	Lavini di Marco 2	Italy	RS	>100	1.19±0.2 BP	^{14}C cal.	?

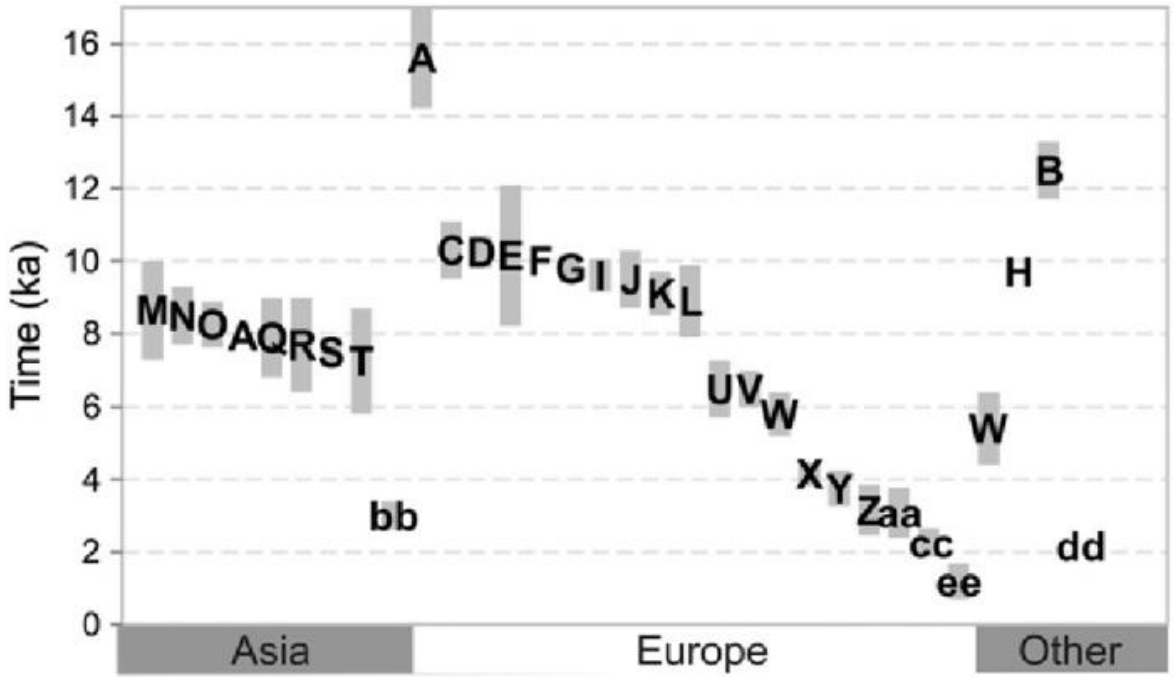

Figure 2.1.2. Ages of global rock slope failure events. Despite regional climatic and geological differences and a small dataset, at this resolution clustering of failure events is evident. Landslide IDs are linked to Table 2.1.1. Where available, dating error is represented by grey bar. Data has been separated into continents with New Zealand and Canada lumped into 'Other'.

While some major landslides initiated prior to deglaciation (Ambrosi and Crosta, 2006), and some were synchronous with deglaciation (Agliardi et al., 2001; Smith, 2001), the majority of documented cases indicates that large post-glacial failures have typically occurred some thousands of years after ice retreat (Table 2.1.1). This 'lag-time' between the destabilising effects of glacier retreat and the failure of slopes has been coined as a '*pre-failure endurance*' by Ballantyne (2002) and explained as the dynamic adjustment of slopes to debuttressing/stress-release through the gradual changes in stresses and strength of the slope. Referring to the European Alps, Le Roux et al. (2009) for example, noted that major landslides typically occurred several thousands of years after glaciers completely retreated, with pre-failure endurances exceeding 5400, 3000, 2500, 4000 and 2000 years for the major Séchilienne, La Clapière, Flims, Val Viola and Fernpass landslides respectively. These very large time-lags, while comparable to lag-times in other places (e.g. Cruden and Hu, 1993), seem an extraordinarily long time for a rock slope to respond to an external factor. There has been little research, other than these few empirical studies, to understand pre-failure endurance and test whether it can sufficiently explain these large time-lags. Other more satisfactory explanations may be needed, such as changes in seismicity or climate.

Ivy-Ochs et al. (2009) suggest that the spate of large slope failures during the mid-Holocene in the European Alps, mentioned above, coincided with a time when climate became markedly warmer and wetter; the Holocene Climatic Optimum (9.0–5.0 ka). This is a view that is consistent amongst several researchers who link climate changes with increased landslide activity, including debris- and earth-flows (Berrisford and Matthews, 1997; Matthews et al., 1997; Dapples et al., 2002; Bertolini et al., 2004; Soldati et al., 2004; Prager et al., 2007; Prager et al., 2008). Abele (1997) however, suggested that it is unlikely that temporal patterns of large, deep-seated rock slope failures would match climatic patterns. This is because rockslides are primarily influenced by internal factors and require particular preparatory factors to have sufficiently reduced stability before climatic triggers could be effective; extreme climatic events have happened many times in the past.

Landslide activity may also be linked to patterns of seismicity, and this could explain the lag time observed. It has been recognised that continental seismicity increased several thousands of years after deglaciation at a similar time to the peak in landslide activity of around 10–8 ka (Section 2.1.3.2.5). It seems a credible explanation, because large (>10 M m^3) landslides, like many of the documented paraglacial slope failures, are typically triggered by earthquakes.

Finally, Bigot-Cormier et al. (2005), Beget (1985), and Tibaldi et al. (2004) have shown that deep seated gravitational slope deformations can exhibit episodic movement interspersed with periods of non-movement or reduced movement lasting several thousand years. This indicates that at least some mass movements remain in a state of critical stability for a long time following deglaciation (or during interglacial periods — Tibaldi et al., 2004) but their activity is driven by a range of processes, some of which are unrelated to the action of long-since vanished glaciers.

2.1.2.2.2 Little Ice Age

The Little Ice Age (LIA) was a period between the 16th and 19th centuries, when a short reversion to cold climatic conditions affected the whole globe, although most evidence for this climate event comes from Northern Hemisphere regions. There were substantial glacial advances during this period due to cooler climate and intensified weather events. Several researchers have linked changes in landslide activity to the

LIA but the reported timing and cause of this activity are varied. Landslide activity in Norway (Grove, 1972) and Italy (Porter and Orombelli, 1981) increased during the LIA, reportedly because of intensified weather events that also caused flood damage. Other researchers report that the decline of the LIA and consequent retreat of glaciers caused an increase in landslide activity (mainly larger scale failures or slope deformation) towards the end of the LIA (Bovis, 1982; André, 1986; André, 1997; Dadson and Church, 2005). Holm *et al.* (2004) documented high post-LIA landslide activity occurring about a century after the retreat of glaciers commenced in Canada.

2.1.2.2.3 Recent and ongoing failures

Several landslides documented in the last few decades have been in deglaciated valleys or valleys still partly occupied by ice. For many, excellent data have been gathered because the features were studied soon after the event. Advances in technology such as satellite imagery and seismograph networks have improved the amount of data available and have helped to constrain time of failure for un-witnessed events (e.g. Sigurdsson and Williams, 1991; McSaveney, 2002; Huggel et al., 2008; Bryant, 2010). Despite this, the triggering events and causes of failures have remained elusive and have relied largely on inference. Often there is no observable trigger, even when events were witnessed as was the case for a large failure in Canada in 2007 (Lipovsky et al., 2008a) and another fatal landslide in Chile in 1987 (Hauser, 2002). Despite a common belief that earthquakes and extreme rainfall events are the main triggers for rock slope failures, absence of observable triggering mechanisms appears to be very common, which presents a significant problem for hazard management and science. In a study of 395 reports of historical alpine rock slope failures in the Sierra Nevada (Wieczorek and Jäger, 1996), half of the accounts reported no triggering event. The three largest ($> 10^7$ M m^3) rock slope failures to have occurred in New Zealand in the last 20 years (Owens, 1992; Hancox et al., 2005; Bryant, 2010), as well as many smaller failures (McSaveney, 2002; Cox et al., 2008), all occurred in deglaciated terrain, and without any observable trigger. Whether these rock masses had reached an intrinsic threshold, such might be the case with progressive strength degradation (Eberhardt et al., 2004), or whether some other unidentified external factor was involved, remains uncertain.

Some researchers have considered the cause of recent paraglacial rock slope failures around the world to be directly linked to recent glacier debuttressing

(Sigurdsson and Williams, 1991; O'Conner and Costa, 1993; Evans and Clague, 1994; McSaveney, 2002; Cox et al., 2008; Allen et al., 2011). However, changes in climate or permafrost degradation linked to warming temperatures have also been cited as a cause (Fischer et al., 2006; Geertsema et al., 2006; Huggel, 2008; Allen, 2009; Ravanel and Deline, 2011). In three failures in Iceland investigated by Sigurdsson and Williams (1991), heavy precipitation events were considered to be likely triggers.

Observable triggers are most common for active paraglacial slope failures, which are mostly deep-seated gravitational slope deformations (McLean, 1976; Bovis, 1982; Bovis, 1990; Blair, 1994; Bovis and Stewart, 1998; Corsini et al., 2005; El Bedoui et al., 2009; Le Roux et al., 2009; Gischig et al., 2010). Monitoring of such features has provided insight into some of the drivers of slope deformation, and allows calibration of slope stability models for back-analyses of failure initiation during early deglaciation. These studies have revealed a variety of mechanisms driving slope deformation, for example groundwater fluctuations (Bovis and Stewart, 1998), thermal effects (Gischig et al., 2011a, b), and collapse of moraine wall (McLean, 1976). Another finding was that movement is normally episodic. These studies suggest that the incidence of slope failures following deglaciation is probably driven by a multitude of processes and brings us closer to direct inference of what these processes actually are.

2.1.2.2.4 Rates of talus accumulation

Young (1972, pg. 226) wrote that talus slopes in cold regions can be considered to be in part a relic of deglaciation, and therefore another approach to analyse the timing of rock slope failures is to investigate the accretion rates of talus. By comparing recent rock-fall and talus-accumulation rates to older post-glacial accumulations of known age, it is possible to evaluate any difference in rate of accumulation between the two time periods of interest. Generally such work has indicated that accumulation of rock-fall talus occurred more rapidly immediately after deglaciation than at present (André, 1986; Luckman, 1988; Wieczorek and Jäger, 1996; André, 1997; Hétu and Gray, 2000). Wieczorek and Jäger (1996), for example, estimated that historical (last 150 years) rates of deposition in Yosemite Valley, USA are about half that of the post-glacial average over the last 15,000 years. Wyrwoll (1977) studied rock-wall retreat and talus accumulation in the sub-arctic Canada. Based on modern rates of rock-wall

retreat by frost shattering, he calculated that large accumulations of Holocene talus could not have formed by modern rates of rock wall retreat and suggested that rock-slope failures must have been more common immediately following deglaciation.

2.1.2.3 Numerical modelling of slope failures

Numerical modelling is a powerful tool for investigating complex geological problems. It has been proven useful for studying many landscape processes including landslides, and its use is growing in paraglacial slope stability investigations, such as for modelling stress-release processes (Augustinus, 1995a; Leith et al., 2010a,b), statistical modelling of slope evolution (Dadson and Church, 2005) and in analysis of specific landslides. Analyses of various landslides have shown that the timing of failure following deglacierization is variable: For example, Ambrosi and Crosta's (2006) models of deformation in the Italian Alps, indicate failure initiation as soon as ice begins to retreat, mostly consistent with their field evidence for early post-glacial deformation. Agliardi et al. (2001), on the other hand, show that gravitational deformation in another part of Italy does not occur until the glacier surface has reached the valley floor. Prior to that point, the slope response was an elastic rebound of the slope without failure. The role of pre-existing tectonic joints and other structures (e.g. foliation) is demonstrated to be of critical importance in both of these studies, for example, Agliardi et al. (2001) show that failure does not develop when the pre-existing structures are excluded from their models. Eberhardt et al. (2004) used numerical modelling to investigate the failure mechanism and initiation of the historical Randa rockslides in Switzerland. In this situation, pre-existing geological and structural features played a less important role compared to the post-glacial changes to the rock mass. Their results suggest that a gradual (over 1000s of years) reduction in the rock mass strength and development of a failure surface led eventually to failure. The degradation of the rock mass was initiated by the development of tensile rock damage, which promoted further weakening by loss of cohesion resulting from internal deformation. Their modelling of the erosion and deglacierization of the slope showed that the stress redistributions associated with these processes may have been sufficient to initiate the tensile rock mass damage. However, the degradation of rock-masses over time has also been used to explain the development of mass movements on non-glaciated slopes. For example, modelling by Chemenda et al. (2009) shows that

sackung can develop simply by gradual reduction in rock mass strength caused by weathering and alteration.

Fischer et al. (2010) show how numerical modelling can be used systematically to understand the cause of a catastrophic paraglacial rock slope failure, the 1988 Tschierva rock avalanche in Switzerland. The value of the study comes from their attempt to assess multiple potential influencing factors, including the slope morphology, the geology and rock mass properties, the hydrological setting, the deglacierization history, permafrost conditions, and meteorological data. Although there were some factors that were not modelled, such as stress changes through multiple glacier cycles, creep, progressive strength degradation, and in-situ stress conditions, the results showed that there was still a multitude of contributing factors, and no single factor could be isolated as being the overall cause of failure.

Despite some questionable early results, it seems that, provided appropriate modelling parameters and constitutive models are adopted, numerical modelling has significant potential to aid paraglacial slope stability research. The ability to perform sensitivity analyses on the various parameters adopted in models will improve insight into the relative importance of the various factors influencing stability.

2.1.2.4 Space-for-time substitutions

A space-for-time substitution approach has not been used in paraglacial slope studies but it has been used for the opposite purpose: to infer the length of time it takes glaciers to produce U-shaped valleys and cirque basins (Kirkbride and Matthews, 1997; Brook et al., 2006; Brook et al., 2008). The slope profiles were measured along valleys that had been glacially occupied for different cumulative lengths of time during multiple glaciations, and these relations were used to estimate a rate of profile development. The approach suffers from an inherent problem: during the periods between glacial cycles, slopes would have been adjusting to non-glacial conditions, and corrections should have been made for this.

This approach could be used indirectly to assess patterns of post-glacial rock slope failures. Since critically steepened slopes will adjust to a more stable angle once glacial erosion has ceased, the amount of adjustment may be assumed to be a function of time since deglacierization. In theory, the more distant a slope is from the retreating glacier surface, the longer it has been able to adjust towards its long-term equilibrium angle.

Results from this could be used to inform slope evolution models. However, any interpretation would need to account for the fact that the degree of glacial erosion is not uniform along a valley because slopes further from the head of a glacier have been glaciated for less time.

2.1.2.5 Discussion

The temporal and spatial patterns identified across all scales investigated indicate a direct link between the development of slope instability and glaciation/deglacierization. However, none of the patterns unequivocally proves the processes linking glacial process with slope instability. For example, the different patterns observed in the LIA (Section 2.1.2.2.2) indicate that increases in landslide activity could have been generated by glaciation (i.e. additional slope modification by glacial erosion), deglacierization (i.e. debuttressing or stress-release), and climatic changes (i.e. increased storminess). One of the difficulties arises because glacial processes can influence several related factors; for example, at sites with higher normal and longitudinal ice stresses, basal shear stresses and therefore erosion and over-steepening, as well as potential stress-release, are higher. Rock mass damage, initial slope failures, or other climatic factors acting after deglaciation may reduce the stability of a deglaciated slope further but these same factors may also be important prior to deglaciation. Numerical modelling studies serve to highlight the fact that many factors may combine to influence the overall stability of a slope and that slopes are varyingly sensitive to different triggering factors. Hence, the response of individual slopes to glaciation and deglaciation is spatially and temporarily variable and many interrelated factors need to be considered to understand the response. Only a few studies have managed to achieve a detailed investigation of the failure mechanisms and causes of an individual 'paraglacial' rock slope failure (e.g. Bovis and Stewart, 1998; Agliardi et al., 2001; Ambrosi and Crosta, 2006; Fischer et al., 2010). In most other studies the causes have had to be based on assumptions and speculation because insufficient information was available. The next section addresses each of the major factors identified in this section in an attempt to assess their general importance for rock slope stability.

2.1.3 Causes and triggers of slope instability

It has been found useful to group the paraglacial factors that result in rock slope failures into three types: preconditioning, preparatory and triggering factors (Glade and Crozier, 2005) (Table 2.1.2). Preconditioning factors are those which are static and inherent. Preparatory factors are dynamic and reduce the stability of a slope over time without actually initiating movement. Triggering factors initiate movement by changing the slope from a 'marginally stable' to 'actively unstable' state.

Table 2.1.2 Factors involved in paraglacial rock-slope stability, separated into preconditioning or preparatory factors, and triggers. The importance of each factor is qualitative and based on the literature reviewed and author's judgement.

Factors	Preconditioning	Preparatory	Trigger
Lithology	Always		
Intact rock strength	Always		
Rock mass quality	Always		
Joint characteristics	Often		
Structure (e.g. bedding)	Often		
Pre-glacial erosion	Often		
Pre-existing stresses	Often		
Debuttressing		Sometimes	Sometimes?
Glacial erosion		Often	Unknown
Sheet jointing		Often	Often
Static fatigue		Always	Unknown
Seismicity		Unknown	Often
Climatic changes:			
Water		Unknown	Often
Permafrost		Sometimes	Often?
Weathering		Always?	Unknown

2.1.3.1 Preconditioning factors

Rock-slope stability and long-term equilibrium slope angles are controlled primarily by rock-mass properties. Many researchers have identified this fundamental control on paraglacial rock slope failure distributions (Thorarinsson et al., 1959; Rapp, 1960; Beck, 1968; Bovis, 1982; Augustinus, 1992, 1995b; Alexandrowicz, 1997). As Bovis (1982) pointed out, although steepening and debuttressing occurred in every glaciated valley, not every slope has failed, and he concluded, as others had done (e.g. Thorarinsson et al., 1959; Beck, 1968), that lithology and rock structure are (preconditioning) factors that provide ultimate control of stability and the distribution of rock slope failures. Any attempt to understand slope-failure patterns first requires an understanding of the rock strength and deformability, bedding, foliation, joints and faults and their orientations and conditions; these factors control the overall ability of a

slope to resist the stresses acting on it, and therefore also determine the geometry that a slope can maintain. However, while the inherent strength of a slope is 'fixed' by the preconditioning factors, the stability of the slope can change with time due to a variety of preparatory and triggering factors. Hence, it is these time-dependent preparatory factors and triggers that are the main focus of paraglacial slope stability studies.

2.1.3.2 Preparatory and triggering factors

2.1.3.2.1 Glacial erosion

Glaciers produce steep-sided and deep valleys, thereby steepening and lengthening valley-sides and increasing the shear and self-weight stresses within the slopes. The slopes become less stable as the ratio of slope strength to those stresses decreases. When the ratio reaches unity, failure occurs. The term 'oversteepened' has been used to describe the state of large steep slopes produced by glacial erosion. However, as Augustinus (1995b) pointed out, such a term may be misleading because it implies that the slope is inherently unstable and close to failure. This may not be so when the rock-mass strength is high. To describe a failed slope as having been 'oversteepened' by glacial erosion may also be misleading, since there are many other factors that could have reduced the stability, such as weathering which reduces rock strength. The term 'glacially oversteepened' should be avoided unless an evaluation of the strength to stress ratio indicates that steepening has had a critical effect on stability. Glacial erosion may sufficiently increase the stresses above a critical value but it may simply expose rock-mass defects (planes of weakness) that are oriented in such a way that failure becomes kinematically feasible. Further, fluvial processes can also steepen and deepen slopes, and most valleys have been formed by both fluvial and glacial erosion over many glacial cycles, so the entire history of the slope should be considered before attributing the cause of failure to glacial erosion.

Reducing slope stability by steepening, deepening, or undercutting by a glacier, may have three outcomes. First, it may increase stresses and reduce the stability of the slope but not to the point of critical instability; failure may occur later, possibly long after the ice has gone, when additional stresses or weakening becomes the trigger. This type of slope modification is a preparatory factor and is probably involved in most paraglacial slope failures. Second, the erosion may reduce the stability of the slope to a critical state but catastrophic failure of the slope is prevented while the ice remains as a

buttress. The steepening is still a preparatory factor but failure would be triggered upon sufficient glacier retreat or thinning at the toe of the unstable rock mass. A third outcome is that the critically stable slope is not prevented from failure by the ice and instead is accommodated by deformation of the ice. This has been proposed as a failure mechanism based on the recognition that rock has a greater density than ice and the buttressing ice will flow in response to applied stresses (Bovis, 1982; McColl et al., 2010). In this outcome, glacial erosion directly triggers failure.

2.1.3.2.2 Glacial debuttressing

Ballantyne (2002) described glacial debuttressing to be "the removal of the support of adjacent glacier ice during periods of downwastage and the consequent stress-release". Including 'stress-release' in the definition may have caused some confusion in the literature. In this review, 'stress-release' is treated as a separate, albeit related, mechanism because an ice buttress may simply be holding up a rock mass that has already failed.

A glacier provides a load or force acting on the base of a slope. Debuttressing, or the removal of this load, can be either a preparatory factor or a trigger for slope failure. As a preparatory factor, the unloading would reduce the stability of the slope but without triggering failure, and other processes may reduce stability further and trigger failure long after glacial retreat. As a trigger, debuttressing may cause rapid slope collapse if slope stability is already critical. However, this may not always be the case. McColl et al. (2010) argue that because ice is less dense than the rock and flows under low applied stresses, and because some of the ice load is supported by basal water pressures, glaciers may not 'buttress' slopes, or at least not continuously when basal water pressures are high. Therefore, slopes could potentially begin to collapse before ice has retreated; but glacier retreat would probably hasten that collapse.

2.1.3.2.3 Rock stress redistributions and jointing

In Section 2.1.2.1 it was seen that many paraglacial slope failure surfaces are controlled by joint distributions, which are a preconditioning factor on stability – joints weaken the rock mass, provide failure surfaces, and also provide pathways for water and additional surface areas for weathering processes. This section explores the

possibility that glacial processes can generate new joints, in which case the development of jointing would be a preparatory factor.

While tectonic stresses are the most common cause of stress-induced rock mass jointing, usually forming two vertical orthogonal joint sets, other joint systems, some of which may result from glacial processes, seem to be important for paraglacial slope failure (Section 2.1.2.1). Nichols (1980) explains that non-tectonic joints are usually easily distinguished from tectonic joints because they are dominantly extensional fractures; usually sub-parallel to the local topography; increase in density towards the surface; are very local in extent; normally have very little or no filling material; and sometimes crosscut or terminate at tectonic fractures (Figure 2.1.3). They occur in a wide range of lithologies including hard (e.g. sandstone and limestone) and weak (e.g. clay and shale) sedimentary rocks as well as metamorphic and crystalline rock types, although their distributions within these lithologies may be different. These joints have long been recognised as non-tectonic in origin (Gilbert, 1904), and have been referred to as exfoliation, sheeting joints, or more recently, stress-relief or -release joints. Sheeting joints is adopted here because the term does not assume any process of formation. Balk (1939) was one of the first to suggest that sheeting joints may play an important role in post-glacial rock slope processes. While several mechanisms have been proposed to explain the formation of these joints, including the mechanical effects of fire, thermal cycles, vegetation and chemical weathering, it has generally been accepted that they are generated by gravitational stresses and usually triggered by unloading (Brunner and Scheidegger, 1973).

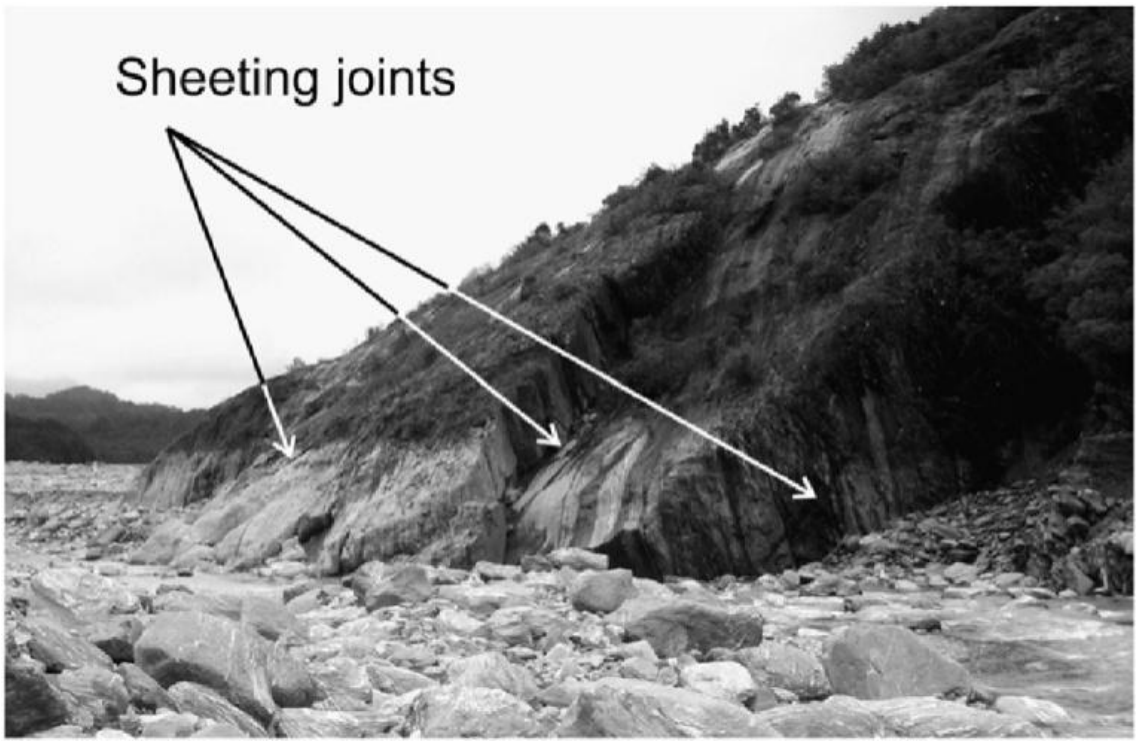

Figure 2.1.3 (previous page). Sheeting joints in schist 200 m down valley from the present-day terminus of the Franz Josef Glacier in New Zealand. The joints appear to be pathways for water flow and surfaces upon which several small rock slabs have failed. The foliation in the schist is sub-vertical and perpendicular to the joints. It is possible that these joints formed as a result of erosional and/or ice unloading; the slopes here are too gentle for the sheeting joints to have formed from high slope-parallel gravity-induced stresses, although this may have been the reason for sheet joint development on very steep slopes further up-valley.

In many locations where sheeting joints have been observed, the stresses, as determined by direct measurement or observation of other geological phenomena, are higher in the horizontal (or slope-parallel) than vertical (or slope-perpendicular) orientation (Figure 2.1.4) (Hencher et al., 2011). The high horizontal to vertical stress ratios, σ_h/σ_v, and the development of joints parallel to the land surface indicate that failure may have been induced by compressive stresses (i.e. by stresses parallel to the joint orientation). It is well known that tensional stresses can develop from compressional applied stresses, as is commonly observed in uniaxial compressive or Brazilian tests on rock specimens. When the induced tensional stresses exceed the tensional strength of the rock, joints propagate by crack development and extension. As in laboratory experiments, the development of these joints is inhibited by sufficient confining pressures (Brunner and Scheidegger, 1973), so that a substantial amount of overburden would prevent development of joints in the rock mass. In deep underground man-made rock excavations or tunnelling, the excavation of rock removes the confining load, inducing spalling fractures on the free face. Laboratory experiments have also ruled out the possibility that tensile stresses induced by surface processes are sufficient to produce sheeting joints; cyclical elastic compression and decompression of rock specimens in laboratory tests does not produce tensile fracturing (Twidale, 1973). However, when lateral confining stresses are maintained upon loading and unloading, then compressive stresses are generated and extensional fractures can develop (Nichols, 1980). These laboratory experiments also confirm the role of compressive stresses in forming rock bursts or ‘pop-ups’, which are the rapid ‘explosion’ of rock at the surface or buckling, often occurring after mining operations that remove overburden or in terrain that has undergone natural erosion (Bain, 1931; Jacobi et al., 2007; Everitt, 2009).

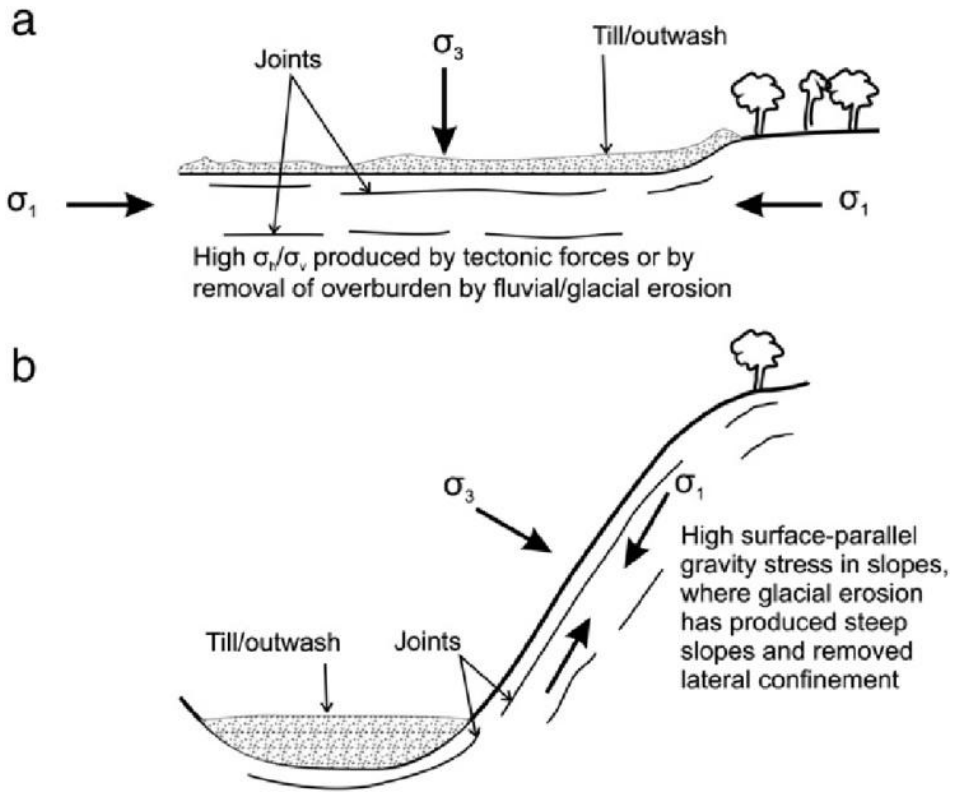

Figure 2.1.4. Stress conditions for the formation of surface parallel joints in (a) situations where high horizontal to vertical stress ratios develop, and (b) steep slopes where gravity stresses acting parallel to the slope are high. σ1 =major principal stress; σ3 =minor principal stress. Modified from Hencher et al. (2011).

High ratios of shear horizontal to shear vertical stresses diminish with depth, as does the density of jointing. High values at the surface (often >1.5 and sometimes as great as 7 for strong rock) and this kind of stress distribution cannot be explained by an elastic and horizontally confined lithostatic overburden (Nichols, 1980). In such a case the gravitationally induced σ_h, would be related to σ_v by

$$\sigma_h = \frac{\nu}{1-\nu}\,\sigma_v \qquad (2.1.1)$$

where ν is Poisson's ratio, and would therefore be lower than vertical stresses for most geological materials. Naturally high ratios, or high surface-parallel stresses, could be achieved in three situations: (1) topographic stress concentration; (2) maintenance of horizontal stresses during unloading of vertical elastic stress; or (3) present-day applied

tectonic loading, such as might be expected in a compressional orogenic setting (Figure 2.1.4). Release of stress upon disturbance of elastic residual strains locked into the rock as a result of past gravitational and/or tectonic forces may also play a role in generating unusual stress conditions, but they are generally considered to be of subsidiary importance (Harper and Nichols, 1982). In the first situation (1), stress concentrations produced by self-weight loading on the slope may increase at the glaciated parts of the slope when confining stresses are removed either through glacial erosion (i.e. steepening the slope) or through unloading of ice (Figure 2.1.3). The second situation (2) may arise because removal of overburden will release vertical/normal elastic stress (i.e. perpendicular to the free-face), but the gravitationally-induced horizontal/slope parallel stresses may be maintained because of lateral confinement provided by the surrounding rock mass. The removal of overburden could be in the form of erosion of rock, stripping of sediments, or the removal of the ice itself. In the third situation (3), regional tectonic loading of the lithosphere from plate motions may generate high horizontal stresses. All of these processes result in reorientation of the major principal stresses at free surfaces, and can result in high surface-parallel (compressive) stresses. Therefore, particularly by situations (1) and (2) above, glaciation and deglacierization may produce compressive stresses at the surface.

Whether or not the surface-parallel or horizontal stresses produced by glaciations and deglaciation processes are sufficiently high to produce extensional failure is uncertain. It seems that the long-term erosion of overburden and modification of slopes, especially where intense erosion occurs such as in glaciated valleys or gorges, certainly could induce sufficiently high slope-parallel stresses in some situations (e.g. as demonstrated by Eberhardt et al., 2004). However, in many situations, additional regional tectonic stresses would be necessary (Leith et al., 2010a; Pascal et al., 2010). The relative contributions of ice unloading and erosional unloading have been long debated (Matthes, 1936; Jahns, 1943; Lewis, 1954; Harland, 1957; Twidale, 1973) but it seems that the loading and unloading of ice itself may seldom be sufficient to produce sheeting joints, as indicated by field evidence of sheeting joints and rock slope failure distributions (Section. 2.1.2.1). Indeed, Brunner and Scheidegger (1973) commented that many observed sheeting joints are pre-glacial in origin. However, the unloading of ice may act as a trigger for sheeting joint development if sufficient horizontal or surface-parallel stresses have developed during glaciations, through

erosion, tectonic stresses, or release of locked-in elastic stresses, and if these stresses are maintained by the confinement of the ice until it disappears.

Stress-redistribution varies from site to site because of differences in: the erosional history of a site; a site's ability to sustain elastic stresses during erosion; the regional tectonic regime and locked-in stresses; the orientation of surfaces relative to these; and differences in rock mass properties, particularly the elastic modulus and strength, anisotropy, fracture density, rock density and moisture content (Wyrwoll, 1977; Nichols, 1980; Selby, 1993; Augustinus, 1995a; Leith et al., 2010a; Hencher et al., 2011). For example, Selby (1993, pp. 41-42) explains that the higher the value of Poisson's ratio for a given material, the higher the gravitationally-induced horizontal stresses for any given vertical stress. The density of pre-existing joints influences the development of sheeting joints because the pre-existing joints accommodate the relief of stresses (Hencher et al., 2011), as such sheeting joints are rarely found in intensely-jointed granite for example (Twidale, 1973). Further, at individual sites within uniform rock masses, the development of sheeting joints will be spatially variable because of variation in stress redistribution.

Much uncertainty remains around the timescales over which sheeting joints develop following deglaciation. The concept of pre-failure endurance (Section 2.1.2.2.1) postulates that there is a period of time from the geomorphic perturbation (e.g. unloading) to the associated stress-reorientations and development of the jointing, to the eventual propagation and formation of joint-networks, until complete failure of the slope proceeds. For example, a slope in Scotland is thought to have failed 7 ka after deglacierization because of progressive propagation of joint networks (Ballantyne et al., 1998). It has been suggested that there is a time-dependent response of rocks to stress-redistributions (Wyrwoll, 1977), which is supported in the field with pop-ups occurring at different times following deglacierization (Jacobi et al., 2007). In the laboratory, however, the response time measured is relatively short (Nichols, 1980) and spalling failures in tunnelling are usually instantaneous upon removal of confining pressures. Understanding the effect on the response time of the scale, rate and magnitude of unloading, as well as the rock mass properties, pre-existing stress state, and the dissipation of stresses, seems like a critical area of future research. Engelder and Sbar (1977) demonstrated that pre-existing joint structures can accommodate some of the stress-release. Essentially this translates to a long response time if the valley wall

has good quality rock. If the rock mass is highly fractured, stress-release may happen very soon after deglacierization, or even during glacier thinning or retreat, but additional jointing may not result. This may partly help explain Jarman's (2006) observations of post-glacial rock slope failures clustering in areas that have undergone only one cycle of glacial erosion. Sites that had developed sheeting in previous glaciations could accommodate strain on those pre-existing joint structures. For individual sites, with specific geology, and geomorphological and environmental histories, the timescale for generating sheeting joints may vary considerably. Until a better knowledge of these timescales and their variation is achieved, pre-failure endurance remains speculative.

Another phenomenon resulting from stress-redistribution that may influence landsliding is the development of gouge weaknesses in horizontal sedimentary strata from flexure of the layers after unloading rebound (Selby, 1993, p. 48). Slip at sedimentary bedding contacts may produce a weak gouge (zone of weak comminuted rock) by grinding and milling of the adjacent rock surfaces. Mattheson and Thompson (1973) show that in several locations in Canada, where rapid formation of valleys has occurred because of large deglacial-melt rivers, the horizontal strata spanning the valley have rebounded and 'flexed' sufficiently to cause slip between the bedding planes. They suggest that in places where this slip has produced weak gouge near the base of slopes, a reduction in slope stability would be expected. Because this mechanism requires specific conditions to operate (i.e. weak horizontal sedimentary strata), it is unlikely to be a common factor influencing paraglacial rock slope failures. However, the differential loading and unloading by ice and the differential unloading by erosion may generate additional (shear) stresses in all geological terrains that may have some further influence on jointing.

Static fatigue (or stress corrosion; Molnar, 2004) is the reduction in strength caused by long-term, relatively low stresses acting on a material (Brideau et al., 2009). It causes cracks to propagate in intact rock, usually in the presence of water, and unlike sheet-joint formation, it operates at stresses well below the failure strength. Slopes are constantly under gravitational stress through self-weight loading and although not yet proven, it is likely that static fatigue has played a role in many slope failures (McSaveney, 2002), especially those relatively common failures for which no other trigger is obvious (Section 2.1.2.2.3). Stress-redistribution created by glaciation and

deglacierization, which generally results in higher differential stresses as slopes are steepened and made larger, may therefore increase static fatigue and consequently reduce the strength of the slope faster. Stress-fatigue may also act faster during and after deglaciation because of melting permafrost adding additional water to rock masses.

In summary, there is little doubt that stress-redistributions from glaciation and deglacierization may be significant in causing or triggering some paraglacial rock slope failures. However, further research should aim at improving our understanding of the particular situations in which it is important and the time-scales over which sheeting joints and static-fatigue develop. This will likely require numerical modelling, lab-testing, and possibly in-situ stress measurements of slopes that have recently been deglaciated and slopes that have been deglaciated for longer amounts of time.

2.1.3.2.4 Seismicity

Earthquake shaking is a common trigger for rock slope failure. Variations in seismicity would be expected to influence paraglacial slope failure distributions in combination with other pre-conditioning and preparatory factors. There is substantial evidence suggesting that glacial cycles have an influence on seismicity and several researchers have linked a period of more active seismicity during the late-Glacial and early Holocene with an increase in landslide activity during the same period (Thorarinsson et al., 1959; Sissons and Cornish, 1982; Ballantyne, 1991; Hippolyte et al., 2006; Hormes et al., 2008; Lagerbäck and Sundh, 2008; Sanchez et al., 2009). Sanchez et al. (2009), for example, use cosmic ray exposure dating of fault-slip, glaciated surfaces and landslides in the French Southern Alps, and reveal close timing between fault activity and landsliding shortly after deglaciation in the early Holocene.

The mechanism(s) responsible for higher seismic activity during deglaciation is an area of continuing research. Factors such as rebound or decompression (elastic recovery) from flexure or compression of the lithosphere by ice masses, past glacial erosion or redistribution of sediment overburden, porewater pressure changes, sea-level changes, and release of locked-in stresses or elastically stored tectonic stresses have been discussed (Mörner, 1978; Gudmundsson, 1994; Mörner, 1995; Arvidsson, 1996; Beck et al., 1996; Firth and Stewart, 2000; Fjeldskaar et al., 2000; Muir-Wood, 2000; Stewart et al., 2000; Wu and Johnston, 2000; Zoback and Grollimund, 2001; Karrow

and White, 2002; Persaud and Pfiffner, 2004; Becker et al., 2005; Wu and Mazzotti, 2007; Lagerbäck and Sundh, 2008; Turpeinen et al., 2008; Gregersen and Voss, 2009; Bungum et al., 2010; Calais et al., 2010; Hampel et al., 2010; Wu et al., 2010). Despite some ongoing debates, it seems likely that the large-scale unloading of continental ice masses is sufficient to generate, enhance, or trigger seismicity on a regional scale. Further, because of the long response time of stress changes at crustal scales (Muir-Wood, 2000) periods of enhanced post-glacial seismicity can be expected to lag deglaciation. This lag time may explain in part the lag-time in peak post-glacial landslide activity.

2.1.3.2.5 Climatic changes

Climate drives glacial cycles and it may also directly influence slope failure. There appears to be a link between the timing of climatic events or climatic transitions and the occurrence of landslides. In Europe significant slope failures occurred when temperatures in the Western Alps were 1–2 °C higher than present-day, and the annual precipitation and density of forest cover were greater (Le Roux et al., 2009). In Poland, numerous landslides have been correlated with climatic transitions over the last 15,000 years (Alexandrowicz, 1997). Other research has indicated that spikes in landslide activity in Europe have coincided with climatic deteriorations (colder, wetter and glacier advances), throughout the Holocene (Starkel, 1997), including the Little Ice Age (Grove, 1972). Climatic factors may have individually or collectively influenced rock slope stability at time scales varying from tens of thousands of years to annual cycles. Weather-related triggers of slope failure can operate as discrete and spasmodic events, making it difficult to quantify the importance of any particular element of climate or event as being a paraglacial factor influencing slope stability. Some of the climatic factors that have been addressed in the paraglacial literature are discussed next.

Rainfall events and prolonged wet periods are a well-recognised trigger or preparatory factor of rock slope failure, usually because of increased pore-water pressures. In Wieczorek and Jäger's (1996) study of post-glacial slope failures in Yosemite, rain storms (and earthquakes) individually accounted for the greatest cumulative volumes of deposits from recognised triggers of all types of historical slope movements. Shallower landslides can be triggered by single rainfall events, but deeper-

seated (>10 m deep) landslides are more likely triggered by prolonged wet periods because of the larger amount of water required (van Asch, 1997). The susceptibility of a slope to triggering by hydrological conditions depends on the strength, the hydraulic conductivity and the flow regime within the slope. The nature (frequency, magnitude, intensity, duration) of rainfall events or wet periods is influenced by the climate, and therefore by glacial cycles. Grove (1972) related an increase in mass-movements to the Little Ice Age in Norway, as did Porter and Orombelli (1981) to intensified weather events in Italy. Dortch et al. (2009) recognised that most of the ancient large landslides of known age in Northern India occurred during periods of enhanced monsoonal activity. Such patterns of increased landsliding associated with climatic changes were identified in other regions through several periods since the Last Glacial Maximum (Brunsden and Ibsen, 1997; Starkel, 1997; Soldati et al., 2004; Le Roux et al., 2009; Borgatti and Soldati, 2010). As Thomas (2003) points out, these same patterns are observed in places unaffected by glaciation (e.g. Reneau et al., 1986; González Díez et al., 1996; Reid and Thomas, 2006). All of these suggest that, independently of other paraglacial preparatory factors, rainfall patterns can account for at least some of the slope failure patterns being observed in many localities during or following glacial retreat.

Melting of snow and ice may be another source of increased pore-water pressures in rock slopes. The transition from a landscape dominated by freezing conditions to one dominated by liquid water has been suggested as a trigger or preparatory factor for paraglacial slope failure. Whalley et al. (1983) suggested that the rapid melting of glaciers in Iceland may have raised cleft-water pressures in the surrounding rock. In temperate glaciers, which can have high water tables even during peak glaciations, deglacierization may only serve to lower slope water tables; although, increased rainfall and higher temperatures during deglaciation may lead to more rapid snow-thaw during melt-seasons and produce anomalously large peaks in the pore-water pressure regimes at those times. Rises in pore-water pressure caused by seasonal snow melt are known to drive slope deformations in the modern alpine environments (Le Roux et al., 2009; Hansmann et al., 2010). However, in a study of deformation of the Randa alpine rock slope by Gischig et al. (2010), deformation was shown to be unaffected by snow-melt and instead most deformation occurred during cold periods. Thermal stress changes or water freezing in joints were thought to drive deformation, rather than pore-

water pressures; in the fractured, permeable slopes pore-water pressures were not high enough to initiate movement. These studies serve to highlight that slopes in similar environments behave differently and careful monitoring is required to understand the mechanisms involved.

Excess joint/cleft-water pressures are a potential trigger for rock slope failure. The water present in a rock joint exerts a hydrostatic pressure (if not flowing) and seepage pressure (if flowing) on the walls of the joint and an 'excess' pressure when the water pressure in the joint is greater than the water pressure in the surrounding (low-permeability) rock mass. The excess pressure acts to dilate the joint and reduce the normal stresses acting across the joint surface, which could be sufficient to trigger failure. Excess joint-water pressures may develop where water inflow, rapid draw-down, seismic loading or deformations in the slope raise joint-water pressures faster than they can dissipate. One reason for pressures not dissipating fast enough is if the joint terminations at slope surfaces experience freezing conditions. Water at the joint openings may freeze, inhibiting drainage and hence raising the water pressure. Excess water pressure in joints has been well recognised as a failure trigger in rock slopes (Terzaghi, 1962) and has been suggested to be a cause of many post-glacial slope failures especially where no other triggering mechanism is evident (Whalley et al., 1983; McSaveney, 2002). The combination of increasingly wet ground conditions, permafrost degradation, the development of fracture networks through enhanced mechanical weathering and earthquake shaking, together with the possibility of freezing conditions in alpine areas during deglaciation, certainly seems to support a view that excess joint water pressures may have a role in paraglacial slope failures.

Degradation of permafrost has also been considered to influence paraglacial slope failure. The pore- and cleft-water in much high-altitude alpine rock remains permanently frozen as permafrost. The bonding action of the ice creates a more intact, stronger rock mass while the ice remains sufficiently cold (Davies et al., 2001). During deglaciation the permafrost level rises, reducing the rock mass strength below this level. This may arise from reduced shear strength or from excess porewater pressures where joints are not free-draining (Matsuoka and Sakai, 1999; Davies et al., 2001; Gruber and Haeberli, 2007). Permafrost degradation has been suggested as a cause of many rock falls and large-scale slope failure (e.g. Dramis et al., 1995; Gruber et al., 2004; Fischer et al., 2006; Hormes et al., 2008; Ravanel and Deline, 2011). Permafrost

degradation may not follow a similar pattern in all parts of a mountain range. Despite cold temperatures during glaciations, temperate glacier cover may prevent freezing by holding the water at the pressure melting point (Wegmann et al., 1998). Subsequent retreat of the glacier exposes the rock to cold atmospheric temperatures, which may result in freezing conditions penetrating the rock mass. There may then be an initial increase in the rock mass strength as permafrost develops (accompanied by freezing-induced joint opening) and a lag-time before atmospheric conditions warm up enough to begin degrading the permafrost (Wegmann et al., 1998). This is a possible explanation for the lag in peak landslide activity following deglaciation.

Freeze–thaw weathering, also known as frost shattering and frost or ice wedging, is the repeated freezing and melting of interstitial water present in rock masses and is another factor considered to influence rock slope stability (Matsuoka and Murton, 2008). This mechanism has been treated separately from permafrost degradation because it is the repeated freezing and melting of interstitial water, a process which by definition does not occur in permafrost but is likely to develop in the same sites following permafrost degradation. It is thought that five different physical processes are involved in freeze– thaw weathering, all of which alter the conditions of fractures: loss of bonding; ice segregation; volume expansion; hydrostatic pressure or cleft-water pressures; and reduction of shear strength (Gruber and Haeberli, 2007). Freeze-thaw weathering has been monitored in the field (Matsuoka, 2001) and is known to cause rock fall (Matsuoka and Sakai, 1999; Noetzli et al., 2003; Gruber et al., 2004; Matsuoka, 2008; Ravanel et al., 2010). Many researchers considered such processes important in increased talus development during deglaciation (e.g. Rapp, 1960), who was perhaps the first to link the process with rock-fall activity at glacier margins). There is also evidence to suggest that freeze–thaw weathering may play a role in large-scale rock slope failures (Wegmann and Gudmundsson, 1999; Davies et al., 2001). Freeze–thaw weathering operates most effectively when there are regular fluctuations in temperature around the freezing point of water. That these conditions are likely to be more common some time after deglaciation once day-time air temperatures have risen sufficiently may be another explanation for the delay in peak landslide activity. Freeze–thaw weathering is likely to extend and weaken the joints in pre-existing joint networks developed by other processes, such as tectonic stress and stress-release mechanisms.

Chemical weathering of rock mass joints will in most situations reduce the rock mass strength and therefore could contribute to the development of large rock slope failures (e.g. La Clapière landslide, France; Chemenda et al., 2009). The rate of chemical weathering is controlled mostly by the availability of water (Hall et al., 2002; Nicholson, 2009; Orwin et al., 2010). Because deglaciation is likely to increase the amount of surface water and water in rock masses, as well as expose more rock to the elements, chemical weathering rates may be expected to be more important during interglacials than during glacials.

2.1.3.3 Discussion

As Varnes (1978 pg. 26) states, "seldom, if ever, can a landslide be attributed to a single definite cause"; a host of preconditioning and preparatory factors may have developed to bring the slope to a point of critical stability. The final trigger, which sets the landslide in motion, cannot be regarded as the only cause, even though it was necessary in the chain of events. Those rock slope failures that sometimes occur long after deglaciation can be caused by a range of factors, some of glacial origin, others related to climate, weathering or tectonics (Wilson and Smith, 2006). To complicate matters such factors may be interdependent. A paraglacial slope failure may have been triggered by an earthquake but this could have arisen from a glacio-isostatic adjustment. A slope failure in a valley that has never been occupied by ice may have occurred in a wet period associated with a glacial climate transition. Glaciation and deglaciation have a wider context than simply the presence and absence of glaciers, because they extend to other processes influenced by glacial cycles. Conversely, glacial valleys can clearly have slope failures in which ice has had no direct role. The term 'paraglacial' must be used carefully because in some cases it may be misleading.

The reality is that slopes adjust to a stable form through a number of processes, and likewise are put out of equilibrium by many factors. In steep mountainous terrain, slope failure usually plays a dominant role in the erosion of the landscape with or without glaciations. Identifying any one factor or combination of factors responsible for a paraglacial slope failure is very difficult and care is required when attempting to link failure to paraglacial processes. The 1967 Steinsholt landslide described by Kjartansson (1967) illustrates this well. A deep-seated failure occurred on a slope steepened by glacier action and affected by glacier thinning. However, 7–8 years of

observable deformation preceded a catastrophic failure that was triggered by very rapid thawing of snow and heavy rainfall.

2.1.4 Research applications

2.1.4.1 Slope evolution models

Whalley et al. (1983) analysed the timing of a dataset of rock slides in Iceland, originally described by Jonsson (1976), and considered multiple paraglacial explanations for them. They realised that it is useful to generalise failure patterns in the form of models: "In general, geomorphologists are not yet in a position to say very much about precise causes for any scale of cliff mass failure. Not only are the mechanisms complex and difficult to evaluate but site investigation is obviously restricted in both space and time. We are thus forced back onto a more probabilistic type of analysis linked in with possible mechanical models." In their models they recognise the importance of slope conditions that evolve through time. Over the succeeding three decades further attempts were made to statistically model paraglacial slope evolution and distribution, using data from Canada. Initially, steady-state models were used (Evans and Gardiner, 1989). These assume that the probability of an event does not change through time and the interval between events is estimated by the number of events during a period of time. It was recognised, however, that most of the rock slides modelled occurred on over-dip slopes created by glacial erosion, and that the dip slopes remaining after failure were stable, so that the number of potential landslide sites diminished with time. An exhaustion model was developed to provide a declining probability of failure as failure sites were used up (Cruden and Hu, 1993; Cruden, 1997). The model did not address other factors controlling stability and was not generalised for other slope types. Dadson and Church (2005) developed a more complex model of slope evolution that considered both deep-seated and shallow landslides. They used a numerical model of an idealised recently-deglaciated valley to describe the development of slope failures and the relaxation of the slope through time. In the model deep-seated landsliding was spatially random whereas shallow landslide activity was controlled by slope angle. Their results showed that steep upper slopes decayed rapidly and that the bulk of adjustment took place over a few thousand years.

Factors such as heightened storminess increased the short-term rate of activity but did not produce an increase in the long-term rate.

To gain the maximum potential benefit from such slope evolution models, extra complexity is required to account for the non-random distribution of rock slope failures that is recognised in the landslide distributions. Dadson and Church's (2005) model, for example, could be extended by making deep-seated landsliding sensitive to external factors such as heightened seismicity, climate changes, as well as internal factors such as rock type and time-dependent variables such as rock mass degradation. Only then may they begin to describe and perhaps predict a more realistic slope evolution. These models are needed for successful management of paraglacial landslide hazard, since the hazard varies non-linearly with time. Such models may feed into decision-making flowcharts, such as that developed by Holm et al. (2004), which aids identification of landslide hazards associated with glacial retreat. Further development of slope evolution models coupled with hazard management tools within paraglacial frameworks seems a worthwhile investment, and should be an ultimate goal for paraglacial research.

2.1.4.2 Landslides as a paleoclimatic proxy

The inextricable link between landslides and climate has often been considered to lend itself to the use of landslides as a proxy for past climates, despite some issues and caveats (Berrisford and Matthews, 1997; Brunsden and Ibsen, 1997; Crozier, 1997; van Asch, 1997; Crozier, 2010). Crozier (2010) suggested that to achieve this, it is necessary to have unequivocal evidence of the timing and causes of extensive landslide activity. The non-climatic processes influencing paraglacial slope response that have been highlighted in this chapter, will make using landslide distributions as a proxy for climate particularly difficult in glaciated regions. However, paraglacial studies have the potential to make this possible through the growing number of landslide inventories with accurate event ages, and by further clarifying the links between slope failures and other non-climatic processes, such as post-glacial seismicity and the development of sheeting joints. Only when the influence of non-climatic processes can be accounted for and removed from the trends will landslide distributions provide a reliable proxy for climate.

2.1.5 Conclusions and recommendations

There is compelling empirical evidence that glaciation and associated climatic change influence patterns of rock slope stability. Both spatial and temporal patterns in the distributions of post-glacial landslides suggest a temporary increase in slope instability following deglaciation — a finding that has been attributed to several processes but in reality is difficult to explain by simple and direct observation. Many mechanisms driving post-glacial slope failures make linking of cause and effect a challenge. Efforts to classify the factors influencing paraglacial slope stability into those that either precondition the slope or act as preparatory factors or triggers help to focus and rank the problem and guide modelling. The overall controls on paraglacial rock slope stability are the geological preconditioning factors, which operate mostly independently of glacial processes. Glacial erosion and associated stress-redistributions provide a secondary control on the spatial and temporal distributions of rock slope failures. Erosion and stress-redistributions are widespread in the landscape, but unique to glaciers is the way their dominance ceases abruptly during rapid deglaciation. A key challenge is to explain why there is often a significant lag-time between glacier retreat and peak landslide activity. Three possible reasons arise from the literature reviewed here. First, that there is a lag-time between local slope stress-redistribution and the development of sheeting joints. Continued development of numerical modelling along with in-situ rock stress-measurements and monitoring of deglaciated valley slopes seems critical in this area of research. This should focus on assessing the time-scale of stress-redistribution and development of rock mass degradation in different rock masses.

The second reason is a lag between regional glacio-isostatic rebound and a period of enhanced seismicity. This link seems largely accepted in the literature despite debate about the mechanism(s) producing enhanced seismicity. More research could focus on the magnitude of the increase and whether it is significant for landsliding; coseismic landslides are generally triggered by earthquakes greater than M_w =6 (Keefer, 1984; Malamud et al., 2004), and more studies like that of Sanchez et al. (2009) are needed in other regions to confirm the link with landslide distributions. Most studies of glacio-isostatic rebound and seismicity have been on large continents affected by ice sheets and with low levels of tectonic seismicity; it would be interesting to test whether a glacio-isostatic signal in seismicity and large landslide patterns can be detected in

tectonically active locations such as New Zealand which have experienced smaller mountain glaciations without the development of ice sheets. Another avenue of research could be on how seismic shaking of glaciated slopes is suppressed or enhanced by ice cover, and how glacial erosion may change seismic resonance of slopes; these factors will influence the shaking intensity and therefore the likelihood of coseismic triggering of landslides.

The third reason for a lag-time may be that those climatic factors such as warmer temperatures and increased rainfall were more significant in the late-Glacial and early Holocene. As discussed earlier in the chapter, there is a need for more statistically robust landslide distribution and climate data to confirm these links.

An understanding of the cause of paraglacial slope failure, and therefore effective management of hazard, is inhibited by the complexity of the processes involved in paraglacial rock slope failure. Numerical slope stability modelling offers a relatively cheap tool to help simulate paraglacial processes and perhaps cut through some of the complexity. For example, testing whether or not glacial debuttressing plays an important role in destabilising slopes may best be achieved with the development of, or application of existing, analytical or numerical models. Those models must use realistic (visco-elastic) constitutive models and glacier fluid pressures to accurately model buttressing processes; ice is a ductile material that flows under low applied stresses and the forces ice exerts on slopes depend on the basal water pressures of the glacier. The numerical models should be supported by field evidence of contemporary collapse of slopes into glacier ice masses. Whether deformation can be initiated during glaciation because of toe erosion, or can be initiated only when glaciers have retreated (de-buttressed) sufficiently is an important question. If glaciers do not completely 'buttress' slopes then it is possible that slope failure may be initiated prior to ice retreat; then debuttressing may only change the rate of landslide movement. This would have implications for glacier erosion processes as well as for slope evolution. In any case, it seems that the mechanism of debuttressing has likely been overstated in literature and surprisingly few examples have been reported where failure appears to have corresponded closely in time with historical ice retreat (e.g. Reitner et al., 1993). In many instances where debuttressing has been invoked to explain failure, it is likely that other preparatory factors that operate within the rock and on its surfaces while the glacier is present and afterwards may have been more critical.

As detailed investigations continue to improve our understanding of failure mechanisms, better inferences about the relative importance of the many factors influencing paraglacial slope failure and slope evolution can be drawn. A key target must be to develop sufficiently robust means to transfer this knowledge to hazard managers and enable them to make better-informed predictions and decisions about how to manage slope-failure hazards in a changing environment. This will be aided by the improvement of slope- and landscape-evolution models that can help predict the destabilisation of slopes in scenarios of anticipated climatic changes or continued deglacierization. To date, simple models of some processes have been developed but higher-complexity models are needed that can help evaluate the role of multiple processes and provide more generally applicable results. Such models are not out of reach in geomorphology; generalised models have now become commonplace in such areas as lake and catchment research where they have had the effect of triggering new understanding, new lines of research and new water management tools (Caminiti, 2004).

Improving landslide inventories, especially for failure patterns across a wide range of glaciated landscapes, and gaining a better understanding of benchmark rates of failure in non-glaciated landscapes would also help to clarify the contribution of paraglacial slope failure in landscape evolution. Many long-term estimates of alpine erosion rates suggest that glaciers are more effective agents of erosion than rivers (MacGregor et al., 2000; Montgomery, 2002; Brook et al., 2006) and considering that landslides are the dominant source of primary erosion and sediment generation in the modern alpine environment (Hovius et al., 1997), it would be surprising if this could remain true in the absence of significant landslide activity during glaciation. After all, those preconditioning factors that provide the overall control on slope instability are largely the same before and after deglaciation. Therefore, the apparent increase in landslide activity may in fact be the result of increased preservation of landslide features in a deglaciated landscape, and the gradual decrease in landslide activity that follows may occur simply because slopes no longer have a glacier undercutting them and because failure sites become exhausted. However, as records grow and absolute dating techniques are applied more widely, there is an opportunity to develop statistically robust regional or even global landslide databases, which may confirm that deglaciation initiates an anomalously large and widespread amount of rock slope

destabilisation, a conclusion which would have implications for landslide hazard management, understanding of long-term erosion rates, sediment budgets and landscape evolution. The research focus could then shift to quantifying the duration of paraglacial processes and exploring what other processes lead to the gradual stabilisation of slopes. For example, post-glacial sedimentation in valleys may eventually bury and stabilise slopes; Kellerer-Pirklbauer et al. (2010) consider such a scenario for the stabilisation of a deep-seated gravitational slope failure in Austria.

This review highlights some problems with how the term 'paraglacial' is defined. If using Ballantyne's (2002) definition (Section 2.1.1.1), a slope failure that occurs during deglaciation as a direct result of glacial erosion would be considered a paraglacial failure, whereas it is not according to Slaymaker (2009) who suggests that 'paraglacial' should refer to events occurring in the transition between glaciation and deglaciation regardless of whether they were a direct result of deglaciation. Alternatively, if permafrost degradation triggers a failure of a slope elevated above the influence of ice, it would be a paraglacial failure under Slaymaker's definition but may not be under Ballantyne's. The present review has attempted to carefully separate the various processes directly attributable to glaciers and those that are not, but it has also revealed many grey areas where the processes overlap or are inseparable with the methods currently available. For practical purposes, use of the term 'paraglacial' to describe a slope failure may require a certain amount of personal judgement of the relative importance of the various factors influencing stability. If, 10,000 years after glacier retreat a glaciated slope fails as a direct result of human slope modification or undercutting by a river, it should not be considered paraglacial in origin; but if it failed on what are unequivocally sheeting joints caused by glacial slope modification, or is a reactivation of earlier slope deformation likely to have been initiated by glacial debuttressing, then the use of the term paraglacial may be more appropriate. Perhaps the point is that we cannot yet precisely define the boundary of the glacial to non-glacial transition. As more detail is gained on the underlying mechanisms of paraglacial failure processes we will be able to transfer more meaning to the words we use.

Acknowledgements: Prof. Timothy Davies and Dr. Mauri McSaveney have been instrumental in alerting me to the problems and inconsistencies in the literature on

paraglacial slope stability, and motivated the writing of this review. I thank Dr. Rob McColl for his perceptive analyses, suggestions and edits which vastly improved the manuscript. Prof. Davies and David Alexander also revised and commented on the manuscript and I am grateful to the reviewers and Editor Prof. Takashi Oguchi for their suggestions and edits.

2.2 PART B: GLACIAL BUTTRESSING – A CRITICAL REVIEW

McColl, S.T., Davies, T.R.H., McSaveney, M.J., 2010. Glacier retreat and rock-slope stability: debunking debuttressing. Geologically active: delegate papers 11th Congress of the International Association for Engineering Geology and the Environment, Auckland, Aotearoa, 5-10 September 2010. Auckland, New Zealand. pp. 467-474

Only formatting and pagination has been modified for production in the thesis

Abstract: Deglaciation is often assumed to be the cause of post-glacial alpine slope failures but the mechanisms behind these failures have received little critical examination. This chapter considers the mechanical properties and behaviour of glacier ice and its interaction with rock slopes. Debuttressing of valley slopes as glaciers retreat is rejected as a significant mechanism causing rock slope instability, on the grounds that: ductile glacier ice allows rock deformation; temperate glaciers do not provide significant slope support due to buoyancy; stress-release joints result from erosion of rock and not glacier unloading; slopes dewater as glaciers withdraw. Other reasons for post-glacial landsliding and sediment generation are outlined. We conclude that in the context of paraglacial slope stability, glaciers have left their mark long before they have retreated.

2.2.1 Paraglacial rock slope failure

The continuing impacts of glaciation, long after massive glaciers have all but completely melted, are the basis of paraglacial geomorphology (Ryder, 1971; Church and Ryder, 1972; Ballantyne, 2002) and some are an important focus for landslide hazard research. There are many reports linking alpine slope failure activity to deglaciation (e.g. Beget, 1985; Haeberli et al., 1997; Smith, 2001; Holm et al., 2004; Geertsema et al., 2006; Lipovsky et al., 2008b; Agliardi et al., 2009a; Allen and Cox, *in review*).

Rock-slope stability and long-term slope angles are controlled primarily by the rock-mass properties but erosion can reduce stability, such as when glaciers carve out deep and steep-sided U-shaped valleys. It is thought by some that during glaciation slopes do not adjust to oversteepening because of the buttressing support of glacier-ice

and that slope adjustments (or failure) occur only after the glacier has retreated and de-buttressed the slope (Ballantyne, 2002). The glacial-debuttressing mechanism has had little substantive justification. In this chapter we examine the interactions between glacier ice and rock slopes during both glaciation and deglaciation to re-evaluate the role of debuttressing, and then turn to other factors influencing post-glacial slope stability. We also discuss whether the post-glacial increase in slope failure frequency and magnitude is real or apparent. First though, it is useful to consider how a buttress works.

2.2.2 Slope buttress and debuttressing

In rock slope engineering toe-of-slope buttresses are used to provide external support to a slope by adding a vertical load surcharge to the toe (A in Figure 2.2.1) and by providing additional sliding (shear) resistance (B in Figure 2.2.1). The former is a function of the weight of the buttress and works by counterbalancing the driving load at the head of the slope. The shear resistance generated along the base of the buttress, which is a function of the buttress weight and the base roughness and slope-angle (Wyllie and Mah, 2004), increases the (shear) strength of the slope. Engineering-buttresses are used only if there is ample room for the large volume of material required, usually waste rock, and the material needs to be free-draining to prevent build-up of water behind the buttress, which may otherwise reduce the stability of the slope.

Removing an engineering-buttress on a critically stable slope is likely to cause failure. Similarly this concept has been applied to glaciated valleys – the glacierised valleys are assumed to have critically stable slopes that are being supported by the glacier-buttress. The following discussions explain why the glacier-buttress may not work.

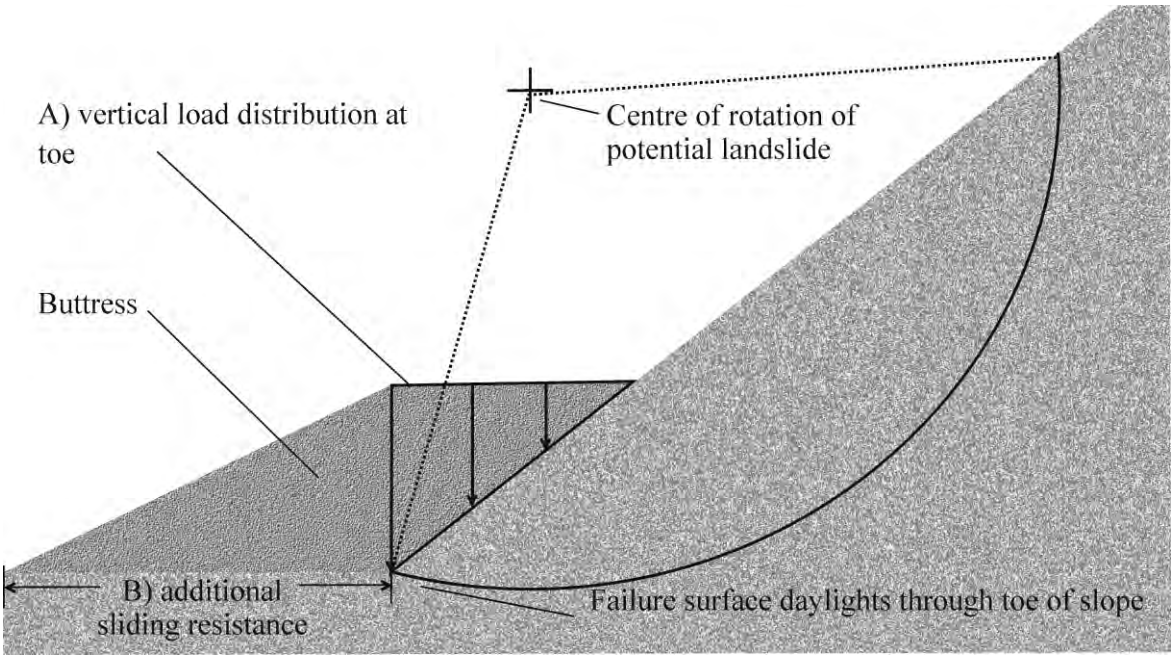

Figure 2.2.1. Rock slope with potential slope failure being buttressed. A toe-of-slope buttress provides external support to a slope by adding a vertical load surcharge to the toe (A) and by providing additional sliding (shear) resistance (B). The buttress counterbalances the forces driving landslide displacement.

2.2.3 Ice and rock slope interactions

The effectiveness of a glacier-buttress at influencing rock slope stability depends on the mechanical properties of the rock mass and ice, and their interactions. These factors are considered in the following discussions.

2.2.3.1 Ice mechanics

Glacier ice is a crystalline material that exhibits a range of mechanical behaviours, from brittle to ductile; these are affected by grain size, temperature, confinement, stress regime and strain rate (Glen, 1955). Ice flows under low strain rates, which implies that ice may not be capable of supporting unstable rock slopes over timescales that allow ice to flow. The ductile or brittle behaviour of ice is strongly related to the rate of strain (Schulson, 1990). Under strain rates less than 10^{-3} to 10^{-4} s^{-1}, at temperatures of -10°C, ice will undergo ductile creep (or flow). Strength (or the yield stress) of the ice is independent of grain size, but increases with decreasing temperature. Under these conditions, microstructural cracks which develop during deformation due to internal stresses are able to relax through creep deformation (Schulson, 1999).

In contrast, strain rates above 10^{-3} to 10^{-4} s^{-1} produce brittle failures. In this regime, strength increases with decreasing grain size and decreasing temperature. Unlike in ductile deformation, internal stresses building at the tips of microstructural cracks have insufficient time to relax, so they coalesce and propagate, leading to brittle failure.

The brittle strength of ice limits high strain rates within an adjacent rock mass, reducing the possibility of rapid, catastrophic failure. However, slow-moving slope deformation or gravitational-creep may be possible at strain rates below the brittle-ductile transition of the ice, if the stresses exerted by the deforming slopes are above those required for ice flow. Glen's law of ice flow (1955) states that ice will flow under very low applied stresses. Consequently, the stresses exerted by a slow creeping rockslide are likely to induce ice-flow. The velocity of the deforming slope will be limited by the maximum strain rates of ductile ice behaviour (10^{-3} to 10^{-4} s^{-1}) but over thousands of years of glacier occupation the magnitude of displacement may be quite significant. Creep failure is a common feature of steep mountain slopes and many creep features (or *sackungen*) have been identified in deglaciated valleys (Bovis, 1982; Bovis and Stewart, 1998; Holm et al., 2004; Agliardi et al., 2009a; Hippolyte et al., 2009; Pánek et al., 2009). There is little evidence for slope deformation during glacier occupation, as rates of slope deformation at the ice-rock interface are extremely difficult to measure. However, many post-glacial catastrophic failures are preceded by slope deformation (Holm et al., 2004) and it is possible that some of this deformation (and indeed the development of the failure surface) took place during glacial occupancy.

2.2.3.2 Glacier buoyancy

Temperate glaciers, like those found in New Zealand and many other mid-latitude localities, contain significant volumes of liquid water and this reduces the effective glacier load. The englacial and sub-glacial hydrology is spatially and temporarily highly variable and at times the sub-glacial water pressures can exceed that of the ice overburden pressure (Fountain & Walder, 1998), which means the ice is floating. Even during peak glaciation with cooler climate, temperate glaciers still contain abundant liquid water. Evidence for this is the ubiquity of Last Glacial moraines in New Zealand typically composed of mostly outwash material as opposed to classic glacial tills which would form in a relatively dryer depositional environment (Shulmeister et al., 2009).

Most of the time glacierised slopes are being only partially buttressed by the glacier and at times not at all (Figure 2.2.2). Load from the liquid water can be ignored because the rock slope is permeable to liquid water (but not ice). Water pressures either side of the rock/ice interface equilibrate over the time scales relevant to deglaciation (100s to 1000s of years). The retreat of glaciers does not necessarily cause a significant or unusual unloading of the slope, but only one that is less transient.

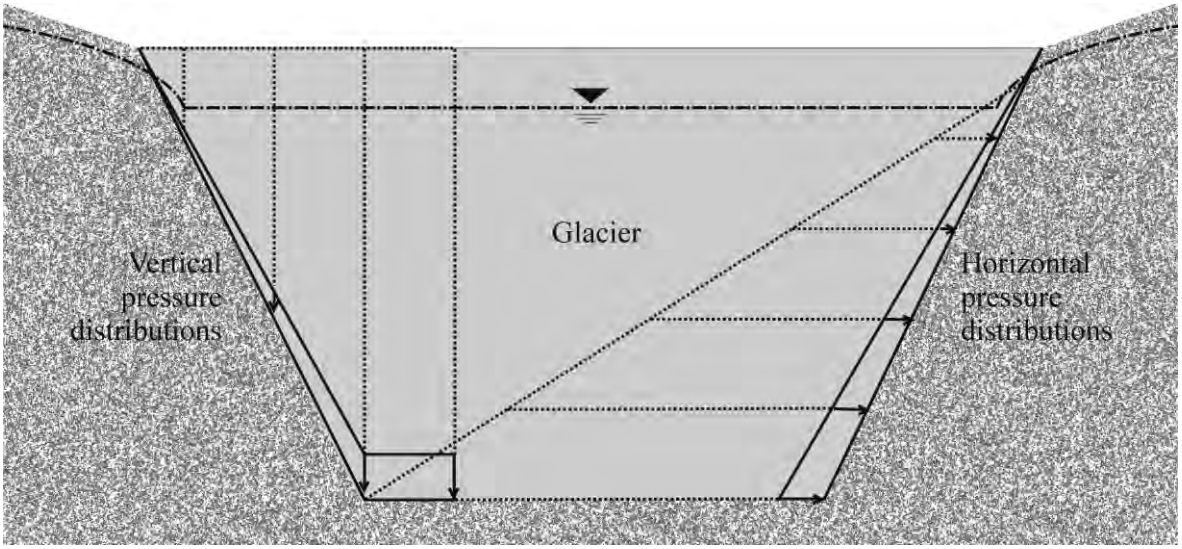

Figure 2.2.2. Glacier load pressure distributions on the floor and slopes of a valley, with a high water table (shown as solid-line pressure distribution), and with no liquid water (dotted-lines). With the high-water table the glacier provides very little slope support and is close to floating.

2.2.3.3 Stress-release

Stress-release joints (or exfoliation or sheeting joints) developed in glaciated valley walls are often considered to result from the unloading of glacier ice (Ballantyne, 2002). Stress-release joints weaken the rock mass and also form failure surfaces for mass movements. We do not support an ice-unloading origin for stress-release joints for reasons given in the preceding section, but instead favour an alternative view that they form from erosion (Balk, 1939; Jahns, 1943; Lewis, 1954; Bradley, 1963; Wyrwoll, 1977; Lo, 1978). The fact that stress-release joints are also found in fluvial valleys (Matthes, 1936) adds significant support to this hypothesis.

Glacier load stresses are negligible when compared to the internal stresses present within rock masses and the unloading caused by erosion. With the possible exception of a glacial valley where the bedrock is composed of young (e.g. volcanic) material, the bedrock has high internal over-consolidation stresses (Bain, 1931; Farmin, 1937; Lo, 1978). Erosion causes the over-consolidated elastic rock mass to dilate and develop

stress-release joints, often parallel to the erosion surface (Jahns, 1943; Bradley, 1963; Lo, 1978).

The relative effects of ice versus erosion unloading can be considered conceptually: the total normal stress at the base of a slope caused by dry glacier ice with a density of 0.9 t m^{-3} and ice thickness of 1 kilometre is approximately 9 MPa; but the *effective* normal stress would be drastically less when water tables are high. The unloading from erosion as the 1 km deep valley was carved out over millions of years equates to approximately 27 MPa (assuming a rock density of 2.7 t m^{-3}). Additionally, the regional erosion during each glacial cycle needs to be accounted for. It is estimated that in the New Zealand Southern Alps the long term erosion rate, matched by uplift, is approximately 10 mm per year (Adams, 1980; Hales and Roering, 2005). Extrapolating this value over a 50,000 year glaciation gives an additional unloading, through regionally averaged erosion, of 13.5 MPa. Total normal stresses reduced by the removal of hundreds of metres of rock over several glacial cycles is therefore greater than the stresses exerted by temperate glacier ice.

Removal of large masses of glacier ice and liquid water during regional deglaciation can de-stress the crust to cause an isostatic rebound of the crust on a regional scale. This is different to the stress-release joints causing local slope failures because the crust is responding to regional rather than local stresses.

2.2.3.4 Slope porewater pressure

It is important to consider the role of groundwater in both glaciated and deglacierized slopes. Phreatic surfaces in the glacier control the phreatic surfaces in the adjacent slopes and this means that changes to the glacier hydrology must affect slope stability. The upper, mid and lower parts of the slope are affected differently. During full glacial conditions, the phreatic surface in the upper slope is higher than what it would be in the absence of the glacier (Figure 2.2.3). This reduces effective normal stresses and makes the upper slope more unstable and susceptible to changes in porewater pressures due to meteoric fluctuations. The mid and lower slopes may be affected by rapid drawdown during glaciation because of steep hydraulic gradients created by fluctuating water tables in the glacier which has a higher hydraulic conductivity than the rock. Glaciers have high hydraulic conductivity because ice is impermeable yet there are many open fractures and conduit networks within the ice mass. Rapid drawdown could potentially trigger slope deformation. The lower slope is

probably less affected by rapid drawdown because the temperate glacier is probably rarely dry and water pressures either side of the ice-rock interface will be more balanced. As glaciers retreat, the slopes will gradually dewater, stabilising the upper slope but potentially shifting the failure zone lower down the slope – Bovis and Stewart (1998) demonstrate that groundwater fluctuations during deglaciation were the dominant factor generating slope displacements in a marginally stable alpine landslide.

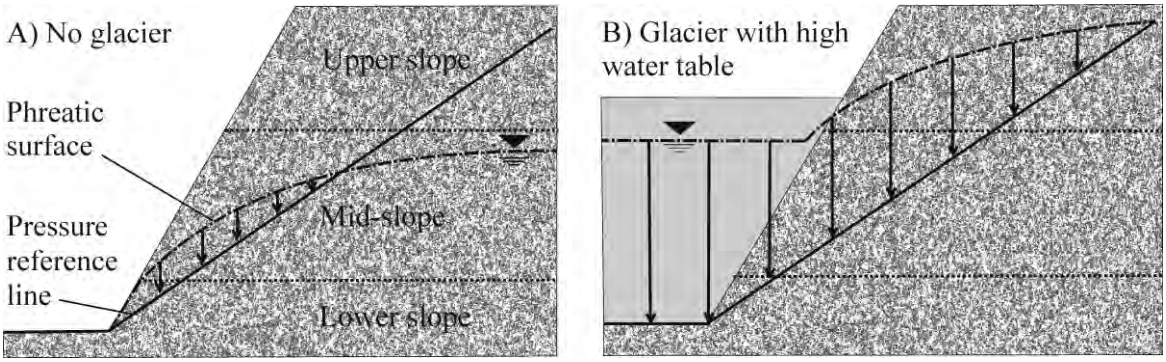

Figure 2.2.3. Glaciers influence the groundwater conditions in adjacent slopes as shown by the water pressure distributions along the same reference line in A and B. The high water table increases the slope's porewater pressure distribution and hydraulic gradient. Parts of the slope (separated by the dotted lines in both A and B) are affected differently.

2.2.3.5 Deamplification of seismic waves

Glacier ice may affect the seismic response of valley slopes. Topographic amplification is the enhancement of seismic shaking through topography. Seismic shaking is enhanced at ridge crests and its amplitude is controlled primarily by the height and shape of the ridge (Buech, 2008). Under the applied strain rates common during seismic shaking, valley ice will act as a rigid material because there is insufficient time for ice-flow to occur. It is therefore likely that the presence of glacier-ice reduces the effective topography, correspondingly reducing the topographic amplification effect on high valley slopes. If, during glacier occupation, the topographic amplification effect is significantly reduced, then coseismic shaking will cause fewer slope failures. The slopes will become steeper and higher from glacial erosion as they adjust to less intense seismic shaking. Once glaciers have withdrawn, subsequent earthquakes can be expected to be more damaging. This, together with the likely increase in seismicity accompanying deglaciation as large-scale crustal stresses develop from ice-unloading and sea-level rise (e.g. Stewart et al., 2000; Zoback and

Grollimund, 2001), may be a factor in any postglacial increase in large-scale mass movements.

2.2.4 Climate drivers of post-glacial rock slope activity

Climatic changes and events occurring during deglaciation may explain much of the observed post-glacial landslide activity. Enhanced periglacial activity (freeze-thaw) and degradation of permafrost (melting of ice-filled joints) are commonly suggested to explain increased post-glacial landsliding, rockfall and sediment generation.

Freeze-thaw cycles of water in pre-existing rock joints are considered a significant agent of mechanical weathering capable of causing landslides (Matsuoka, 2008; Matsuoka and Murton, 2008). Melting of ice-filled joints with rising temperatures is thought to weaken rock masses by rapidly reducing shear strength and/or increasing porewater pressures (Matsuoka and Sakai, 1999; Davies et al., 2001; Fischer et al., 2006; Gruber and Haeberli, 2007). In some cases the landslides triggered by these processes can be large and catastrophic (e.g. Dramis et al., 1995; Deline, 2009).

Two reasons for enhanced periglacial activity during deglaciation are: a greater fluctuation of regional temperatures above and below freezing, and; an expansion of the periglacial activity zone as glaciers withdraw - glacier ice maintains the underlying rock at a more stable temperature, either below freezing or above freezing where pressure melting occurs (Fischer et al., 2006).

Increased precipitation snow melt are likely to also influence post-glacial landslide activity. The development of more abundant liquid water during early deglaciation may reduce slope stability before the glaciers withdraw completely and dewater the slopes (Whalley, 1983). The landslide record in Iceland and elsewhere (e.g. Cruden and Hu, 1993), shows a postglacial peak in landslide activity that decreases with time, which fits this hypothesis. Specific weather or climatic events may also explain slope-failure activity, for example Grove (1972) relates an increase in mass-movements during the Little Ice Age in Norway to intensified weather events which also caused considerable flood damage. Similar patterns of increased landsliding associated with climatic changes are identified in other regions through several periods since the Last Glacial Maximum (Soldati et al., 2004; Le Roux et al., 2009). Thomas (2003) points out that these same patterns are observed even in places that have not been affected by glaciation (e.g. Reneau et al., 1986; González Díez et al., 1996).

2.2.5 Do we really see enhanced post-glacial landslide activity?

The interpretation of an observed increase in post-glacial landslide activity or sedimentation requires caution. It is impossible to accurately compare the rates of landslide activity observed today to what was occurring during glaciation. Landslide distributions and the types of landslides may be very different and many more landslide deposits formed during glaciation will have been poorly preserved and are missing from the records compared to the few we have identified in deglaciated terrain. Intense rates of post-glacial sedimentation occur in the absence of any increase in primary erosion because of reworking of glacial sediment and high deposition rates in the deep valleys that glaciers leave in their wake (e.g. Curry et al., 2006). Furthermore, long-term estimates of alpine erosion rates suggest that glaciers are more effective agents of erosion than rivers (MacGregor et al., 2000; Montgomery, 2002; Brook et al., 2006). It would be unlikely for this to be true in the absence of significant landslide activity during glaciation considering mass-wasting is the most important form of erosion in many mountains (Korup, 2005).

2.2.6 Conclusions

Ice does not make a good engineering-buttress and likewise a temperate glacier does not make a good natural slope buttress. Glacial debuttressing is probably not as important as fluctuating groundwater, climatic changes and post-glacial seismicity. This hypothesis is supported by examination of the interactions between ice and rock slopes in a deglaciation context. Interpreting the cause of post-glacial slope failures and sedimentation needs care and should be done with the slope history in mind, as well as the multitude of factors influencing stability. The transition from a U-shape glacial valley to a V-shape fluvial valley may reflect a change in sediment transport and storage and the end of intense oversteepening, but not necessarily an increase in mass-wasting. In the context of post-glacial slope stability, glaciers have left their mark on the landscape before they have retreated. We are in the process of validating and quantifying some of the ideas presented above using a combination of physical and numerical modelling of slope stability and ice-rock slope interactions.

CHAPTER 3: THE NZ SOUTHERN ALPS

The New Zealand landscape is ideally suited for studying the influence of deglaciation on slope stability; it has high-relief mountainous topography of variable lithology, strong precipitation gradients, past and present glaciation, and extremely high erosion and uplift rates. Actively retreating and accessible glaciers make it an ideal place to study the short-term, immediate effects of deglaciation but the preservation of Quaternary and Holocene sediments and other glacial landforms also make it suitable for studying longer timescales. Specific reference to New Zealand and case-studies are given throughout the thesis; therefore, the geologic, geomorphic, and glacial setting of the Southern Alps and surrounds, as well as a brief review of paraglacial work in New Zealand follow.

3.1 GEOLOGICAL SETTING

New Zealand is situated along the boundary of two obliquely converging tectonic plates; the Pacific and the Australian (Figure 3.1). Active dextral transpressional movement along this major boundary leads to crustal shortening and uplift of the Southern Alps orogen. Inferred inter-plate velocities are c. 37 mm per year during the last 3 Ma; about two-thirds of this is accommodated by movement along the 800 km Alpine Fault (Norris and Cooper, 2001). The central Southern Alps are comprised of well-indurated greywacke and argillite of Torlesse composite derived from sediments eroded from the ancient Gondwana continent. These rocks progressively give place to schist of increasing metamorphic grade towards the west, where the schists are being exhumed in the hangingwall of the Alpine Fault. Schist is also more common in the south of the alps, in the Otago region, where the bedrock is low to high grade schists of Rakaia and Caples terrane. The rocks of the central Southern Alps formed during the Triassic, metamorphosed and tectonically deformed during the Cretaceous, and uplifted during the ongoing Kaikoura Orogeny (Cox and Barrell, 2007). Further south, in the Fiordland area, the bedrock of the alps are older granites, diorites and metamorphosed sediments associated with the Australian plate (Turnbull, 2000; Turnbull et al., 2010).

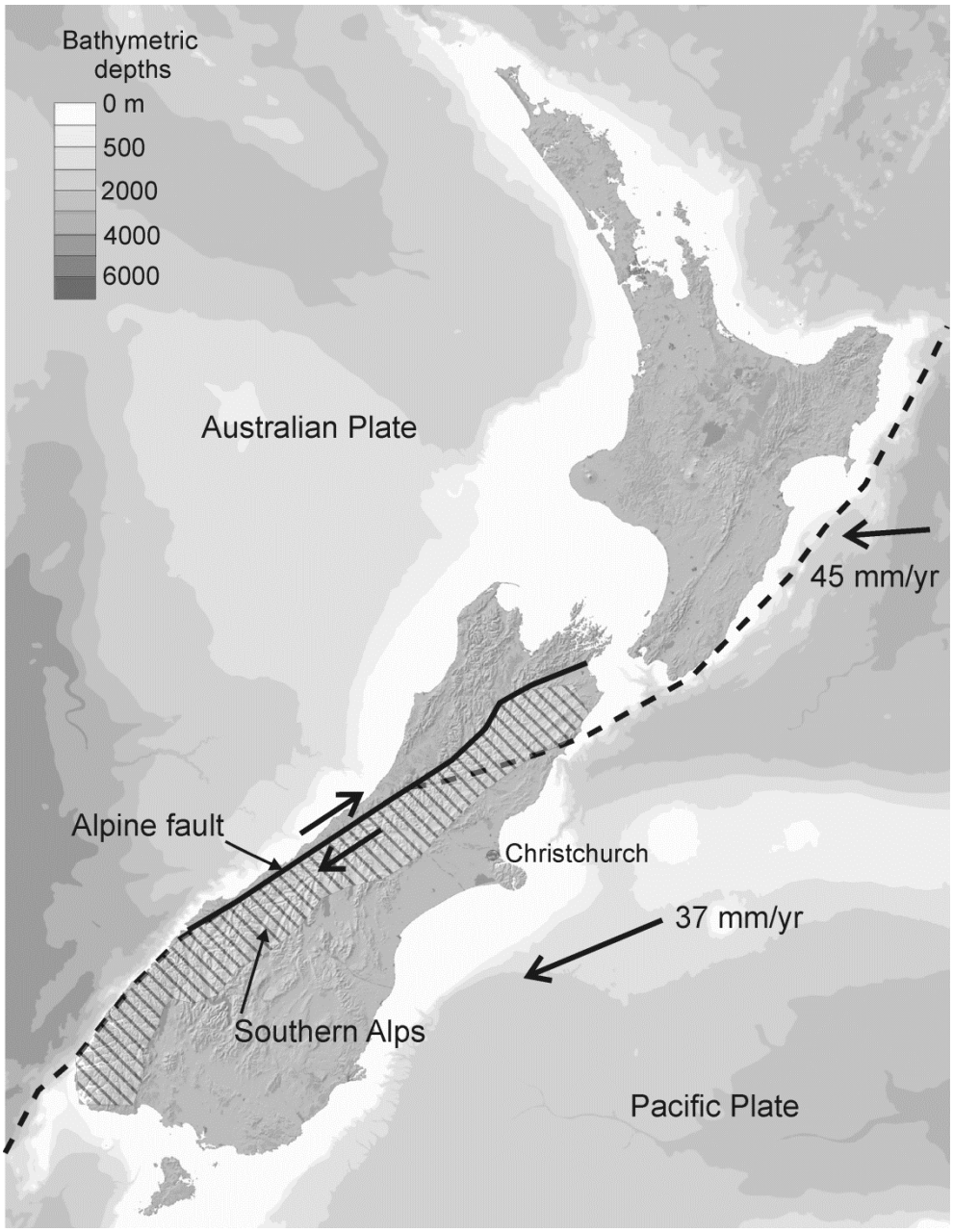

Figure 3.1: New Zealand with the location of the Southern Alps (striped area), location of plate boundary (dashed line), the Pacific and Australian Plates and relative plate motion vectors, and the location of the Alpine Fault (solid line). The bathymetry data is sourced from NIWA.

3.2 GEOMORPHOLOGICAL SETTING

Much of the Southern Alps (Figure 3.1) terrain is steep and intensely eroded, with some of the highest uplift and erosion rates in the world. Uplift, associated with folding and faulting, continues to the present day at rates of about 10 mm/yr and the entire area is subject to severe earthquake shaking every 100-300 years. Passage of moisture-laden

north-westerly airflow from the Tasman Sea and Southern Ocean is intercepted by the Southern Alps, resulting in strong orographically-enhanced precipitation of up to 14 metres per year near the main divide (Henderson and Thompson, 1999; Kerr et al., 2007). The combination of rapidly uplifting and tectonically damaged rock, steeply incised terrain and high precipitation and seismicity contribute to mass movement being a dominant form of erosion and landscape modification (e.g. Hovius et al., 1997; Korup et al., 2004). Smaller (< 1 M m^3) mass movement events occur frequently (e.g. Cox et al., 2008) but larger (> 1 M m^3) rock slope failures also occur relatively often, about once per decade (e.g. Whitehouse, 1983; Hancox et al., 2002; McSaveney, 2002; Hancox et al., 2005; Massey et al., 2008), and very large (> 100 M m^3) failures occur every few thousand of years or so (e.g. Hancox and Perrin, 2009). As well as these rapid, catastrophic failures, the Southern Alps host many slow moving gravitational failures, both active and relict. These are particularly numerous in the foliated schist ranges of the Otago region. Although fewer have been identified in the central Southern Alps, they are not entirely absent; ridge rent (or sackung or antiscarp) features have been observed and documented in several places (Beck, 1968; Pere, 2009), and an ongoing ridge collapse and creeping rockslide have been identified in Mount Cook National Park (Blair, 1994; Hancox, 1998).

3.3 GLACIAL HISTORY

Elevated topography situated in a temperate climate zone with high precipitation has resulted in extensive glaciation of the Southern Alps. Several times during the Pleistocene, ice has advanced across about one-third of the South Island landscape (Barrell, 2011 fig. 75.2), at times extending below modern-day sea levels. Erosion by large valley glaciers and small ice caps has resulted in the creation and modification of large glacial troughs (Figure 3.2), steep valleys (Figure 3.3), truncated spurs (Figure 3.4), and sharp (arête) topography (Figure 3.5). The generation, transport, and delivery of vast quantities of sediment in the glacial system has resulted in the formation of extensive outwash plains (Figure 3.6), thick loess sequences (Figure 3.7), moraines, and considerable other glacial landforms and deposits. Today, higher parts of the Southern Alps intersect inter-glacial snowlines and more than 3000 valley and cirque glaciers continue to flow; however, many of these glaciers have been in a

retreat/thinning phase since historical observations have been made (e.g. Figure 3.9). Barrell (2011) provides a review of the last century and a half of research of the regional glaciations of the Southern Alps and wider New Zealand.

Figure 3.2 Wakatipu glacial trough with the northern (upvalley) end of Lake Wakatipu in view. The lake is one of the deepest in New Zealand, reaching depths of about 400 metres, and extending 100 metres below sea level. Photo taken from atop Mt Alfred, which is a 1000 metre high mass of rock that has been covered with ice of the Wakatipu glacier during several Pleistocene glaciations. The delta at the head of the lake is continuing to grow as gravels deposited by the Rees (left) and Dart (right) rivers; several thousands of years ago the head of the lake was some 17 km further upvalley.

Figure 3.3: Precipitous rock slopes of a fiord produced by glacial erosion of the Milford Sound valley in Fiordland.

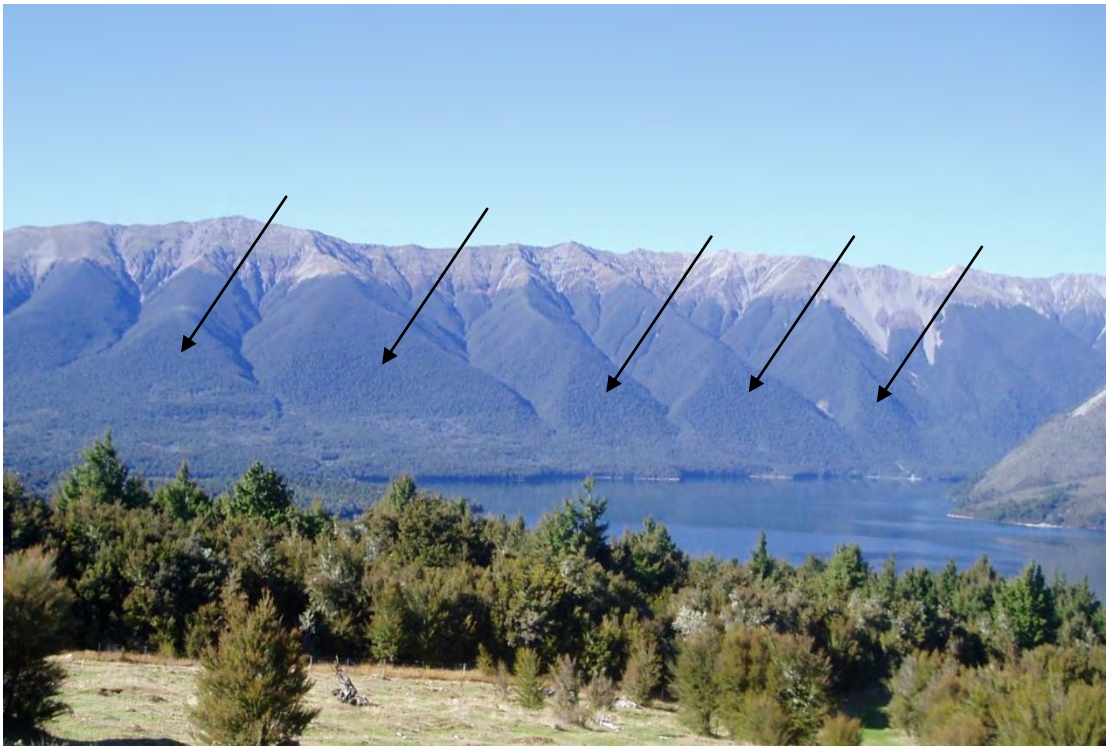

Figure 3.4: Fluvially produced spurs truncated by glacial erosion at Lake Rotoiti, Nelson Lakes National Park. Ice flow was from right to left. Arrows point to truncated spurs. Moraine is visible beneath truncated spurs and in photo foreground.

Figure 3.5: Sharp arête of the Mount Sefton Ridge formed by glacial erosion, Mt Cook National Park. The high peak is Mount Sefton and the low peak at right is Footstool. Photo is taken from the Sealy Range at sunrise.

Figure 3.6: Outwash gravels of the Canterbury Plains (photo centre), the Waimakariri River (photo centre-left), Southern Alps foothills (foreground) and Banks Peninsula (background), which is now connected to the mainland by the build up of Pleistocene outwash gravel.

Figure 3.7: Loess derived from the last (Otiran) glaciation overlaying basalt on the Otago coastline, East Coast of the South Island.

Figure 3.8: Tasman glacier proglacial lake, which has only developed in the last century. The debris-covered Tasman glacier terminus is indicated by lower arrow. The Murchison valley is the tributary at top left and the Murchison proglacial lake is just visible (top arrow). Photo taken February 2009.

3.4 PARAGLACIAL SLOPE STABILITY RESEARCH

Little research on paraglacial slope processes has been undertaken in New Zealand despite the suitability of New Zealand for studying the effect of deglaciation on slope instability. Slope collapse, where glacier downwasting has destabilised moraine, has been documented when it has caused problems for climber access, safety, or has threatened infrastructure (Blair, 1994; Kirkbride and Warren, 1999; McSaveney et al., 2003). Recent rock avalanches have, in some cases, been attributed to deglaciation (Cox et al., 2008; Allen et al., 2011), while some of New Zealand's very large and giant rockslides are thought to have been influenced by deglaciation (Hancox and Perrin, 1994, 2009). Beck (1968) attributed the development of slow creeping gravity failures in New Zealand to the retreat of glaciers; Pere (2009) investigated the process in more detail, using several New Zealand case-studies. Augustinus (1992, 1995a, b) developed a framework for the response of deglaciated valley slopes in the Southern Alps, which related the slope failure type and response time following deglacierization to the rock mass properties and lithology. It is hoped that, apart from these few studies

and the additions presented in this thesis, the New Zealand landscape will receive greater attention from paraglacial geomorphologists. If glaciers continue to retreat and permafrost limits continue to rise, there will be excellent opportunities to record the influence it has on the geomorphic evolution of slopes and the rest of the fluvial system.

CHAPTER 4: RESEARCH CONTRIBUTIONS

4.1 PART A: INVESTIGATION OF A LARGE ICE-CONTACT ROCKSLIDE

Abstract: The thinning and retreat of glaciers is thought to contribute to the development of or the acceleration of slope movements. Understanding the mechanisms involved in this process has been hindered by a lack of direct observation. The Mueller Rockslide in Aoraki/Mount Cook National Park, New Zealand, is a large slow-moving rockslide whose toe is in contact with the side of the Mueller Glacier. The rockslide has been investigated over a two-year period to assess the rates and patterns of slope movement and to explore the factors that have led to the development of instability and slope movement. Field and aerial-imagery mapping and a range of surveying techniques were used to determine the structural controls on the distribution and rate of slope deformation. The rockslide extends ~600 m in elevation from the top of the ridge to the bottom of the valley, is ~1200 m wide, and has a volume of between 100 and 200 M m3. Movement is deep-seated, taking place on dip-slope bedding planes that form the limb of an overturned and plunging anticline. Total downslope movement measured on the lower part of the rockslide was ~4.5 metres over the two years; much of which appears to be associated with a period of heavy rainfall. Large tension cracks are present on the ridge above the rockslide and some of these have opened further since measurements were first made in 1994. The top of the ridge therefore appears to be undergoing dilation, and possibly subsidence, in response to displacement of the rockslide mass. Movement of the slope threatens a popular alpine hut situated at the top of the rockslide, and runout of the debris into the proglacial lake at the terminus of the Mueller Glacier, in the event of catastrophic collapse, presents a serious hazard for a nearby community. The ongoing monitoring of this site, and, ideally, the implementation of a warning system, would be prudent measures to help reduce the impact of a catastrophic failure. These monitoring data will also contribute to knowledge of how large-scale slope movements in glaciated valleys develop and behave during glacier recession.

4.1.1 Introduction

Despite much research on the relationship between slope instability and deglaciation over the last few decades (reviewed by Ballantyne, 2002; and in Section 4.2; McColl, 2012), there is limited field evidence for contemporary slope failure processes associated with glacier retreat. Much of the previous research has focussed on the link between prehistorical rock slope failures and their timing with the retreat of ice from the last glaciation. Although these studies have revealed valuable information about the timing of failures and possible links to processes such as enhanced seismicity, their inferences could be strengthened by physical evidence or suitable contemporary analogies. The physical link between deglacierization and slope collapse can be studied directly by examining contemporary slope collapse in valleys presently containing glaciers. This is a necessary step for improving understanding of the causes, controls, and timing of slope collapse during glacier downwasting, which may eventually help to reduce the impacts on society by providing advanced warning of where and when slope failures will occur.

The Mueller Rockslide is a large, active mass movement in the glaciated Mueller Valley of New Zealand; the base of the rockslide is in contact with the side of the Mueller Glacier. The Mueller Glacier appears to be about 100-200 metres thick at the rockslide. Initiation of the rockslide, possibly within the last 1000-2000 years, is likely to have been related to undercutting of the slope by the Mueller Glacier and subsequent thinning of the glacier – but other factors such as seismicity probably contributed to the development of instability. Continued thinning or complete retreat of the glacier may result in accelerated movement of the slope and possibly catastrophic collapse. Runout of the debris, in the event of rapid collapse, could threaten infrastructure and people downvalley, especially if it enters the proglacial lake and generates tsunami waves. The collapse may also increase and speed up the collapse of the ridge above the rockslide, which threatens a popular alpine hut and walking access along the Sealy Range.

The accessibility of the Mueller Rockslide presents an opportunity to investigate the development of a slope during glacier downwasting, and the information collected may also be used to help mitigate impact from the potential catastrophic failure of the slope. In the following, I present and discuss the results of mapping, monitoring, and

engineering geological investigation of the Mueller Rockslide with respect to the geologic, geomorphic, and glacial controls on stability.

4.1.2 Study site

The Mueller Rockslide is a large (~1.1 M m^2; 100-200 M m^3) very slow moving translational rockslide situated on the Sealy Range in Mount Cook National Park. It extends west from near the crest of the Sealy Range (c.1800 m.a.s.l) to the Mueller Glacier some 600 metres below (Figure 4.1.1) in the central alpine region of the Southern Alps (Figure 4.1.1 inset).

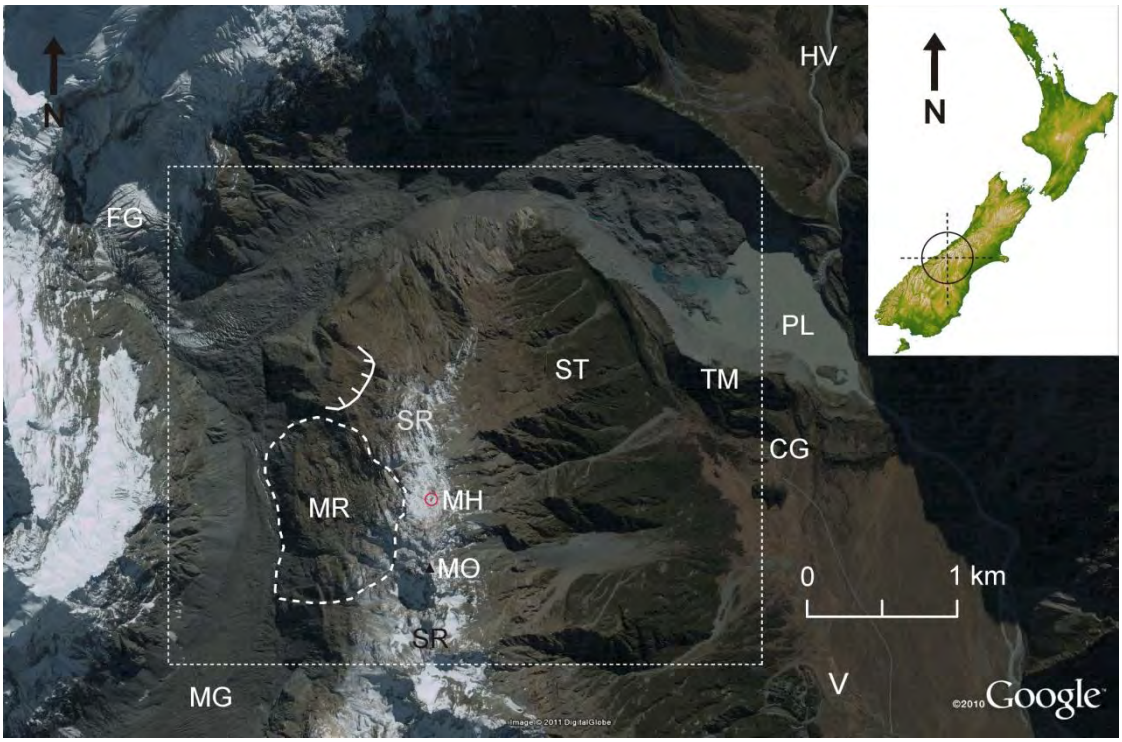

Figure 4.1.1 – Overview of the Mueller Rockslide (MR) site and location within the South Island, New Zealand (inset). The rockslide boundary is shown by the white thick-dashed polygon. An adjacent mass movement feature is indicated with the white arc with tic-marks. The white thin-dashed white rectangle is the map extent for Figure 4.1.2. HV = Hooker Valley; FG = Frind Glacier – tributary of the heavily debris covered Mueller Glacier (MG); PL = Mueller Glacier proglacial lake; ST = Sealy Tarns; TM = Mueller Glacier terminal moraine (late-glacial to Holocene); SR = Sealy Range; CG = White Horse camping ground; MH = Mueller Hut (1816 m.a.s.l.); MO = Mt Ollivier (1933 m.a.s.l.); V = Aoraki/Mount Cook Village (750 m.a.s.l.). Centre point of image (at approximately ST) is 170° 04′ 32″ E; 43° 42′ 48″ S. Image is from GoogleEarth®, dated 5/04/2006.

4.1.2.1 Geology

In the central Southern Alps greywacke and argillite progressively give place to schist of increasing metamorphic grade towards the Alpine Fault on the western side of

the range. The well-indurated rock is Torlesse composite, predominantly Rakaia terrane, formed during the Triassic, metamorphosed and tectonically deformed during the Cretaceous, and uplifted during the ongoing Kaikoura Orogeny (Cox and Barrell, 2007). The 60 km long N-NNE trending Main Divide Fault Zone (MDFZ) separates the non-metamorphosed rock in the east from semi-schistose and schistose rock to the west and closer to the Alpine Fault, where uplift and erosion have removed most of the previously overlaying greywacke and argillite. However, on the Sealy Range the MDFZ is still covered by non-metamorphosed sandstones (Cox and Findlay, 1995).

Sealy Range is formed by a large overturned fold structure, the Kitchener Anticline, which plunges 25 degrees towards the north in the location of the Mueller Rockslide (Lillie and Gunn, 1964) (Figure 4.1.2). The rockslide occurs on the western limb of the anticline, in greywacke sandstone dipping steeply (45-50 degrees) to the west. The bedding is inferred to form the principal slip surface(s) of the rockslide (Figure 4.1.2 cross-section). On the eastern side of the Sealy Range the non-metamorphosed rock is faulted against semischist by the steeply dipping Green Rock Fault. Further east the semi-schist is faulted against non-metamorphosed greywacke sandstone by the steeply dipping Great Groove Fault.

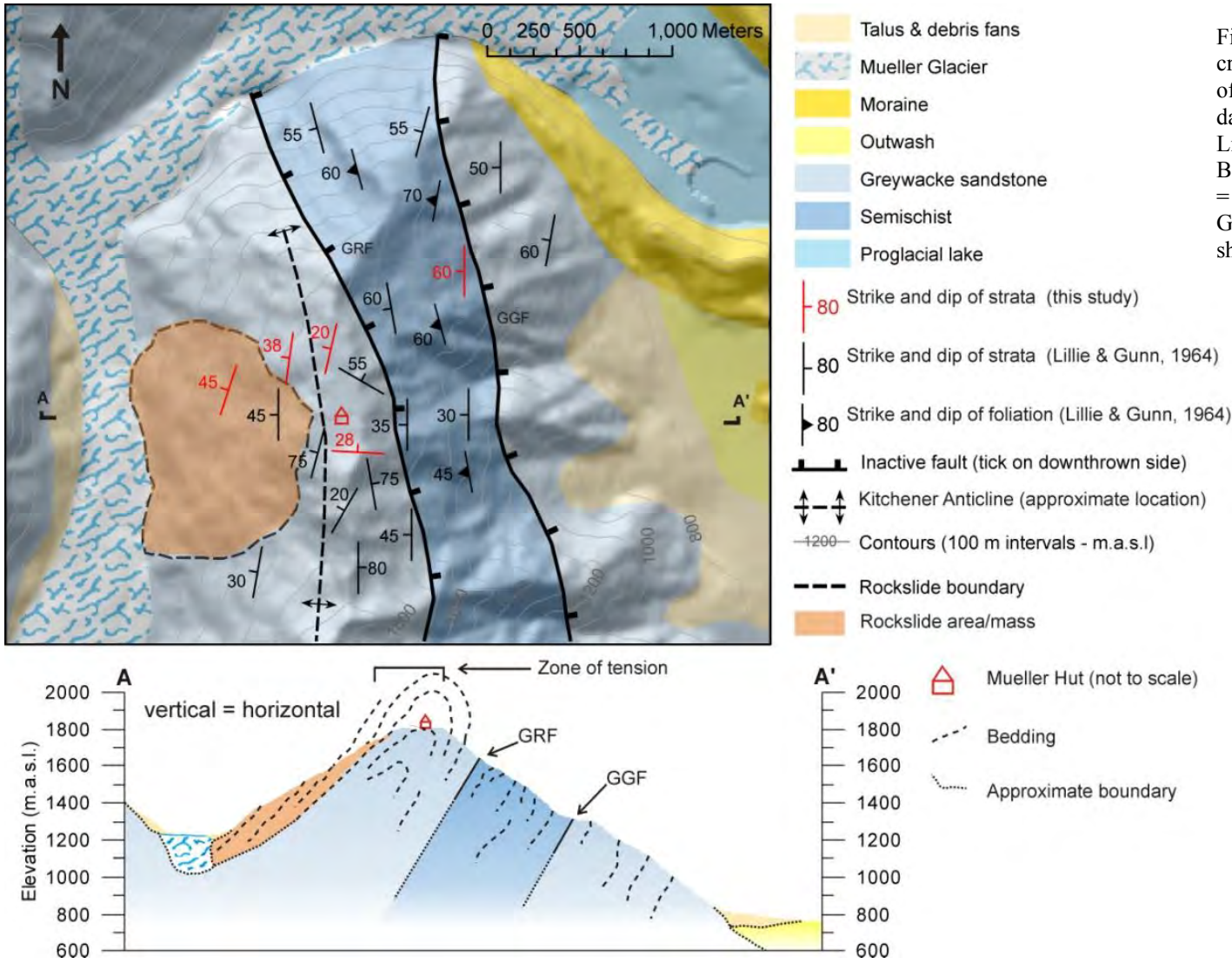

Figure 4.1.2: Geological map and cross-section for the northern end of the Sealy Range. The geological data and interpretations are from Lillie and Gunn (1964), Cox and Barrell (2007), and this study. GRF = Green Rock Fault; GGF = Great Grove Fault. Extent of map is shown in Figure 4.1.1.

4.1.2.2 Engineering geology and geomorphology

The Mueller Rockslide occurs in unweathered grey to slightly weathered pinkish-grey very strong greywacke sandstone; it is inter-bedded with strong argillaceous siltstone/mudstone. Joints are widely spaced and mostly narrow to very wide, many with fresh, clean surfaces. Much of the rockslide ground-surface appears disturbed, with dilated joints, chaotic rock blocks and patchy veneers of angular debris on the surface (Figure 4.1.3A). This is probably related to a combination of landslide movement, seismic shaking, rockfall, freeze-thaw weathering, and snow creep. Vegetation cover is sparse, comprising a few small alpine plants. Annual precipitation may be as high as 10 metres per year (Kerr et al., 2007), much of which falls as snow. Snow covers much of the rockslide ground-surface for about two thirds of the year and in late summer a few small patches of névé usually remain (Figure 4.1.3A). Near the head of the rockslide, and on the top of the ridge, large smooth rock slabs, marked with striations oriented sub-perpendicular to the Mueller valley long-axis, indicate that small cirque glaciers may have existed in the past (Figure 4.1.3B).

4.1.2.3 Glacial history

The region was extensively glaciated during the last ice age and the largest valley glaciers have undergone over 50 km of retreat and hundreds of metres of thinning since that time (c. 18-24 ka). Many tens of metres of downwasting and retreat of the Mueller and other nearby glaciers has occurred over the last 200 years, as evidenced by the abandonment and exposure of terminal and lateral moraines, and the development of proglacial lakes over this period (Gellatly, 1985; Kirkbride and Warren, 1999). Based on valley cross-section extrapolation, the Mueller Glacier is approximately 100-200 metres thick at the rockslide location (Figure 4.1.2 cross-section). It is likely to continue thinning and eventually retreat beyond the Mueller Rockslide in perhaps as little as two hundred years (based on thinning and retreat over the previous c.200-year period).

Figure 4.1.3: (A) View looking north from near the crest of the Sealy Range ridge above the rockslide. The flattish area in view has numerous tension cracks and a chaotic boulder-covered surface, with the head of the rockslide out of view beyond the break of slope at upper left of photo. Photo taken late summer when there are only small patches of névé remaining. During winter and spring, snow can be over 5 metres deep, frequently burying Mueller Hut (building in upper centre of photo) up to the roof. (B) Smooth convex hollow (white dashed line) below main scarp (approximately 40 metres high, shown with line i). The hollow has numerous striations on surface, indicating surface modification by the scraping of rocks across the surface by cirque glaciation or sliding of annual snowpack. The surface is being destroyed by retrogressive block toppling from the down-slope edge (area indicated by line iii and incipient block topple cleft shown with line ii). (C) A large block has detached from the main rockslide scarp, in the northern area of the landslide, photo taken looking south with Mueller Glacier to the right. (D) Lateral moraine ridge in the middle part of the landslide at the southern end. The ridge is several metres high and about 100 metres long with faceted, striated, and sub-angular to sub-rounded boulders.

4.1.2.4 Previous investigations

Instability of the Sealy Range has been investigated previously by Hancox (1994, 1998), for the Department of Conservation in relation to the safety and re-positioning of the Mueller Hut. The current Mueller Hut (Figures 4.1.1 to 4.1.5) is a large (28 bunk) and popular hut, often at full capacity during the summer months. It was repositioned and rebuilt (for a fifth time) in the current location in 2003 after concerns about the stability of the rock foundations of the previous site (at approximately the location of Monitoring line A in Figure 4.1.5). Here the hut had 'gone bump in the night' as reported by several occupants, and it was deemed to be positioned on an active slumped bench (Figure 4.1.5). Other cracks in the area and a 'rift' in the ridge just west of the slumped bench were at this time considered to be associated with movement of the Mueller Rockslide (referred to by Hancox as the Mueller Landslide). Historical aerial photographs showed that the rift had developed in only the last decade (since 1985) and possibly after 1992 (Hancox, 1994). Two monitoring lines were set up in 1994 to monitor movement at the hut site (monitoring line A) and further south on the ridge (monitoring line B). Soon afterwards it was decided on to move the hut to the current, more stable location. This is about 125 m metres from monitoring line B, which had been established to monitor further opening of a 3 m wide tension crack thought to have developed recently. Evidence at the time indicated that the crack may have formed, or widened substantially, during the previous winter and following a heavy rainfall event in the summer of 1994. Hancox (1994) suggested that the crack is part of the aforementioned rift zone, but a different interpretation has been developed in this study (Section 4.1.4.1). Re-monitoring of these survey lines was not carried out again until 2011 (this study).

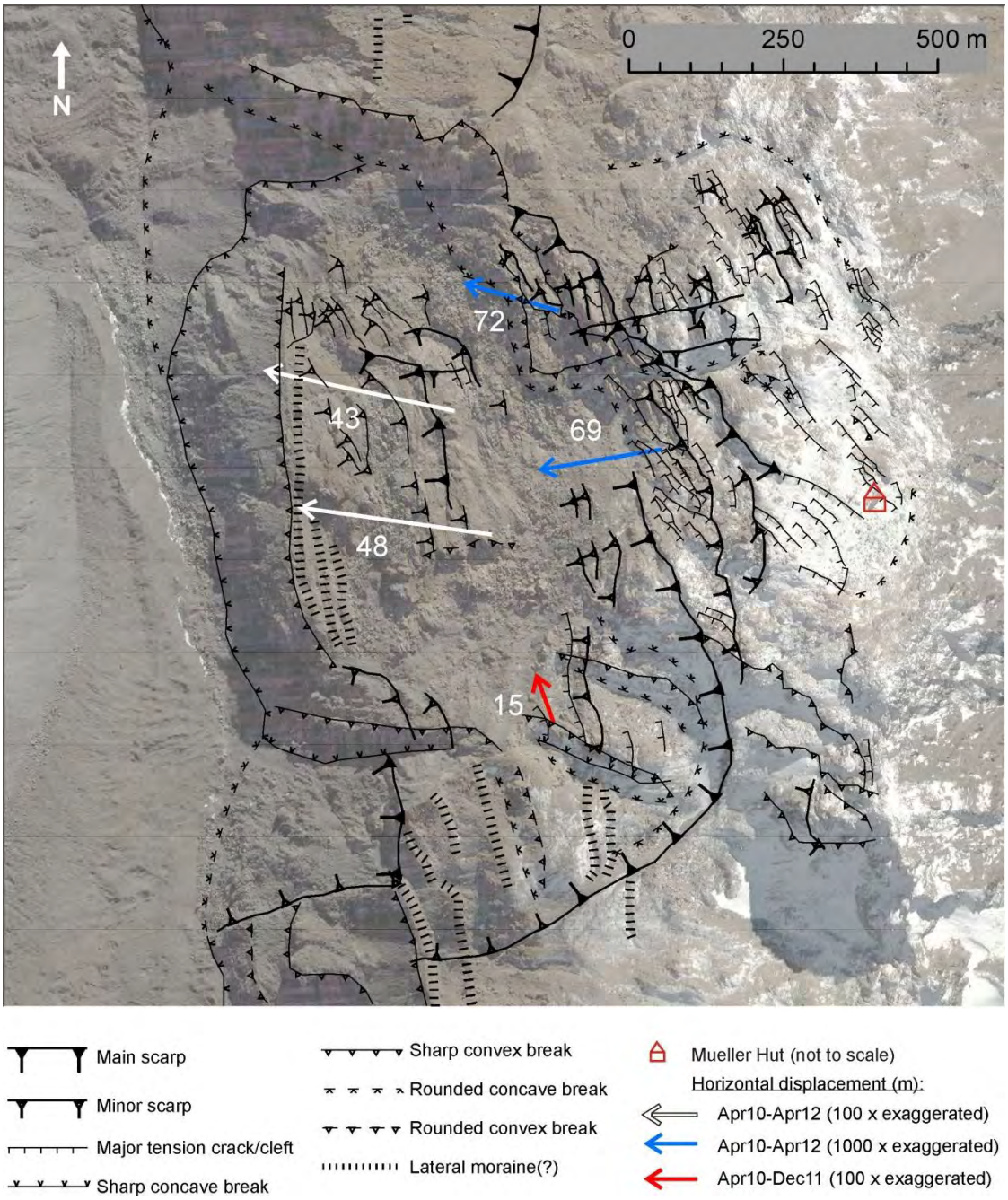

Figure 4.1.4: Geomorphological map overlaid on GoogleEarth® imagery. The numbers alongside the displacement arrows are angle of inclination below the horizontal. The base of the arrow is the location of each corresponding survey mark.

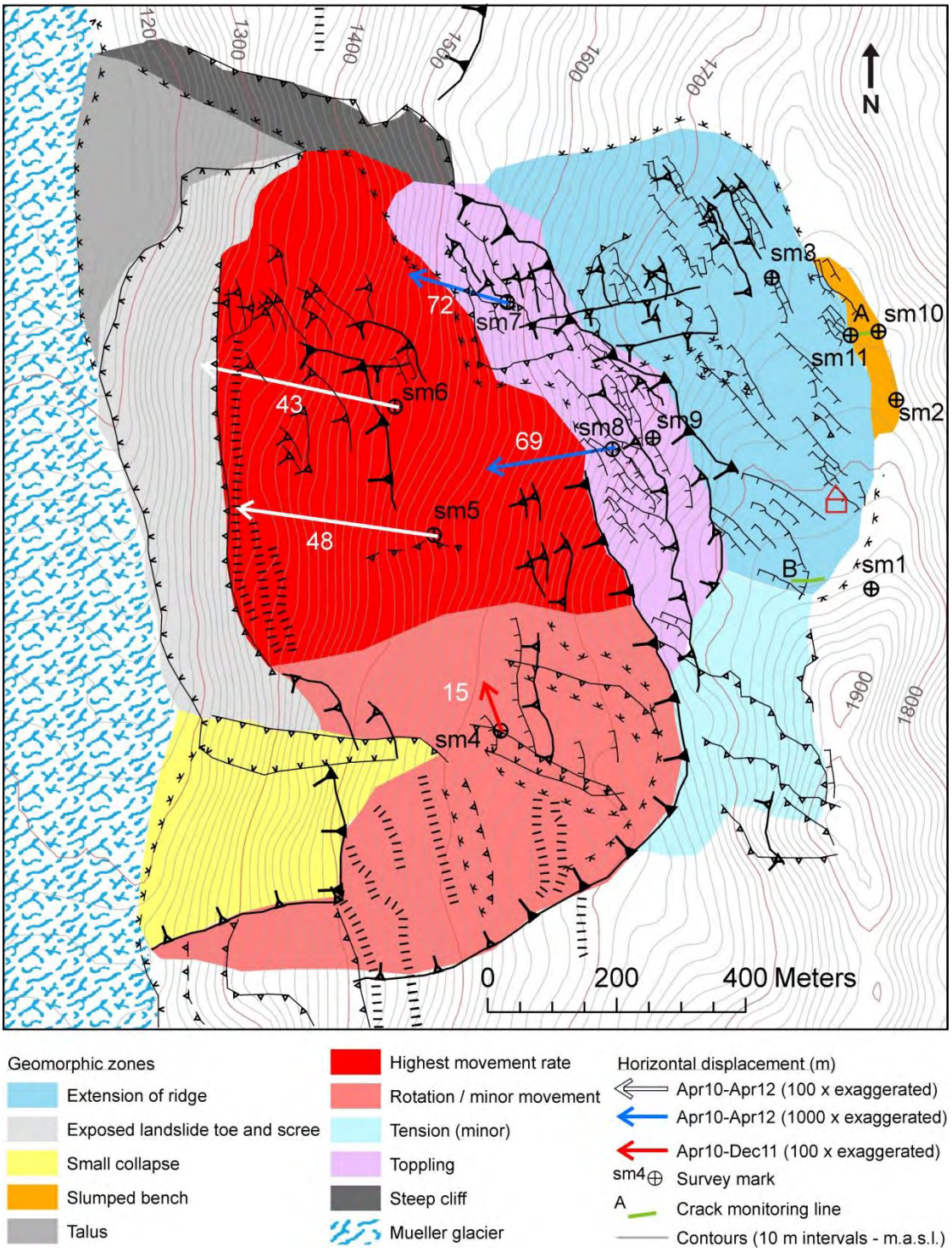

Figure 4.1.5 Map of Mueller Rockslide showing: geomorphic zones based on geomorphological mapping and movement data; location of survey marks; horizontal displacement vectors and inclination angles; and location of crack monitoring lines A and B. The geomorphic legend is the same as Figure 4.1.4.

4.1.3 Methodology

To define the rockslide boundary, kinematics, and structural controls, geological and geomorphological field and remote (aerial photo and satellite imagery) mapping were undertaken. Engineering properties of the rockslide mass were quantified by field description and laboratory testing. Precipitation data provided by the National Institute of Water and Atmospheric Research (NIWA) were analysed. These datasets were compiled to characterise the rockslide and analyse the controls on movement rate.

4.1.3.1 Differential GPS surveying

Repeat surveying of the slope using differential GPS (DGPS) was undertaken to determine the spatial variability in slope movement. Geomorphological mapping allowed different movement zones within the slope to be identified, which were then used in selecting locations for survey marks (2 cm round aluminium survey disks, fastened to the rock surface with an epoxy resin). Survey marks sm4, sm5 and sm6 were positioned in the lowest safely accessible parts of the rockslide and were expected to record the largest displacements (Figure 4.1.5). Although survey marks were carefully placed to avoid unrepresentative rockslide movement (i.e. not on ground directly affected by individual block topples, or collapse), this was not always practical. Survey mark sm4 was positioned on an apparently stable block of rock that later disintegrated; December 2011 was the last survey of this mark.

Three survey marks were installed in the zone of toppling (sm7, sm8, sm9; Figure 4.1.5). Survey mark 7 was located in the northern part of this zone and survey marks sm8 and sm9 in the central part of the rockslide below the main scarp. Due to their position immediately below the main scarp, it was expected that sm8 and sm9 would record similar displacements to the survey marks lower on the rockslide.

Survey mark sm3 was located above the main scarp, in the region of the ridge that was thought to be undergoing extension. Survey mark sm2, and later sm10 and sm11, were positioned to assess movement of the slumped bench to the east of the Mueller Rockslide described by Hancox (1998) (Figure 4.1.5). Survey mark sm10 is on an old cleft monitoring line pin (monitoring line A, pin 2, Hancox 1998) and sm11 is a wooden stake constructed in this study.

Survey mark sm1 was positioned in a (relatively) non-active part of the slope near the top of the ridge to provide control on the relative movements in more active locations (so that regional tectonic deformation could be removed).

Surveying at each survey mark was done using an external antenna (Trimble Hurricane) mounted on top of the survey mark for a minimum occupation of 15 minutes and until a post-processed horizontal accuracy of less than 12 cm was achieved. The GPS data were differentially-corrected against the LINZ permanent Mount John Observatory base station (located 41 km from the site). The first survey was in April 2010 and subsequent ones in March 2011, December 2011 and April 2012 (except for sm9, sm10 & sm11 which were first established and surveyed in December 2011 and resurveyed in April 2012).

4.1.3.2 Continuous GPS

A continuous GPS (CGPS) device (Trimble NetRS) was installed at survey mark sm9 in April 2010 to provide a near-continuous record (30 second recording intervals) of displacement at one site on the rockslide (Figure 4.1.6). The purpose was to assess the relationship between movement and external variables such as seasonal changes (rainfall, snow loading and thaw) or seismic triggers, and to determine whether or not there is a creep (constant background deformation) component to the motion of the rockslide. The site selected for installation was chosen because of its accessibility, its position within an active part of the rockslide (based on preliminary geomorphic assessment) and distance from localised movement (e.g. rock toppling at the edge of scarps), adequate exposure to sky view for satellites and solar power generation, and the low likelihood of snow avalanche or rock fall damage. As it turned out, the position chosen was considerably less active than the lower section (according to the DPGS surveying), and during the winter/spring of 2010 the equipment was badly damaged from snow-pack sliding. Further attempts to re-establish new equipment were abandoned because of lack of an alternative site that matched all of the criteria above. The short monitoring life and the absence of recording during the winter months because of snow cover (causing loss of power and satellite reception), meant that the recorded data were sporadic and of short duration. The 30 second data were differentially corrected using the AUSPOS Online GPS Processing Service (version: AUSPOS 2.0). The program used 13 reference stations for differential correction, 9 of which were located within the South Island, New Zealand, and the closest station being the (41 km) Mount John

Observatory station. A mean position was calculated for each 24 hour period from the 30 second observations. The reported geodetic precision of corrected data, at one sigma, is better than 5 mm on all days, and better than 1 mm on most days, for east, north, and vertical movement directions. The geodetic positions are reported as ITRF2008 coordinates with GRS80 ellipsoidal heights.

Figure 4.1.6: The continuous GPS on the Mueller Rockslide. The aerial is protruding 30 cm above the ground to the left. The GPS (NetRS) and power supply are on the framing behind the 80W solar panel. The frame was anchored to the rock with expansion bolts. Snowpack sliding buckled and sheared the aluminium framing and anchor bolts, and bent the 20 mm diameter stainless steel rod supporting the aerial.

4.1.3.3 Crack monitoring

A crack monitoring line established in 1994 (monitoring line A, Hancox 1998) was resurveyed in 2012, and a second monitoring line established in 1998 (monitoring line B, Hancox 1998) was re-surveyed in 2011 and in 2012 (Figure 4.1.5). Monitoring line A was established at the previous site of the Mueller Hut to monitor development of an active slump feature on the eastern side of the ridge where the hut was situated. It was resurveyed in this study to assess further movement of the slump and its relationship to movement of the rockslide. Monitoring line B was set up to monitor expansion of a

several-metre wide crack that had developed about 150 metres from the current Mueller Hut site. This was re-surveyed in this study to assess the extension of the ridge in this location. The original monitoring lines consisted of steel expansion bolts drilled into rock. A steel measuring tape was used to re-survey the distances between bolts (achieving accuracy better than 5 mm).

4.1.4 Results

4.1.4.1 Rockslide extent

The approximate boundary, location of major features of the rockslide, and structural data are presented in Figure 4.1.4 and 4.1.5. The rockslide is interpreted to extend from the near top of the ridge to approximately 150 m below the Mueller Glacier surface. The crown of the rockslide is interpreted to be defined by a discontinuous scarp (herein referred to as 'main scarp'), of 15-40 metres height, extending the width of the rockslide. The crown is situated below a subtle curvilinear break in slope at the western side of the flattish ridge top (Figure 4.1.4). The location of this scarp is likely to be related to the change in bedding orientation associated with the fold axis. The continuation of this main scarp into lateral scarps and the change from a highly disrupted surface to the surrounding more-intact rock indicates the lateral boundary of the slide mass, although there is some evidence (scarp mapped in Figures 4.1.1 & 4.1.4) that the entire western flank of the Sealy Range north of the rockslide boundary is affected by gravitational collapse.

The interpretation of the landslide boundary in this study differs from previous interpretations by Hancox (1994, 1998). Hancox had interpreted the landslide to continue farther up the ridge, with its eastern boundary defined by the edge of the large rift (adjacent to the slumped bench in Figure 4.1.5). It appears to the author that this rift feature identified by Hancox is related to the slumping of the bench on the eastern side of the ridge, rather than movement of the ridge. The orientation of bedding in the upper part of the ridge in the area of the fold axis is variable but appears to be dipping in a northerly direction, so the failure surface of the Mueller Rockslide is probably unlikely to continue to the eastern side of the ridge. However, movement of the Mueller Rockslide certainly appears to be causing extension (relaxation) of the upper part of the ridge (Figure 4.1.5; Section 4.1.4.2). The curious flat cross profile of the ridge in this

area may be in part a result of gradual subsidence of the ridge as the rockslide has advanced. However, this shape may also be structurally controlled or a result of previous cirque glaciation – there are several planar to concave, smoothed surfaces with striations in this area.

The mapped above glacier (slope) surface area of the rockslide is ~1.1 M m^2 (based on the area shown for the rockslide boundary in Figures 4.1.1 and 4.1.2) and the volume of the rockslide is estimated to be between and 100 and 200 M m^3. The large uncertainty in volume arises from large uncertainty in the depth of the sliding surface (with a maximum estimated depth of 200 metres). The overall volume for the mass movement may be as much as 50% larger if the part of the ridge above the rockslide undergoing extension is also included.

4.1.4.2 Failure mechanisms

Based on morphology and structural analysis, the failure mechanism for the main rockslide is most likely translational sliding along the (45 - 50°) inferred bedding surfaces of the dip slope (Figure 4.1.7). It appears that the projected failure surface may 'daylight' from the rock slope at some position below the surface of the Mueller Glacier, which would suggest that the presence of glacier is currently influencing the stability of the rockslide.

In the upper part of the ridge above the rockslide, where there are numerous tension cracks, extension in response to rockslide displacement – effectively steepening and unloading the upper part of the ridge – appears to be occurring. Two systematic joint sets are recognised from structural mapping (JS1&2; Figure 4.1.7), which are oriented sub-perpendicular to each other. Many of the tension cracks mapped on the ridge above the rockslide (Figure 4.1.5), some over 100 metres in length, are similar in orientation to those of JS2 and are likely to be part of the same joint set; these were not included in the stereonet because their dip is unknown as they were mapped mostly from aerial imagery. Both joint sets have many widely open joints, of which the surfaces are often fresh (unweathered and clean), and the direction of slope movement is at an angle approximately half-way between the intersection of the two joint sets; this suggests that the dilation of the joints is related to rockslide movement. It also suggests that the systematic joint-set orientations are unfavourable for the ongoing stability of the upper part of the ridge if the rockslide continues to move. Some of the joints may be recent in origin, having formed in response rockslide displacement; however, some of the joint

surfaces have thin deposits of calcite or quartz, indicating a less recent origin for at least some of them.

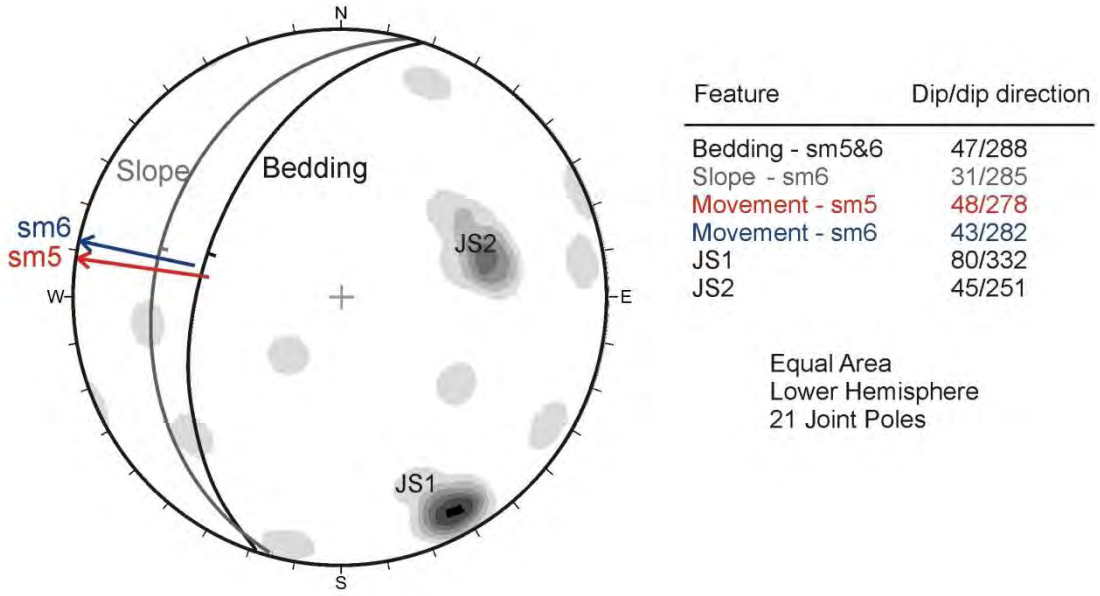

Figure 4.1.7: Stereographic analysis on a lower hemisphere stereonet showing: joint pole distribution contours; great circles for average bedding orientation at the sm5 and sm6 survey mark locations; slope angle at the sm6 survey mark location; and trend/plunge of movement of survey marks sm5 and sm6. Slope angle at survey mark sm6 was calculated by taking the elevation 200 metres above and below the survey mark and the aspect was estimated from contour line orientations in Figure 4.1.5. JS1 and JS2 data are from the ridge above the rockslide. Orientation of stereonet is relative to true north.

There are a number of secondary failure mechanisms within the rockslide complex, in addition to the dominant sliding and the relaxation of the upper part of the ridge mentioned previously. The upper part of the rockslide, below the main scarp, appears to have a large component of vertical (downwards) movement. In this area, the rock is breaking away from the main scarp and other minor scarps by toppling (Figure 4.1.3B). As a consequence of toppling and disintegration, the slopes underneath are covered with angular boulders and debris – some of this debris will have been transported to the lower slope by snow avalanching and rockfall. As well as this debris cover, much of this area is undergoing disintegration, with extensive (c. 100 m^2) areas containing many (> 5 m wide) chaotic, rotated, and precariously balanced rock blocks. These debris and rock blocks prevented observation of the underlying 'in-situ' geology to allow assessment of the rockslide behaviour in this area. In the lower zone of the rockslide (in proximity of sm5 and sm6), some 'bedrock' is exposed and the appearance of >50 m long rock swales (smoothed several-metre-high rock ridges) may be associated with compressional

stresses. The lowest third of the rockslide, below the elevation of survey mark sm6, was inaccessible and was mapped only with remote imagery. On the aerial imagery it is obvious that the frontal part of the rockslide (exposed landslide toe zone in Figure 4.1.5) has been exposed by glacier thinning and is affected by rockfall and slope-wash.

In the southern part of the frontal zone (rockslide toe) there is a separate slope collapse within the main rockslide boundary ('small collapse' shown in Figure 4.1.5). Although there is no geological information to confirm it, the failure of this part of the slope may have been caused by daylighting of the bedding planes forming the main (?) rockslide failure surface. The anticline is plunging towards the north at approximately 25 degrees, whereas the glacier gradient at the rockslide is approximately 8 degrees. Therefore, it is likely that in the southern part of the rockslide, bedding is considerably higher and would daylight earlier than the bedding further north during glacier recession.

4.1.4.3 Slope movement

Visual indications of recent activity, including fresh cracks and scarps, are confirmed with slope movement monitoring data. These are presented below.

4.1.4.3.1 Differential GPS surveying

Movement recorded with DGPS surveying of the eleven survey marks is provided in Table 4.1.1 and horizontal displacement vectors and movement inclination are shown in Figures 4.1.3 and 4.1.4 for survey marks within the active zones of the rockslide.

In the upper part of the ridge, outside of the mapped rockslide boundary, movement is mostly less than the error of the GPS equipment (c. 0.5 m) but a total of about 1 metre of movement in a south-west direction is recorded at sm3, consistent with the interpretation of this part of the ridge undergoing gradual extension towards the west as a result of rockslide movement. A total of about 0.5 m of movement in a south-east and downwards direction is recorded at sm2, consistent with this being located on an actively slumping bench. Survey mark sm1, which was thought to be in an inactive part of the ridge, has moved less than half a metre, in a general direction of north-west. This is within the error of the survey but is also consistent with the regional deformation recorded 4 km away on the Sealy Range by the continuous GPS site (NETT) maintained by GeoNet; it records a net movement vector for April 2010 to April 2012 of approximately 80 mm NNW. In the central part of the rockslide (sm8) approximately 0.3 metres of movement steeply downward towards the west has been recorded, which is

possibly too close to survey error to be considered reliable; however, a similar magnitude and direction was recorded at sm7. Both have been mapped in the zone of toppling directly below the main rockslide headscarp, and therefore a westerly movement direction with a high component of vertical downwards displacement was expected here. Towards the southern part of the rockslide at survey mark sm4, net movement was in a NNW direction at a low downward inclination (15°). A possible explanation for the lower magnitude and more northerly movement at the southern site (sm4) is that the southern part of the rockslide is being slowly released by displacement of the faster moving northern zone (sm5 and sm6), and therefore is moving northwards to fill the space.

In the lower, central part of the rockslide (sm5 and sm6) movement has been on the order of 1 to 5 metres with a net movement direction and inclination similar to the angle and azimuth of dip (47/288) of the strata at these locations. In the final monitoring interval between December 2011 and April 2012, the data shows a different pattern, but one that is questionable for such a short monitoring interval. Both sites had less than 0.5 m of horizontal displacement, a comparatively large vertical displacement component, and a more southerly movement direction. That significantly more movement was recorded at survey marks sm5 and sm6 during the first 11 month survey interval than in the following 13 months, suggests that the movement is episodic and influenced by some external factors, such as rainfall.

Table 4.1.1: Movement data from the differential GPS surveying. The 'net movement' is a combination of horizontal and vertical movement. The 'net rate' is the average net movement (i.e. total movement divided by the entire monitoring interval), and is therefore not a true rate of movement.

Mark	Survey dates	Days	Horizontal (m)	Vertical (m)*	Net (m) **	Net Rate (m/yr)**	Trend	Plunge **
sm1	Apr '10 - Mar '11	352	0.136	0.368	-0.392	**-0.407**	**270**	**-70**
	Mar '11 - Dec '11	257	0.364	0.362	-0.514	**-0.729**	**320**	**-45**
	Dec '11 - Apr '12	118	0.220	-0.444	0.496	**1.533**	**119**	**64**
	Apr '10 - Apr '12	727	0.246	0.286	-0.377	**-0.189**	**314**	**-49**
sm2	Apr '10 - Mar '11	352	0.395	-0.109	0.410	**0.425**	**129**	**15**
	Mar '11 - Dec '11	257	0.021	-0.341	0.342	**0.485**	**076**	**87**
	Dec '11 - Apr '12	119	0.103	-0.136	0.171	**0.524**	**081**	**53**
	Apr '10 - Apr '12	728	0.486	-0.586	0.761	**0.382**	**118**	**50**
sm3	Apr '10 - Mar '11	352	0.457	0.294	-0.543	**-0.564**	**212**	**-33**
	Mar '11 - Dec '11	257	0.378	-0.574	0.687	**0.976**	**207**	**57**
	Dec '11 - Apr '12	119	0.152	0.296	-0.333	**-1.020**	**076**	**-63**
	Apr '10 - Apr '12	728	0.737	0.016	-0.738	**-0.370**	**201**	**-1**
sm4	Apr '10 - Mar '11	352	0.233	-0.213	0.316	**0.327**	**289**	**42**
	Mar '11 - Dec '11	257	0.716	-0.017	0.717	**1.018**	**355**	**1**
	Dec '11 - Apr '12			Survey mark destroyed				
	Apr '10 - Dec '11	609	0.836	-0.230	0.867	**0.520**	**340**	**15**
sm5	Apr '10 - Mar '11	352	2.780	-3.374	4.372	**4.533**	**274**	**51**
	Mar '11 - Dec '11	257	0.667	-0.197	0.695	**0.988**	**351**	**16**
	Dec '11 - Apr '12	118	0.476	0.078	-0.483	**-1.493**	**209**	**-9**
	Apr '10 - Apr '12	727	3.138	-3.493	4.696	**2.357**	**278**	**48**
sm6	Apr '10 - Mar '11	352	2.764	-3.230	4.251	**4.408**	**284**	**49**
	Mar '11 - Dec '11	257	0.449	-0.337	0.561	**0.797**	**289**	**37**
	Dec '11 - Apr '12	118	0.197	0.639	-0.669	**-2.069**	**168**	**-73**
	Apr '10 - Apr '12	727	3.128	-2.928	4.285	**2.151**	**282**	**43**
sm7	Apr '10 - Mar '11	351	0.314	-1.001	1.049	**1.091**	**122**	**73**
	Mar '11 - Dec '11	257	0.513	-0.012	0.513	**0.729**	**322**	**1**
	Dec '11 - Apr '12	119	0.219	0.516	-0.561	**-1.720**	**208**	**-67**
	Apr '10 - Apr '12	727	0.159	-0.497	0.522	**0.262**	**286**	**72**
sm8	Apr '10 - Dec '11	608	0.159	0.324	-0.361	**-0.217**	**284**	**-64**
	Dec '11 - Apr '12	118	0.082	-0.861	0.865	**2.675**	**213**	**85**
	Apr '10 - Apr '12	726	0.201	-0.537	0.573	**0.288**	**261**	**69**
sm9	Dec '11 - Apr '12	118	0.327	-0.305	0.447	**1.384**	**033**	**43**
sm10	Dec '11 - Apr '12	118	0.537	0.029	-0.538	**-1.664**	**181**	**-3**
sm11	Dec '11 - Apr '12	118	0.538	-0.162	0.562	**1.738**	**180**	**17**

* Negative = down; ** Negative = up

4.1.4.3.2 Continuous GPS data

The movements recorded by the continuous GPS station are presented in Figure 4.1.8. The top graph (A) shows the change in seconds of latitude south, graph B shows change in seconds of longitude east and graph C shows change in elevation in metres

above ellipsoid. Three periods of movement were recorded: (1) Slightly over two months from the end of March until early June. Towards the end of this period there is a sharp change in the recorded positions but this is most likely artificial, created by snow covering the GPS aerial. Prior to snow cover, there is a trend of movement towards the WNW and downwards (i.e. decreasing longitude and elevation, and slightly decreasing elevation). This trend is apparent amongst the scatter in the data and is illustrated in Figure 4.1.8 with manually fitted lines that bound the majority of scatter in the data. Movement appears to be related to related to a creep type mechanism at a movement rate of 10 mm/yr north, 35 mm/yr west and 80 mm/yr down. However, the regional deformation in the area, recorded by the (4 km distant) NETT cGPS station is approximately 35 mm/yr north, 23 mm/yr west and 2.5 mm/yr up. If it is assumed that this background deformation is the same at the Mueller Rockslide site, then the displacement caused by landsliding is actually 25 mm/yr south, 12 mm/yr west and a little over 80 mm/yr down. Recording stopped about two weeks following the burial of the aerial, presumably because snow cover had sufficiently reduced the solar-voltaic power supply.

During July, the solar panel and GPS housing was cleared of snow and several days of recording were achieved before further snow fall (Period 2). There was no evidence of damage to the framing at this time. The GPS aerial was not cleared of snow, so the positions collected during Period 2 in Figure 4.1.8 are not reliable.

In late November the GPS began recording again, presumably several days after the snow had cleared and power was restored. Several days after this, an inspection of the site revealed damage to the GPS aerial and framing. There was no snow covering the rock slab at the time of this inspection. The GPS was removed from the site because it was no longer securely achored to the ground ; unfortuantely, the GPS was removed prior to the heavy rainfall events that started in late December 2011. The GPS aerial stand had been bent by several degrees in an approximately north-west direction, displacing the aerial by about 10 to 15 cm horizontally, and 1 to 2 cm down. This apparent displacement needs to be corrected for at Period 3 in Figure 4.1.8, at least for the plots of latitude and longitude. If the creep rate from Period 1 is projected through to Period 3 (dashed lines in Figure 4.1.8), then the remaining difference between the projected and recorded positions is approximately 12 cm in the northerly direction and 8 cm in the westerly direction. This difference is close to the apparent displacement

amount produced by aerial bending. Therefore, it can be assumed that the creep rate did not markedly differ during the entire monitoring period, and there were no unusually large movements recorded at this site. Consequently, the high movement recorded by the DGPS surveying in the April 2010 to March 2011 interval is quite likely to have occurred after the end of the CGPS monitoring (i.e. after 1st December 2010).

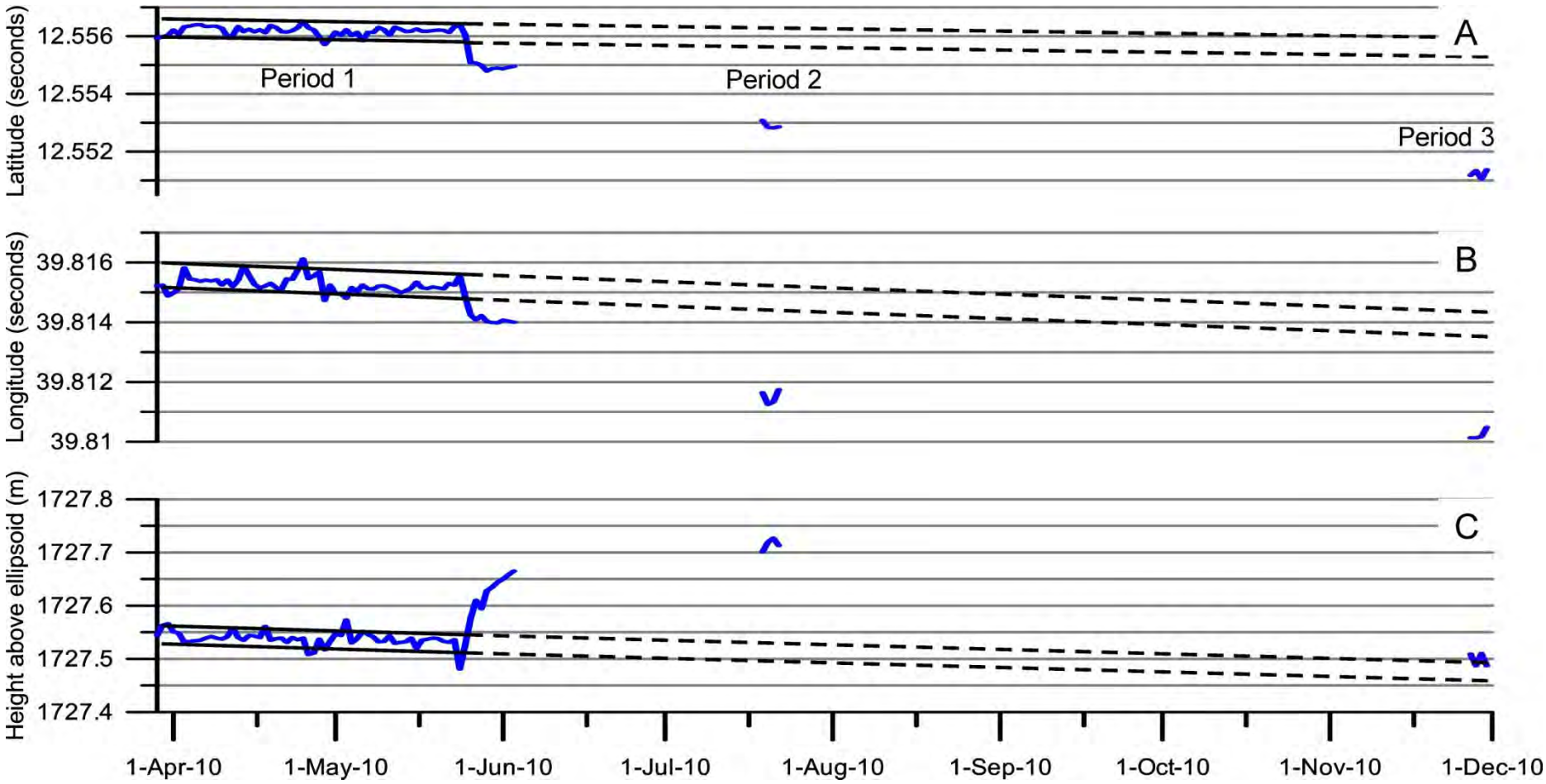

Figure 4.1.8: Mean daily position recorded by the CGPS. At 45 degrees of latitude,1 second of latitude equals approximately 30.87 m and 1 second of longitude equals approximately 21.82 m.

4.1.4.3.3 Cleft-monitoring data

The cleft monitoring data are shown in Table 4.1.2. Because of lost survey pins and uncertainty in pin identification at monitoring line A, interpretation requires caution. It appears that there is likely to have been some continued slumping/displacement of this rock bench, but further monitoring is necessary to determine more accurately how much has occurred.

At monitoring line B there has been a total of 80 mm (15 mm and 67 mm) of crack extension over the 15-year survey interval. This is consistent with the interpretation (based on morphology) that the head of the rockslide is actively undergoing extension at a slow rate (~5mm/yr).

Table 4.1.2: Monitoring line data. Values are in metres. Locations are shown on Figure 4.1.5.

Date:	12/04/1994	3/03/1998	29/03/2011	11/12/2011	7/04/2012
Personnel:	Hancox & Bellringer	Hancox & Bellringer	Vick & Sintenie	McColl & Cook	McColl & Stahl
Monitoring Line A - Previous hut site (slumped bench)					
Hut to Pin 1A	20.0	15.7[a]	missing	snow	16.73[bc]
Pin 1A to Pin 1	11.1	14.8	missing	snow	14.91[cd]
Pin 1 to Pin 2	15.5	15.5	missing	pin 2 found	14.55[d]
Monitoring Line B - Mt Ollivier					
Pin 3 to Pin 4	1.37	[g]	1.75[e]	snow	1.37
Pin 4 to Pin 5	25.1[f]	[g]	25.01	snow	25.01
Pin 5 to Pin 6	18	[g]	18.06	snow	18.067
Pin 6 to Pin 7	7.19	[g]	7.205	7.204	7.205

[a] *Pin 1A lost and replaced for this survey.*
[b] *Hut has been removed. New mark established (nail in end of 4x2 post held upright in centre of cairn) but location may be up to 2 metres from original hut survey position.*
[c] *Pin1A location uncertain - found a steel tube drilled into rock (but no dazzle as reported by Hancox) and it is a couple of metres laterally from expected location on monitoring line transect.*
[d] *Pin1 in expected location but only a dazzle mark was found, not an expansion bolt as had been described by Hancox (1994).*
[e] *Suspicious measurement (different to previous and subsequent measurements, which are identical)*
[f] *Suspected error of original measurement (subsequent measurements have the decimal point shifted)*
[g] *Measurements for this have been lost but Hancox (1998) reports a total increase of 20-80 mm of since 1994.*

4.1.4.3.4 Off-set moraine ridges

During aerial mapping of the rockslide it was noticed that several moraine-like features cut across the slope, potentially providing a means of establishing a longer-term record of movement. The features are 2-5 metre high, linear ridges of debris oriented parallel with slope contours in the mid-lower section of the rockslide (Figures 4.1.3D and 4.1.4.) These appear to be moraines deposited by the Mueller Glacier; striations, rounding, and faceting were apparent on some of the boulders. Some of these features appear to cross, and be offset by, lateral scarps at the rockslide boundary. It was

considered that these features may provide a way to estimate the time that movement initiated and also constrain a long-term movement rate. However, in the field the correlations between the ridges across the scarps, based on visual inspection using morphology and sedimentology, proved very uncertain. Such correlations may be possible with the assistance of quantitative Schmidt hammer rebound-hardness comparisons (e.g. Winkler, 2009), and this will be considered for further field visits.

4.1.4.4 Precipitation records

Comparing seasonal rainfall and snowfall records with the movement data would provide a means to test if there is a relationship between rockslide movement and precipitation. These types of relationship have been identified for other rockslides, for example, the 800 M m^3 Campo Vallemaggia rockslide in Switzerland, in which deformation (measured by inclinometer surveys) could be linked to precipitation events which caused elevated pore-water pressures (Bonzanigo et al., 2007).

An electronic weather station (Mueller Hut EWS) was installed by the National Institute of Water and Atmospheric Research (NIWA) on the Sealy Range close to the Mueller Hut in April 2010. A second active weather station (Mt Cook EWS) is located at Aoraki/Mount Cook village. Unfortunately neither of these stations has a complete record of snowfall or precipitation over the timeframe of interest, but together the data provided by these stations is sufficient to develop a picture of the precipitation pattern.

The rainfall record for Mueller Hut EWS is shown in Figure 4.1.9 over the period between the 14th April 2010, when the site became operational, and mid-December 2011, when instrument/recording errors began; records did not recommence until May 2012. The rainfall pattern shows a distinct seasonality with rainfall totals and rain days being greater in the summer and autumn (December to May) than in winter and spring (June to November). Note the exceptionally large rainfall total of 400 mm on the 28th December 2010, which occurred during a several-week-long wet period. This wet period coincides with the monitoring period in which the greatest displacements were recorded.

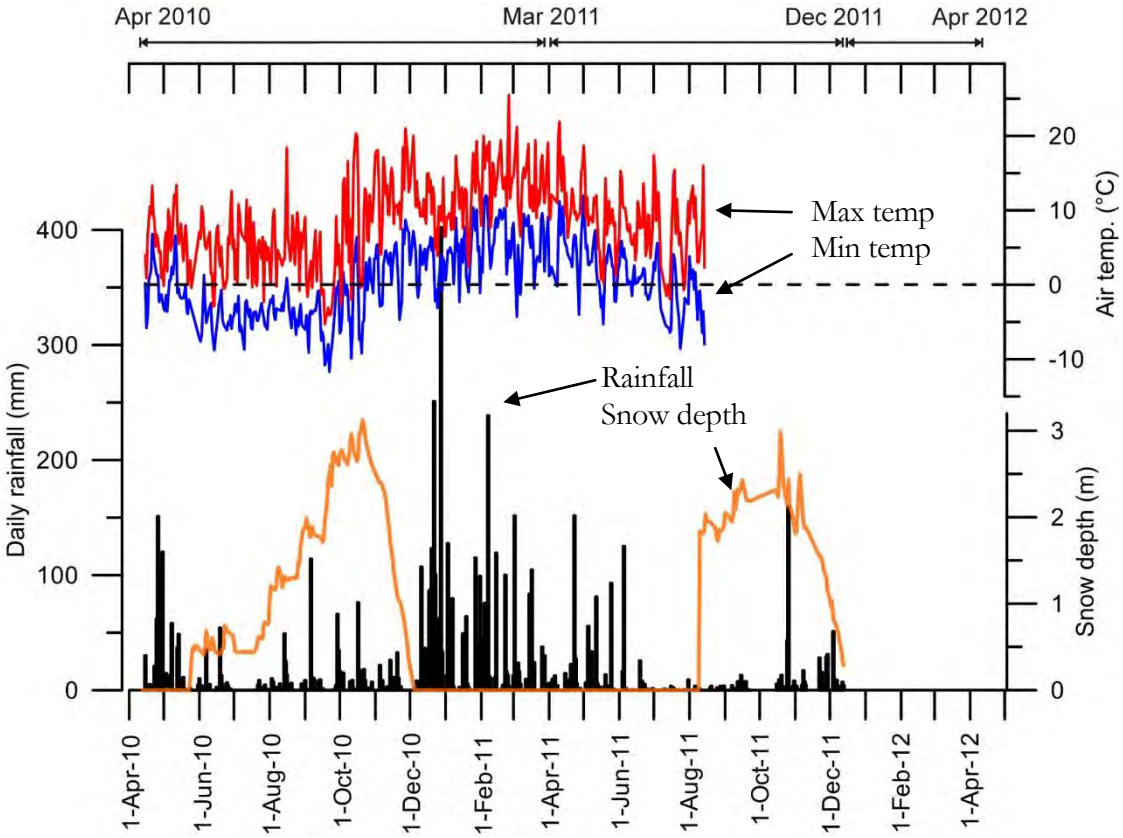

Figure 4.1.9: Daily rainfall totals (black bars), average daily snow depth (orange line), and maximum (red line) and minimum (blue line) air temperature recorded by Mueller Hut EWS. DGPS rockslide monitoring intervals are shown above graph. Rainfall data missing from 23/09/11 to 16/10/11 and after 13/12/11. Snow data missing from 5/12/10 to 9/08/11 and after 12/12/11. Data source: Rainfall and temperature = NIWA CliFlo database; Snow depth = NIWA, manually filtered to remove anomalous spikes. The reliability of the snow data is poor but the author's field observations of snow depth match quite well those of the EWS. For example, the snow depth recorded by the station (0.5 m) in July 2010 fits the field estimate of about 0.4 to 0.7 metres.

Rainfall alone is not representative of total precipitation because much of the precipitation will have fallen as snow during the cooler months from about May to November, as is indicated by the snow depth data in Figure 4.1.9. The relative precipitation contributions from rain and snow correlate with the air temperature, as expected (Figure 4.1.9). Although data are sparse, it appears that, at least compared to 2011, there was heavy snowfall in early spring (September) of 2010 followed by a period of rapid thawing between late-October and the end of November. This is consistent with anecdotal evidence collected by the author (Figure 4.1.10).

To complement the record of precipitation on the top of the Sealy Range, the record from Aoraki/Mount Cook Village is examined (Figure 4.1.11). The station elevation is about 900 m lower than Mueller Hut EWS and further east at the base of the Sealy Range; therefore, it cannot be expected to exactly mimic the conditions at the top of the

ridge, but it should show similar trends. Major (> 200 mm per 24 hr) rainfall events (e.g. 22/12/10; 28/12/10; and 7/2/10) are recorded by both stations. The relative precipitation contributions from snow and rain differ markedly between the two sites. There is much less snow (because the temperature is mostly above 0° C), and there is less seasonal variation in rainfall at Mount Cook EWS. However, at both stations, the period between mid-December 2010 and mid-January 2011 was a particularly wet period with very high daily rainfall totals. This period of rainfall would likely have melted most remaining snow cover on the rockfall; although no snow cover was recorded by the Mueller Hut EWS in early-December, there were still deep pockets of snow in hollows (Figure 4.1.10).

Figure 4.1.10 (on following page): Snow cover on the ground around Mueller Hut at different times of the year: Winter = 17th July 2010; Late spring = 13th November 2009. The toilet (red box) in front of the hut is buried in snow. The thick snow during the spring of 2009 was likely to be similar to that during the spring of 2010. Photo Steve Corin; Early summer = 2nd December 2010. There was surprisingly little snow remaining considering the heavy snow falls in spring. Photo Julia Valigore; autumn = 29th March 2010. Typically there is very little snow remaining by the end of summer, but on occasion it can be completely absent. Photo, Natalya Reznichenko.

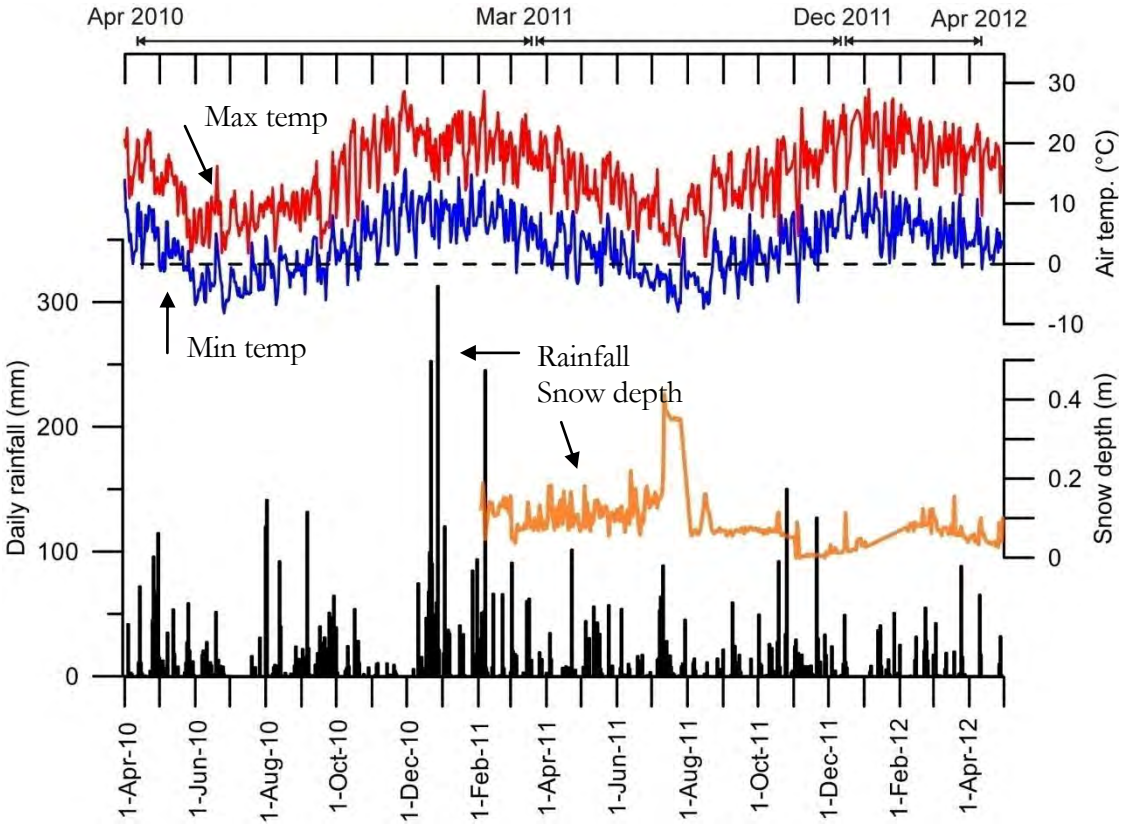

Figure 4.1.11: Daily rainfall total (black bars), daily average snow depth (orange line), and maximum (red line) and minimum (blue line) daily air temperatures for Mt Cook EWS. Data source: NIWA CliFlo database. Note, only large rises in snow depth data are reliable, e.g. July 2011. DGPS rockslide monitoring intervals are shown above graph.

4.1.5 Discussion

4.1.5.1 Causes and movement-rate controlling processes

A number of preconditioning and preparatory factors are identified here as having made the rockslope susceptible to the development of a failure surface, and several processes have been considered that may control the rate of movement. These are presented in Table 4.1.3 and discussed below. Note that in Table 4.1.3, preparatory factors and (initial) triggers are not distinguished because of the difficulty in assessing the relative importance of various preparatory factors in either bringing the slope into an actively unstable state or in the formation of the failure surface. The rate-controlling processes, however, are distinguished because they control the movement rates.

Table 4.1.3: Movement-rate controlling processes and factors considered to have caused or influenced instability of the Mueller Rockslide.

FACTOR	EFFECT	REASON/EVIDENCE
Preconditioning		
Bedding planes and mudstone strata	Creates planar weakness in the otherwise very strong rock	Coincidence of bedding orientation with that of observed slope movement direction (Figure 4.1.7).
Jointing (pre-existing)	Breaks the rock mass up, making it less rigid and less able to elastically respond to tensile, flexural, or shearing stresses.	Coincidence of major joint set orientations with that of the movement direction; toppling and dilation at the top of the ridge consistent with joint control (Figure 4.1.7).
Topography (slope)	Influences the self-weight stresses in the slope, and interacts with the orientation of unfavourable structures, e.g. bedding, joints.	Steep rock slope, at similar orientation to bedding, and the Sealy Range is parallel with one of the joint sets (Figures 4.1.2 & 4.1.4).
Preparatory/trigger		
Glacial erosion	Steepens and undercuts slopes, increasing self-weight stresses can expose unfavourably-oriented structural features	The slope profile is particularly steep towards the lower part of the rockslope (Figure 4.1.2 cross-section). The valley has experienced several glaciations which would have modified the shape of the valley.
Glacier downwasting (debuttressing)	Removes cryostatic confining stresses, reducing the resisting stresses acting on the slope (Section 4.1).	The apparent coincidence of recent (last few hundred years of) glacier downwasting and the development/increased movement of the Mueller landslide.
Stress-release jointing	Erosional and ice unloading of slopes may cause fracturing or growth of existing joints (usually parallel to slope), reducing the frictional strength of the rock mass (Section 2.1.3.2.3).	Dilated and fresh nature of the many of the joints, including many of the slope-parallel bedding joints.
Earthquake shaking	Rock damage caused by earthquake shaking can weaken rock masses and increase site-effects in subsequent earthquakes (e.g. the Rawilhorn rock avalanche, Switzerland; Moore et al., 2012). High ground accelerations can also create new failure surfaces.	Close proximity to the large and active Alpine and Ostler faults. Many large (>100 M m^3) rock slope failures are triggered by earthquake shaking.
Other rock-mass degradation processes	Stress-corrosion, thermal stress, weathering (Section 2.1.3.2)	Unknown influence but appears to be significant in other situations
Rate-controlling processes		
Rainfall/groundwater in the slope	Reduces the normal stress, providing less frictional resistance to movement. This will fluctuate seasonally as well as with weather.	See the following section. There appeared to be a large amount of snow early in the spring of 2010 and a rapid spring thaw, which may have generated a higher water table.
Groundwater fluctuations in the glacier	The cryostatic pressure acting on the valley wall reduces as the water table in the glacier increases. Fluctuations in water table level will cause fluctuations in the slope support provided by the glacier (Section 4.1).	Unknown but the anecdotal evidence of high spring water input may be equally applicable for the glacier.
Changes in the effective viscosity of the glacier	The slope movement rate may depend on the deformation rate of the glacier as the rockslide advances into the ice. This rate will depend on the creep rate of the ice, which is strongly dependent on temperature and stress (Section 4.1).	Unknown but it would likely mean that movement is faster in the warmer months.
Snow loading	Several metres of snowfall on the rockslide, particularly the upper slopes, may be sufficient to increase the driving stress of the landslide.	Unknown, except for the anecdotal evidence of late heavy (and presumably wet/heavy) snow in the spring of 2010.
Seismicity	Ground accelerations from seismic shaking providing transient increases in the driving stress. The duration of response (movement) may be extended considerably because of the gradual deformation response of the glacier.	CGPS data indicates that the 7.1 M_w Darfield earthquake did not cause significant movement, but stronger shaking may trigger movement in the future.

4.1.5.1.1 Preconditioning factors

The geological formation of the rock slope predisposes the slope to instability; the bedding plane weaknesses have been steepened as the anticline formed and flexural fracturing further weakened the rock mass. At this stage however, the specific configuration of the slope may have been sufficiently stable and a failure surface may not have yet developed. This state may have existed for many hundred-thousand years.

4.1.5.1.2 Preparatory factors

The slope may have remained in a stable condition until such a time that erosion, (especially glacial erosion), weathering, or seismic perturbations reduced stability sufficiently for a complete failure surface to develop. However, even if a failure surface had developed, the slope may have existed in a marginally stable state for many thousands of years without moving significantly. Instability would depend on the balance of driving and resisting stresses, and particularly on the cryostatic and viscous support provided by the glacier (Section 4.2). During full glaciation, the glacier would have been in contact with much of the slope. Once the Mueller Glacier began downwasting at the end of the last glaciation (approx. 15 ka), the cryostatic pressure acting on the slope began to reduce and the rock mass may have been weakened further by more intense weathering and stress-release induced joint development. Eventually, but possibly as recently as the last few hundred years, this may have been sufficient to bring the slope to an actively unstable state. At this stage, and in the present-day situation, the movement-rate of the slope is dependent on a number of other factors, some of these external.

4.1.5.1.3 Rate-controlling processes:

The high movement recorded during the first DGPS monitoring interval (April 2010 to March 2011) coincides with both the late spring cold weather and snowfall followed by warm weather, and with the very high rainfall totals and wet period in early summer. These data suggest a possible correlation between slope movement and precipitation.

Precipitation could influence stability in several ways (Table 4.1.3). The additional weight of snow will increase the driving stress (Crozier, 1986, p 45). However, the snow will also increase the normal stresses and therefore frictional strength of the failure

planes, so a reduction in stability for a cohesionless planar failure surface (i.e. a planar rockslide controlled by frictional strength) will only occur if the snow loading is greater at the top of the slope, effectively increasing the angle of the slope. Since there is a reasonably large elevation difference between the top and bottom of the slope (about 600 m), more snow would accumulate in the colder upper part of the slope, especially in the small hollows in the flattish part of the upper ridge. Therefore, snow loading may reduce stability, and increase movement during the winter. It seems unlikely that the increased movement in the first monitoring interval was caused in any significant way by snow loading. This is because although in the first year there was a lot of snow produced in the early spring, the total snow depth and duration of thick snow cover was not greater than in the following year (Figure 4.1.9). The snow in 2010 however, may have marginally lowered the stability of the slope and provided a source of meltwater that further reduced stability later in spring.

Rainfall and snowmelt infiltration of high intensity over a several week period could have increased the groundwater levels in the slope, reducing the stability of the rockslide by increasing the driving, or by reducing the resisting, forces acting in the slope (Crozier, 1986, p. 79) (Table 4.1.3). This could occur in several ways: (i) Rapid infiltration of water to the slope may increase pore-water pressures acting on the failure surface(s), lowering effective normal stresses and therefore the effective shear strength of the failure surface; (ii) increased infiltration may increase pore-water pressure acting on joint surfaces (cleft-water pressures). This will reduce the frictional strength of both horizontal to sub-horizontal joints, and for vertical to sub-vertical joints, the stress may produce additional lateral driving force; (iii) if the hydraulic gradient in the slope is steepened (i.e. flow of water in a down-slope direction increases), this will exert a greater driving (drag) stress in the slope.

High amounts of rainfall, snow and ice melt, and runoff from the catchment are likely to also increase the water table elevation in the glacier. As this occurs, the cryostatic force acting on the toe of the rockslide decreases, therefore reducing the lateral support (discussed in Section 4.2). This assumes that the rock mass is sufficiently permeable, otherwise the hydrostatic pressure will counter the reduced loss of lateral cryostatic support; this is a reasonable assumption because of the jointed nature of the rock mass.

The high movement rate in the first DGPS monitoring interval coincided with the September 2010 Darfield 7.1 M_w earthquake and several other major aftershocks following the September event, including a 6.3 M_w Christchurch earthquake in February 2011. However, the CGPS data does not indicate any significant movement associated with the Darfield earthquake, despite potentially strong ground motions. A strong-motion seismometer at Aoraki/Mount Cook Village recorded peak horizontal ground accelerations of 0.184 m s^{-1} for the Darfield earthquake (Figure 4.1.12), and a Mercalli Modified felt intensity of 4 was reported by two people in the village (Figure 4.1.13). Historical records from New Zealand indicate that slope failures are rarely triggered by earthquakes when the shaking intensity is lower than MM6 (Hancox et al., 2002). This relationship was developed primarily from first-time or catastrophic failures. The reactivation of an existing slope failure or the movement of a slope that is already at a point of critical stability, may be triggered by less intense shaking than this. Further, the shaking experienced on the top of the Sealy Range may have been several times greater than that recorded at the village due to the amplification of seismic waves by topography (Section 4.3.2). Given that the orientation of the ridge was perpendicular to, and the rockslide slope aspect was facing away from the likely direction of seismic wave propagation (from the east), the conditions were favourable for topographic amplification of seismic shaking. Further, although the Darfield earthquake caused relatively few mass movements in the Canterbury area, as compared to locally more intense aftershocks, a moderately large (c. 50,000 m^3) slope failure and several precursor rockfalls occurred 175 km away near Kaikoura in the days following the Darfield earthquake and are thought to have been (partly) triggered by shaking (Hancox, 2010). Therefore, although from the data available it appears that the earthquake shaking did not trigger significant movement, it may have further reduced the stability of the slope or caused minor movement not detected with the CGPS data.

In conclusion from the evidence collected, in appears that there is a component of steady creep movement, of some tens of millimetres per year (which may be considerably greater in the more active lower parts of the rockslide), and heavy rainfall events or prolonged wet periods can cause accelerated movement.

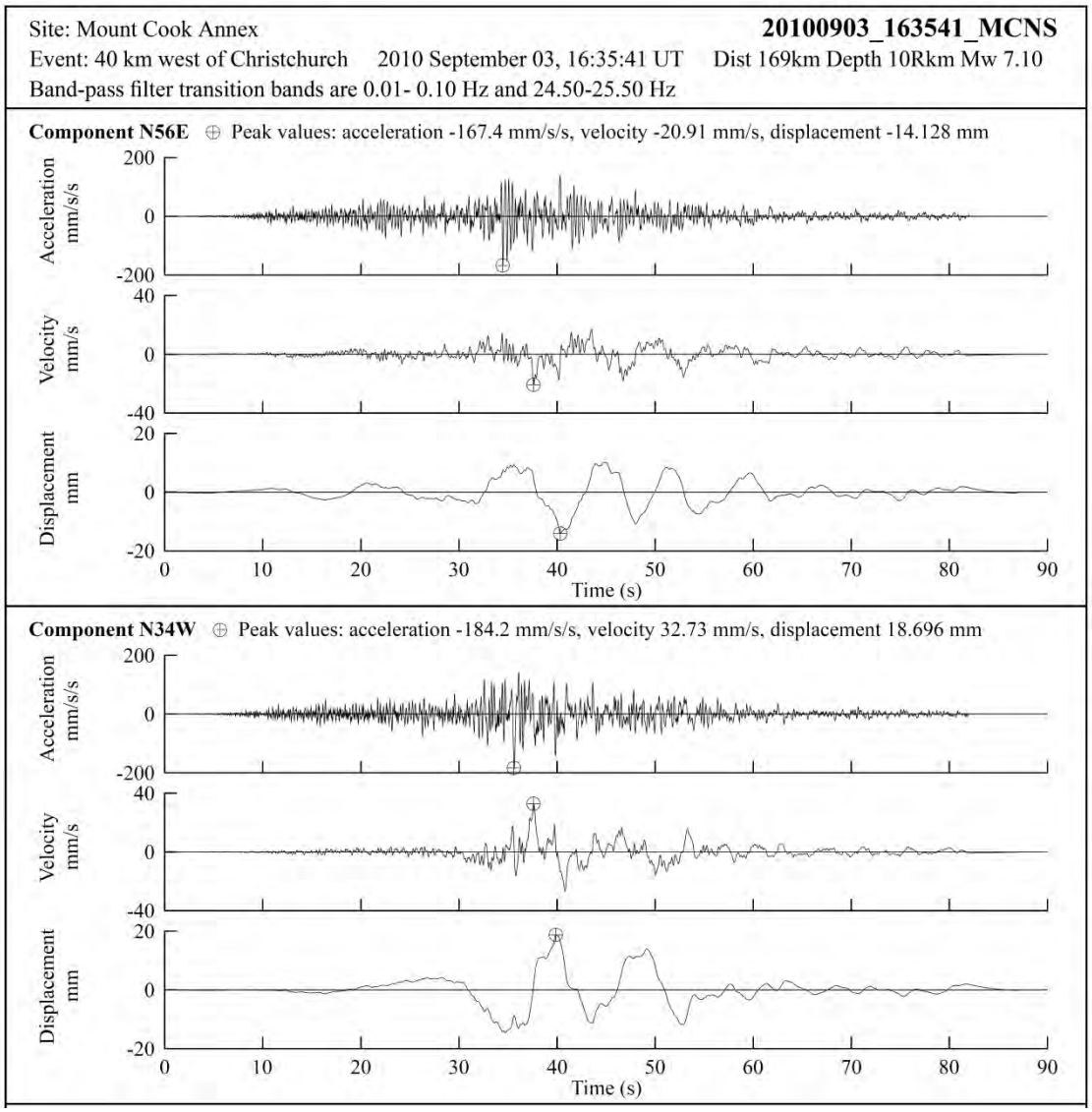

Figure 4.1.12: Horizontal shaking amplitudes and duration for the September 2010 Darfield earthquake, recorded at Aoraki/Mount Cook Village. The vertical motion was about half of that of the horizontal motion. Data source: GeoNet strong motion database. ftp://ftp.geonet.org.nz/strong/processed/Proc/2010/09_Darfield_mainshock_extended_pass_band/Vol2/plots/20100903_163541_MCNS.pdf

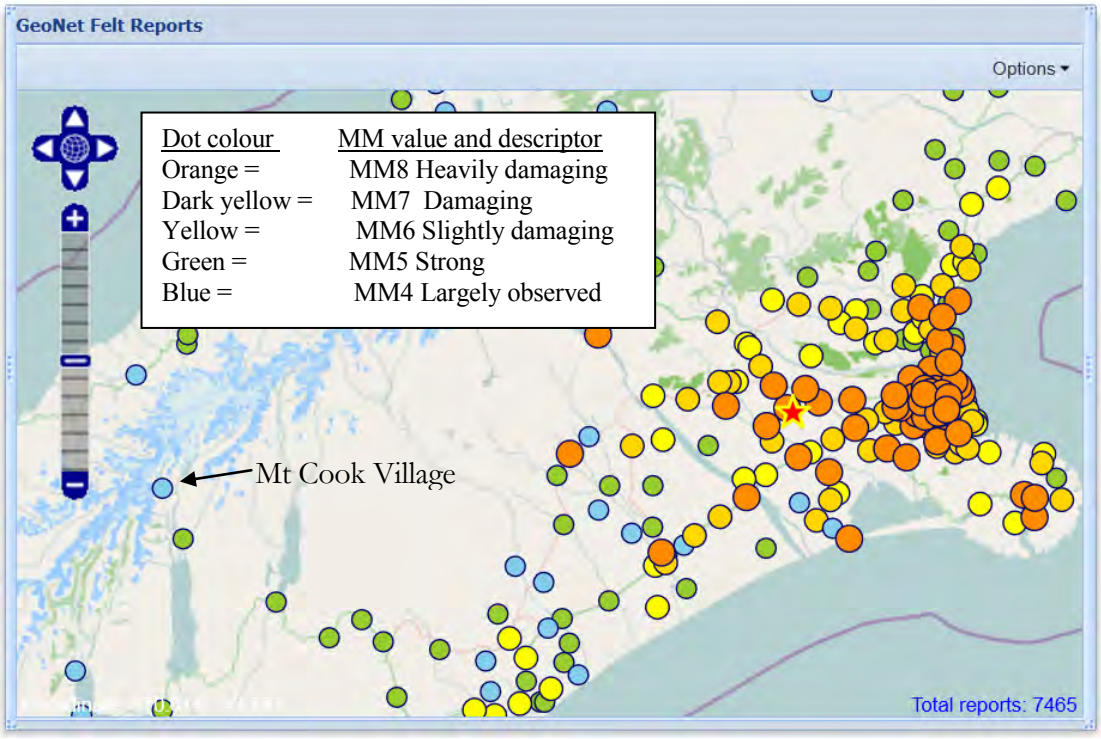

Figure 4.1.13: Modified Mercalli intensity values for the Canterbury region from the September 2010 Darfield earthquake, obtained from GeoNet's online felt reports: (http://geonet.org.nz/earthquake/quakes/3366146g-shaking.html).

4.1.5.2 Impacts of slope movement and catastrophic failure

Here I briefly consider the impacts of continued movement or the catastrophic failure of the rockslide. Continued thinning of the glacier, or gradual reduction in the strength of the slope will reduce the stability of the slope. This is likely to increase the creep rate of the rockslide and reduce the triggering thresholds for movement to occur (e.g. movement will be triggered by smaller rises in groundwater). Aside from co-seismically triggered failures, many catastrophic rockslide failures are preceded by a period of accelerated movement (Voight, 1989; Kilburn and Petley, 2003). This does not mean that the Mueller Rockslide will necessarily follow this pattern and result in catastrophic failure, but it is a possibility. Given the proximity of the site to high-magnitude earthquake sources (the Alpine and the Ostler faults), there is also a high probability that the site could experience severe earthquake shaking, which could be sufficient to trigger catastrophic failure. It is worth considering what consequences these scenarios may have, especially if the failed mass has the potential to become a long-runout rock avalanche.

4.1.5.2.1 Rock-avalanche runout

In the event of a catastrophic failure the collapsed debris may fragment and travel several kilometres down the glacier as rock avalanche. The potential for this to happen can crudely be assessed by comparing some of the geometric characteristics of the rockslide with that of other events that have generated long-runout behaviour. Regression equations between two pairs of three geometric parameters (volume, maximum fall height, and maximum length) for 32 non-volcanic landslides that developed long runout are provided in Table 4.1.4 (Legros, 2002 and references therein). Based on the regression equations, and different estimates of starting volume, predicted distances that rock avalanche debris could attain are provided in Table 4.1.4. In Table 4.1.4, L_{max} and H_{max} are the distance from the top of the failed mass to the distal end of the mobilised material in the horizontal and vertical planes respectively. For a volume of 150 M m^3, the predicted distance and fall height are L_{max} = 5.5 km and H_{max} = 1300 m. Given that the lake at the Mueller Glacier terminus is only about 900 metres below and 5.5 km distant from the top of the Mueller Rockslide (following the path of the glacier), there is potential for mobilised debris to reach the lake, based on this analysis. However, the R^2 values for the correlation between volume and H_{max} and L_{max} are quite low, meaning that there could be high variation (error) in the predicted values for any given event. One of the reasons for the error is likely to be variations in the geometry (e.g. confined or unconfined) and material (e.g. low-friction ice or deformable substrate) of the travel path.

The correlation between H_{max} and L_{max} is slightly better than the correlation between volume and H_{max} and $L_{max,}$ (Table 4.1.4). The potential fall height for the Mueller Rockslide is somewhat limited because after reaching the glacier surface (with a maximum fall of c. 500 m), the runout path down the valley becomes quite gentle (c. 10°) and very gentle (c. 5°) beyond the end of the glacier, and probably then impeded by terminal moraine. On the assumption that H_{max} is limited by about 1100 m, the correlation between H_{max} and L_{max} provides another estimate of L_{max} for the Mueller Rockslide. Using fall height as the variable, the L_{max} predicted for a range of H_{max} estimates from 500-1100 m ranges from about 1.5 km to 5 km – thus slightly more favourable estimates of travel distance.

The likelihood of the debris from catastrophic failure reaching the proglacial lake is however, going to increase as the lake extends further upvalley and the glacier thins. Therefore, although presently the travel distance of the debris would need to be at the upper end of the estimates made here using empirical data, in time the likelihood will increase and this may provide sufficient incentive for developing an early warning system in the event of accelerating movement (Section 4.1.5.2.4).

Table 4.1.4: Estimates of the runout distance and fall height of the Mueller Rockslide resulting from catastrophic failure; based on empirical data for 32 non-volcanic long runout landslides presented (data from Legros, 2002 and references therein).

		Distance L_{max} (km)	Fall Height, H_{max} (km)	Distance L_{max} (km)
	Regression type:	Logarithmic	Logarithmic	Power
	Equation:	y = 1.2106ln(x) + 7.8162	y = 0.1216ln(x) + 1.535	y = 4.1669x1.2684
Variable (x)	R-squared value:	0.4464	0.248	0.657
Volume (km^3)	0.1	5.0	1.3	
	0.15	5.5	1.3	
	0.2	5.9	1.3	
	0.3	6.0	1.4	
Fall Height H_{max} (km)	0.5			1.7
	0.7			2.7
	0.9			3.6
	1.1			4.7

4.1.5.2.2 Dilation of the ridge at Mueller Hut

Another hazard associated with ongoing movement of the slope is the threat to the Mueller Hut and persons in it. Whether or not this part of the ridge could fail catastrophically along with the rockslide is uncertain, but it is likely that as movement continues, and if the rockslide does fail catastrophically, there will be additional and probably accelerated dilation of the ridge. The gradual dilation of the ridge in itself is probably not cause for alarm but continued monitoring of this part of the slope is recommended. Sub-surface investigations could be carried out to confirm whether or not there are unfavourable structures (e.g. bedding) that could provide a failure surface for sliding. If such a surface exists (although geological evidence provided in this study

indicates that bedding is gently dipping to the north at this location; Figure 4.1.2), then relocating, or possibly removing the hut, would seem an appropriate measure to take.

4.1.5.3 Recommendations for future research:

Although the dominant controls on the stability have been identified, without high-resolution temporal (i.e. hourly) data, such as that provided by CGPS, it is impossible to determine the variation and controls on creep and accelerated movement episodes, or to confidently link movement with triggering processes such as precipitation or seismicity. Unfortunately, the attempt to obtain CGPS data in this study was largely unsuccessful because of damage sustained to equipment. Considering that the magnitude of movement that was identified using the DPGS and crack monitoring suggests a high rate of activity, another attempt at high-resolution monitoring would be useful. Perhaps, given that the terrain proved too hostile for installation of equipment on the site itself, alternative monitoring and assessment approaches need to be applied. In this Section I discuss different slope monitoring approaches, what value they can add, and comment briefly on how they may be used to develop a warning system.

4.1.5.3.1 Remote sensing

One (preferred) monitoring approach would be to use an automatic ground-based radar system (GB-InSAR or Slope Stability Radar) to capture regular (i.e. sub-daily) images for interferometry analysis (e.g. Harries and Roberts, 2007; Gischig et al., 2009; Casagli et al., 2010). The advantages of this technique over CGPS are that the equipment can be installed on 'stable' ground off the rockslide (e.g. just north of the rockslide at approximately 1450 m.a.s.l.; Figure 4.1.5), it collects a much wider spatial distribution of data than the CGPS point measurement, and it removes the need for personnel to be on the unstable active parts of the rockslide. The disadvantages of this technique are the limited availability of the technology, intensive data processing (especially for daily image capture), specific requirements for line of sight orientation with respect to movement direction, difficulties comparing movement with traditional survey measurements, and equipment robustness (i.e. needs to sustain heavy snow and wind loading). Similar advantages and disadvantages apply for robotic total stations, which offer another technique for monitoring slow-moving landslides (e.g. monitoring of the

West Taihape Landslide, New Zealand; Massey, 2010). However, for robotic total stations, which take very precise (mm) measurements of survey prisms installed within line of site using an electronic distance meter, a higher precision and reduced processing intensity is offset by a reduced spatial coverage, the need to deploy prisms on the rockslide itself, and, unlike the radar, it requires clear air (i.e. no rain or fog to block the line of sight to the prisms).

These methods could also be complemented with other forms of remote sensing or surveying, such as repeat air-borne Light and Ranging (LiDAR), repeat satellite-borne InSAR, or repeat aerial photogrammetry surveying (Wieczorek and Snyder, 2009). Although these techniques typically cannot achieve the same level of temporal resolution as terrestrial radar or robotic total station surveys, they can provide a wide spatial coverage with relatively good resolution, and can be done remotely (Strozzi et al., 2005; Wieczorek and Snyder, 2009; Strozzi et al., 2010).

Whatever approach is used, to develop a full understanding of the causes of slope movement it may be necessary to monitor the slope for several years in case apparent links between factors like precipitation are only coincidental, as has been found for other rockslide monitoring programs (Eberhardt et al., 2008). This problem is well illustrated with the detailed monitoring program for a rock slope (Checkerboard Creek) in British Columbia, Canada. It was discovered only after several years of monitoring that regular annual periods of increased displacement were not related to precipitation events as indicated in the first years of monitoring, but were actually caused by seasonal changes in temperature (Watson et al., 2007).

4.1.5.3.2 Ground investigation

Even with high-resolution monitoring to relate periods of high movement with an external factor, the mechanism responsible for increasing movement may remain unknown without additional sub-surface information. For example, monitoring of groundwater levels and permeability in the slope and in joints may be required to establish whether a precipitation event causes movement because of increased pore-water pressure, a reduction in cohesion at the failure surface, because of cleft-water pressure, or because of increased seepage forces. This can be done with the installation of ground-water monitoring bore-holes (piezometers) with automatic data logging

capability. Further, the geological model, which for the Mueller Rockslide assumes movement along a failure surface at some depth that daylights somewhere below the surface of the Mueller glacier, will require sub-surface investigations. This could be achieved with core-logging of drill-holes to identify shear surfaces or some form of geophysics to identify failure surface (e.g. ground penetrating padar, seismic refraction, and resistivity surveys used to identify failure surfaces for the Åknes rockslide in Norway; Ganerød et al., 2008). The down-hole installation of devices such as inclinometers or geophones to measure microseismic tremors generated by slip on failure surfaces (e.g. the study of the Randa rockslope in Switzerland; Spillmann et al., 2007), can provide information on the distribution of displacement within the sub-surface and help relate movement at depth with surface movement data.

4.1.5.3.3 Numerical modelling

Numerical analysis can be another useful tool to help confirm the geological model or the link between movement and external factors, as well as providing a tool for helping to predict future behaviour (Eberhardt et al., 2008). The accuracy of the numerical model depends on both the ability of the model to reproduce the mechanical behaviour of the slope and the selection of representative material models and parameters. For the Mueller Rockslide, a discontinuum analysis (e.g. UDEC or alternative discrete element program) is probably necessary for reproducing the slope behaviour because of the strong influence of discontinuities (bedding planes and joints). To be able to model the potential influence of the glacier, an appropriate constitutive model will need to be applied (Section 4.2).

4.1.5.3.4 Warning system: considerations

The scope of this chapter does not include risk assessment for the Mueller Rockslide or a discussion of whether a warning system should or should not be implemented here. However, given that the rockslide is active, very large, and in the vicinity of a village, it appears to be prudent. Successful implementation of a warning system requires adequate understanding of the slope behaviour in order to set appropriate thresholds for triggering an alert (Eberhardt et al., 2008), as well as a process for effectively alerting the end-user; the thresholds may be based on either an internal physical variable (e.g. movement

acceleration; Crosta and Agliardi, 2002; Crosta and Agliardi, 2003; Kilburn and Petley, 2003) or an external environmental variable (e.g. rainfall or snowmelt; Crosta et al., 2012). Successful implementation therefore requires collection of sufficient information, which can be done by using the approaches and tools recommended above. The technology and the equipment required to do this are expensive, and the installation of equipment, disturbance of ground (in the case of drilling), and helicopter logistics within the National Park add to the cost and difficulties of high-resolution and sub-surface monitoring. Further, the environmental conditions (freezing temperatures, snow and high wind), and the possibility of damage to equipment from rockfall, snow avalanche, snow-pack sliding, keas (alpine parrots), and the possibility of complete loss of equipment in the event of catastrophic failure, adds to the risk of adopting some of the monitoring techniques. These costs and constraints need to be weighed up against the benefit, which is a responsibility that ultimately falls on the land manager (DoC).

Note that there is no reliable method for predicting failure triggered by earthquake shaking, so it is not considered here in the context of early warning systems. However, experience from other places has shown that there is a period of increased likelihood of slope failure in the months following a major earthquake because of incremental weakening of the slope during the mainshock and subsequent aftershocks (e.g. Moore et al., 2012). Therefore, if the site experiences strong ground shaking as a result of a large earthquake, the slope should be considered to have a higher likelihood of failure for the proceeding few months.

Another consideration is how much warning time can be achieved after catastrophic failure has commenced. This depends on the rock avalanche velocity and travel distance (~5 km in a few minutes) and tsunami wave velocity and travel distance (~ 5 km in 5 minutes; ~ 10 minutes in total). This small amount of time is insufficient for effective evacuation of the area but it may provide time for persons to shift to higher ground within the area (e.g. ascending the 50 m high moraine at the campground, or for persons in the village to move to the more elevated areas).

4.1.5.4 Summary and conclusions

The development of the Mueller Rockslide is likely to be a result of the combination of unfavourable geology, the modification of the slope by erosion, and the relatively

recent downwasting the Mueller Glacier. The major mechanism of movement appears to be deep-seated sliding on steeply dipping bedding structures, which is in turn causing relaxation and dilation at the top of the slope (retrogressive failure), and toppling and rockfall at scarps.

Geologic and geomorphic evidence (i.e. orientation of bedding and movement direction) suggests that the Mueller Glacier is partly supporting the toe of the rockslide. Given the known ductile behaviour of ice (Section 4.2), the glacier may regulate the movement rate of the rockslide (e.g. true creep or damping of episodic movements). If the glacier continues to thin, the stability of the rockslide is likely to decrease. Eventually, if the driving stresses exceed the strength of the slope (and the brittle strength of the ice), or if a failure plane is exposed, catastrophic slope failure could occur.

Monitoring with DGPS and CPGS since April 2010 indicated that the most active (monitored) part of the rockslide normally crept at a rate of several millimetres per month but episodic movements of several metres may be triggered by rainfall events.

This study provides the groundwork and the justification for a more detailed slope monitoring study. It is recommended that slope monitoring is continued and a high temporal-resolution monitoring system be established. This is necessary to more confidently link periods of movement with external triggers and to assess how the glacier influences movement. Additional sub-surface instrumentation or geophysical surveys, and numerical modelling, may also be required to help interpret surface data and the mechanisms controlling slope deformation. Such tools will also be necessary for setting up a reliable warning system to provide advanced warning in the event of movement acceleration leading to catastrophic failure.

4.2 PART B: LARGE ICE-CONTACT SLOPE MOVEMENTS: GLACIAL BUTTRESSING, DEFORMATION AND EROSION

Large ice-contact slope movements: Glacial buttressing, deformation and erosion, McColl ST; Davies TRH, *Earth Surface Processes and Landforms*, (in press), Copyright © 2012 John Wiley & Sons, Ltd.
http://onlinelibrary.wiley.com/doi/10.1002/esp.3346/full

Only formatting and pagination has been modified for production in the thesis

Abstract: Glaciers and slope movements may act simultaneously to erode and modify glaciated slopes. Undercutting by glaciers can destabilise slopes but the extent to which slope failure may progress prior to subsequent glacier withdrawal has not hitherto been considered. The traditional view has been that the buttressing effect of ice prevents slope movement. The problem with this view is that ice is one-third the density of rock and flows under low applied stress. Consequently, failed slopes may move into the glacier if they exert a stress in excess of the resistance provided by the glacier. Slope movement rate depends on ice rheology and other factors influencing driving and resisting stresses. Simple viscous equations are used to investigate these variables. The equations predict that small (< 125,000 m^3) ice-contact rockslides can deform ice at several mm/year, increasing to several m/year for very large (>10^8 m^3) rockslides. To test these estimates, field evidence is presented of slope movements in glaciated valleys of New Zealand; narrowing or squeezing of glaciers adjacent to unstable rock slopes is demonstrated and considered to be the result of slope movement. For one site, geomorphic mapping and slope movement monitoring data show that movement rates are of similar order of magnitude to those predicted by the viscous equations; closer agreement could be achieved with the application of modelling techniques that can more realistically model the complex slope geometries and stability factors encountered, or by obtaining additional empirical data to calibrate the models. This research implies that, while the concept of glacial debuttressing – the reduction of slope support from withdrawal of glaciers – is valid, complete debuttressing is not a prerequisite for the movement of ice-contact rock slopes. These slope movements may contribute to the

erosional processes of glaciers and the evolution of glaciated slopes in a previously unrecognised way.

4.2.1 Introduction

Over time scales of tens of thousands of years, glacial erosion and mass movements modify the shape of mountains. Glaciers sculpt out landforms such as glacial troughs, hanging valleys and cirques, delivering large volumes of sediment to proglacial systems. At similar time scales, mass movements can completely alter the shape of mountains, but usually doing so in discrete, episodic events; the c. 27 km^3 Green Lake Landslide in Fiordland, New Zealand is a dramatic example of this (Hancox and Perrin, 2009). Landsliding also delivers huge volumes of sediment to valleys (Korup et al., 2004). While both glaciers and mass movements dramatically modify landscapes and produce large quantities of sediment, they are usually studied as independent processes within their respective disciplines. Interactions between the two processes have been gaining attention, for example, increasing awareness of the role that large rock avalanche deposit emplacement onto glacier surfaces has in altering the mass balance of glaciers (e.g. Reznichenko, 2012; and references therein). Also, the role that glacial steepening of valley walls and subsequent deglaciation (debuttressing, i.e. removal of lateral support by the glacier) has in causing slope instability has been a subject of much interest to geomorphologists over the last few decades (see reviews by Ballantyne, 2002; McColl, 2012). However, the possibility that glacial erosion and mass-movements may operate in unison, simultaneously modifying the shape of mountains, has hitherto not been investigated.

Glacier ice is a ductile material that flows under very low applied stresses, and has a density about a third that of rock (~ 920 kg/m^3 cf. ~2700 kg/m^3). It has been proposed that these properties make glaciers incapable of permanently supporting unstable valley walls (McColl et al., 2010). If true, it would add to our understanding of how slope movements in glaciated terrain develop, because previous studies (reviewed by McColl, 2012) have focussed only on their development subsequent to the removal of buttressing support provided by glaciers. Slope failures, initiated by glacial erosion or other factors

such as earthquake shaking, could deform the walls of glaciers and eventually become entrained by the glacier. Consequently, i) the debuttressing of valley walls during recession of glaciers may not be, in all circumstances, a pre-requisite for the initial movement of glaciated slopes; ii) slope movement may constitute a previously unrecognised source of sediment in the glacial system; and iii) slope movement may contribute to the development of glacially-modified valleys during periods of glacial erosion in addition to periods after glacier erosion has ceased.

Deep seated gravitational slope deformation (DSGSD), also known as deep-seated creep, is the very slow (<1.6 m/yr , IUGSWGL, 1995) deformation of rock slope masses larger than about 200,000 m^3 (Dramis and Sorriso-Valvo, 1994; Pere, 2009). This type of slope movement is common in high-relief and glaciated terrains (Beck, 1968; Bovis, 1982; Bovis, 1990; Bovis and Evans, 1996; Holm et al., 2004; Ambrosi and Crosta, 2006; Agliardi et al., 2009b; Hippolyte et al., 2009; Pere, 2009; El Bedoui et al., 2011; Pánek et al., 2011). DSGSDs are typically recognised by features such as scarps and uphill-facing scarps, sackungen, tension cracks and toe bulging, and can involve large (>100 m downslope) displacements of rock at rates of a few millimetres to several metres per year (Figure 4.2.1). DSGSDs are an important mass-wasting process and can develop into catastrophic slope failures (Evans and Couture, 2002; Crosta and Agliardi, 2003), making their study important for understanding landscape evolution and for reducing landslide hazards in mountainous areas.

Most studies of DSDSDs in glaciated terrain have been of slopes long-since disconnected from the glacier. Several of these DSDSDs have been considered to have become active long after ice downwastage or retreat, which is sometimes supported based on either dating of landslide surface features (e.g. Cossart et al., 2008; Agliardi et al., 2009a; El Bedoui et al., 2011) or numerical modelling studies of failure conditions (e.g. Bovis and Stewart, 1998; Ustaszewski et al., 2008; Ambrosi and Crosta, 2011; Ghirotti et al., 2011). In some of these situations this may be the case. However, it is unlikely that datable landslide features, which developed prior to glacier retreat, would be adequately preserved because of glacial erosion and burial in glacial sediments. Further, all of the numerical models have assumed elastic properties for the glacier ice. It is possible that some of those DSGSDs, and others that remain unidentified, initially developed failure surfaces, instability and motion prior to complete glacier retreat – a

process unlikely to be reproduced with models that use elastic ice properties. Subsequent glacier retreat would have accelerated movements and allowed the development and preservation of fully-developed and datable surface expressions. In any case, an understanding of how these slopes develop failure surfaces and begin moving is a critical area of research. Advancing this research requires studies on active ice-contact slope failures and methods for their investigation. Active slopes in contact with ice have been monitored in the Swiss Alps; two active rock slope deformations, in contact with opposite sides of the terminus of the Great Aletsch Glacier, have been monitored using a range of remote sensing and ground based surveying techniques (e.g. Kääb, 2002; Strozzi et al., 2010). Displacements of several centimetres per year have been recorded for these slopes. The extent to which the movement of these slopes affects (deforms) the glacier has not yet been established, but it is a target of investigation.

To test the hypothesis that destabilised ice-contact slopes can move and deform glacier ice, simple equations for estimating the necessary conditions for, and movement rate of, ice-contact slope movements, are tested with field evidence from New Zealand.

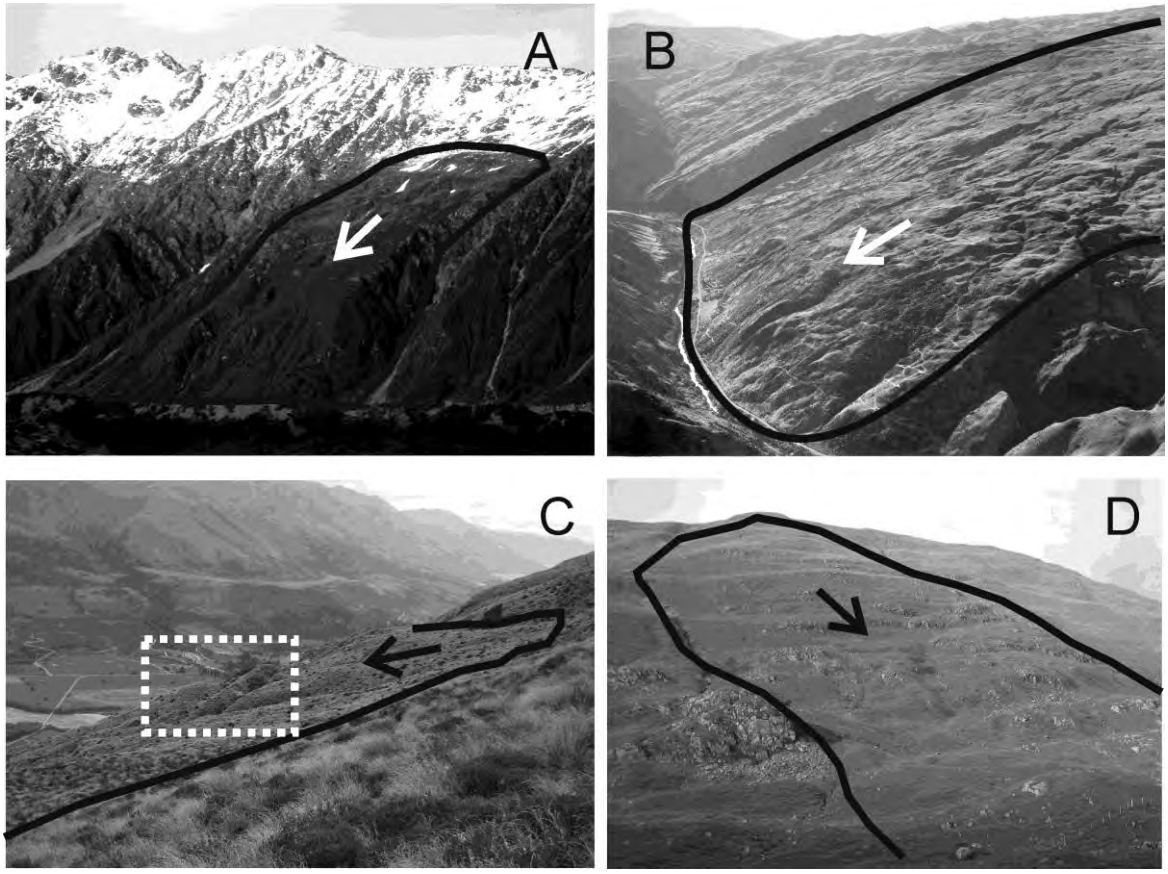

Figure 4.2.1: Deep-seated rock slope deformations outlined with black lines and movement direction indicated with arrow. All sites have been glaciated in the past: (A) Sealy Tarns, on the eastern side of Sealy Range, Mount Cook National Park, New Zealand, with moraine from the Mueller Glacier shown in foreground. Bedrock is well-indurated sandstone with bedding dipping into the slope. The slope outlined is approximately 600 metres high and 400 metres across; (B) Kawarau Landslide, Otago, New Zealand. Bedrock is schist with foliation dipping towards the river in the lower part of the landslide. The slope outlined is approximately 2 km wide (photo Lloyd Homer); (C) Mount Alfred, Otago, New Zealand. Large (c. 10 m high) sackungen outlined in centre. Bedrock is schist with foliation dipping into the slope; (D) A distinctive portion of the Beinn Fhada DSGSD, Scotland. Bedrock is Moine Gneiss with foliation dipping into the slope. Approximate height of the slope is 500 metres. A fence in the lower right provides scale (photo Verne Pere).

4.2.2 A simple model of rock sinking through ice

To understand how slope movement may deform glacier ice, it is necessary to consider the forces involved. Bovis (1982) suggested that valley wall instability caused by glacial erosion may lead to an elastic bulging of the valley wall into a glacier because of the density difference of ice and rock. Non-elastic deformation of the valley wall, produced by rock-creep, sliding, toppling, or a rock-fall mechanism, generates stresses in the ice and will also cause an elastic response in the ice. However, non-elastic ice deformation (i.e. flow) will also occur at strain rates below the ductile-brittle transition for ice, which is about 10^{-3} to 10^{-7} s^{-1} (Schulson, 1999). Consequently, a glacier may be able to prevent rapid catastrophic collapse of a valley wall due to the elastic strength of ice at high strain rates but may not prevent the gradual, permanent deformation of the valley wall. The rate of this deformation will depend on the magnitude of stress and the flow resistance of the ice.

Glacial ice deforms by power-law creep, largely from dislocation slip on the basal plane within individual ice crystals (basal glide), but also from other mechanisms including sliding at grain boundaries within the lattice of ice crystals (Schulson, 1999; Marshall, 2005). Here we simplify this complex mechanical behaviour by approximating ice as a viscous fluid with very high effective viscosity ($\sim 2 \times 10^{13}$ Pa s) and without a definitive yield stress (Hooke, 2005, p13), in order to estimate the rate at which rock slope collapse will deform a glacier.

First, consider a rock suspended in ice beneath the surface of a glacier. The rock exerts a gravitational stress on the ice that is proportional to its buoyant mass. The rock is sinking, albeit very slowly and probably not measurably before the rock is transported

to the end of the glacier or exposed by surface ablation. Following Stokes' law for settling particles, the terminal (steady state) velocity, v_t (m/s), of the (cube-shaped) rock as it sinks through the viscous ice can be approximated by considering the buoyant forces, F_g (N), that cause the rock particle to sink and the drag forces F_d (N) that resist its sinking (Figure 4.2.2A):

$$F_g = g.V\,(\rho_r - \rho_i); \tag{4.2.1}$$

$$F_d = 6.\pi.\eta.r.v; \tag{4.2.2}$$

$$v_t = g.V\,(\rho_r - \rho_i) / 6.\pi.\eta.r \tag{4.2.3}$$

where, g = acceleration due to gravity (m/s^2), ρ_r = the density of the rock (kg/m^3), ρ_i = the density of the ice (kg/m^3), η = ice viscosity (Pa s), V = the volume of rock (m^3), and r = the equivalent spherical radius of the object (m), given by:

$$r = \sqrt[3]{((\tfrac{3}{4}.V) / \pi)} \tag{4.2.4}$$

The stress, σ (Pa), acting on the rock-ice interface is given by:

$$\sigma = g.V\,(\rho_r - \rho_i) / A \tag{4.2.5}$$

where A = the area of the block face in contact with the ice beneath the block (m^2). Only the terminal velocity, v_t, is considered because steady state velocity would be reached practically instantaneously. The assumption of non-turbulent drag for Stokes' law is maintained even for very large particle volumes because the very high ice viscosity prevents high velocities being attained. The velocity is strongly dependent on the stress magnitude (Equation 4.2.5), with the increase in velocity with incremental stress following a positive power-law; Glen's flow law for ice (Glen, 1958), which has been widely used for modelling flow in glaciers, also follows a power-law. Pressure melting is ignored because it would be negligible at the pressures involved (Cuffey and Paterson, 2010; p. 234).

Using equation (4.2.3), a 1 m^3 cube of rock with density = 2500 kg/m^3, would fall through ice (with viscosity = 2 $x10^{13}$ Pa s and density = 920 kg/m^3) at 2 mm per year. A 1000 m^3 cube rock of the same density would fall at a speed of 200 mm per year and for a volume of 125,000 m^3 (the equivalent size of a large rockfall), the speed would be just over 5 metres per year.

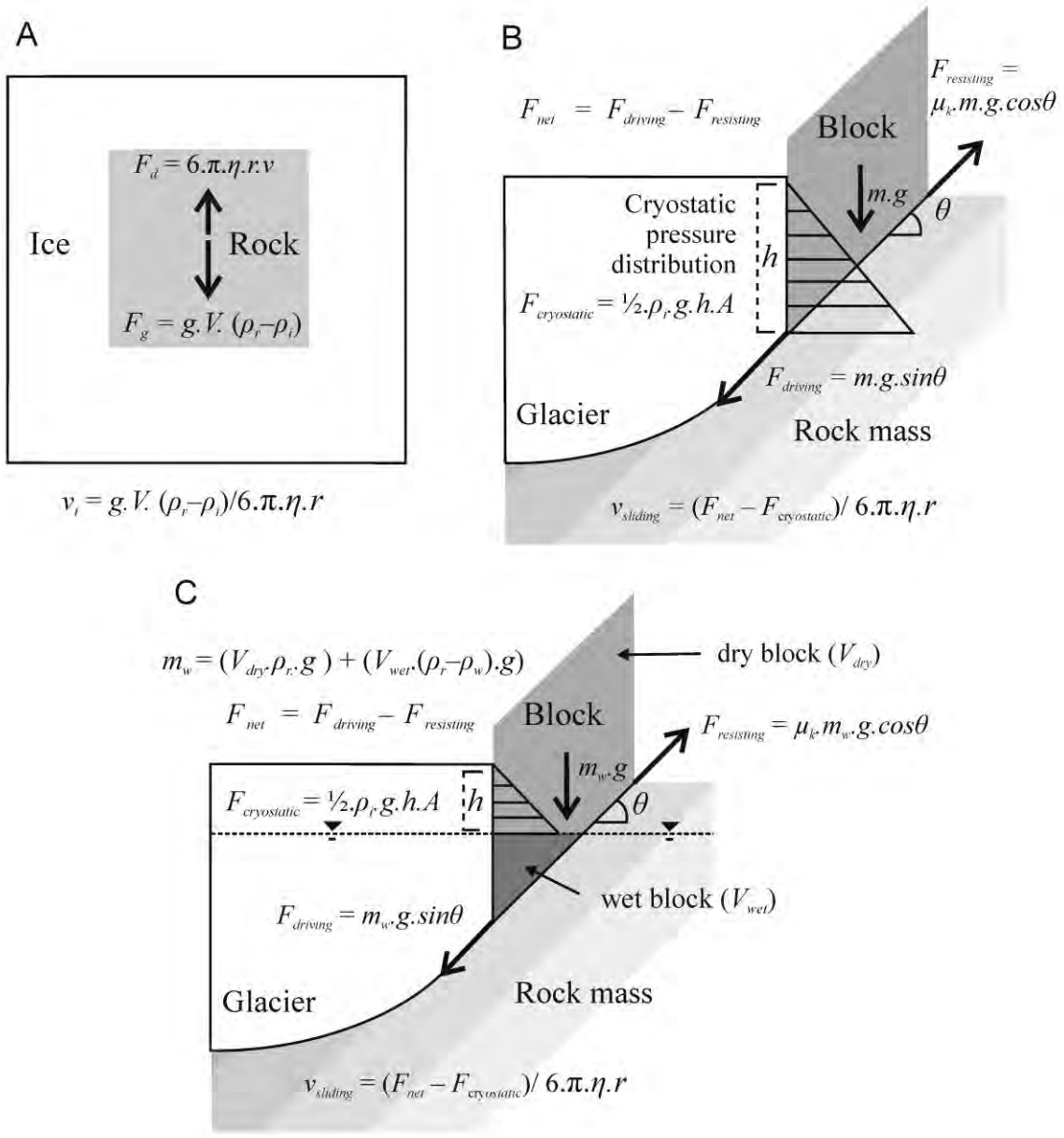

Figure 4.2.2: (A) Force diagram of a rock falling through ice. (B) Forces involved for a block of rock sliding into the side of a glacier when dry and; (C) with a static water table (and permeable rock mass).

So far only a rock suspended within glacier ice has been considered; some modifications are required for modelling the deformation of the ice caused by a collapsing slope. To calculate the speed of a block of rock entering the ice from a slope adjacent to the glacier but underneath the ice surface, additional forces need to be considered. If treated as a rockslide, involving an intact rock block sliding down a planar failure surface (Figure 4.2.2B), then the force exerted on the ice, F_{net} (N) (parallel to the sliding surface), is related to the weight of the block, slope of the failure surface, and coefficient of friction between the sliding surface and overlying block:

$$F_{net} = F_{driving} - F_{resisting}: \tag{4.2.6}$$

$$F_{driving} = m.g.\sin\theta; \tag{4.2.7}$$

$$F_{resisting} = \mu_k.m.g.\cos\theta, \tag{4.2.8}$$

where θ is the angle of the planar sliding surface (°) and μ_k is the coefficient of kinetic friction between the block and the sliding surface (Tan[friction angle]). When the driving force exceeds the resisting force, $F_{net} > 0$, there is an unbalanced force on the block and it will tend to move. Whether or not the block will move will then depend on how much resistance is provided by the ice. A dynamic force is generated on the face of the block in contact with the ice by the movement of the glacier past the block. This force is proportional to the square of the velocity of the glacier and because the glacier velocity is so small, the force will be negligible; consequently, this force is ignored here. A considerably larger force exerted by the glacier arises from cryostatic force, also known as glaciostatic force, ($F_{cryostatic}$, N) generated by ice against the block:

$$F_{cryostatic} = ½\,\rho_i.g.h.A, \tag{4.2.9}$$

where h = the height of the ice above the bottom of the block (m) and A = the area of the rock block face in contact with the ice (m^2) (Figure 4.2.2B).

Water within the glacier and adjacent rock mass also influences the forces involved. Water within the glacier will eliminate the cryostatic pressure acting on the block for any

part of the block below the water table (Figure 4.2.2C). Thus, if the water table is at the glacier surface, $F_{cryostatic}$ is completely eliminated. Warm-based glaciers probably have basal water pressures fluctuating above zero and may even have basal water pressures that temporarily exceed the overburden pressure of the ice (i.e. the glacier temporarily floats) (Fountain and Walder, 1998). Therefore, it is reasonable to assume that for temperate glaciers, the cryostatic force will, at the least, fluctuate below its maximum dry value. The water table in the glacier is likely to influence the water table in the adjacent rock mass – joint networks make rock masses permeable to water. A static water table within the rock mass reduces the net force exerted on the ice by the portion of the block below the water table when there is a positive force balance and increases the net force when there is a negative force balance – a positive force balance exists when the slope angle of the failure plane exceeds the angle of sliding friction (i.e. $F_{driving} > F_{resisting}$). This is because water reduces the weight ($m.g$) of the block through hydrostatic uplift (Figure 4.2.2C); the consequence is a reduction in both (driving and resisting) force components but a proportionately larger reduction in the larger of the two components. A negative water pressure gradient in the slope (i.e. water flow towards the glacier) and excess water pressure (exceeding hydrostatic water pressure) between the block and the sliding surface will however, increase the driving force and reduce the sliding resistance of the block respectively. The influence of these water-pressure variations in the glacier and slope are not explored in the present study but are a target of investigation. Water is likely to play a role in mediating the slope movement rate but perhaps also in providing stress-release in the rock mass by reducing the cryostatic pressure exerted on the rock mass; stress-release could allow the growth of joints and therefore the initiation of further slope failures while glaciers are still present. A major difficulty is how to model groundwater fluctuations and their effects over longer periods.

Ignoring the effects of water in the glacier and in the slope, for a 2500 m^2 block face, 50 metres below the ice surface the cryostatic force generated by the (dry) ice is greater than 5 MN. The velocity of the sliding block, $v_{sliding}$, can now be represented by the following adaptation of equation (4.2.3) that incorporates this additional counter force:

$$v_{sliding} = (F_{net} - F_{cryostatic})/ 6.\pi.\eta.r \qquad (4.2.10)$$

Using equation (4.2.10) and applying the same rock and ice properties as above, the smallest block size required for movement on a planar sliding surface (θ = 50° and μ_k = tan30°), is slightly less than 13,000 m^3. The velocity of a 13,000 m^3 block is approximately 7 mm per year, increasing to about 10 metres per year for a block with a volume = 1 M m^3.

The calculations above provide only approximations; they do not account for variations in the effective viscosity of glacier ice, which is known to be strongly dependent on the strain rate, temperature, grain-size, confinement, and presence of liquid water at grain boundaries (Glen, 1955; Marshall, 2005), and only simple geometries and dry conditions have been considered. In general, the velocities are likely represent minimum values because the ice viscosity value used here (2 $x10^{13}$ Pa s) is conservatively high for temperate glaciers, and water tables in the glacier and the slope will generally increase the sliding block velocity. This simple analysis is a first attempt at exploring the time-scales over which slope movement forces could be sufficient to cause deformation of ice. The results indicate that medium to large rockslides could feasibly deform into glaciers at sufficiently high velocity for measurable movement to occur. Even if a 13,000 m^3 block moved at a rate of only 6 mm per year, over the thousands of years that a glacier exists, the cumulative displacement could become many tens of metres.

If this analysis is realistic, we should expect to find field evidence of rock slope failures protruding into glaciers, and associated slope collapse should be expected as a consequence of glacier thinning.

4.2.3 Field evidence

At least ten rock slope movements (DSGSDs) that appear to be associated with deformation of valley glaciers were identified in the Southern Alps of New Zealand using (Google Earth® and SPOT) satellite imagery. Identification was based on the coincidence of slope deformation features (scarps, hummocky terrain, sackungen, slope bulging, slumping, or large cracks) above glacier surfaces with a corresponding

narrowing or squeezing of the glacier. It is possible that more DSGSDs, entirely hidden beneath the glaciers, or evident at scales not examined in the present study, exist in the Southern Alps, but they remain unidentified. Further, those recognised here likely represent only a small proportion of the total number of these types of features that have existed in the New Zealand Southern Alps during its more extensive periods of glaciation, especially in the schist terrain, which is well-known to be prone to large-scale creep (McSaveney et al., 1992; Turnbull, 2000) (Figure 4.2.1B&C).

4.2.3.1 Site 1: Dart Glacier

Several slope deformation features have been identified at the Dart Glacier in Otago (Figure 4.2.3 & 4.2.4). The Dart Glacier, now only 6 km long, was once part of the much larger glacier that occupied Lake Wakatipu, and extended about 130 km farther down the valley in the last glaciation (ending ~ 15 ka) (Barrell, 2011). The rock type in this region, Haast schist (Turnbull, 2000), hosts hundreds of examples of large creeping slope movements, many of which are active. The DSGSDs identified at the Dart Glacier appear to have pushed into the sides of the glacier, causing the glacier to appear laterally constrained (Figure 4.2.4). Two of the features (shown in boxes 'a' & 'b') on the true left of the glacier are relatively well-defined. They display numerous scarps, appear blocky in nature, and are likely to be structurally controlled by foliation that dips steeply towards the north-west. Part of the feature identified at the Dart Glacier terminus (b in Figure 4.2.4), appears to have been partly entrained/removed by the glacier, based on the volume of the source area versus volume of displaced material. There may be another large slope deformation on the opposite side of the glacier, (indicated by scarps and dashed lines, Figure 4.2.4) that has also caused deformation in the glacier ice (dashed arrows, Figure 4.2.4), but it in this case, debris from the slope movement may be the cause of the apparent bulging in the glacier wall.

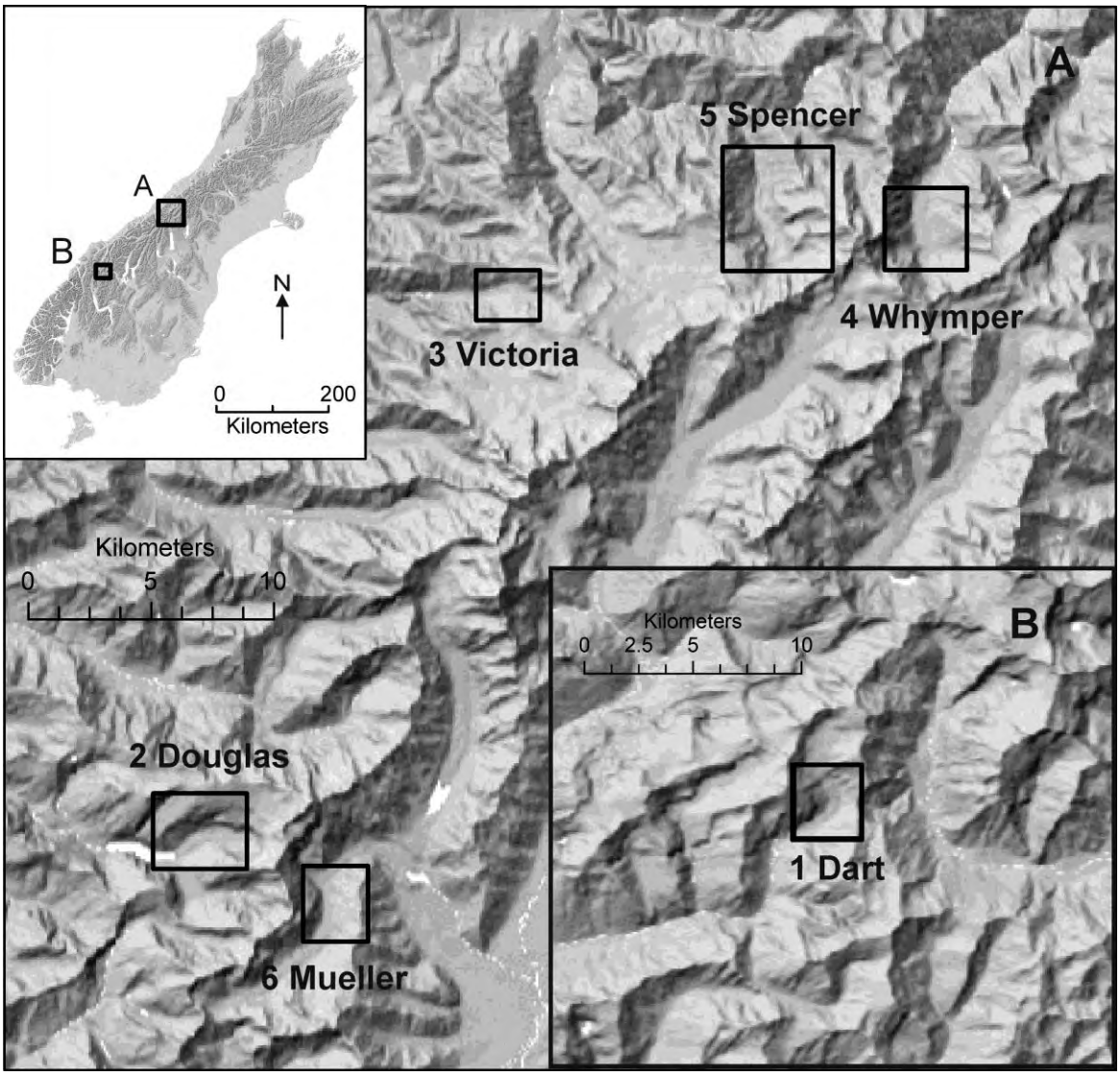

Figure 4.2.3: Location of study sites in the South Island, New Zealand (inset upper left) superimposed onto 100 m hillshade maps (A = glacier sites 2 to 6; B = glacier site 1). White infill represents water bodies. Data source: Geographx Ltd, downloaded from Koordinates.com.

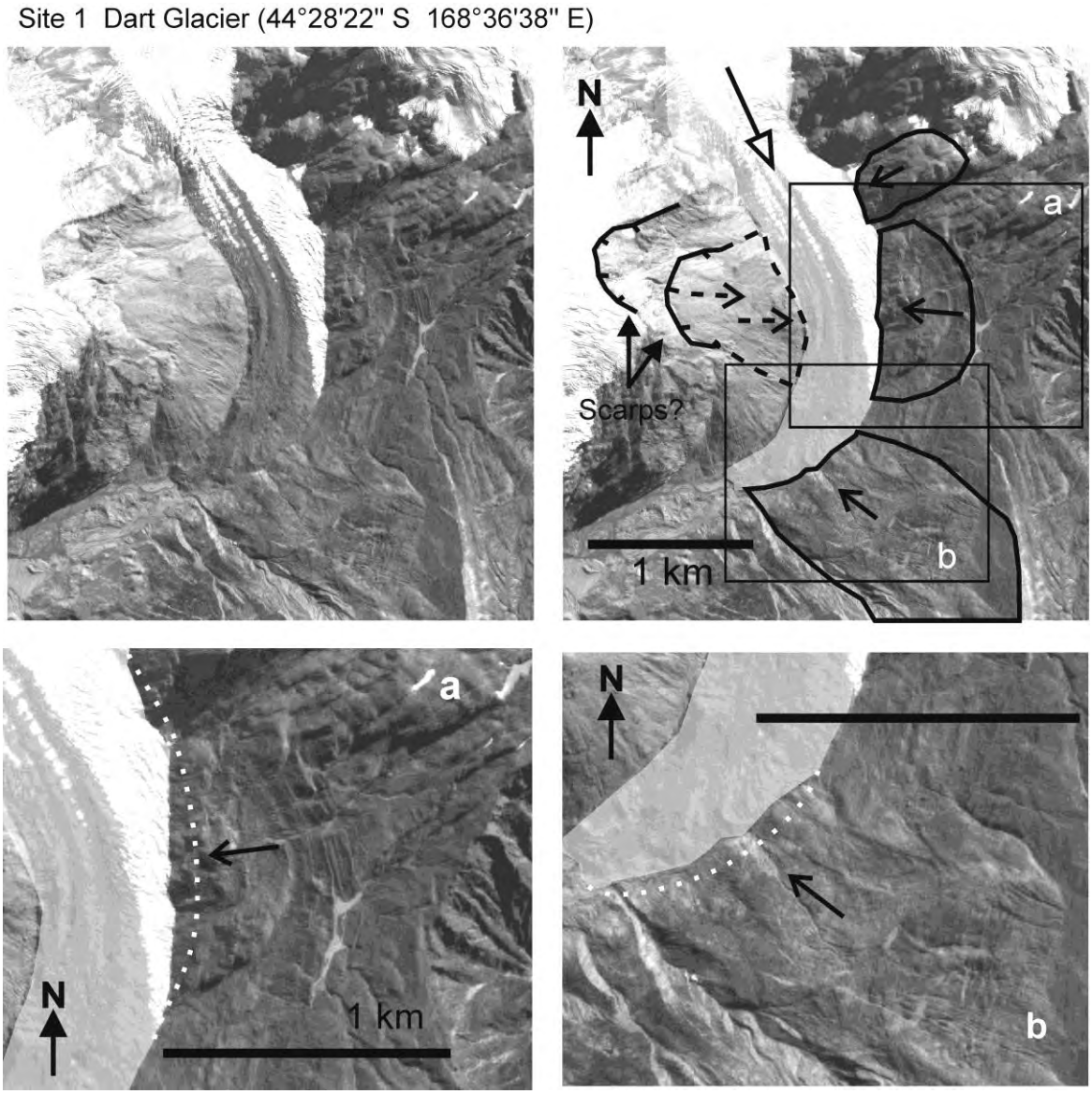

Figure 4.2.4: Sites 1 (Dart Glacier) referred to in text and Figure 4.2.3. Annotated SPOT image at right shows DSGSDs (solid outline for certain, and dashed outline for uncertain) and glacier (white shading – supraglacial debris makes it difficult to see glaciers). Solid/dashed arrows indicate slope movement direction and open arrow indicates glacier flow direction. Boxes 'a' and 'b' are enlarged in the lower images, and the estimated limit of the glacier before slope movement is shown on these by the dotted white line.

4.2.3.2 Site 2: Douglas Glacier

Two large slope deformations in Haast schist have been identified at the Douglas Glacier on the western side of the Main Divide of the central Southern Alps (Figures 4.2.3 & 4.2.5). The Douglas Glacier, and the Victoria, Whymper, and Spencer glaciers

mentioned below, flow westwards from the topographic divide of the Southern Alps. All of the glaciers were of considerably larger extent during the last glaciation (Barrell, 2011). The mass movement on the southern side of the Douglas Glacier is a deep-seated slope deformation with clearly-visible lateral and internal scarps (Figure 4.2.5; solid outline). The movement appears to have caused the glacier to deform laterally. The glacier surface also appears to be slightly elevated adjacent to the slope movement feature but, in the absence of high-resolution topographic data, the magnitude of bulging cannot be reliably measured and it will remain speculative that the bulging is associated with slope deformation without monitoring both the glacier surface and the slope. The second mass-movement, on the northern side of the glacier at the terminus, appears to have caused deformation of the ice (Figure 4.2.5; dashed outline). However, the feature as been outlined as 'uncertain' because it was not possible to tell if the apparent squeezing of the ice was instead debris/talus derived from the slope and resting on the ice surface.

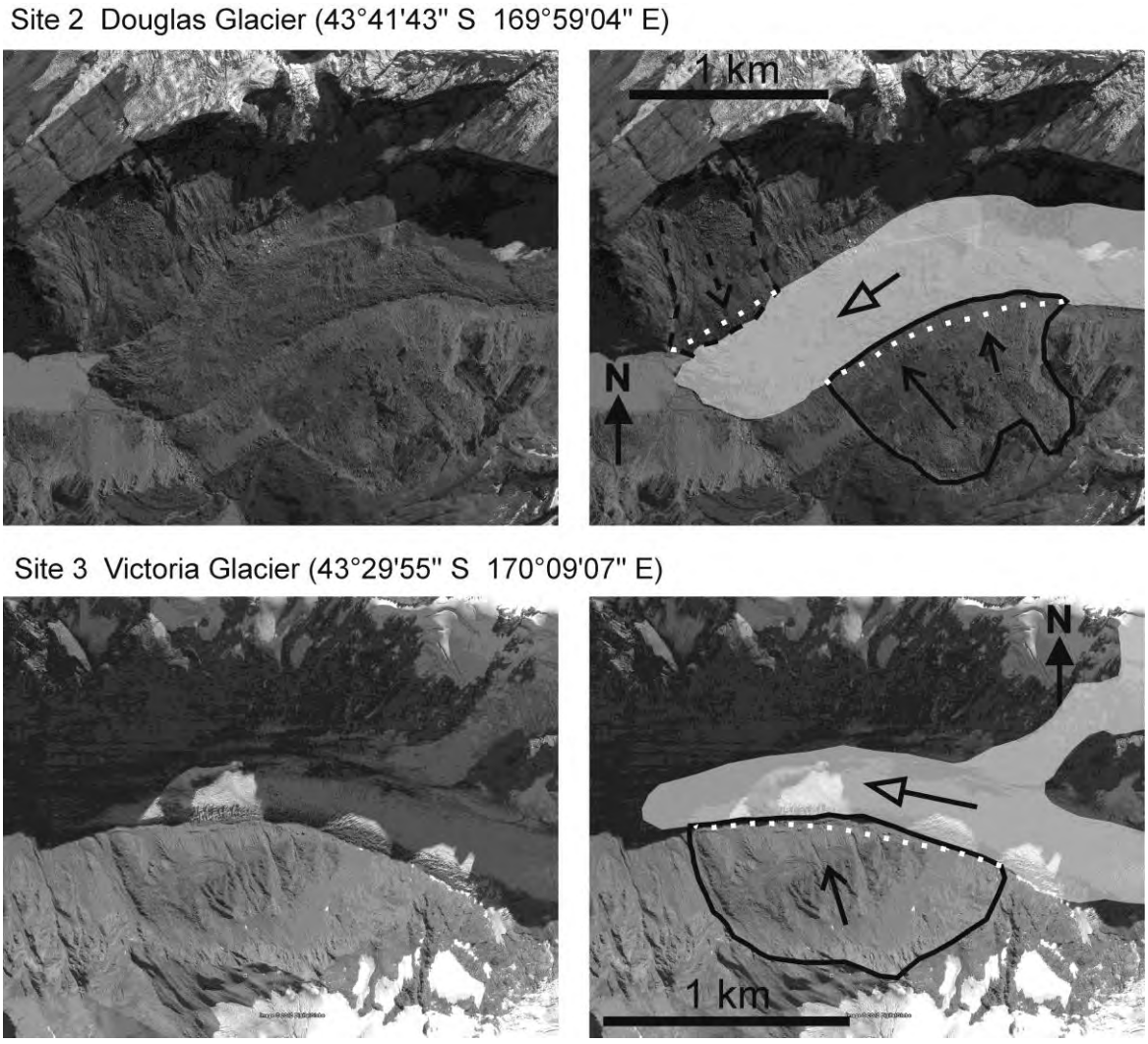

Figure 4.2.5: Sites 2 and 3 referred to in text and Figure 4.2.3. Annotated images at right show DSGSDs (solid outline for certain, and dashed outline for uncertain) and glacier (white shading – supraglacial debris makes it difficult to see glaciers). Solid/dashed arrows indicate slope movement direction and open arrow indicates glacier flow direction. The white dotted line represents the estimated limit of the glacier prior to slope movement. Latitudes and longitudes locations are for the centre-point of each image. Images are from GoogleEarth®.

4.2.3.3 Site 3: Victoria Glacier

Farther north, in similar lithology, a large slope deformation has been identified at the Victoria Glacier (Figure 4.2.3 & 4.2.5) (also mapped by Cox and Barrell, 2007). Here, the head scarp is nearly 100 metres in height and the slope appears to move as a large block; no internal scarps can be identified, although surface features may be obscured by debris (Figure 4.2.5). The slope movement appears to have caused the glacier to narrow and bend slightly where the slope movement enters the glacier.

4.2.3.4 Site 4: Whymper Glacier

The Whymper Glacier, situated in the northern part of the central Southern Alps and also in Haast schist, has a large slope deformation developing on its eastern side (Figures 4.2.3 & 4.2.6). The deformation of the rock slope is identified by a chaotic and hummocky surface with numerous internal scarps, clefts near the top of the slope, and well-defined lateral scarps (on the northern side). The slope movement appears to have caused a slight deformation of the glacier wall but the deformation of ice appears less well-developed than in the previous examples.

The apparent narrowing of the Whymper glacier on the western side (beginning centre-left of image and continuing north) appears to be produced by the overlapping of ice and rock talus on to the glacier surface, rather than slope movement. The crevassed ice at the southern part of this overlapping material, looks to have been part of a glacier once connected to the slopes above, and/or accumulation snow and ice talus.

Figure 4.2.6 (on following page): Sites 4 and 5 referred to in text and Figure 4.2.3. Annotated images at right show DSGSDs (solid outline for certain, and dashed outline for uncertain) and glacier (white shading – supraglacial debris makes it difficult to see glaciers). Solid/dashed arrows indicate slope movement direction and open arrow indicates glacier flow direction. For site 5, the northern most mapped feature may have deformed the glacier more in the past but the terminus has almost retreated beyond the extent of the slope movement. Zoomed-in image is provided for box 'a' for site 5, with the dashed line here representing the estimated limit of the glacier prior to deformation. Latitudes and longitudes locations are for the centre-point of each image. Images are from GoogleEarth®.

Site 4 Whymper Glacier (43°28'49" S 170°21'50" E)

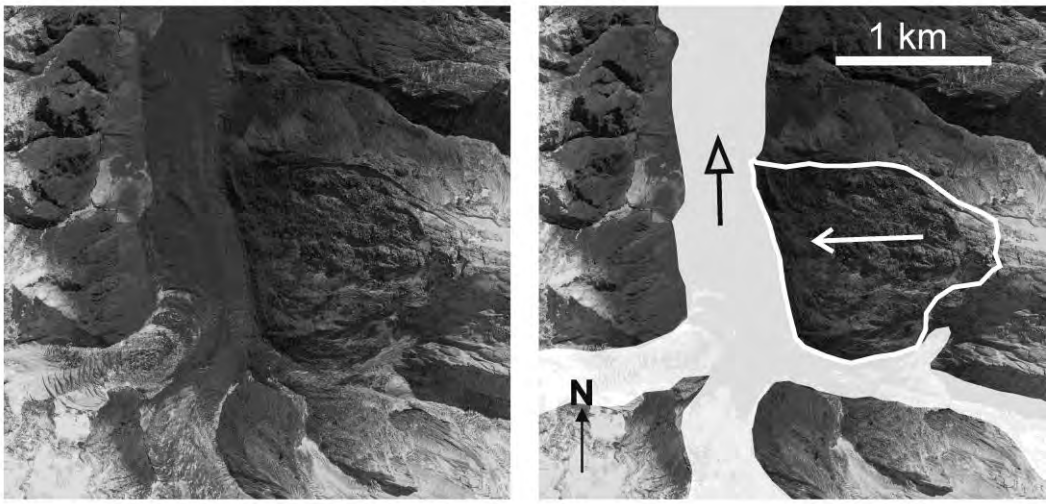

Site 5 Spencer Glacier (43°28'15" S 170°17'09" E)

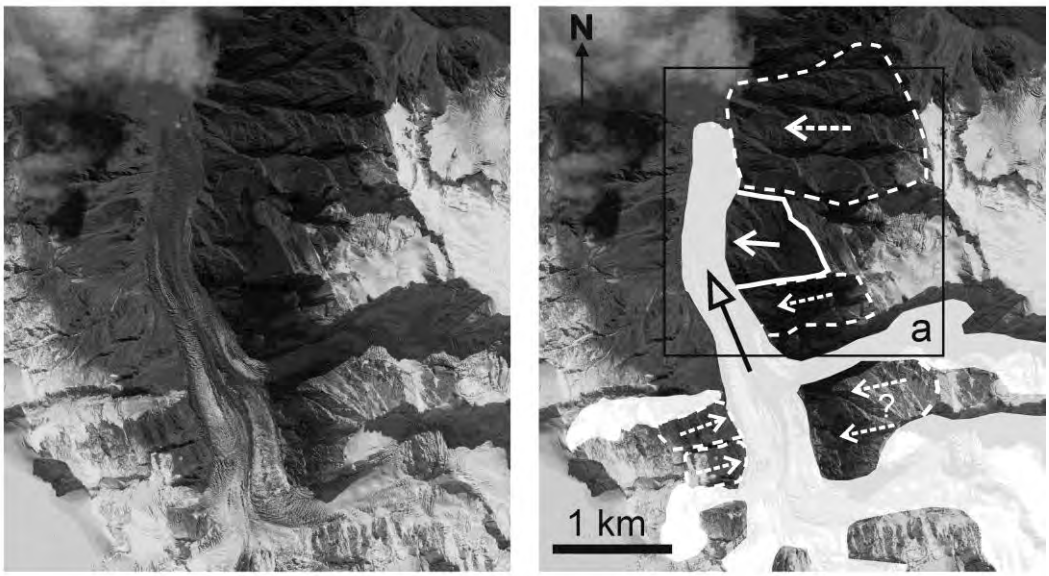

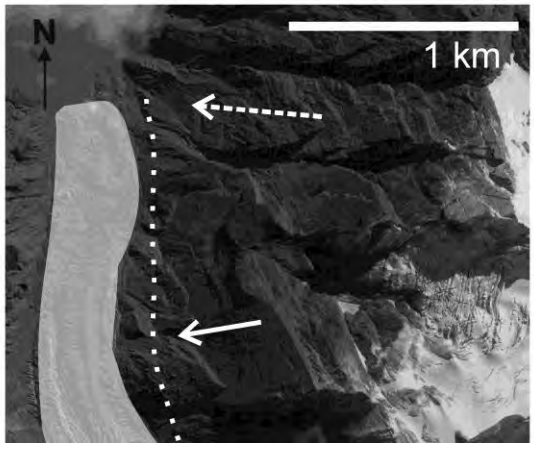

4.2.3.5 Site 5: Spencer Glacier

The Spencer Glacier is located 6 km north-west of the Whymper Glacier (Figure 4.2.3 & 4.2.6). Several significant slope deformations have been mapped here in Haast schist (Figure 4.2.6). The features appear to be strongly structurally-controlled, with those identified to the east appearing to slide as a series of slabs dipping steeply towards the glacier (zoomed in on in the lower image 'a'). The feature with the solid arrow has caused significant deformation of the glacier, forcing it inwards by about one hundred metres. Several other unstable slopes adjacent to this glacier may also be deforming the glacier (dashed lines and arrows).

4.2.4 Site 6: Mueller Rockslide case study

The field evidence examined so far indicates that slope movements may be able to cause deformation of glacier ice, but alone, the imagery examined does not provide compelling evidence. Further, these snap-shots in time reveal little information on the rate that these features develop. Higher-resolution imagery and topographic data, along with repeat observations through time, may provide one way to reduce these uncertainties. Here we provide additional evidence in the form of geological, geomorphological, and slope movement data for one site, the Mueller Rockslide. The Mueller Rockslide has previously been described by Hancox (1994; 1998; referred to therein as Mueller Landslide), but is recognised here as another example of a DSGSD that has caused glacier deformation (Figure 4.2.7). Despite being the only DSGSD described here in non-schistose lithology, this rockslide is used to study the process of slope deformation in more detail because of its accessibility. The rockslide morphology has been mapped using aerial and satellite imagery and in the field. Survey marks, installed in 2010, have been periodically re-surveyed to assess movement behaviour (McColl et al., in prep; Section 4.1.2).

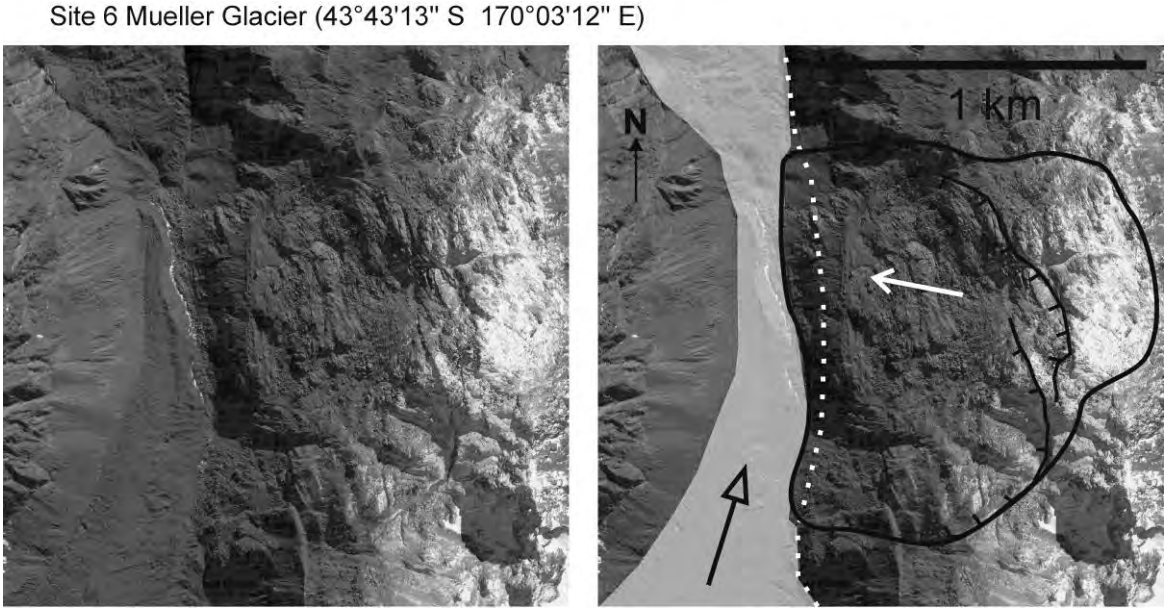

Figure 4.2.7: Site 6, the Mueller Rockslide. The annotated image at right shows the rockslide outline (black solid line), the main scarp (black line with tick marks) and the Mueller Glacier (white shading). Solid white arrow indicates slope movement direction and open black arrow indicates glacier flow direction. The dashed white line indicates assumed lateral extent of Mueller Glacier prior to narrowing by movement of the Mueller Rockslide. Latitude and longitude are for the centre-point of the image. Image is from GoogleEarth®.

4.2.4.1 Geology and geomorphology

Situated on the Sealy Range in Mount Cook National Park (Figure 4.2.3), the Mueller Rockslide is a 100-200 M m^3, very slow-moving rockslide that extends west from the ridge crest at c.1800 m.a.s.l to the Mueller Glacier 600 metres below (Figure 4.2.8). The Sealy Range is formed by a large overturned fold structure, the Kitchener Anticline, plunging towards the north (Lillie and Gunn, 1964). On the west of the range, bedding dips steeply (45-50 degrees) to the west (under-dip slope) and is inferred to form the principal slip surface/s for the Mueller Rockslide.

The Mueller Rockslide occurs in unweathered to slightly-weathered pinkish- grey, distinctly-bedded, non-metamorphosed greywacke sandstone. The rock is very strong with widely-spaced open joints. Bedding alternates between metre to tens of metres thick sandstone and decimetre-thick, dark grey, moderately strong, mudstone (argillite). Much of the rockslide surface appears disturbed by rockslide movement; scarps – block topples, dilated joints, and chaotic blocks at the surface (Figure 4.2.9). Little vegetation exists on the rockslide except for small alpine plants.

Annual precipitation may be as high as 10 metres per year (Kerr et al., 2007) and much of this probably falls as snow. Snow covers most of the rockslide for about two thirds of the year. In late summer a few small patches of névé remain (Figure 4.2.9B) and there may have been small glaciers on the rockslide in the past (Figure 4.2.9C).

Figure 4.2.8 (on following page): Geomorphic map of Mueller Rockslide and surrounding ridge, showing the main and other minor landslide scarps, area of ridge under tension, bedding plane orientations, and exaggerated horizontal displacement vectors (m) measured from survey marks between April 2010 and April 2012. The number alongside each displacement vector arrow is the angle from horizontal, with positive values in the down direction. Survey marks with less than 0.5 m net and horizontal displacements do not have vectors shown. Topographic data are based on University of Otago 15 m digital elevation model (Columbus et al., 2011). Corresponding cross-section (A-A′) shows the inferred bedding orientations at depth, failure surface, depth of glacier, and scree thickness.

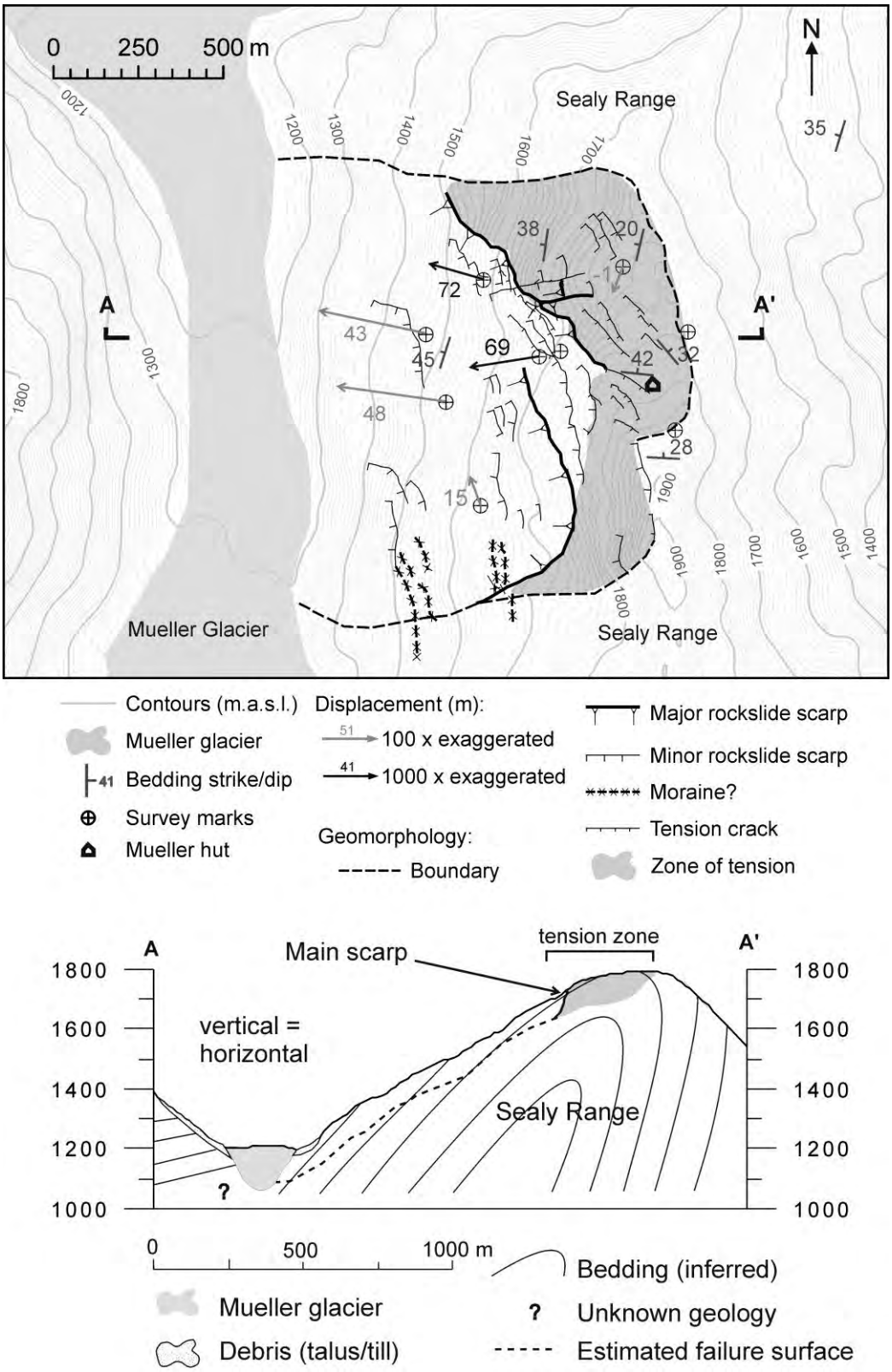
0 250 500 m
N
Sealy Range
35
A
A'
38
20
72
43
69
45
42
32
48
28
15
1800
1300
1200
1400
1500
1600
1700
1900
Mueller Glacier
Sealy Range
Contours (m.a.s.l.)
Mueller glacier
41 Bedding strike/dip
Survey marks
Mueller hut
Displacement (m):
51 100 x exaggerated
41 1000 x exaggerated
Geomorphology:
Boundary
Major rockslide scarp
Minor rockslide scarp
Moraine?
Tension crack
Zone of tension
A
A'
Main scarp
tension zone
vertical = horizontal
Sealy Range
1800
1600
1400
1200
1000
?
0 500 1000 m
Bedding (inferred)
Mueller glacier
Debris (talus/till)
? Unknown geology
Estimated failure surface

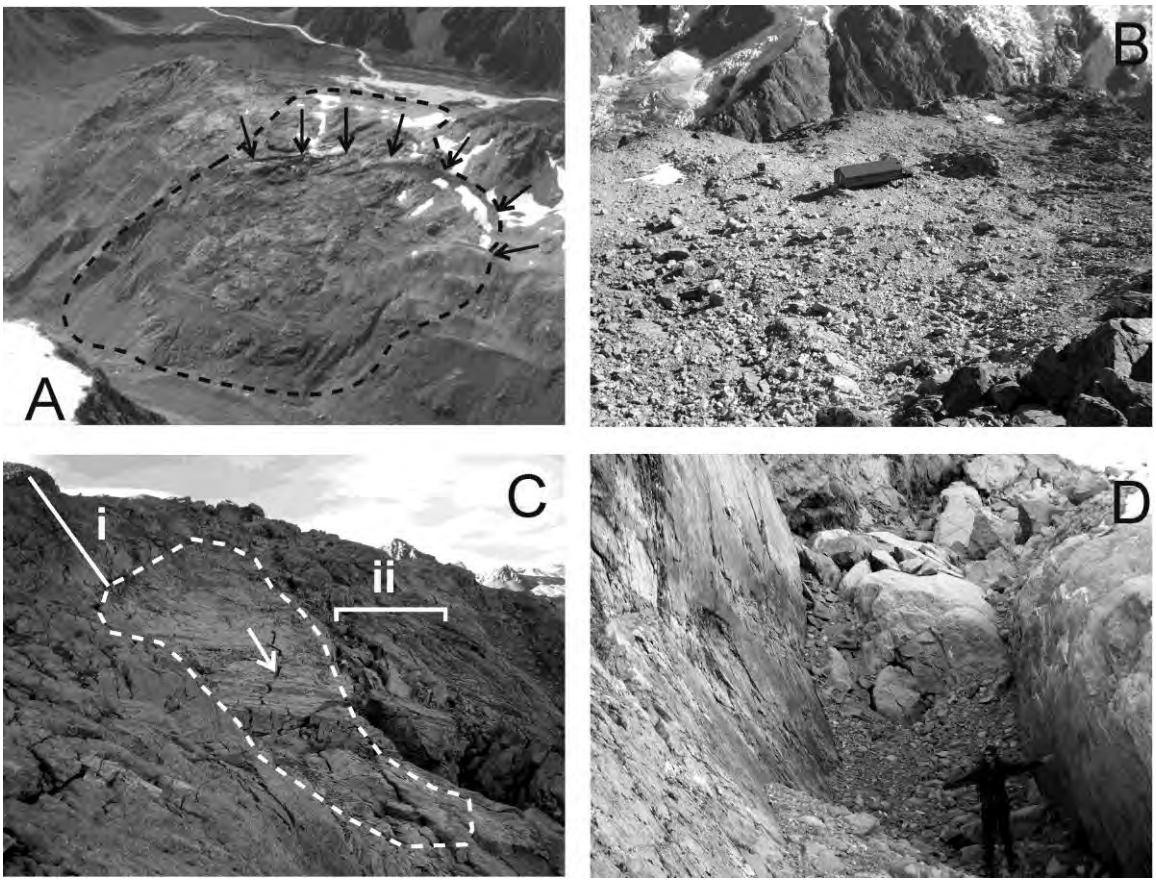

Figure 4.2.9: Surface features and morphology of the Mueller Rockslide. (A) View from south-west looking down towards the Mueller Rockslide on Sealy Range. The main scarp (indicated on Figure 8A) is clearly visible. Mueller Glacier is seen bending around the end of Sealy Range with the terminus and immature pro-glacial lake visible in the background (photo Mauri McSaveney, approx 1980s). (B) Chaotic surface near the top of the rockslide, in a zone of tension above the main scarp, which is beyond break of slope at upper left of photo. Firn patches visible have been present each summer for the last few years. Mueller hut (building in upper-centre of photo) is situated in an area actively dilating and probably subsiding in response to slope movement. (C) Smooth convex hollow (white dashed line) below main scarp (approximately 40 metres high, shown with line i). The hollow has numerous striations on surface, indicating surface modification by cirque glaciation or sliding of annual snowpack. The surface is being destroyed by retrogressive block toppling from the down-slope edge (area indicated by line ii and incipient block topple crack feature shown with arrow). (D) Part of the main rockslide scarp in the northern area of the rockslide, photo taken looking south.

4.2.4.2 Glaciation and glacier retreat

Glaciers in the Mount Cook region have undergone substantial downwasting over the last 200 years, as evidenced by the abandonment of terminal and lateral moraines, and the development of proglacial lakes (Gellatly, 1985; Kirkbride and Warren, 1999). During the peak of the last glaciation, at around 18-22 ka, the Mueller Glacier may have been several hundred metres thicker at the rockslide. Since that time the glacier surface has probably undergone several phases of lowering before reaching the present day

elevation. Based on valley cross-section projections, it is estimated that the ice thickness remaining at the toe of the rockslide is 100-200 metres. Today, the Mueller Glacier upvalley of the rockslide appears to flow relatively slowly and contribute little ice to the glacier terminus. For example, boulders observed (using Google Earth® imagery) on the glacier surface near the rockslide travelled approximately only 43 metres down valley between 16/01/2004 and 4/5/2006. The Frind and Huddleston tributary glaciers joining the Mueller Glacier downvalley of the rockslide appear to contribute greater flow; boulders observed on the glacier surface downvalley of the rockslide travelled approximately 185 metres during the same period.

4.2.4.3 Rockslide morphology and movement

The failure mechanism is most likely translational sliding along bedding forming a step-wise failure surface, with extension and possibly subsidence at the head of the slope behind the main scarp (Figure 4.2.8 cross-section). Mapping indicates that the rockslide is most active below the 10-40 m high main scarp that extends most of the way across the rockslide (Figure 4.2.8). Below the main scarp are large block topples, cracks, and extensive ground disturbance. Between the main scarp and the top of the ridge, the ground is less disturbed but large tension cracks are present.

Movement data collected by GPS surveying of 7 survey marks over a two year period (April 2010 to April 2012) (McColl et al. in prep) support these field interpretations. The net (vertical and horizontal) movement has varied between 1 and 4 metres per year in the most active parts of the rockslide. The net movement in the active area is in a down-dip direction at an inclination angle similar to that of the dip-angle (Figure 4.2.8). The movement rate was 2 to 4 times greater in the first year of monitoring than the second year but the rate-controlling processes remain unknown. Several rate-controlling processes are the target of ongoing investigation: (i) snow loading on the rockslide surface causing additional driving force, in which case greater movement would be expected in the winter and during heavy snow years; (ii) variable snow or ice melt and rainfall causing fluctuation of water table levels in both the rockslide and the glacier, consequently changing the driving and resisting forces that control rockslide

movement; (iii) earthquake ground acceleration, for example, during the September 2010 M_w 7.1 Darfield earthquake (epicentral distance c. 170 km).

4.2.4.4 Deformation of the Mueller Glacier

Like the previous examples of field evidence presented, the deformation of the Mueller Rockslide appears to be at least partly accommodated by deformation of the glacier. This can be seen as (i) the slight protrusion of the (visible) toe of the rockslide farther out into the valley than the adjacent more stable slopes and (ii) the narrowing of the glacial valley here (Figure 4.2.7). Further, (iii) morphologically, the rockslide appears to be a deep-seated structure moving on bedding planes that appear to project below the glacier surface (Figure 4.2.8 cross-section) and (iv) the displacement vectors indicate that the movement is in a down-dip direction at approximately the dip angle of 45 - 50 degrees, whereas the slope angle for the rockslide surface is about 35-40 degrees. Additionally, (v) if the glacier was acting as a solid buttress and not yielding to the rockslide, then the movement in the upper part of the rockslide would be causing upward bulging of the rockslide toe. Neither the surface morphology nor displacement data available indicate bulging; however, the monitoring data do not cover the lower half of the rockslide where bulging would be greatest.

4.2.4.5 Application of the model from Section 4.2.2.

The equation for predicting the movement rate of an ice-contact slope was applied to the Mueller Rockslide. A movement rate of 167 metres per year is calculated with the following parameters in equation (4.2.10): $\eta = 2 \times 10^{13}$ Pa s; $\rho_i = 920$ kg/m^3; $h = 150$ m; $\rho_r = 2700$ kg/m^3; $\mu_k = \tan 38°$; $\theta = 45°$; $A = 180000$ (h * rockslide width of 1200 metres) m^2; rockslide volume = 100 M m^3; and with the drag force being reduced to $F_d = 6.\eta.v.(½\ \pi.r)$ to account for the tabular shape of the rockslide (i.e. a smaller surface area in contact with the ice for the given volume). The coefficient of friction used here (tan38°) is the average value measured in the field using tilt-block tests on smooth blocks of sandstone against argillite (the average values for rough sandstone = tan45°; smooth sandstone against smooth sandstone = tan38°; and argillite against argillite = tan33°). The rockslide volume (100 M m^3) is a lower-bound estimate based on the assumption that the upper half of the rockslide is under tension, as evidenced by numerous tension cracks and

scarps, and therefore does not contribute a driving force at the rockslide toe. An upper-bound volume estimate of 150 M m^3 produces a movement rate of 250 metres per year. The associated strain rates (1.8 $x10^{-8}$ and 2.6 $x10^{-8}$ s^{-1}, for 167 m/year and 250 m/year respectively) are still well below the strain rate transition (10^{-3} to 10^{-7} s^{-1}) to brittle deformation of ice. The results are one to two orders of magnitude greater than the measured movement rate of 1 - 5 metres per year. This large deviation from the observed movement rate is hardly surprising and likely to be because of poor estimation of some of the model parameters. The geometry of Mueller Rockslide and the failure surface is undoubtedly more complex than is being represented by our model and the strength of the rockslide cannot realistically be represented by a single value of friction. For example, the model treats the rockslide as moving on a single planar surface, whereas in reality, there are probably multiple surfaces, of varying strength, and additional resistance is likely to be provided by the lateral shear planes. Further, effective viscosity (η) of glaciers is known to vary by orders of magnitude with relatively small changes in temperature; for example, modelled effective ice viscosity for the Greenland Ice Sheet ranges from less than 10^{12} to over 10^{17} for ice at temperatures between 0 and -15 °C respectively, for a range of stress conditions (Marshall, 2005). For the purposes of the simplistic modelling objective here, it is not possible, or indeed necessary, to determine all of these parameter values to within better than order of magnitude. However, it is reasonable to adjust some of these parameters to calibrate the model to get a closer match between observed and modelled movement for the purposes of exploring how changes in ice thickness may influence movement rate; field calibration is an approach used for developing empirical models of any natural-system behaviour.

In order to be able to more confidently use the equations to assess how ice thickness influences movement rate, two of the parameters (θ and μ_k) are varied until a closer match between the modelled and observed movement rate is achieved. The movement rate is very sensitive changes in these two parameters, both of which influence the magnitude of stress applied to the ice. A new coefficient of friction of tan41° is applied. This is not unrealistically high because although the argillite beds have the lowest sliding friction, the argillite bedding planes are less continuous than the thicker sandstone beds, far less abundant, and their contacts and associated bedding joints are less planar. The sliding surface angle was then reduced until the predicted and measured movement rates

were within order of magnitude of each other, with a final value of $\theta = 42.1°$ being used. This angle is also realistic because the original inclination used for the sliding surface was based on the assumption that the bedding orientation at depth is consistent with the orientation of bedding observed at the surface; this may not be the case because the bedding at the surface may have been rotated and steepened due to toppling or other deformation caused by landsliding, and it is likely that the failure surface does not occur on a single bedding plane, but steps across multiple surfaces. For these new values of θ and μ_k the model predicts a movement rate of 3 m/year for the 100 M m^3 block and a movement rate of 35 m/year for the 150 M m^3 block. With the model now predicting movement rates closer to those observed, it is used to postdict how much glacier thinning was required for initiation of the Mueller Rockslide motion, and to predict how the movement rate will change under scenarios of continued glacier thinning.

Keeping all the other parameters the same, an additional 3 and 38 metres of ice thickness (h) for the 100 M m^3 and 150 M m^3 rockslides, respectively, reduces movement to zero. When h is halved to 75 metres, the velocities predicted are 56 and 81 metres per year, respectively. Based on these crude extrapolations, the movement on the present failure surface may have started in the last few hundred years (c. 35 metres) of ice thinning. It is also likely that continuing thinning of the Mueller Glacier will allow the rockslide to accelerate, and possibly to fail catastrophically. Nevertheless, until these equations can be improved by calibration from additional empirical data, or their complexity is increased to model behaviour more realistically, the values provided here remain speculative – but not unrealistic or unhelpful.

4.2.5 Discussion

4.2.5.1 Glacial erosion and entrainment

The equations and field evidence presented here indicate that slope movements of sufficient mass, for example > 100,000 m^3, could feasibly deform adjacent glacier ice, and this could happen at velocities of 10^{-2} to 10^2 metres per year. Such rates of slope displacement would be significant over hundreds to thousands of years and may contribute significant volumes of sediment to the glacial system. However, in most of

the field examples the glaciers do not appear to have significantly entrained the displaced mass. Instead, the glaciers seem to have been forced to narrow. This situation may arise when glaciers are small, slow flowing, and not highly erosive, and therefore incapable of entraining the displaced mass. The glaciers may be gradually plucking or quarrying out smaller blocks of the displaced and broken-up mass, but not removing the material fast enough to keep up with slope movement. Therefore, in the present situations, the rates of slope movement probably exceed the erosion rates of these glaciers. Eventually, the slope mass may move sufficiently far into the flow of the glacier to become fully detached from the slope and entrained within the glacier. It is also possible that further narrowing of a glacier as slope movement continues would cause ice flow, and therefore erosion capacity, to increase. Nevertheless, as glaciers continues to thin, the slopes are likely to move faster and farther; eventually they may collapse catastrophically, especially if the failure surface becomes exposed above the ice surface. This could happen before the glacier terminus has retreated past the slope.

Slope movements that occur in this way may provide a previously-overlooked source of sediment in glaciated catchments. Some measurements of landscape-averaged erosion indicate that erosion is greater during periods of glaciation, suggesting that glaciers are more effective agents of erosion than are rivers (MacGregor et al., 2000; Montgomery, 2002; Brook et al., 2006). However, in modern alpine mountains, mass movements rather than rivers or glaciers are the dominant source of primary erosion and sediment generation (Hovius et al., 1997). Given the potential role of mass movements in the glacier systems examined here, the same may also be true during glaciations; however, the glacier still plays a role in destabilising the slopes because undercutting and steepening of the slopes by glacial erosion contributes to the initiation of slope movements in glaciated valleys. Glacial erosion is not the only factor that can destabilise a glaciated slope. For example, a failure surface may develop during a strong earthquake, or by gradual degradation of the rock mass caused by weathering processes (e.g. stress corrosion). Regardless of how failure is initiated, the velocity of the slope movement will depend on a variety of factors, such as the variation of driving and resisting forces as the slope adjusts, continued erosion by the glacier, degradation of rock strength, water table fluctuations, and changes to the level of the glacier. Quantifying the contribution of ice-contact slope movement to slope evolution and sediment generation

during glacial cycles is challenging. Using field evidence of past slope activity is difficult because of poor preservation of landslide evidence; the debris from slope movements that occur in glaciated valleys will be removed and reworked by the glaciers and buried by glacial outwash and other sediments after glacier retreat. However, as our understanding of contemporary ice-contact slope movement increases, their role in the glacial system and for slope evolution will become more apparent.

4.2.5.2 Glacial buttressing and stress release

The results of this research may change our understanding of how slope movements develop during stages of deglaciation, a subject of great interest because of its importance for landslide hazard and sediment fluxes in glaciated catchments (McColl, 2012). Glacial debuttressing and stress release are often assumed to have caused destabilisation of slopes and enhanced slope movement activity during deglaciation. Glacial debuttressing of slopes is the removal of support of adjacent glacier ice during periods of downwastage (Ballantyne, 2002). Stress-release is the development of tensile stresses within the rock mass upon unloading of ice, and often results in the propagation of surface-parallel (sheeting) joints, which create weaknesses in the rock mass. Debuttressing and associated stress-release necessitate the build up and *maintenance* of elastic strain energy during periods of glacial erosion (i.e. increases in self-weight stresses in the slope) and the release of that energy upon glacier retreat. Maintenance (or storage) of this energy requires that ice behaves elastically and that sufficient confining pressures are maintained by the glacier during its life. Here we have shown that elastic strain is unlikely to be stored in a slope; deformation of the slope can be accommodated by permanent non-elastic deformation of the ice. However, glacier thinning and retreat will reduce the cryostatic ice pressures acting on slopes, consequently reducing slope support and thus increasing the movement rate of existing slope failures or allowing new failures to develop.

4.2.5.3 Suggestions for further research

A step towards furthering our understanding of ice-contact slope movement and being able to more accurately quantify the process is to conduct further investigation of contemporary features. In particular, this should include the application of more

powerful remote sensing and slope monitoring tools, such as aerial or terrestrial light detecting and ranging (LiDAR), or terrestrial or satellite-borne radar interferometry (InSAR). Information provided by these studies can then be used to further test the equations developed here and provide empirical basis for their improvement and wider applicability. It may also be possible to expand the applicability of these simple models to include other types of mass movement in glaciated terrain. For example, glacier thinning can also destabilise ice-contact moraines, and in some instances the failure of these develops as slow moving slumping/mass movement (e.g. Blair, 1994). For very large moraines still partially in contact with the glacier, the weight of the moraine may be sufficient to deform the ice; to model this process, as for rockslides, will require different considerations for the failure surfaces (i.e. probably curved), and different geometries and densities for the slope material.

The present work has identified at least some of the major processes and parameters controlling the behaviour of ice-contact rock slopes, in particular the plastic, rather than elastic, response of ice to an applied stress. However, it is recognised that the approach used so far is limited and the models likely fail to account for other important processes. As discussed earlier, these may include the variable mechanical behaviour of ice at different temperatures, pressures and strain rates; fluctuations in water pressure both within the glacier and slope; and the geometrical and mechanical complexities of the deforming or sliding rock mass. Further, the models provide only an instantaneous assessment of the sliding velocity, but as the slope movement develops and the glacier continues to flow past the slope the forces operating will change. Perhaps a better approach for modelling these processes than the simple equations used here, for all types of slope movement, is to apply numerical techniques that can include a more complete representation of the material behaviour, physical conditions involved, and the forces as the system evolves. This will necessarily require the expertise of numerical modellers as well as those with expertise in rock and ice mechanics, and the modelling will be greatly improved by field calibration if high resolution monitoring data can be obtained for both the slope and the glacier.

4.2.6 Conclusions

Failure and movement of ice-contact slopes appear to be important, but as yet still poorly-constrained, processes involved in slope evolution and glacial erosion. The initiation and development of some slope failures in glaciated valleys may occur significantly earlier than previously recognised. Glacier ice cannot always prevent the movement of slope failures, but has a significant role in mediating the rate of slope movement. Force analysis demonstrates that large glaciated rockslides can deform glacier walls and move at a rate of 10^{-2} – 10^{2} metres per year. Mapping with satellite imagery suggests that these features exist; they are identified by the coincidence of visible slope deformation with associated glacier narrowing. Monitoring of one rockslide reveals a variable movement rate; the rate may depend on changes in the slope, glacier conditions, or external factors. We hope that the study will motivate searches for additional field evidence of such phenomena in different physiographical locations and the application of more powerful remote sensing techniques and slope monitoring capability to help to investigate the rate-controlling processes, particularly the role of water pressure. Further, it is hoped that the study will help motivate numerical modelling studies aimed at quantifying these processes and predicting catastrophic slope failure, as well as guide the application of appropriate material properties and physical constraints used in those models.

Acknowledgements: We are grateful to Patrick Kailey for revising the manuscript and Simon Cook for providing SPOT imagery, and to both for useful discussion on the topic. We thank reviewers Christian Huggel and Philip Deline, and editorial staff for their constructive comments.

4.3 PART C: THE EFFECT OF GLACIATION ON THE INTENSITY OF SEISMIC GROUND MOTION

The effect of glaciation on the intensity of seismic ground motion, McColl ST; Davies TRH; McSaveney MJ, *Earth Surface Processes and Landforms,* 37: 1290-1301. Copyright © 2012 John Wiley & Sons, Ltd
http://onlinelibrary.wiley.com/doi/10.1002/esp.3251/full

Only formatting and pagination has been modified for inclusion in this thesis

Abstract: Seismicity is known to contribute to landscape denudation through its role in earthquake-triggered slope failure; but little is known about how the intensity of seismic ground motions, and therefore triggering of slope failures, may change through time. Topography influences the intensity of seismic shaking – generally steep slopes amplify shaking more than flatter slopes – and because glacial erosion typically steepens and enlarges slopes, glaciation may increase the intensity of seismic shaking of some landforms. However, the effect of this may be limited until after glaciers retreat because valley ice or ice-caps may damp seismic ground motions. Two-dimensional numerical models (FLAC 6.0) were used to explore how edifice shape, rock stiffness and various levels of ice inundation affect edifice shaking intensity. The modelling confirmed that earthquake shaking is enhanced with steeper topography and at ridge crests but it showed for the first time that total inundation by ice may reduce shaking intensity at hill crests to about 20–50% of that experienced when no ice is present. The effect is diminished to about 80–95% if glacier ice level reduces to half of the mountain slope height. In general, ice cover reduced shaking most for the steepest-sided edifices, for wave frequencies higher than 3 Hz, and when ice was thickest and the rock had shear stiffness well in excess of the stiffness of ice. If rock stiffness is low and shear-wave velocity is similar to that of ice, the presence of ice may amplify the shaking of rock protruding above the ice surface. The modelling supports the idea that topographic amplification of earthquake shaking increases as a result of glacial erosion and

deglaciation. It is possible that the effect of this is sufficient to have influenced the distribution of post-glacial slope failures in glaciated seismically active areas.

4.3.1 Seismic implications of glaciation

Glacial cycles have wide-spread effects on much of the landscape system beyond the direct influence of waning and waxing of global ice masses. One such consequence is glacio-isostatic stress changes in the crust of the earth and associated changes to crustal deformation and seismicity. Glacio-isostatic uplift since the last glaciation has been on the order of 10^1 to 10^2 m on some continents (Stewart et al., 2000). Increases in fault slip and in the amount and distribution of pre-historic as well as contemporary seismicity have also been linked to glacial rebound (Hetzel and Hampel, 2005). It has also been recognized that as well as large continental ice sheets, smaller ice masses have affected uplift, seismicity and slip on faults in glaciated mountains belts (e.g. Persaud and Pfiffner, 2004; Barletta et al., 2006; Ustaszewski et al., 2008).

Another consequence of glacial cycles is the change to factors affecting mountain slope stability. A clustering of landslides in the post-glacial period has been thought to be mostly a response to a decrease in slope stability caused by glacial steepening/deepening and the subsequent glacial debuttressing, stress release, and mechanical weathering occurring with deglaciation (Ballantyne, 2002). However, a period of more intense coseismic landslide triggers, produced during glacial-rebound enhanced seismicity, has also been proposed to explain these post-glacial landslide distributions; coseismic landslide densities correlate with both earthquake magnitude (Keefer, 1984; Keefer, 1994) and shaking intensity (Meunier et al., 2007). Therefore, an increase in seismicity (or systematic shaking intensity) can be expected to influence landslide distributions. For example, Sanchez et al. (2009) use cosmic-ray exposure dating of fault-slip, glaciated surfaces and landslides in the French Southern Alps to reveal close temporal correlation between fault activity and landsliding shortly after deglaciation in the early Holocene. The following section discusses how glaciation and deglaciation may also alter the intensity of earthquake shaking.

It has been observed that coseismic landslides often occur on steep slopes and at the crests of ridges (Geli et al., 1988; Murphy, 2006). This is probably in part because of the way landform topography can enhance ground motions, a process referred to as topographic amplification. Meunier et al. (2008) explain that topographic amplification of seismic shaking occurs when seismic waves entering the base of a mountain edifice are partially reflected back into the rock and diffracted along the free surface. This causes the waves to converge at the slope convexities, in particular at ridge crests, and enhance ground motions at these locations. The importance of topographic amplification for coseismic landslides is confirmed by a statistical study of landslide distributions produced by earthquakes in three different locations (Meunier et al., 2008). These authors found that, as well as correlating with epicentre proximity, landslide distributions correlated with topographic conditions and the landslides were preferentially located at ridge-crests or the upper flanks of slopes. Changing the topography of a landscape is likely to influence topographic amplification and affect coseismic shaking intensities. Because glacial erosion can produce steep topography – it can truncate slopes, form steep valley cross-profiles, and create sharp arêtes and glacial horns – it may increase the potential for topographic amplification of earthquake shaking in these locations. However, during glaciation, while glaciers still occupy valleys and mantle topography, glacier ice may in fact damp seismic shaking (Figure 4.3.1). Ice cover may damp seismic shaking because: (1) some seismic energy propagating through the rock, that otherwise would be reflected back into the bedrock at the free-surface, will instead travel into the ice, and (2) ice provides a confining mass that is rigid at dominant earthquake frequencies and able to reduce the shaking amplitude experienced in the bedrock. Based on these factors, the intensity of ground shaking should vary with ice inundation and so should the probability of coseismic rock-slope failure. Numerical modelling is used to test the hypothesis that deglacierization enhances topographic amplification of earthquake shaking on glacially steepened bedrock.

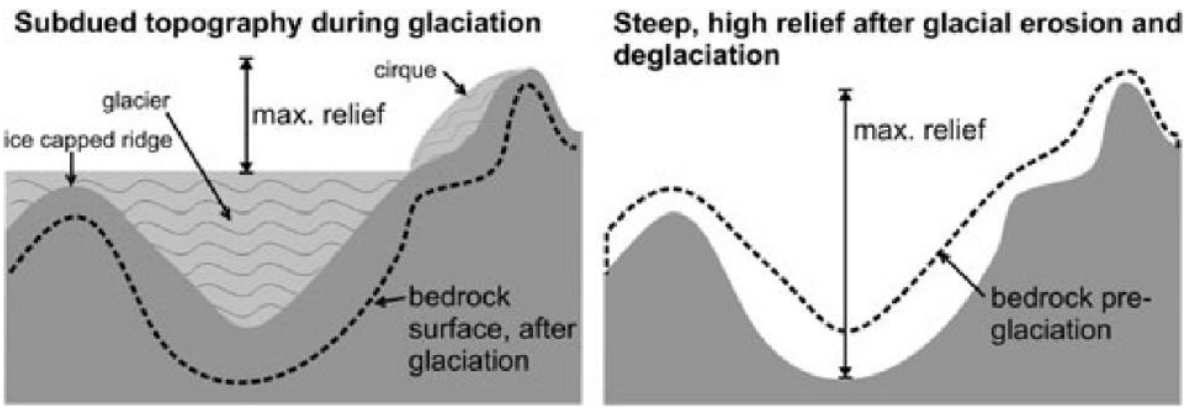

Figure 4.3.1. Schematic of topographic relief at the start of glaciation (bed-rock profile underneath ice at left and dashed line at right), during glaciation (ice surface at left), and after glaciation (bedrock profile at right and dashed line at left).

4.3.2 Topographic site-effects

Earthquakes do not shake the ground equally everywhere. In geotechnical engineering, the term 'site-effects' is used to describe the entire range of factors causing local variations in shaking at the ground surface due to a given earthquake. Topographic amplification is just one of the many site-effects influencing ground motions during earthquakes (others include source-motion characteristics, seismic-path effects, and local soil, geological, structural, and hydrological conditions), but it is one of the more important factors in steep mountainous terrain (Boore, 1972). For example, field measurements of seismic ground motions on the crest of a greywacke ridge in New Zealand were amplified 300 -1100% compared to those measured on flat ground near the base of the ridge (Buech et al., 2010).

Topographic amplification has been investigated theoretically, empirically, and through numerical and physical modelling (e.g. Boore, 1972; Geli et al., 1988; Benites and Haines, 1994; Sepúlveda et al., 2005; Bouckovalas and Papadimitriou, 2006; Buech, 2008; Meunier et al., 2008; Dhakal, 2009; Di Fiore, 2010). Results indicate that edifice shape, material stiffness, and the direction and frequency composition of the seismic input strongly influence the local topographic amplification or deamplification of seismic ground motions. Steeper slopes and convexities in slopes generally produce stronger shaking, and amplification is inversely proportional to rock stiffness. Amplification is significantly greater for horizontal ground motion than it is for the vertical components, and greater for motion perpendicular to a ridge than for those parallel. Focussing of shaking on the far side of ridges occurs if the incoming seismic energy is oblique to the hill instead of propagating vertically upwards underneath the

ridge. The response has maxima at the resonant and harmonic frequencies of the edifice, and is generally greatest at ridge crests (Buech et al., 2010).

The way in which seismic shaking destabilizes edifices has not been closely investigated, but it is clear that traditional models of coseismic slope stability (e.g. Newmark sliding block and pseudo-static methods) fail to capture some of the physical processes adequately. We suggest that an edifice responds to an incoming seismic wave-field by developing overall motions reflecting its size, shape and elastic properties; numerical methods, for example discrete element modelling simulations by Bazgard et al. (2009), indicate that horizontal deformations at the edifice crest greatly exceed those at mid-height, and may be out of phase with them. Bazgard et al. (2009) showed that these motions generate high shear stresses deep within the edifice. This leads to the development of deep-seated failure surfaces and correspondingly large-volume landslides. This is in part why the modelling performed here only considers horizontally polarized shear waves. Additionally, vertically polarized shear waves are excluded because they are more challenging to model and because vertical motions are less affected by topographic amplification than are horizontal motions (Buech et al., 2010), and consequently, any effects observed for horizontal shear waves are likely to be less for vertical waves. It is acknowledged however, that both vertical and horizontal seismic ground motions may play a role in triggering landslides (e.g. Huang et al., 2001; Ingles et al., 2006).

4.3.3 Methodology

A two-dimensional explicit finite difference program, FLAC 6.0 (Itasca Consulting Group, 2008), was used to model the effect of inundation by ice in modifying the response of mountainous terrain to seismic shaking. Two-dimensional modelling was preferred over three-dimensional for its simplicity; however, it is recognized that the response of a mountain edifice to seismic loading is strongly influenced by the angle of incidence of the seismic waves, and that their interaction with the mountain edifice is controlled by its three-dimensional shape, and to that extent this work is exploratory.

The study was carried out in two stages. First, several idealized mountain edifice cross-sections, bounded by various thicknesses of ice, were dynamically loaded (shaken) by (cosine) waves of various frequencies. The purpose of this was to explore edifice-shape and wave-frequency dependence of the ice's effect on the response of the edifice. The second stage involved modelling cross-sections of two New Zealand mountain edifices, one affected in the past by a large valley glacier, and one by cirque glaciers. For the seismic input in this stage, real earthquake seismographs were used in addition to the artificial cosine waves.

4.3.3.1 FLAC 6.0 model setup and parameters

The following section describes the conditions and parameters used in the modelling. The models were implemented using the built-in FLAC programming language FLACish (FISH) in addition to the pre-set commands provided in the graphical interface.

4.3.3.1.1 Grid generation: idealized mountain edifices

The geometries for all models were created by dissecting a rectangular grid, made up of 10 m^2 zones, with lines defining the geometrical shapes and assigning material properties (ice or rock) to regions within the geometrical shapes, and assigning regions of zero stress outside of these. Three 1000 m high mountain geometries were created, the first two with rectilinear slopes of 45° and 65°, and a third with a break in slope at mid-height (Figure 4.3.2). The first two geometries were used to study the effect of slope angle on amplification, while the last geometry represented a mountain steepened by glacial valley erosion. The edifice size was an important consideration; the greatest amplification occurs when the wavelength of the incoming seismic wave is approximately equal to the height or half-width of the mountain edifice (Geli et al., 1988; Buech, 2008). For the chosen materials (Table 4.3.1), the 3 Hz wavelength was close to the 1000 m height selected for the idealized mountain edifices. The idealized mountains were partly to completely submerged in ice representing various levels of ice inundation (Figure 4.3.2).

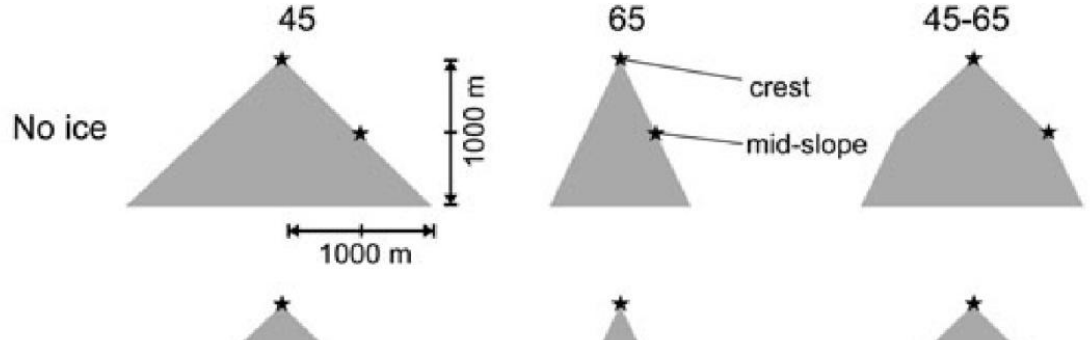

Figure 4.3.2. Model geometries with no ice, with a 'glacier', and with complete ice cover. The grid zone size in each model is 10 m by 10 m. The monitoring locations at the crest and mid-slope are shown with black stars.

Table 4.3.1: Properties and model parameters for the materials used in the FLAC analyses.

	Greywacke			Schist	Ice		
Parameter	High	Average	Low	Average	Low	Average	High
ρ (kg/m^3)[1]	2680			2800	916	916	
E (GPa)[1]	80	57	15	47	8	10	11
v[1]	0.25			0.13	0.31		
K (Equation 4.3.2) (GPa)	53	38	10	21	7	8.7	9.8
G (Equation 4.3.3) (GPa)	32	23	6	21	3	3.8	4.3
C_s (Equation 4.3.1) (m/s)	3455	2919	1496	2734	1810	2036	2160

Note: The low and high values for each material were used for defining the HRS and LRS model material properties. [1]From Stewart (1997) for unweathered intact sandstone; from Brown et al. (1980) for unweathered intact schist; and from Petrovic (2003), based on testing by Gold (1988) for intact ice at 10°C.

4.3.3.1.2 Grid generation: realistic mountain edifices

Two real mountain edifices were modelled. The sites chosen were mountains in New Zealand that are known to have been glaciated. Although not part of the criteria for selecting the chosen sites, they were both in high-seismicity regions affected by large

landslides. Cross-sections were constructed using a (Landcare Research Ltd) 25-m digital elevation model. The depth to bedrock below any contemporary ice or post-glacial valley sediment infill was roughly estimated by extrapolation of the exposed bedrock surface beneath the overburden. Different ice thicknesses were then introduced in subsequent models.

4.3.3.1.2.1 *Mount Alfred.*

Mount Alfred [44°45′40″S; 168°21′50″E; 1375 metres above sea level (m.a.s.l.)] is located at the head of Lake Wakatipu, New Zealand (Figure 4.3.3). The edifice is an isolated mass of schist situated in the middle of the Dart valley and was surrounded by ice of the Wakatipu glacier during Pleistocene glaciations (Figure 4.3.4) (Turnbull, 2000; Barrell, 2011). In this study, the last glacial maximum (LGM) ice surface was estimated to have reached approximately 800 m a.s.l. at Mount Alfred, some 500 m below its summit. This ice limit is based on recognition of a consistent spur truncation along the opposite (west) valley slopes and kame-terraces at this height on the opposite (eastern) valley slopes. The entire edifice was overridden by ice during a previous glacial advance, corresponding to another consistent spur truncation identified higher (at about 1400 m.a.s.l.) on the opposite (western) valley slopes. However, Barrell (2011) suggested considerably greater ice volumes for the last glaciation and interprets these features as being of LGM age. Regional seismicity is high, with the large and active Alpine (dextral) and Nevis–Cardrona (reverse) faults within 60 km. In a regional probabilistic hazard model (Stirling et al. 2002), a non-amplified peak ground acceleration of 0.7 g for a 475 year return interval is estimated for the Mount Alfred area.

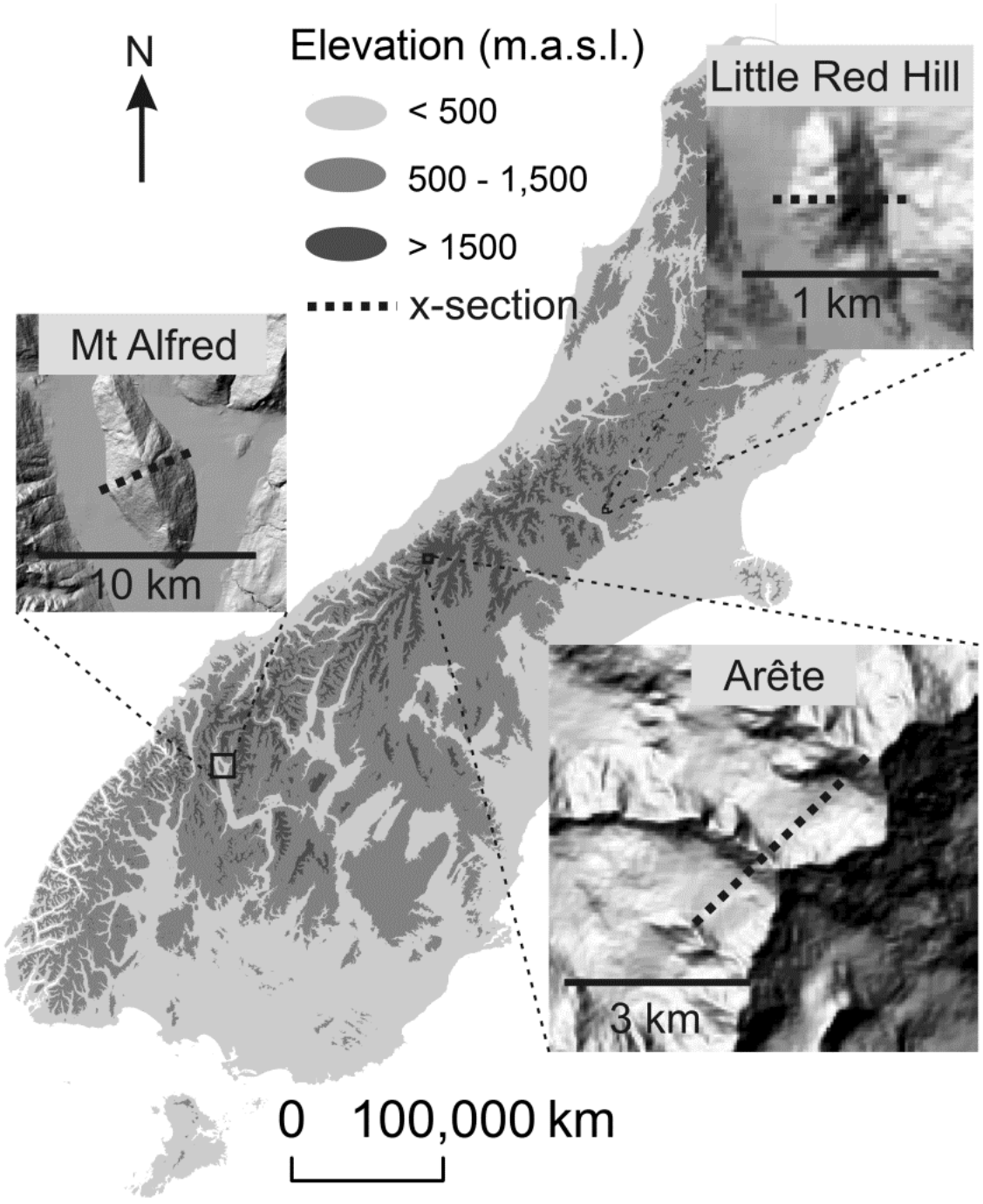

Figure 4.3.3. Location of sites in South Island, New Zealand. Cross-sections are shown on the hill-shade insets.

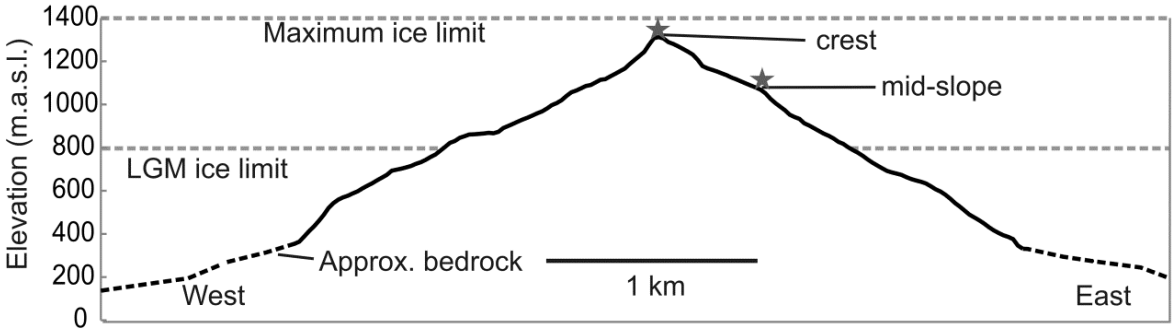

Figure 4.3.4. Mount Alfred cross-section with approximate ice limits adopted in model. Monitoring locations at the crest and mid-slope are shown with grey stars.

4.3.3.1.2.2 *Arête.*

An unnamed narrow arête of bedrock (43°34′22" S; 170°08′35" E; 3071 m.a.s.l.) lies near Mount Tasman. This arête was chosen to represent the sharp topography typical of glaciated landforms in this region (e.g. Kirkbride and Matthews, 1997) (Figure 4.3.3 inset). Today the arête is exposed above small glaciers but it is possible that it, and others like it, were completely submerged in ice during peak glaciation. Hypothetical surfaces have been reconstructed (Figure 4.3.5) to represent this arête without ice and inundated with various ice thicknesses. Regional seismicity is high with the large and active Ostler (reverse) fault and the (dextral) Alpine fault both within 50 km and contributing to a non-amplified probabilistic peak ground acceleration for a 475 year return interval of 0.8 g at the arête location (Stirling et al., 2002).

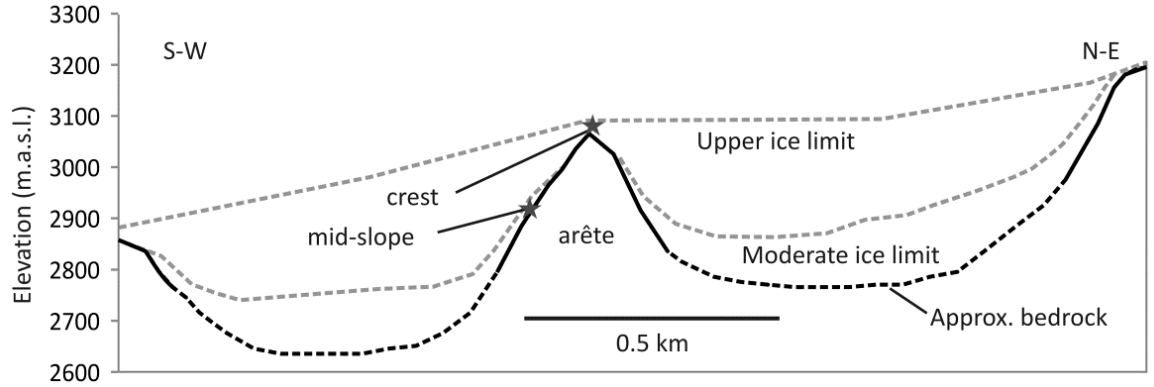

Figure 4.3.5. Arête cross-section with approximate ice limits adopted in model. Monitoring locations at the crest and mid-slope are shown with grey stars.

4.3.3.1.3 Material properties and constitutive model

Material properties influence the response to seismic inputs, with greater stiffness and higher shear-wave velocities producing less intense shaking responses. The shear wave velocity, C_s is related to the material stiffness (shear modulus, G) and the density (ρ) by:

$$C\_s = \sqrt{(G/\rho)} \tag{4.3.1}$$

Because G and C_s vary with rock type, rock-mass quality, depth and temperature, it was not practical to model the entire range of variability; instead representative values were chosen (Table 4.3.1). However, to provide upper and lower bounds for the expected variation, the models were run with upper-bound and lower-bound values of G and C_s for ice and lower-bound and upper-bound values for rock (herein referred to as high relative ice stiffness, or HRS and low relative ice stiffness, or LRS, respectively) (Table 4.3.1). It was expected that HRS ice would damp seismic shaking more, and that LRS would damp seismic shaking less, because more similar shear wave velocities in the rock and ice should result in less reflection of energy back into the bedrock, and stiffer ice should provide more resistance to shaking.

Isotropic-elastic constitutive models were used to represent the behaviours of ice and rock because the objective was to investigate the relative amplifications of seismic energy, not mass failure, and to provide general indications of response rather than site-specific assessments. For an elastic model, three material parameters are required: density, and the bulk and shear moduli. Bulk modulus, K (a measure of stress induced volume change) is related to Young's Modulus, E (a measure of elasticity) and Poisson's ratio, v (ratio of longitudinal strain to axial strain) by:

$$K = E/[3(1 - 2\upsilon)] \tag{4.3.2}$$

and the shear modulus, G (a measure of stress induced shear strain) to these variables by:

$$G = E/[2(1 + \upsilon)\,] \quad (4.3.3)$$

Typical (and lower and upper bound) material properties for unweathered New Zealand greywacke sandstone were used for the conceptual and arête models (Stewart, 1997). For Mount Alfred, properties for a site in Otago schist (Brown et al., 1980) were used. Despite the known influence of foliation orientation on deformation moduli, an isotropic model was used for the schist because: (1) Mount Alfred is a synform with foliation dipping into the slope on either side (Turnbull, 2000) so the weakness cannot be exploited; and (2) the modulus values chosen were derived from laboratory testing of a sample of schist for which the results were treated as isotropic (Brown et al., 1980).

4.3.3.1.4 Seismic wave propagation

In setting up the model grid, a compromise was made between computational time and ensuring accurate propagation of the seismic wave by limiting the zone size. The recommended spatial zone size is one-tenth of the wavelength or smaller (Itasca Consulting Group, 2008). Using a grid with zone size of 10 m^2 allowed the maximum wave frequency *f*, before wave distortion, to be 29 Hz for the sandstone, 27 Hz for the schist, and 20 Hz for the ice, based on $f = C_s/100$. Although the maximum allowable wave-frequency (20 Hz) for ice is just within the upper range of frequencies used in the earthquake input data (25 Hz and 0.1 Hz), the distortion of the wave should be negligible because most of the energy is contained within frequencies below 15 Hz (Figure 4.3.6).

Quiet and free-field boundary conditions were applied at the base and edges of all model grids to eliminate wave interference and to ensure that energy propagated as if the model was of infinite extent at the boundaries. The quiet boundary uses viscous dashpots attached to the base of the model to provide normal and shear tractions, thus preventing the reflection of downward-propagating waves back into the model. The free-field boundary condition is applied to the edges of the model, and similarly, dashpots enforce free-field motion at the boundary so that outward propagating waves are not reflected back into the model (Itasca Consulting Group, 2008).

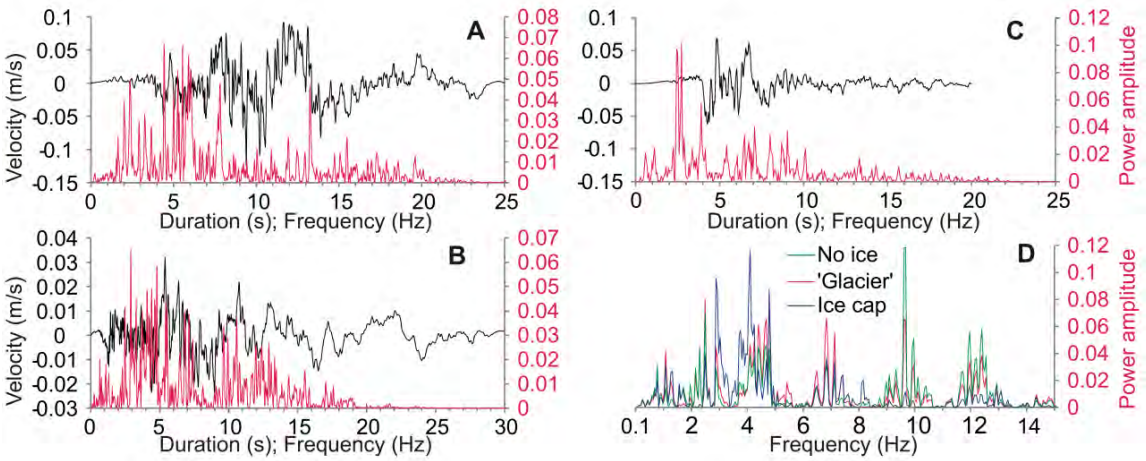

Figure 4.3.6. Velocity histories (black line) and power spectrum (red line) for (A) Loma Prieta, (B) Morgan Hill and (C) Christchurch earthquakes. (D) Example of Morgan Hill power spectrum for undamped arête model using HRS material values, illustrating the effect of shifting the predominant frequencies with addition of different thicknesses of ice.

4.3.3.1.5 Seismic input

4.3.3.1.5.1 *Idealized mountain edifice*

The elastic strain energy radiated in an earthquake is a mix of body waves of many different frequencies making it impractical to model the entire wave spectrum here. Instead, for the basic mountain edifice modelling a single horizontal shear-wave cycle of a specific frequency (between 0.5 and 12 Hz) and with a shear particle velocity of 1 m/s was used as the input for each model run. This was sufficient to allow comparison of the way seismic energy was amplified in each of the model geometries. This frequency range was chosen because it brackets the frequencies usually associated with strong ground motions (1–10 Hz) and the fundamental frequencies of the models. The shear wave was applied to the entire base of the model as an applied shear stress σ_s calculated by:

$$\sigma_s = 2(\rho C_s)V_s \tag{4.3.4}$$

where, ρ is the mass density (of the rock), C_s is the speed of shear-wave propagation through medium and V_s is the input shear particle velocity (1 m/s), with the factor of two accounting for dividing the energy into an upward and a downward propagating wave at the grid boundary.

4.3.3.1.5.2 *Real mountain edifice*

As well as applying the same artificial seismic input as that used for the idealistic geometries, seismic inputs based on three recorded earthquakes were applied to the real mountain models: the 1989 Loma Prieta and 1984 Morgan Hill (California) earthquakes, and the February 2011 Christchurch (New Zealand) earthquake. These earthquakes represent a range of similar magnitudes and fault rupture mechanisms to that which might be expected for large earthquakes at the study sites (i.e. greater than 6.0 moment magnitude and produced by reverse-oblique or strike-slip faulting). The Californian earthquake data were extracted from the Pacific Earthquake Engineering Research Centre ground motion database and the Christchurch earthquake data were extracted from the GeoNet FTP site of GNS Science. Velocity histories are shown in Figure 4.3.6 (A, B & C), and the characteristics of the earthquakes and the criteria used for selecting them and the recording sites (seismometers) are in Table 4.3.2. Filtering and linear-baseline correction were applied using SeismoSignal 4.1.2. The velocity history was used as the input shear particle velocity (v_s) in Equation 4.3.4.

Table 4.3.2: Earthquake characteristics and seismometer selection criteria

	Earthquake			Reason
Parameter/type	Loma Prieta	Morgan Hill	Christchurch	
Mechanism	Reverse/oblique	Strike-slip	Reverse	Similar to local faults
M_W	6.9	6.2	6.3	Large coseismic rock-slope failures are normally triggered by EQs > 5–6 M_W
Distance to fault (km)	12	15	15	> 10 to avoid near-to-source interference and < 30 to avoid attenuation effects
Motion component	Fault-parallel	Fault-parallel	North-South	Arbitrary
Average C_S in top 30 m, V_S30 (m/s)	714	1428	> 700	To ensure the seismic data are appropriate for the bedrock being modelled, i.e. C_S between 700–10 000 m/s
Filtering (Hz)	> 0.1, < 25	> 0.1, < 25	> 0.1, < 25	To remove noise
Predominant frequency (Hz)	4–6	2–5	2–3	Broad range to test wave-frequency-dependence in modelling

4.3.3.1.5.3 *Cyclic energy damping*

In any natural system there is energy loss (attenuation) during wave propagation, both through loss as the wave radiates out from a point source (geometrical spreading), and through frictional losses and slippage at grain boundaries. Attenuation will offset

some of the amplification of ground motion by topography because seismic energy reaching the top of a topographic high-point will have travelled farther and therefore attenuated more energy than the seismic energy only travelling as far as the base of the topographic feature. Geometrical spreading is significant only over large distances and because of the relatively small masses modelled here it was considered sufficient to treat the incoming wave as planar. Attenuation from frictional losses and slippage at grain boundaries however, was considered important, but only for the realistic modelling. Attenuation could be ignored for the idealized models because the models were of equivalent size and the objective was to investigate how shape and the presence of ice modify relative amplifications, rather than to model real ground motions.

For the realistic modelling, attenuation was forced using the Rayleigh method, which uses a viscous dashpot to damp seismic energy proportional to the material mass (Itasca Consulting Group, 2008). Although the attenuation of seismic energy travelling through rock is frequency-dependent, for the purposes of this modelling it was assumed that the damping was frequency-independent over the range of dominant frequencies. This was achieved by setting the centre-frequency of the damping factor to within the range of the predominant frequencies of the model system. The predominant frequencies of the model system are a combination of the spectral frequency of the dynamic input and the natural mode of the system, and were determined by applying the earthquake (with no damping) and then analysing the resulting power spectral density (power versus frequency) for a central, representative location in each model (Figure 4.3.6 A, B, & C). A damping value of 3% (of critical) was used because it is within the 2–5% range for typical damping of geological materials (Newmark and Hall, 1982). Three per cent damping reduced peak ground motions at the crest of the arête and Alfred models by about 20 and 30%, respectively.

4.3.3.1.6 Model outputs

The ground motion amplification effect was explored by examining the modelled horizontal velocity of the mountain at equivalent surface point locations in each model. These locations were at the crest and mid-slope position of each mountain (Figures 4.3.2, 4.3.4 and 4.3.5). The motions at the crest were of critical importance because ground motion high on the edifice has been shown to lead to deep-seated failure surfaces

such as those seen in coseismic landslides (Bazgard et al., 2009). Vertical ground motions produced by the sideways flexing of the edifice were recorded but excluded from analysis because they were an order of magnitude smaller than the horizontal motions.

4.3.3.1.7 Modelling test

To check that FLAC was capable of realistically modelling topographic amplification it was tested using data from a greywacke edifice known as Little Red Hill (Figure 4.3.7) whose seismic response to several far-field and regional earthquakes has been measured (Buech, 2008). Buech (2008) determined that the greatest motions occurred for waves with frequencies around 5 Hz and perpendicular to the main axis of the ridge. At the crest of the ridge he found that accelerations were typically amplified by about 500% compared to those on flat land near the base of the ridge. A cross-section across Little Red Hill was constructed to coincide with the crest (Figure 4.3.7) and the values for the material properties were those used by Buech based on typical properties for New Zealand greywacke. Dynamic input was applied as described for the idealistic models and with 3% Rayleigh damping. Similarly to the field measurements, the modelled peak ground response occurred around 5 Hz. The maximum amplification modelled at the crest was about 150% higher than at the base of the slope (Figure 4.3.7). The modelled amplification was considerably lower than that measured by Buech, consistent with a common disparity found between field observations and modelled amplifications (Geli et al., 1988). Geli et al. (1988) suggest that models may underestimate amplification because of inadequate representation of geological conditions, three-dimensional effects, and topographic complexities. At Little Red Hill, it is possible that the crest of the ridge has a lower rock mass shear wave velocity than the base because, as noted by Buech, the crest of the hill showed evidence of catastrophic coseismic rock damage. Another reason for the disparity may be failure to model ground motions produced by compressional, shear vertical and surface Rayleigh waves, all of which can also be amplified by topography (Benites and Haines, 1994; Savage, 2004). In summary, the FLAC models reproduce the natural site-period of the edifice but underestimate the magnitude of amplification by topography.

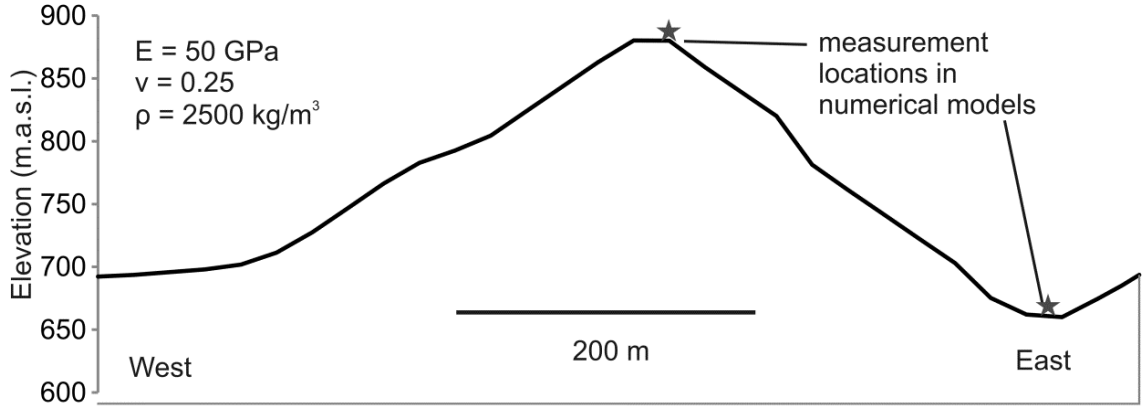

Figure 4.3.7. Cross-section of Little Red Hill model. Monitoring locations at the crest and base are shown with stars.

4.3.4 Results

4.3.4.1 Idealized models

Peak ground motions recorded at the crest and mid-slope positions for each idealistic model are presented in Figure 4.3.8. Velocities of greater than 2 m/s at the crest for all wave frequencies represent an amplification of ground motion compared to that for flat topography; a value of 2 m/s results from the velocity-doubling effect of the free-surface. In all of the idealized modelling, topography amplified seismic shaking when no ice was present. At the crest this ranged from a maximum amplification, compared to a flat surface, of 50% for the 45° geometry at a wave frequency of 3 Hz, to a maximum of 200% for the 45°–65° geometry at 12 Hz, and a maximum of 450% for the 65° geometry at 5 Hz (Figure 4.3.8). Amplification was significantly more pronounced at the crest than at the mid-slope, for which amplifications were less than 50% for all model geometries. Excluding the exceptions noted later, complete ice inundation ('full ice cover' in Figure 4.3.8) reduced the maximum velocity to close to or below the velocities measured for flat topography (i.e. 2 m/s, or zero amplification). Wave frequencies above 3 Hz resulted in slight deamplification in the 45° model. Velocities measured at the mid-slope positions were also reduced under an ice cover, to about half the amplification found for no ice cover. The ice cover reduced the velocities measured most for the 65° model, and slightly more for the 45°–65° than the 45° model. Wave frequency also influenced how much effect ice cover had, with significantly less influence for frequencies below 2–3

Hz. Only for the 45° HRS (high relative ice stiffness) model were the velocities similar, at the crest and (even slightly higher) at the mid-slope, when ice cover was present.

Partial ice inundation ('glacier' in Figure 4.3.8) for the 45° and 45°–65° models generally reduced peak crest velocities, but to a lesser extent than complete inundation. At the mid-slope there was little difference to velocities compared to the 'no ice' situation. For the 65° model the velocities at the crest were similar to the 'no ice' situation whereas the mid-slope velocities were higher. With HRS materials, there was a marked difference in response between the model geometries. For the 45° model, partial ice inundation resulted in much lower velocities than both complete ice inundation and the 'no ice' situation, whereas for the 65° model partial ice inundation increased amplification beyond that for the 'no ice' situation at frequencies above 2 Hz. There was little difference between the LRS (low relative ice-stiffness) materials and average materials.

Thus the ability for ice to damp seismic shaking in the models depended on the model geometry, the amount of ice cover, the wave frequencies and the material properties of the rock and ice. In general, ice cover reduced the effect of topographic amplification most for steepest slopes, and when ice was thickest, wave frequencies were higher than 3 Hz, and the slopes had relatively high shear stiffness.

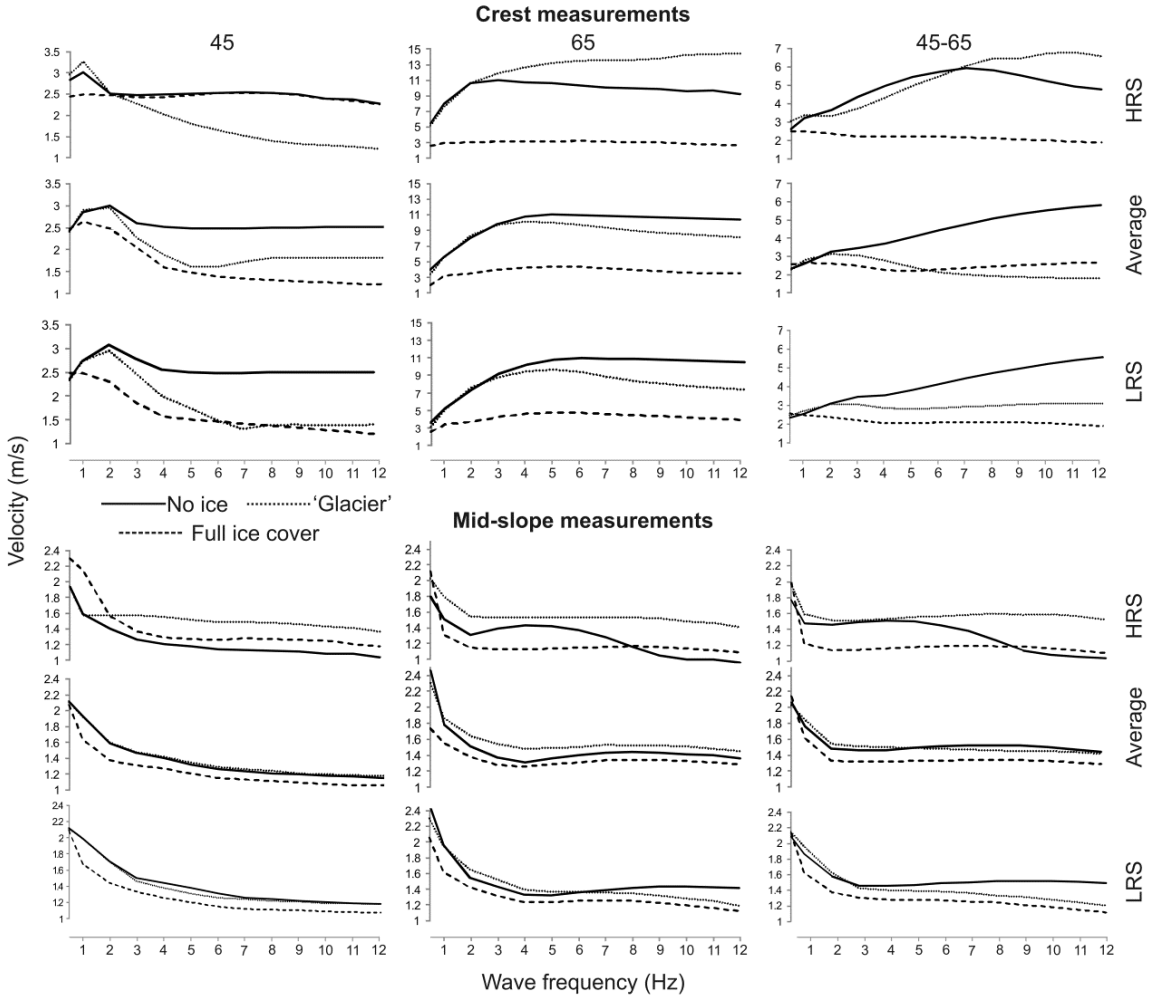

Figure 4.3.8. The response of each idealistic model to 1 m/s dynamic inputs with wave frequencies between 0.5 and 12 Hz, measured as peak velocity at the equivalent crest and mid-slope. Note that for flat topography the peak velocity at the surface for all wave frequencies is 2 m/s because of a velocity doubling at the free-surface. HRS, high relative ice stiffness; LRS, low relative ice stiffness.

4.3.4.2 Real-mountain models

4.3.4.2.1 Mount Alfred

Peak ground motions generated by the artificial seismic input at the crest and mid-slope positions of the Mount Alfred model are presented in Figure 4.3.9. A maximum amplification of about 50% occurred for frequencies between 3 and 5 Hz and complete inundation with ice resulted in a small amplification at frequencies less than 3 Hz, and a small deamplification occurred at higher frequencies. Partial inundation by ice had no significant effect on ground response. For the earthquakes modelled here, the edifice amplified shaking (peak velocities) relative to that experienced at the base of the edifice

by up to 300% at the crest and 200% at the mid-slope (Figure 4.3.10). The range in amplification produced by the three earthquakes, especially between the Loma Prieta and Christchurch earthquakes, which had similar peak velocities but different wave-frequency power distributions (Figure 4.3.6), reflects the wave-frequency dependence of topographic amplification. Ice inundation generally reduces peak velocities for all of the earthquakes modelled but does not remove the topographic amplification effect altogether. When the edifice is completely covered by ice, the amplification effect is reduced to about 60–75% to that of the ice-free edifice and reduced by only a few per cent when partially inundated by a 'glacier' (Figure 4.3.11).

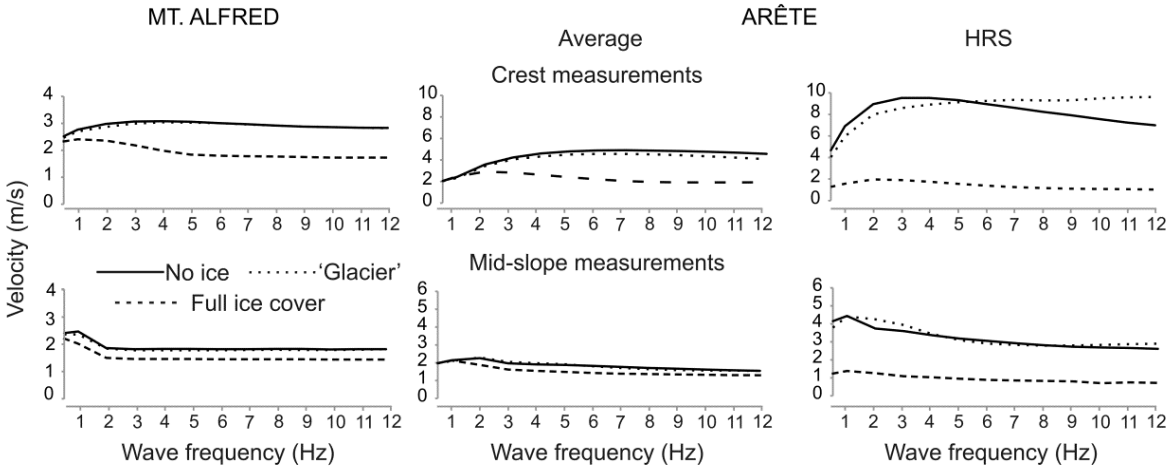

Figure 4.3.9. The response of Mount Alfred and the arête models to the artificial 1 m/s shear waves at frequencies between 0.5 and 12 Hz.

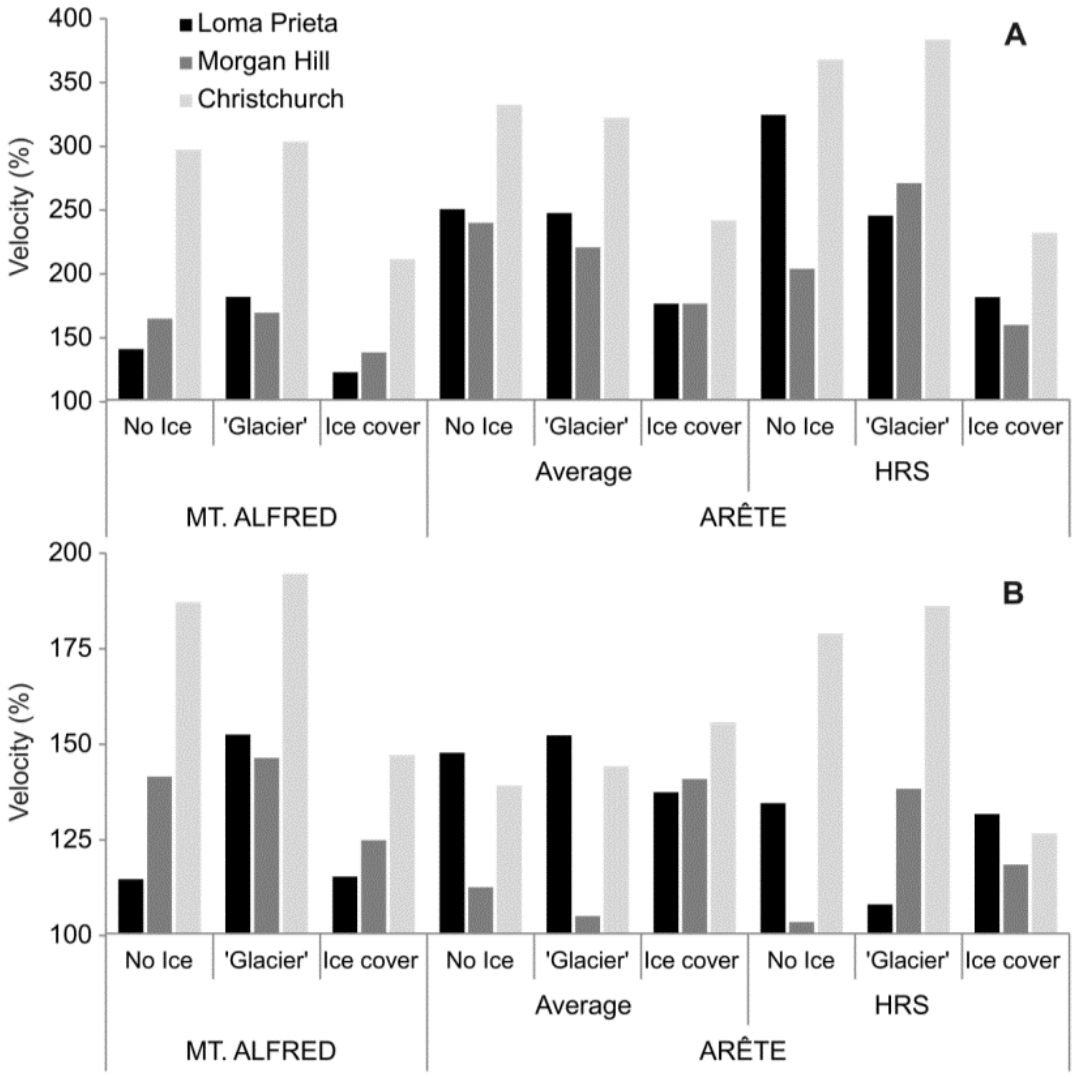

Figure 4.3.10. Percentage of peak recorded velocities of the Mount Alfred and arête models at the crest (A) and mid-slope (B) compared to that recorded at the base of each model. Note that the peak velocity recorded at the base of each model varied slightly between models for the same earthquake input and material properties, reflecting differences in geometry.

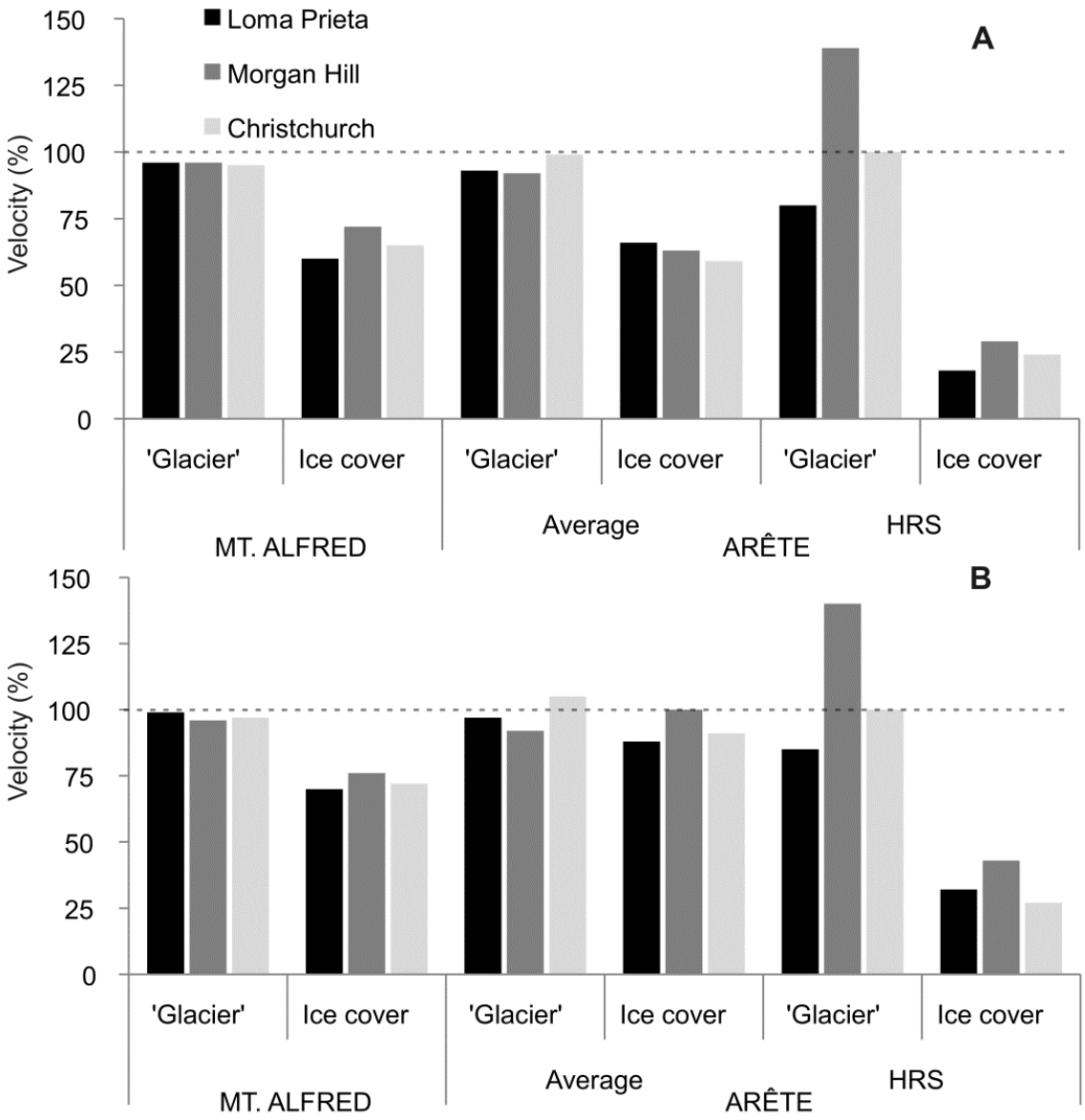

Figure 4.3.11. Percentage of peak recorded velocities of the Mount Alfred and arête 'glacier' and ice covered models at the crest (A) and mid-slope (B) locations compared to that recorded at the equivalent locations in the models with no ice inundation. Values falling under the dashed line represent a reduction in shaking, whereas values exceeding the line represent an increase in shaking.

4.3.4.2.2 Arête

Peak velocities for the arête models were higher than those for Mount Alfred (Figures 4.3.9 and 4.3.10), as expected with the steeper and narrower profile of the mountain. Peak ground motions generated by the artificial seismic input at the crest and mid-slope positions of the arête models are presented in Figure 4.3.9. For average relative ice stiffness, a maximum amplification of about 150% occurred for frequencies

between 6 and 8 Hz and complete inundation with ice reduced the amplification to zero for frequencies greater than 5 Hz and to about 50% for frequencies between 2 and 4 Hz. With high relative ice stiffness, a maximum amplification factor of nearly 400% occurred for frequencies between 3 and 4 Hz, while complete inundation completely removed this effect and caused a slight deamplification at frequencies other than 2 to 3 Hz. Partial inundation by ice produced a slightly lower amplification factor for frequencies below 5 Hz but increased amplification at higher frequencies. In response to the real earthquakes, the edifice amplified shaking (peak velocities) relative to that experienced at the base of the edifice by a maximum of almost 400% at the crest and 185% at the mid-slope (Figure 4.3.10). Similarly to Mount Alfred, an ice cover reduced the response to about 50–60% but had little influence on the peak velocities recorded at the mid-slope (Figure 4.3.11). When HRS material values were used, the complete ice cover reduced the velocities at the crest and mid-slope to about 25–40% of that of an ice-free edifice (Figure 4.3.11). Partial inundation by the 'glacier' for the HRS models had a greater degree of variation between the earthquakes for both the mid-slope and crest locations: Compared to the 'no ice' situation, velocities were less for the Loma Prieta earthquake, similar for the Christchurch earthquake, and higher for the Morgan Hill earthquake. The reason this occurred is likely that the predominant frequency components of the three earthquakes (Figure 4.3.6, Table 4.3.2) more broadly spanned the natural frequency of the HRS 'glacier' model, which closely matched to the predominant frequency of the Morgan Hill earthquake. In general, it demonstrates the frequency-dependence of the phenomena under investigation.

4.3.5 Discussion

In all of the models, complete ice inundation reduced shaking intensity (peak velocity), suggesting that if mountain crests and steep topography were deeply mantled in ice, bedrock shaking intensity could be reduced to at least 20–50% of that experienced in similar earthquakes in the absence of the ice cover. The effect diminishes to about 80–95% for glaciers that reach to about half of the mountain slope height. However, given

the tendency of FLAC to underestimate field amplifications, the actual effects of ice inundation may be greater than modelled (Section 4.3.3.1.7).

The effect of ice on damping seismic energy has been shown here to be dependent on the earthquake-frequency spectrum, being greatest for frequencies higher than 2–3 Hz for the chosen idealized geometries. Considering that each earthquake emits a unique spectrum of seismic energy and that topographic amplification is known to be a wave-frequency dependent phenomenon, it was not surprising that the three earthquakes modelled here produced different ground motions under both identical and geometrically- and physically-varied conditions. Some of this variability has been accounted for in the modelling by testing different geometries, materials and earthquakes. One surprising result is that the presence of glaciers could amplify shaking in situations where the rock crest rises above the ice surface, and particularly where topography is steep and the rock stiffness is low (Figures 4.3.8 and 4.3.10). This may be because ice, with low stiffness and shear wave-velocity, produces stronger ground motions than the rock. The energy from those ground motions may be transferred and concentrated into the protruding rock mass, consequently generating sufficient extra shaking (especially when the rock also has low stiffness). This may offset and outweigh the reduction in topographic amplification effect provided by the ice.

4.3.5.1 Other post-glacial processes modifying topography

So far it has been assumed that deglaciation will only increase the topographic relief because of glacier recession, but there are other non-glacial processes that may have the opposite effect during deglaciation. Mountain-slope instability is commonly thought to increase following deglaciation (Cruden and Hu, 1993; Ballantyne, 2002), and indeed the steepest and highest slopes are presumably likely to be the first to fail, increasing the stability of those slopes through time as the more probable failure sites are consumed and the slopes are lowered and brought to a stable equilibrium angle. The colluvium generated in these slope failures, as well as other material washing off valley walls, may accumulate in scree-fans and scree-aprons, to broaden and buttress the base of the mountain edifice, making the valley cross-profile less steep. Post-glacial valley sedimentation also lessens the relief as sediment accommodation spaces vacated by

glacier ice are progressively filled (Eyles et al., 1990). It is uncertain how these sediments may influence seismic ground motions but it is possible that, as shown here with ice, they will reduce topographic amplification. Topographic amplification of the seismic shaking may be at its peak immediately following deglaciation and gradually reduce through these slope denudation and valley sedimentation processes (Figure 4.3.12).

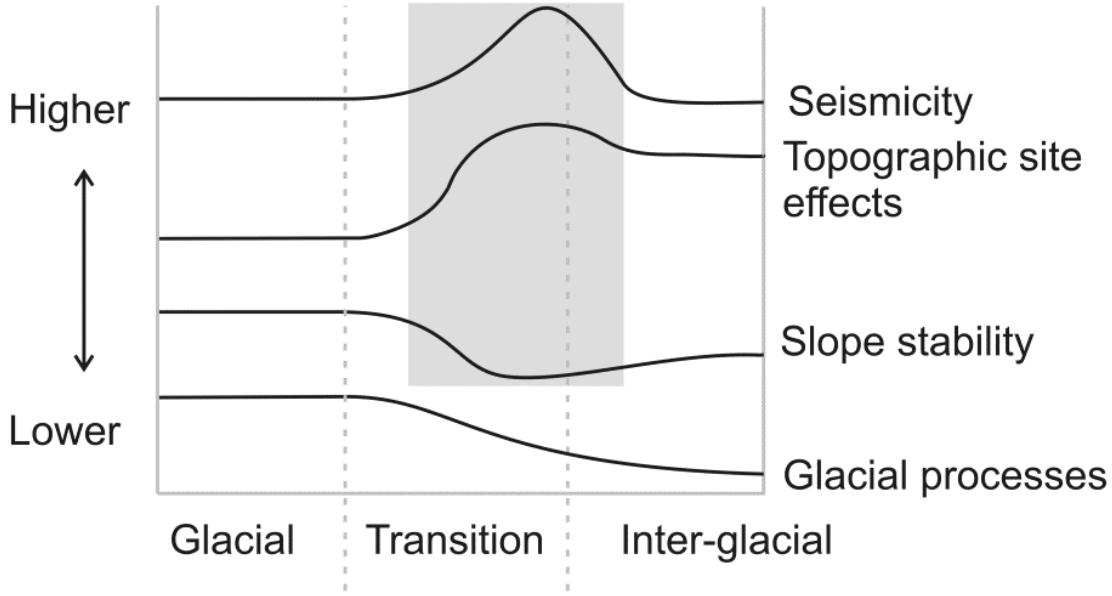

Figure 4.3.12. Conceptual model for the evolution of coseismic landslide susceptibility as a result of changing levels of topographic amplification effect and ice damping, changing glacial-rebound induced seismicity, and changes in slope stability as influenced by deglaciation processes (such as permafrost degradation and glacier retreat). The grey area marks the period when coseismic landslide susceptibility is greatest.

4.3.5.2 Other site-effects and heterogeneity

The present modelling has assumed that bedrock is homogenous and uniform throughout the edifice, but in reality the stiffness and shear wave velocities will vary depending on lithological variations, bedding or foliation, joint distributions, and weathering. Generally, the shear-wave velocities and stiffness will decrease closer to the surface where weathering and jointing are greatest. The development of joint networks and weathering profiles, as might be expected following deglaciation (McColl, 2012), will likely increase the susceptibility of sites to intense ground motions during

earthquakes. The ice properties will also vary, especially because ice elastic properties are affected by temperature (Gold, 1988). It has been assumed that the ice-rock contact is fixed but this is not always true, such as at bergschrunds, so the ice will be more effective at damping seismic energy in some places than at others.

4.3.5.3 Slope stability implications

The implications of these findings for slope stability are conceptualized in Figure 4.3.12, which shows the evolution of coseismic landslide susceptibility partly as a result of changing levels of topographic amplification effect and ice damping. The model also accounts for changing glacial-rebound induced seismicity – it is assumed that, during full glacial conditions, the background seismicity is not zero. The model can ignore other factors, such as the frequency spectrum and magnitude of the earthquake; proximity to the source and angle of incidence; attenuation between source and mountain; duration and cyclic loading; kinematic feasibility of failure; and the rock-mass strength. These factors influence whether a particular earthquake will trigger a coseismic slope failure or not but they are assumed to not vary appreciably with changing glacial conditions. The model does account for changes to other factors, *sensu* Glade and Crozier (2005), affecting the stability of slopes in deglaciated terrain; aside from the pre-conditioning factors of lithology and structure, these may include preparatory factors such as glacial steepening, slope debuttressing, stress release, freeze–thaw weathering, stress fatigue, and hydrological factors associated with the climatic changes (McColl, 2012). The model assumes that during glaciation, fewer sites are able to fail catastrophically because ice buttresses their slopes. Proportionally fewer catastrophic coseismic landslides occur during full glaciation when ice inundates the landscape and lessens rock-mass degradation from coseismic rock damage and weathering. Once seismicity and intensity ramps up again during deglaciation, and once other preparatory factors influenced by deglaciation have developed, the likelihood of coseismic landslides increases. This is consistent with other studies, reviewed by McColl (2012), that report a high frequency of large rock slope failures developing during and after the last deglaciation. Several non-seismic reasons have been suggested to explain this increase of landslide activity, such as glacial debuttressing and degradation of permafrost, but seismicity seems likely

to have been an important factor because many of the post-glacial slope failures conforming to this pattern are large (> 10 M m^3), making it likely that failure has been triggered by strong earthquake shaking. Further, landslide activity lags behind deglacierization by some thousands of years but coincides with a period of enhanced seismicity thought to coincide with glacial rebound (Thorarinsson et al., 1959; Sissons and Cornish, 1982; Ballantyne, 1991; Hormes et al., 2008; Lagerbäck and Sundh, 2008). If topography is more likely to amplify coseismic strong ground motions during this period of reduced glacier ice and enhanced seismicity, the likelihood of slope failure would be greater than at other times. The process described by the model may be important in seismically-active mountainous areas that have been affected by severe glaciations, such as Antarctica. Much of the Antarctic continent underlying the ice is mountainous, for example the Gamburtsev Mountains (Ferraccioli et al., 2011), and large (> M_w 8.0) earthquakes in the region may occur as a result of glacial rebound (Tsuboi et al., 2000). Mountain crests exposed during inter-glacials when the ice sheets are thinner are likely to experience higher than normal shaking because of topographic amplification effects coupled with rebound-induced seismicity. A recent example of how topographic amplification of seismic shaking seems likely to have been a factor in the location of landslides in deglaciated mountainous terrain is landsliding during the 2002 Denali earthquake in Alaska. Numerous failures were initiated from high on glacially-modified slopes, such as the rock avalanches at the Black Rapids Glacier (Figure 4.3.13). If the same earthquake occurred several millennia earlier when the glacier was thicker, the ground motions on the slope may have been insufficient to initiate failure.

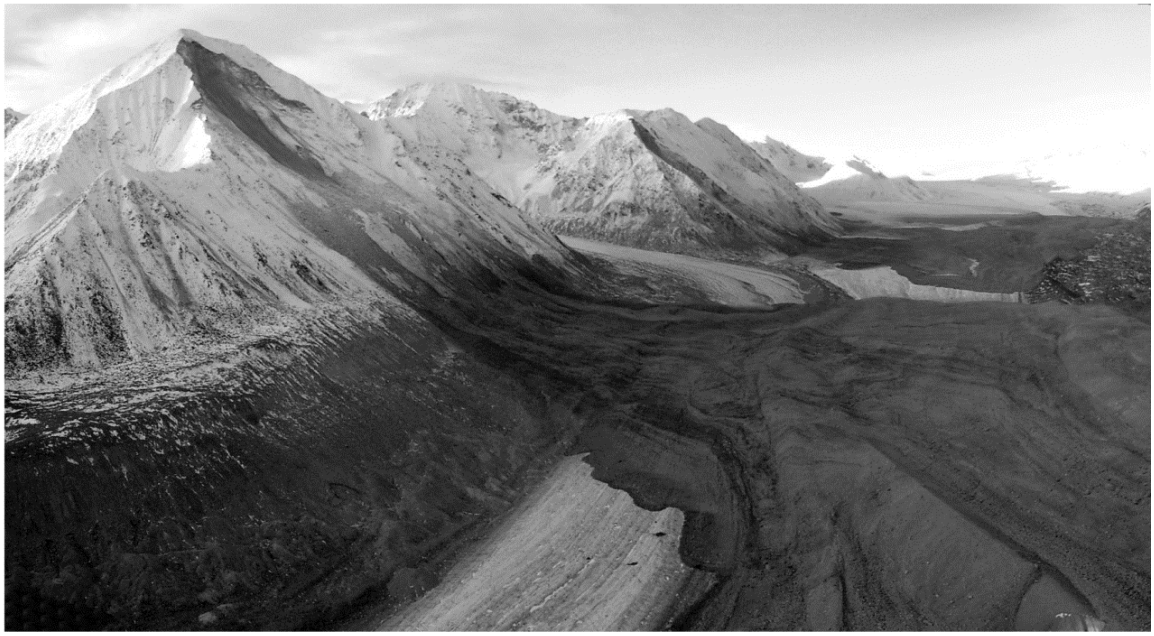

Figure 4.3.13. Coseismic rock avalanche source areas and their deposits on the Black Rapids Glacier, Alaska. Photograph Rod March, US Geological Survey.

4.3.6 Conclusions

Numerical modelling supports the hypothesis that glaciers may reduce topographic amplification of seismic shaking at mountain edifices; this effect is greatest when glaciers completely mantle a mountain, and is most pronounced for steeper slopes, and near the crests of mountains. Modelling real mountain edifices subject to real earthquake loading demonstrates that the shaking amplitudes could be at least 50–80% lower when the mountain is surrounded by ice. Small valley glaciers, like much of the ice remaining in many present-day temperate mountain ranges, however, probably have negligible influence. In situations where the rock mass protruding above these glaciers has a low stiffness (e.g. poorly indurated or highly weathered rock), and where the presence of the glacier alters the natural frequency of the ground conditions such that it matches the predominant frequencies of the earthquakes, small glaciers may actually enhance shaking intensity.

It can be expected that during parts of a glacial cycle the potential for intense seismic shaking in mountainous terrain could be increased; this is because glacier erosion often steepens topography and steeper topography amplifies seismic shaking more than gentler topography. This is likely to result in increased probability of

coseismic failure at the end of a glacial cycle and it may help to explain some of the coseismic rock-slope failure patterns observed in deglaciated terrain. It could also provide another factor in post-glacial slope-evolution models (e.g. Cruden and Hu, 1993), which usually predict an initial high rate of landslide activity immediately following glaciation that diminishes with time. Deciphering the relative importance of topographic amplification in affecting patterns of coseismic rock slopes, over the other factors in operation through glacial cycles, is impractical. However, the results reported herein indicate that it may be a factor that influences rock-slope failures in concert with glacial cycles, and should not be ignored.

Acknowledgements: Itasca Consulting Group Inc. graciously supplied a second copy of the FLAC 6.0 software after the original delivery failed to turn up because of chaos following the February 22, 2011 Christchurch earthquake. Ali Bazgard provided guidance on using FLAC and modelling topographic amplification. The authors are grateful to the editors and reviewers for their edits and constructive advice.

CHAPTER 5: SYNOPSIS

The primary aim of this research was to study the relationship between rock slope stability and glacial processes. One of the motivations for this was to help minimise the impacts of slope instability as the climate continues to transition towards interglacial conditions. It was suggested that to achieve this it is necessary to identify and evaluate the causes of slope instability during glacial cycles. In this thesis, some progress towards this goal has been made, by achieving, to varying degrees of success, the major research objectives:

Objective 1 was to identify and evaluate the various factors and processes influencing rockslope instability during glacial cycles; this was achieved in Section 2 with an extensive review and discussion of the available literature.

Objective 2 was to re-evaluate the mechanism of glacial debuttressing and its role in causing and triggering rock slope failure; this was achieved by i) developing a theoretical basis for glacial debuttressing (Section 2 Part B) and developing in Section 4 Part B a viscous model for glacier ice; ii) by collecting field evidence of movement of ice-contact slopes (Section 4 Part A & B). In general, the thinning and retreat of glaciers does remove a supporting element from a rock slope, but it is not a prerequisite for movement initiation.

Objective 3 was to observe, evaluate and model the movement of ice-buttressed rock slopes. This was achieved by the mapping and interpretation of rock slope failures in Section 4 Part B and the monitoring of a rock slope in Section 4 Part A. The monitoring data collected supports the existence of ice-contact rock slope movement as a mechanism of rock slope deformation. The movement rate appears to be strongly influenced by rainfall for the slope investigated. However, the study was preliminary in nature and limited by equipment failure; higher resolution monitoring and more accurate models will need to be developed to better understand the movement rate-controlling processes.

Objective 4 was to quantify the changes to seismic shaking intensity in mountainous terrain brought about by glacial erosion and changes in extent of glacial-ice cover. This was achieved in Section 4 Part C by the application of numerical modelling, which allowed the response of mountains to earthquake shaking to be measured for

scenarios of varying ice inundation and edifice shape. The modelling indicated that earthquake shaking intensities may be reduced to less than half that when no ice surrounds a mountain. The modelling approach taken could be improved by accounting for the three-dimensional effects that may be involved with topographic amplification, and by modelling the ice-rock interface as non-continuous (as opposed to the continuum model).

A key element in achieving Objectives 2 to 4 was the recognition that the rock slope response to glacier erosion and the withdrawal of glaciers depends on the mechanical behaviour of ice during its response to different interactions with the surrounding rock. On the one hand, the erosion by glacial action and the ductile nature of the ice favours the failure and movement of slopes (Chapter 4 Part A and B). On the other hand, the glacier provides a degree of (elastic) support to those slopes, and during earthquake shaking the presence of the glacier reduces the intensity of ground shaking that otherwise would occur (Chapter 4, Part C).

Objective 5 was to develop a conceptual model of rockslope instability during glacial cycles; this model is presented below and incorporates the ideas developed in this thesis:

5.1 A conceptual model of rockslope evolution

The period of greatest susceptibility to slope failure appears to be during the transition to deglaciation, during the time when glaciers begin to retreat and culminating some thousands of years after glaciers retreated beyond the rock slopes – this is supported by the evidence of the timing of slope failures, examined in Chapter 2. This is mostly consistent with previous interpretations of paraglacial slope instability (Ballantyne, 2002; Slaymaker, 2009), except that here it is recognised that slope movements may develop prior to complete debuttressing, and that other factors, such as the intensity of seismic shaking also influence failure patterns.

The model of rock slope evolution presented in Figure 5.1 includes three time stages within a glacial cycle: (1) glaciation, (2) transition, and (3) interglacial. In each stage, the stability of the rock slope, the dominant type of failure, and the main factors influencing these are presented. The model applies only to slopes affected by glacial action; slopes

affected by only periglacial processes are excluded. The factors increasing stability reduce the probability of failure (the green lines on the left) are separated from those that reduce the stability or increase the probability of failure (the red lines on the right). The factors have weightings applied according to their importance, as judged by the author; thicker lines equal a higher importance. The graph in the centre represents the summation of all of these factors, and it shows lower stability/higher probability of failure during the transition period, but also a slightly lower stability in the glacial period than in the interglacial period. The black lines on the right also show the dominant type of mass-movement changing through time; creeping rock slope movements are the dominant type of mass-movement operating during periods when glaciers both erode slopes and regulate the movement rate of large slope failures, but they become less dominant, but not absent, as glacier vanish.

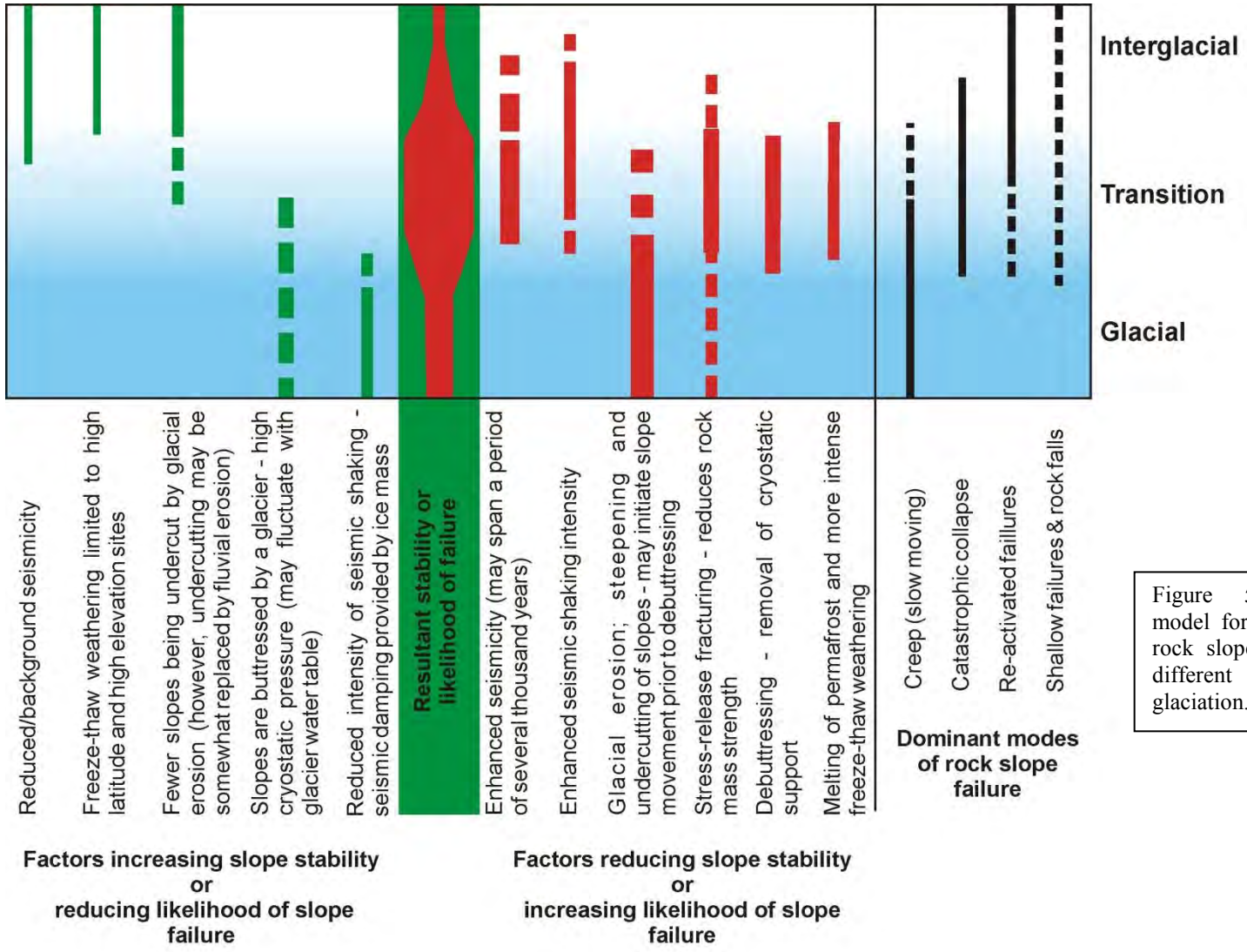

Figure 5.1: Conceptual model for the evolution of rock slope stability during different stages of glaciation.

In the following explanation of the conceptual model and the stability of slopes during the three stages of the glacial cycle, the terms *stable*, *marginally stable*, and *actively unstable* are used (*sensu* Crozier, 1986). Stable slopes are those that remain stable and will not undergo movement when affected by common transient forces such as fluctuations in groundwater level, or minor to moderate seismic events. Marginally stable slopes are those that will fail at some time in response to transient forces (triggers) reaching a certain threshold. Actively unstable slopes are those in which the transient forces result in continuous or episodic movement. These states of stability are representatives on a continuum from a high margin of stability at one end to continuous instability (movement) at the other end; preparatory factors can change where on this spectrum a particular slope lies.

Stage 1 Glacial: During the glaciation stage, the geological formation of the rock slope, and other preconditioning factors, predispose the slope to either a favourable (stable) or unfavourable margin of stability. Some slopes, therefore will be susceptible to failure (marginally stable), while others may require dramatic modification to reduce their stability. An unfavourable change to the preconditioning factors could occur if tectonic deformation increases the slope angle of bedding and more slopes may become marginally stable. The marginally stable slopes may resist movement for a long time until either the triggering factors increase or preparatory factors reduce the margin of stability further. During glaciation, these factors may include weathering, erosional induced stress-release joint development, seismic shaking, and, in particular, glacial erosion. Generally, for the slope to become marginally unstable, a failure surface will need to develop. The development of this surface may be a gradual process involving fracture propagation aided by increased stresses in the slope or stress corrosion. Alternatively, the development of the failure surface may be rapid in a situation when there is a rapid increase in stress or cyclic stresses, such as during an earthquake. However, during full glaciation, the seismic activity may be somewhat reduced by glacial loading (although, initially this could be higher as the crust is loaded at

the beginning of a glacial cycle); and further, the seismic shaking intensity may be substantially subdued (Section 4.3).

At this stage, the movement of marginally stable slopes will depend strongly on the balance between the buttressing action of the glacier and the stresses exerted on the glacier by the rock slope (Section 4.2); the thicker the glacier, the greater the cryostatic support. The Mueller Rockslide (Section 4.2) may have existed in this marginally stable state for many thousands of years; glacier thinning or another preparatory factor must have reduced stability sufficiently for movement to begin in the recent past. Movement of marginally or actively unstable slopes at this time will most likely be very slow creep; the rate of movement will depend on the excess of driving stresses and the response of the glacier to the applied stress, with the ice strain rate being a function mostly of stress magnitude and temperature (Section 4.1). There is no field evidence for this type of slope movement existing during full glacial conditions, but evidence of slope movement in partly deglaciated terrain (Section 4.1 & 4.2) indicates that it may have occurred in any situation where the stresses exerted on the ice by movement of the slope are sufficient to overcome the resistance provided by the glacier. Note that subaerial mass movements, such as rockfall, will still occur from exposed slopes during Stage 1, but their role is probably limited because the subaerial exposure of rock during glaciation is reduced.

Stage 2 Transition: During the transition stage, major changes to the condition of glaciated slopes begin to occur as the temperatures warm and glaciers begin to retreat. Glacier downwasting reduces the cryostatic pressure acting on the slope. This in turn may trigger further stress-release joint development, and expose new rock to weathering processes (such as freeze-thaw, and chemical) which will weaken the rock mass, but both of these processes may take many thousands of years to have a large influence (Section 2.1.3.2). Regional loss of ice may initiate rebound-enhanced seismicity – this too could be delayed for several thousand years (Section 2.1.3.2.4) – and the exposure of steep topography will provide opportunity for intense ground shaking during earthquakes (Section 4.3). Warmer air temperatures will eventually thaw permafrost and increase the elevation of permafrost limits. Melting of permafrost will reduce the strength of frozen joints and allow

the development of freeze-thaw weathering, both of which will reduce rock mass strength, and also provide more opportunity for excess-cleft water pressures to develop, which can trigger rock slope failure (Section 2.1.3.2.5). Now three outcomes may occur: a) A previously stable slope may become less stable, but still have sufficient strength to have a high margin of stability; b) if the slope was previously marginally stable, it may now become actively unstable. This was likely to have been the situation for the Mueller Rockslide when the Mueller Glacier began more rapid retreat in the late Holocene; and c) if the slope was actively unstable the movement rate may increase or the slope could fail catastrophically, especially if the failure surface is exposed by glacier withdrawal. During this stage, the stability and movement of slopes and the development of new failures becomes more strongly controlled by non-glacial processes, such as weathering, precipitation, and seismicity, and is less influenced by, or no longer influenced by, glacial erosion. Creeping rock slope movements may become less important as shallow failures, rockfalls, and catastrophic failures begin to overtake as the dominant form of (gravitational) slope modification. Some of the creeping slope movements may become more stable, or stop moving entirely, as they return to a state of equilibrium without the further destabilising effect of erosional steepening by a glacier. Such a situation may have occurred in the schist terrain of Otago, New Zealand, where many of the now marginally stable rock slopes were thought to be active during periods of glacial erosion (Bell, 1976; McSaveney et al., 1992).

Stage 3 Interglacial: During the final interglacial stage, the glaciers have all but disappeared. Glacial erosion ceases to undercut and steepen slopes, although other processes such as river erosion or human modification may fill this role to a certain extent. Weathering rates probably become more constant as climate stabilises. Seismicity will begin returning to normal background tectonic levels. The susceptibility of the mountain peaks to topographic amplification will be lessening as deep glacial valleys fill up with sediments and the sharp topography associated with glaciations begins to lessen (Section 4.3). By this stage, only non-glacial processes influence slope movement and modify stability; however, the stability of the slope remains influenced by the inherited legacy of glacial erosion and the other glacial processes that have altered stability in the past. Any of the remaining actively-

unstable slopes may fail catastrophically if triggered by normal climatic or seismic processes. Non-glacial factors, such as weathering or human modification, may lead to first-time failure of marginally stable slopes, or may cause reactivation of existing failures. These conditions may endure for a long-time until the cycle is renewed when climate deteriorates enough for glaciers to substantially re-advance.

The model provides a general view of rock slope evolution; the response of specific slopes, catchments, or regions may differ, particularly because of variable preconditioning factors, scales, and climates. As more information is collected, in the form of field data and the results of numerical analysis of rock slope processes, the accuracy of the conceptual modelling can be improved and more locally applicable models can be developed. These models provide a tool for helping to manage the hazards associated with rock slope failure in glaciated terrain, and therefore their constant improvement is worthwhile.

5.2 Ideas for further research

Several research ideas and unresolved issues were identified in the thesis. Below is a summary of suggestions for further research within the field of paraglacial slope stability (with reference given to the relevant section of the thesis:

- **Investigation of the time-scales required for the development of stress-release jointing following the unloading of glacier ice and glacial erosion (Section 2.1).** This could be achieved by using a combination of field-evidence and numerical modelling. Field evidence for the timing of stress-release jointing could be collected by mapping stress-release joint abundance and persistence in similar environments but which have been free of ice for differing lengths of time from very recently to many thousands of years. Numerical techniques could be used to help distil what factors control this development.

- **Investigating the role of stress-corrosion/static-fatigue in priming and triggering rock slope failures (Section 2.1).** This may best be achieved by: First, comparing the number of modern rock slope failures that do have known triggers to those that do not. Second, doing detailed analysis of several modern slope failures for which there are very good climate, groundwater, and seismic records in order to rule out more common triggering factors for those failures. These two approaches will provide a sense of how important static-fatigue may be in triggering slope failures (although it is recognised that there may be additional triggering factors other than static-fatigue that also go undetected). Third, for a number of modern rock-slope failures with known triggers, an assessment of how many times in the past the slopes in their modern configuration and conditions have been subjected to similar triggers without failing could be done. This will provide a sense of how important static-fatigue is in priming rock slope failures (i.e. weakening the rock slope). Forth, failing insight gained from existing literature on static-fatigue in other materials, attempt to use scaled laboratory testing of rock specimens to measure the time-scales over which crack-propagation and rock failure occur at a range of pre-failure stress magnitudes. Scaling laws could be applied to relate these experiments to the conditions in rock slopes. Fifth, the laboratory results could be used to help guide numerical techniques to model the development of stress-fractures and the complete development of failure planes for rocks under static loading conditions.

- **Modelling and monitoring of ice-contact rock slope movements (Section 4.1 & 4.2).** (i) In this thesis, the narrowing of a glacier adjacent to a slope movement was observed and some limited movement monitoring was done for one slope. More detailed observation and monitoring of the deformation of the ice may provide additional information on the rates of deformation and the effect the ice deformation has on the glacier flow dynamics. This could be achieved by mapping the crevasse distributions and shapes in the glacier and monitoring changes as a result of ice-contact slope movement. The change in crevasse orientation and closure would provide information on the stress conditions in the ice, at least near the surface. Mapping of these changes could be done with the analysis of high-resolution (low-altitude) aerial imagery for a period spanning several years to decades. (ii) There is little known of the way that the rock slope deforms below the ice surface and how the rock may be entrained by the glacier. Geophysical surveys (e.g. seismic reflection or GPR) could be used to observe the ice-rock contact below the ice-surface and measure how it changes. (iii) It is recommended that more ice-contact rock slope movements are searched for in aerial imagery from sites outside of New Zealand, and that some of these sites be monitored using remote sensing (e.g. satellite-borne InSAR). This would provide a wider understanding of the range of conditions (geological and glaciological) under which ice-slope movement occurs and a better estimate of the range of movement-rates. (iv) Other recommendations for detailed monitoring of ice-contact slope movements were put forward in Section 4.2, with the main recommendation being the application of terrestrial InSAR to

measure movement and a borehole ground investigation to identify the failure surface/s and monitor pore-water pressures.

- **Growth of paleo-landslide inventories (Section 2.1).** There are hundreds of large rock slope failures in the New Zealand Southern Alps and other Alps around the world that have been identified but are of unknown age. Establishing age-dates for at least the largest of these would be useful to help identify and/or confirm links between the timing of these features and the timing of other processes such as deglaciation, changes in climate, and seismicity. This will likely require a combination of radiocarbon dating and terrestrial cosmogenic exposure dating techniques. Further, the accurate identification of rockslides and their associated deposits will require careful observations to ensure the deposits identified are mass-movement in origin; McColl and Davies (2011; Appendix A) provide an example of how this can be achieved.

5.3 Conclusions

The development of rock slope instability and the style of slope failure during glacial cycles has been investigated in this thesis. Where the preconditioning (geological) conditions allow it, the erosion of rock slopes by glaciers is sufficient to destabilise rock slopes. Some of these slopes will fail once the glacier has retreated sufficiently (and de-buttressed the slopes); these failures will continue to occur until the slopes have returned to a long-term equilibrium angle. However, the ductile nature of glacier ice allows the movement of destabilised slopes that are still in contact with a glacier, when the stresses exerted by the

rock slope on the ice exceed the counter-stress provided by the ice. In this situation, rock slope movement can cause the glacier to deform; the movement rate will depend largely on the effective viscosity of the ice and the glacier thickness above the sliding mass. The erosion by glaciers and subsequent glacial retreat is also likely to cause rock mass-damage, through mechanical weathering and stress-release jointing processes. The rock mass-damage, as well as permafrost degradation in some areas, will reduce the stability of rock slopes further. Increased rainfall associated with climate warming (i.e. more precipitation falling as rain), increased seismicity associated with glacial-rebound and increases seismic shaking intensities associated with increases to the topographic amplification effect, will increase the triggering of slope failures, especially in the few thousands of years following deglaciation. The evolution of rock slopes during glacial cycles is therefore a result of the specific geological conditions that influence stability, the effectiveness of glacial erosion, and any further changes to stability as the glaciers recede, the climate warms, and seismicity changes. The failure of the slopes can be either rapid and catastrophic, or slow and gradual, or some combination of the above, depending on the specific combination of factors influencing stability and triggering movement. The timescales over which these processes operate in different areas and under different conditions will vary, and any attempt to model the evolution of rock slopes during deglaciation will need to account for these differences if it is to have wide applicability. This research has advanced our understanding of how slopes respond to deglaciation, but much work is still required to be able to fully quantify and predict this response.

REFERENCES

Abele, G., 1997. Influence of glacier and climatic variation on rockslide activity in the Alps. In: Matthews, J.A., Brunsden, D., Frenzel, B., Gläser, B., Weiß, M.M. (Eds.), Rapid Mass Movement as a Source of Climatic Evidence for Holocene. Gustav Fisher Verlag, Stuttgart, 1-6.

Adams, J., 1980. Contemporary uplift and erosion of the Southern Alps, New Zealand: Summary. Geological Society of America Bulletin 91: 2-4.

Adams, J., 1981. Earthquake-dammed lakes in New Zealand. Geology 9: 215-219.

Adams, J., 1989. Postglacial faulting in eastern Canada: nature, origin and seismic hazard implications. Tectonophysics 163: 323-331.

Agliardi, F., Crosta, G., Zanchi, A., 2001. Structural constraints on deep-seated slope deformation kinematics. Engineering Geology 59: 83-102.

Agliardi, F., Crosta, G.B., Zanchi, A., Ravazzi, C., 2009a. Onset and timing of deep-seated gravitational slope deformations in the eastern Alps, Italy. Geomorphology 103: 113-129.

Agliardi, F., Zanchi, A., Crosta, G.B., 2009b. Tectonic vs. gravitational morphostructures in the central Eastern Alps (Italy): Constraints on the recent evolution of the mountain range. Tectonophysics 474: 250-270.

Alexandrowicz, S.W., 1997. Holocene dated landslides in the Polish Carpathians. In: Matthews, J.A., Brunsden, D., Frenzel, B., Gläser, B., Weiß, M.M. (Eds.), Rapid Mass Movement as a Source of Climatic Evidence for Holocene. Gustav Fisher Verlag, Stuttgart, pp. 75-83.

Allen, S., 2009. Geomorphic Hazards associated with Glacial Change, Aoraki/Mount Cook region, Southern Alps, New Zealand. Ph.D. Thesis, University of Canterbury, Christchurch, 161 pp.

Allen, S., Cox, S., Owens, I., 2011. Rock avalanches and other landslides in the central Southern Alps of New Zealand: a regional study considering possible climate change impacts. Landslides 8: 33-48.

Allen, S.K., Cox, S.C., *in review*. Landsliding in glacial terrain: A regional-scale study of landslide distribution and potential climate change impacts in the central Southern Alps of New Zealand. Landslides

Ambrosi, C., Crosta, G.B., 2006. Large sackung along major tectonic features in the Central Italian Alps. Engineering Geology 83: 183-200.

Ambrosi, C., Crosta, G.B., 2011. Valley shape influence on deformation mechanisms of rock slopes. Geological Society, London, Special Publications 351: 215-233.

André, M.-F., 1986. Dating slope deposits and estimating rates of rock wall retreat in Northwest Spitsbergen by lichenometry. Geografiska Annaler. Series A, Physical Geography 68: 65-75.

André, M.F., 1997. Holocene rockwall retreat in Svalbard: a triple-rate evolution. Earth Surface Processes and Landforms 22: 423-440.

Arvidsson, R., 1996. Fennoscandian earthquakes: Whole crustal rupturing related to postglacial rebound. Science 274: 744-746.

Augustinus, P.C., 1992. The influence of rock mass strength on glacial valley cross-profile morphometry: A case study from the Southern Alps, New Zealand. Earth Surface Processes and Landforms 17: 39-51.

Augustinus, P.C., 1995a. Glacial valley cross-profile development: the influence of in situ rock stress and rock mass strength, with examples from the Southern Alps, New Zealand. Geomorphology 14: 87–97.

Augustinus, P.C., 1995b. Rock mass strength and the stability of some glacial valley slopes. Zeitschrift fur Geomorphologie 39: 55-68.

Bain, G.W., 1931. Spontaneous rock expansion. The Journal of Geology 39: 715-735.

Balk, R., 1939. Disintegration of glacial cliffs. Journal of Geomorphology 2: 305-334.

Ballantyne, C.K., 1991. Holocene geomorphic activity in the Scottish Highlands. Scottish Geographical Magazine 107: 84 - 98.

Ballantyne, C.K., Stone, J.O., Fifield, L.K., 1998. Cosmogenic Cl-36 dating of postglacial landsliding at The Storr, Isle of Skye, Scotland. The Holocene 8: 347.

Ballantyne, C.K., 2002. Paraglacial geomorphology. Quaternary Science Reviews 21: 1935–2017.

Ballantyne, C.K., 2003. Paraglacial landform succession and sediment storage in deglaciated mountain valleys: theory and approaches to calibration. Zeitschrift für Geomorphologie, Supplementband 132: 1-18.

Ballantyne, C.K., Stone, J.O., 2004. The Beinn Alligin rock avalanche, NW Scotland: cosmogenic 10Be dating, interpretation and significance. The Holocene 14: 448-453.

Ballantyne, C.K., 2008. After the ice: Holocene geomorphic activity in the Scottish Highlands. Scottish Geographical Journal 124: 8 - 52.

Barletta, V.R., Ferrari, C., Diolaiuti, G., Carnielli, T., Sabadini, R., Smiraglia, C., 2006. Glacier shrinkage and modeled uplift of the Alps. Geophys. Res. Lett. 33: L14307.

Barrell, D.J.A., 2011. Quaternary glaciers of New Zealand. Developments in Quaternary Science, 15: 1047-1064

Beck, A.C., 1968. Gravity faulting as a mechanism of topographic adjustment. New Zealand Journal of Geology and Geophysics 11: 191-199.

Beck, C., Manalt, F., Chapron, E., Rensbergen, P.V., Batist, M.D., 1996. Enhanced seismicity in the early post-glacial period: Evidence from the post-Würm sediments of lake annecy, northwestern Alps. Journal of Geodynamics 22: 155-171.

Becker, A., Ferry, M., Monecke, K., Schnellmann, M., Giardini, D., 2005. Multiarchive paleoseismic record of late Pleistocene and Holocene strong earthquakes in Switzerland. Tectonophysics 400: 153-177.

Beget, J.E., 1985. Tephrochronology of antislope scarps on an alpine ridge near Glacier Peak, Washington, U.S.A. Arctic and Alpine Research 17: 143-152.

Bell, D.H., 1976. Slope evolution and slope stability, Kawarau valley, Central Otago, New Zealand. Bulletin of Engineering Geology and the Environment 13: 5-16.

Benites, R., Haines, A.J., 1994. Quantification of seismic wavefield amplification by topographic featuresInstitute of Geological and Nuclear Sciences Limited Client Report 343901, 108 pp.

Berrisford, M.S., Matthews, J.A., 1997. Phases of enhanced rapid mass movement and climatic variation during the Holocene: a synthesis. In: Matthews, J.A., Brunsden, D., Frenzel, B., Gläser, B., Weiß, M.M. (Eds.), Rapid mass movement as a source of climatic evidence for Holocene. Gustav Fisher Verlag, Stuttgart, pp. 409-440.

Bertolini, G., Casagli, N., Ermini, L., Malaguti, C., 2004. Radiocarbon data on late-Glacial and Holocene landslides in the Northern Apennines. Natural Hazards 31: 645-662.

Bigot-Cormier, F., Braucher, R., Bourlès, D., Guglielmi, Y., Dubar, M., Stéphan, J.F., 2005. Chronological constraints on processes leading to large active landslides. Earth and Planetary Science Letters 235: 141-150.

Blair, R.W., Jr., 1994. Moraine and valley wall collapse due to rapid deglaciation in Mount Cook National Park, New Zealand. Mountain Research and Development 14: 347-358.

Bonzanigo, L., Eberhardt, E., Loew, S., 2007. Longterm investigation of a deep-seated creeping landslide in crystalline rock—Part 1: Geological and hydromechanical factors controlling the Campo Vallemaggia landslide. Canadian Geotechnical Journal 44: 1157-1180.

Boore, D.M., 1972. A note on the effect of simple topography on seismic SH waves. Bulletin of the Seismological Society of America 62: 275-284.

Borgatti, L., Soldati, M., 2010. Landslides as a geomorphological proxy for climate change: A record from the Dolomites (northern Italy). Geomorphology 120: 56-64.

Bouckovalas, G., Papadimitriou, A., 2006. Aggravation of seismic ground motion due to slope topography. First European Conference on Earthquake Engineering and Seismology, Paper number 1171

Bovis, M.J., 1982. Uphill-facing (antislope) scarps in the Coast Mountains, southwest British Columbia. Geological Society of America Bulletin 93: 804-812.

Bovis, M.J., 1990. Rock-slope deformation at Affliction Creek, southern Coast Mountains, British Columbia. Canadian Journal of Earth Sciences 27: 243-254.

Bovis, M.J., Evans, S.G., 1996. Extensive deformations of rock slopes in southern Coast Mountains, southwest British Columbia, Canada. Engineering Geology 44: 163-182.

Bovis, M.J., Stewart, T.W., 1998. Long-term deformation of a glacially undercut rock slope, southwest British Columbia. Eighth International Congress, International Association for Engineering Geology and the Environment: 1267-1276

Bradley, W.C., 1963. Large-scale exfoliation in massive sandstones of the Colorado Plateau. Geological Society of America Bulletin 74: 519-528.

Brideau, M.-A., Yan, M., Stead, D., 2009. The role of tectonic damage and brittle rock fracture in the development of large rock slope failures. Geomorphology 103: 30-49.

Brook, M.S., Kirkbride, M.P., Brock, B.W., 2006. Quantified time scale for glacial valley cross-profile evolution in alpine mountains. Geology 34: 637-640.

Brook, M.S., 2008. George Leslie Adkin (1988-1964): glaciation and earth movements in the Tararua Range, North Island, New Zealand. In: Grapes, R.H., Oldroyd, D., Grigelis, A. (Eds.), History of Geomorphology and Quaternary Geology. Geological Society, London, Special Publications, pp. 315-328.

Brook, M.S., Kirkbride, M.P., Brock, B.W., 2008. Temporal constraints on glacial valley cross-profile evolution: Two Thumb Range, central Southern Alps, New Zealand. Geomorphology 97: 24-34.

Brunner, F.K., Scheidegger, A.E., 1973. Exfoliation. Rock Mechanics and Rock Engineering 5: 43-62.

Brunsden, D., Ibsen, M.L., 1997. The temporal occurence and forecasting of landslides in the European Community: summary of relevant results of the European Community EPOCH Programme. In: Matthews, J.A., Brunsden, D., Frenzel, B., Gläser, B., Weiß, M.M. (Eds.), Rapid Mass Movement as a Source of Climatic Evidence for Holocene. Gustav Fisher Verlag, Stuttgart, pp. 401-407.

Bryant, J.M., 2010. North Young Rockslide Dam. Geologically active : Extended abstracts 11th Congress of the International Association for Engineering Geology and the Environment, 5-10 September 2010. Auckland, New Zealand.pp. 49-55.

Buech, F., 2008. Seismic response of Little Red Hill - towards an understanding of topographic effects on ground motion and rock slope failure, University of Canterbury, Christchurch, 285 pp.

Buech, F., Davies, T.R., Pettinga, J.R., 2010. The Little Red Hill seismic experimental study: Topographic effects on ground motion at a bedrock-dominated mountain edifice. Bulletin of the Seismological Society of America 100: 2219-2229.

Bungum, H., Olesen, O., Pascal, C., Gibbons, S., Lindholm, C., VestÃ¸l, O., 2010. To what extent is the present seismicity of Norway driven by post-glacial rebound? Journal of the Geological Society 167: 373-384.

Caine, N., 1982. Toppling failures from alpine cliffs on Ben Lomond, Tasmania. Earth Surface Processes and Landforms 7: 133-152.

Calais, E., Freed, A.M., Van Arsdale, R., Stein, S., 2010. Triggering of New Madrid seismicity by late-Pleistocene erosion. Nature 466: 608-611.

Caminiti, J.E., 2004. Catchment modelling - a resource managers's perspective. Environmental Modelling & Software 19: 991-997.

Casagli, N., Catani, F., Ventisette, C.D., Luzi, G., 2010. Monitoring, prediction, and early warning using ground-based radar interferometry. Landslides 7: 291-301.

Chemenda, A.I., Bois, T., Bouissou, S., Tric, E., 2009. Numerical modelling of the gravity-induced destabilization of a slope: The example of the La Clapière landslide, southern France. Geomorphology 109: 86-93.

Church, M., Ryder, J.M., 1972. Paraglacial sedimentation. A consideration of fluvial processes conditioned by glaciation. Geological Society of America Bulletin 83: 3059–3072.

Columbus, J., Sirguey, P., Tenzer, R., 2011. A free, fully assessed 15-m DEM for New Zealand. Survey Quarterly 66: 16-19.

Corsini, A., Pasuto, A., Soldati, M., Zannoni, A., 2005. Field monitoring of the Corvara landslide (Dolomites, Italy) and its relevance for hazard assessment. Geomorphology 66: 149-165.

Cossart, E., Braucher, R., Fort, M., Bourlés, D.L., Carcaillet, J., 2008. Slope instability in relation to glacial debuttressing in alpine areas (Upper Durance catchment, southeastern France): Evidence from field data and 10Be cosmic ray exposure ages. Geomorphology 95: 3-26.

Cox, S.C., Findlay, R.H., 1995. The Main Divide Fault Zone and its role in formation of the Southern Alps, New Zealand. New Zealand Journal of Geology & Geophysics 38: 489-499.

Cox, S.C., Barrell, D.J.A. (compilers). 2007. Geology of the Aoraki area. Institute of Geological and Nuclear Sciences 1:250 000 geological map 15. 1 sheet + 71 p. Lower Hutt, New Zealand GNS Science.

Cox, S.C., Ferris, B.G., Allen, S., 2008. Vampire rock avalanches, Aoraki/Mount Cook National Park, New Zealand. GNS Science, GNS Science Report 2008/10, 34 pp.

Crosta, G., Agliardi, F., 2002. How to obtain alert velocity thresholds for large rockslides. Physics and Chemistry of the Earth 27: 1557-1565.

Crosta, G., Agliardi, F., Sosio, R., Rivolta, C., Leva, D., Dei Cas, L., 2012. Long term real-time monitoring of large alpine rockslides by GB-InSAR: mechanisms, triggers, scenario assessment and Early Warning. Geophysical Research Abstracts 14

Crosta, G.B., Agliardi, F., 2003. Failure forecast for large rock slides by surface displacement measurements. Canadian Geotechnical Journal 40: 176-191.

Crozier, M.J., 1986. Landslides: Causes, consequences and environment. Croom Helm Ltd, London, 252 pp.

Crozier, M.J., 1997. The climate-landslide couple: a Southern Hemisphere perspective. In: Matthews, J.A., Brunsden, D., Frenzel, B., Gläser, B., Weiß, M.M. (Eds.), Rapid Mass Movement as a Source of Climatic Evidence for Holocene. Gustav Fisher Verlag, Stuttgart, pp. 333-354.

Crozier, M.J., 2010. Deciphering the effect of climate change on landslide activity: A review. Geomorphology 124: 260-267.

Cruden, D., 1997. Rapid mass movement and climate: a North American perspective. Paläoklimaforschung 19: 371-378.

Cruden, D.M., Eaton, T.M., 1987. Reconnaissance of rockslide hazards in Kananaskis Country, Alberta. Canadian Geotechnical Journal 24: 414-429.

Cruden, D.M., Hu, X.Q., 1993. Exhaustion and steady state models for predicting landslide hazards in the Canadian Rocky Mountains. Geomorphology 8: 279-285.

Cruden, D.M., Varnes, D.J., 1996. Landslide types and processes: Chapter 3. In: Turner, A.K., Schuster, R.L. (Eds.), Landslides: Investigation and mitigation. Special Report 247. Transportation Research Board, National Research Council, Washington D.C., pp. 36-75.

Cuffey, K.M., Paterson, W.S.B., 2010. The physics of glaciers. Butterworth-Heinemann, Burlington, 704 pp.

Curry, A.M., Cleasby, V., Zukowskyj, P., 2006. Paraglacial response of steep, sediment-mantled slopes to post-'Little Ice Age' glacier recession in the central Swiss Alps. Journal of Quaternary Science 21: 211-225.

Dadson, S.J., Church, M., 2005. Postglacial topographic evolution of glaciated valleys: a stochastic landscape evolution model. Earth Surface Processes and Landforms 30: 1387-1403.

Dapples, F., Oswald, D., Raetzo, H., 2002. Holocene landslide activity in the Western Swiss Alps - a consequence of vegetation changes and climate oscillations. In: Rybar, J., Stemberk, J., Wagner, P. (Eds.), Landslides: Proceedings of the first European conference on landslides, Prague, Czech Republic, June 24-26, 2002. Taylor and Francis Group, pp. 349-354.

Davies, M.C.R., Hamza, O., Harris, C., 2001. The effect of rise in mean annual temperature on the stability of rock slopes containing ice-filled discontinuities. Permafrost and Periglacial Processes 12: 137-144.

Deline, P., 2009. Interactions between rock avalanches and glaciers in the Mont Blanc massif during the late Holocene. Quaternary Science Reviews 28: 1070-1083.

Dhakal, S., 2009. Dynamic modelling in slopes using finite difference program. Bulletin of the Department of Geology 12: 89-94.

Di Fiore, V., 2010. Seismic site amplification induced by topographic irregularity: Results of a numerical analysis on a 2D synthetic models. Engineering Geology 114: 109-115.

Dortch, J.M., Owen, L.A., Haneberg, W.C., Caffee, M.W., Dietsch, C., Kamp, U., 2009. Nature and timing of large landslides in the Himalaya and Transhimalaya of northern India. Quaternary Science Reviews 28: 1037-1054.

Dramis, F., Sorriso-Valvo, 1994. Deep-seated gravitational slope deformations, related landslides and tectonics. Engineering Geology 38: 231-243.

Dramis, F., Govi, M., Guglielmin, M., Mortara, G., 1995. Mountain permafrost and slope instability in the Italian Alps: The Val Pola Landslide. Permafrost and Periglacial Processes 6: 73-81.

Dufresne, A., Davies, T.R., 2009. Longitudinal ridges in mass movement deposits. Geomorphology 105: 171-181.

Eberhardt, E., Stead, D., Coggan, J.S., 2004. Numerical analysis of initiation and progressive failure in natural rock slopes--the 1991 Randa rockslide. International Journal of Rock Mechanics and Mining Sciences 41: 69-87.

Eberhardt, E., Watson, A.D., Loew, S., 2008. Improving the interpretation of slope monitoring and early warning data through better understanding of complex deep-seated landslide failure mechanisms. Landslides and engineered slopes from the past to the future. Proceedings of the Tenth International Symposium on Landslides and Engineered Slopes, 30 June–4 July 2008. Xi'an, China.39-51.

El Bedoui, S., Guglielmi, Y., Lebourg, T., Pérez, J.-L., 2009. Deep-seated failure propagation in a fractured rock slope over 10,000 years: The La Clapière slope, the south-eastern French Alps. Geomorphology 105: 232-238.

El Bedoui, S., Bois, T., Jomard, H., Sanchez, G., Lebourg, T., Trics, E., Guglielmi, Y., Bouissou, S., Chemenda, A., Rolland, Y., Corsini, M., Pérez, J.L., 2011. Paraglacial gravitational deformations in the SW Alps: a review of field investigations, 10Be cosmogenic dating and physical modelling. Geological Society, London, Special Publications 351: 11-25.

Engelder, T., Sbar, M.L., 1977. The relationship between *in situ* strain relaxation and outcrop fractures in the Potsdam Sandstone, Alexandria Bay, New York. Pure and Applied Geophysics 115: 41-55.

Evans, S.G., Gardiner, J.S., 1989. Geological hazards in the Canadian Cordillera. In: Fulton, R.J. (Ed.), Quaternary geology of Canada and Greenland. Geology of North America, Vol. K-1. Geological Society of America, pp. 702-713.

Evans, S.G., Clague, J.J., 1992. Glacier-related hazards and climatic change. AIP Conference Proceedings 277: 48-60.

Evans, S.G., Clague, J.J., 1994. Recent climatic change and catastrophic geomorphic processes in mountain environments. Geomorphology 10: 107-128.

Evans, S.G., Couture, R., 2002. The 1965 Hope Slide, British Columbia; catastrophic failure of a sagging rock slope. Geological Society of America, Abstracts with Programs 34: 16-26.

Everitt, R.A., 2009. Pop-ups and related damage in granite at the Medika Pluton in southeastern Manitoba. Canadian Geotechnical Journal 46: 9.

Eyles, N., Mullins, H.T., Hine, A.C., 1990. Thick and fast: Sedimentation in a Pleistocene fiord lake of British Columbia, Canada. Geology 18: 1153-1157.

Farmin, R., 1937. Hypogene exfoliation in rock masses. The Journal of Geology 45: 625-635.

Ferraccioli, F., Finn, C.A., Jordan, T.A., Bell, R.E., Anderson, L.M., Damaske, D., 2011. East Antarctic rifting triggers uplift of the Gamburtsev Mountains. Nature 479: 388-392.

Firth, C.R., Stewart, I.S., 2000. Postglacial tectonics of the Scottish glacio-isostatic uplift centre. Quaternary Science Reviews 19: 1469-1493.

Fischer, L., Kääb, A., Huggel, C., Noetzli, J., 2006. Geology, glacier retreat and permafrost degradation as controlling factors of slope instabilities in a high-mountain rock wall: The Monte Rosa east face. Natural Hazards and Earth System Science 6: 761-772.

Fischer, L., Amann, F., Moore, J.R., Huggel, C., 2010. Assessment of periglacial slope stability for the 1988 Tschierva rock avalanche (Piz Morteratsch, Switzerland). Engineering Geology 116: 32-43.

Fjeldskaar, W., Lindholm, C., Dehls, J.F., Fjeldskaar, I., 2000. Postglacial uplift, neotectonics and seismicity in Fennoscandia. Quaternary Science Reviews 19: 1413-1422.

Fountain, A.G., Walder, J.S., 1998. Water flow through temperate glaciers. Reviews of Geophysics 36: 299-327.

Ganerød, G.V., Grøneng, G., Rønning, J.S., Dalsegg, E., Elvebakk, H., Tønnensen, J.F., Kveldsvik, V., Eiken, T., Blikra, L.H., Braathen, A., 2008. Geological model of the Åknes rockslide, western Norway. Engineering Geology 102: 1-18.

Geertsema, M., Clague, J.J., Schwab, J.W., Evans, S. G., 2006. An overview of recent large catastrophic landslides in northern British Columbia, Canada. Engineering Geology 83: 120-143.

Geli, L., Bard, P.-Y., Jullien, B., 1988. The effect of topography on earthquake ground motion: a review and new results. Bulletin of the Seismological Society of America 78: 42-63.

Gellatly, A.F., 1985. Historical records of glacier fluctuations in Mt Cook National Park, New Zealand: A century of change. The Geographical Journal 151: 86-99.

Ghirotti, M., Martin, S., Genevois, R., 2011. The Celentino deep-seated gravitational slope deformation (DSGSD): structural and geomechanical analyses (Peio Valley, NE Italy). Geological Society, London, Special Publications 351: 235-251.

Gilbert, G.K., 1904. Domes and dome structure in the High Sierra. Bulletin of the Geological Society of America 15: 29-36.

Gischig, V., Loew, S., Kos, A., Moore, J.R., Raetzo, H., Lemy, F., 2009. Identification of active release planes using ground-based differential InSAR at the Randa rock slope instability, Switzerland. Nat. Hazards Earth Syst. Sci. 9: 2027-2038.

Gischig, V., Moore, J.R., Evans, K.F., Loew, S., 2010. Seasonal changes of rock mass deformation rate due to thermal effects at the Randa rock slope instability, Switzerland. Geologically active : delegate papers 11th Congress of the International Association for Engineering Geology and the Environment, Auckland, Aotearoa, 5-10 September 2010. Auckland, New Zealand.pp. 179-186.

Gischig, V.S., Moore, J.R., Evans, K.F., Amann, F., Loew, S., 2011a. Thermo-mechanical forcing of deep rock slope deformation - Part II: the Randa rock slope instability. Journal of Geophysical Research

Gischig, V.S., Moore, J.R., Evans, K.F., Amann, F., Loew, S., 2011b. Thermo-mechanical forcing of deep rock slope deformation - Part I: conceptual study of a simplified slope. Journal of Geophysical Research

Glade, T., Crozier, M.J., 2005. The nature of landslide hazard impact. In: Glade, T., Anderson, M.G., Crozier, M.J. (Eds.), Landslide Hazard and Risk. John Wiley & Sons Ltd, Chichester, pp. 43-74.

Glen, J.W., 1955. The creep of polycrystalline ice. Proceedings of the Royal Society of London. Series A, Mathematical and Physical Sciences 228: 519-538.

Glen, J.W., 1958. The flow law of ice: A discussion of the assumptions made in glacier theory, their experimental foundations and consequences. IAHS 47: 171-183.

Gold, L.W., 1988. On the elasticity of ice plates. Canadian Journal of Civil Engineering 15: 1080-84.

González Díez, A., Salas, L., Ramon Díaz de Terán, J., Cendrero, A., 1996. Late Quaternary climate changes and mass movement frequency and magnitude in the Cantabrian region, Spain. Geomorphology 15: 291-309.

Gregersen, S., Voss, P., 2009. Stress change over short geological time: the case of Scandinavia over 9000 years since the Ice Age. Geological Society, London, Special Publications 316: 173-178.

Grove, J.M., 1972. The incidence of landslides, avalanches, and floods in western Norway during the Little Ice Age. Arctic and Alpine Research 4: 131-138.

Gruber, S., Hoelzle, M., Haeberli, W., 2004. Permafrost thaw and destabilization of Alpine rock walls in the hot summer of 2003. Geophys. Res. Lett. 31

Gruber, S., Haeberli, W., 2007. Permafrost in steep bedrock slopes and its temperature-related destabilization following climate change. J. Geophys. Res. 112: F02S18, doi:10.1029/2006JF000547.

Gudmundsson, G.H., 1994. An order-of-magnitude estimate of the current uplift-rates in Switzerland caused by the Würm Alpine deglaciation. Eclogae Geologicae Helvetiae 87: 545-557.

Haeberli, W., Wegmann, M., Vonder Muhll, D., 1997. Slope stability problems related to glacier shrinkage and permafrost degradation in the Alps. Ecologae Geologicae Helvetiae 90: 407-414.

Hales, T.C., Roering, J.J., 2005. Climate-controlled variations in scree production, Southern Alps, New Zealand. Geology 33: 701-704.

Hall, K., Thorn, C.E., Matsuoka, N., Prick, A., 2002. Weathering in cold regions: some thoughts and perspectives. Progress in Physical Geography 26: 577-603.

Hampel, A., Hetzel, R., Maniatis, G., 2010. Response of faults to climate-driven changes in ice and water volumes on Earth's surface. Philosophical Transactions of the Royal Society A: Mathematical, Physical and Engineering Sciences 368: 2501-2517.

Hancox, G.T., 1994. Report on Mt Cook National Park hut site inspections and establishment of monitoring lines, April 1994. Institute of Geological and Nuclear Sciences, Client Report 353902.20, prepared for Department of Conservation, Mt Cook National Park, 32 p.

Hancox, G.T., Perrin, N.D., 1994. Green Lake landslide: a very large ancient rock slide in Fiordland, New Zealand. Institute of Geological ; Nuclear Sciences sciences, IGNS Science Report 93/18, June 1994,

Hancox, G.T., 1998. Pilot study for Baseline Geological Inspection of DOC Backcountry Huts: Inspections of alpine hut sites in the Mt Cook and Westland National Parks, March 1998. Institute of Geological and Nuclear Sciences, Client Report 43713B, prepared for Department of Conservation, Mt Cook National Park, p 1-6.

Hancox, G.T., Perrin, N.D., Dellow, G.D., 2002. Recent studies of historical earthquake-induced landsliding, ground damage, and MM intensity in New Zealand. Bulletin of the New Zealand Society for Earthquake Engineering 35: 59-95.

Hancox, G.T., McSaveney, M.J., Manville, V.R., Davies, T.R., 2005. The October 1999 Mt Adams rock avalanche and subsequent landslide dam-break flood and effects in

Poerua River, Westland, New Zealand. New Zealand Journal of Geology and Geophysics 48: 683-705.

Hancox, G.T., Perrin, N.D., 2009. Green Lake Landslide and other giant and very large postglacial landslides in Fiordland, New Zealand. Quaternary Science Reviews 28: 1020-1036.

Hancox, G.T., 2010. Report on the landslide that blocked SH 1 and the railway line near Rosy Morn Stream south of Kaikoura on 10 September 2010. GNS Science Report 2010/59, 33 p.

Hansmann, J., Loew, S., Evans, K., 2010. A mathematical model of observed, recharge controlled, reversible rockslope deformations in the central Swiss Alps. Geologically active : delegate papers 11th Congress of the International Association for Engineering Geology and the Environment. Auckland, New Zealand.pp. 2961-2972.

Harland, W.B., 1957. Exfoliation joints and ice action. Journal of Glaciology 3: 8-10.

Harper, T.R., Nichols, T.C., Jr, 1982. Discussion on 'Rebound, its nature and effect on engineering works', by T.C. Nichols, Jr. Quarterly Journal of Engineering Geology and Hydrogeology 15: 63-65.

Harries, N., Roberts, H., 2007. The use of Slope Stability Radar (SSR) in managing slope instability hazards. Rock Mechanics: Meeting Society's Challenges and Demands, Proceedings of the 1st Canada-US Rock Mechanics Symposium. Vancouver, Canada.53-59.

Harrison, S., 2009. Climate sensitivity: Implications for the response of geomorphological systems to future climate change. Geological Society Special Publication: 257-265

Hauser, A., 2002. Rock avalanche and resulting debris flow in Estero Parraguirre and Rio Colorado, Region Metropolitana, Chile. In: Evans, S.G., DeGraff, J.V. (Eds.), Catastrophic landslides: effects, occurence and mechanisms, pp. 135-148.

Hencher, S., Lee, S., Carter, T., Richards, L., 2011. Sheeting joints: Characterisation, shear strength and engineering. Rock Mechanics and Rock Engineering 44: 1-22.

Henderson, R.D., Thompson, S.M., 1999. Extreme rainfalls in the Southern Alps of New Zealand. Journal of hydrology (NZ) 38: 309-330.

Hétu, B., Gray, J.T., 2000. Effects of environmental change on scree slope development throughout the postglacial period in the Chic-Choc Mountains in the northern Gaspé Peninsula, Québec. Geomorphology 32: 335-355.

Hetzel, R., Hampel, A., 2005. Slip rate variations on normal faults during glacial-interglacial changes in surface loads. Nature 435: 81-84.

Hewitt, K., 1999. Quaternary moraines vs catastrophic rock avalanches in the Karakoram Himalaya, Northern Pakistan. Quaternary Research 51: 220-237.

Hippolyte, J.-C., Brocard, G., Tardy, M., Nicoud, G., Bourlès, D., Braucher, R., Ménard, G., Souffaché, B., 2006. The recent fault scarps of the Western Alps (France): Tectonic surface ruptures or gravitational sackung scarps? A combined mapping, geomorphic, levelling, and 10Be dating approach. Tectonophysics 418: 255-276.

Hippolyte, J.-C., Bourlès, D., Braucher, R., Carcaillet, J., Léanni, L., Arnold, M., Aumaitre, G., 2009. Cosmogenic 10Be dating of a sackung and its faulted rock glaciers, in the Alps of Savoy (France). Geomorphology 108: 312-320.

Hoek, E., Carranza-Torres, C.T., Corkum, B., 2002. Hoek-Brown failure criterion-2002 edition. Proceedings of the fifth North American rock mechanics symposium, Toronto, Canada, vol. 1, 2002. p. 267-273

Holm, K., Bovis, M., Jakob, J., 2004. The landslide response of alpine basins to post-Little Ice Age glacial thinning and retreat. Geomorphology 57: 201-216.

Hooke, R.L., 2005. Principles of glacier mechanics. Cambridge University Press, Cambridge, 429 pp.

Hormes, A., Ivy-Ochs, S., Kubik, P.W., Ferreli, L., Maria Michetti, A., 2008. 10Be exposure ages of a rock avalanche and a late glacial moraine in Alta Valtellina, Italian Alps. Quaternary International 190: 136-145.

Hovius, N., Stark, C.P., Allen, P.A., 1997. Sediment flux from a mountain belt derived by landslide mapping. Geology 25: 231-234.

Huang, C.-C., Lee, Y.-H., Liu, H.-P., Keefer, D.K., Jibson, R.W., 2001. Influence of surface-normal ground acceleration on the initiation of the Jih-Feng-Erh-Shan landslide during the 1999 Chi-Chi, Taiwan, Earthquake. Bulletin of the Seismological Society of America 91: 953-958.

Huggel, C., 2008. Recent extreme slope failures in glacial environments: effects of thermal perturbation. Quaternary Science Reviews 28: 1119-1130.

Huggel, C., Gruber, S., Caplan-Auerbach, J., Wessels, R.L., Molnia, B.F., 2008. The 2005 Mt. Steller, Alaska, rock-ice avalanche: A large slope failure in cold permafrost. Proceedings Ninth International Conference on Permafrost, 29 June - 3 July, 2008. Fairbanks, U.S.A.pp. 747-752.

Ingles, J., Darrozes, J., Soula, J.-C., 2006. Effects of the vertical component of ground shaking on earthquake-induced landslide displacements using generalized Newmark analysis. Engineering Geology 86: 134-147.

ISRM, 1985. Suggested method for determining point load strength. International Journal of Rock Mechanics and Mining Science & Geomechanics Abstracts 22: 51-60.

Itasca Consulting Group, I., 2008. FLAC - Fast Lagrangian Analysis of Continua, Ver. 6.0 User's Manual. Itasca, Minneapolis.

International Union of Geological Sciences Working Group on Landslides, 1995. A suggested method for describing the rate of movement of a landslide. Bulletin of Engineering Geology and the Environment 52: 75-78.

Ivy-Ochs, S., Poschinger, A.v., Synal, H.-A., Maisch, M., 2009. Surface exposure dating of the Flims landslide, Graubünden, Switzerland. Geomorphology 103: 104-112.

Jacobi, R.D., Lewis, C.F.M., Armstrong, D.K., Blasco, S.M., 2007. Popup field in Lake Ontario south of Toronto, Canada: Indicators of late glacial and postglacial strain. Geological Society of America Special Papers 425: 129-147.

Jahns, R.H., 1943. Sheet structure in granites: Its origin and use as a measure of glacial erosion in New England. The Journal of Geology 51: 71-98.

Jarman, D., 2006. Large rock slope failures in the Highlands of Scotland: Characterisation, causes and spatial distribution. Engineering Geology 83: 161-182.

Jonsson, O., 1976. Berghlaup. Raektunar felag Norourlands, Akurekri, Iceland, 623 pp.

Kääb, A., 2002. Monitoring high-mountain terrain deformation from repeated air- and spaceborne optical data: examples using digital aerial imagery and ASTER data. Journal of Photogrammetry and Remote Sensing 57: 39-52.

Karrow, P.F., White, O.L., 2002. A history of neotectonic studies in Ontario. Tectonophysics 353: 3-15.

Keefer, D.K., 1984. Landslides caused by earthquakes. Geological Society of America Bulletin 95: 406-421.

Keefer, D.K., 1994. The importance of earthquake-induced landslides to long-term slope erosion and slope-failure hazards in seismically active regions. Geomorphology 10: 265-284.

Kellerer-Pirklbauer, A., Proske, H., Strasser, V., 2010. Paraglacial slope adjustment since the end of the Last Glacial Maximum and its long-lasting effects on secondary mass wasting processes: Hauser Kaibling, Austria. Geomorphology 120: 65-76.

Kerr, T., Owens, I., Henderson, R., 2007. An extreme average annual precipitation gradient measured in a lee mountain catchment, South Island, New Zealand. Geophysical Research Abstracts EGU2007 9: 11607

Kilburn, C.R.J., Petley, D.N., 2003. Forecasting giant, catastrophic slope collapse: lessons from Vajont, Northern Italy. Geomorphology 54: 21-32.

Kirkbride, M., Matthews, D., 1997. The role of fluvial and glacial erosion in landscape evolution: The Ben Ohau Range, New Zealand. Earth Surface Processes and Landforms 22: 317-327.

Kirkbride, M.P., Warren, C.R., 1999. Tasman Glacier, New Zealand: 20th-century thinning and predicted calving retreat. Global and Planetary Change 22: 11-28.

Kjartansson, G., 1967. The Steinsholtshlaup, central-south Iceland on January 15th, 1967. Jökull 17: 249-262.

Korup, O., McSaveney, M.J., Davies, T.R.H., 2004. Sediment generation and delivery from large historic landslides in the Southern Alps, New Zealand. Geomorphology 61: 189-207.

Korup, O., 2005. Large landslides and their effect on sediment flux in South Westland, New Zealand. Earth Surface Processes and Landforms 30: 305-323.

Korup, O., Clague, J.J., 2009. Natural hazards, extreme events, and mountain topography. Quaternary Science Reviews 28: 977-990.

Kubik, P.W., Ivy-Ochs, S., Masarik, J., Frank, M., Schlüchter, C., 1998. 10Be and 26Al production rates deduced from an instantaneous event within the dendro-calibration curve, the landslide of Köfels, Ötz Valley, Austria. Earth and Planetary Science Letters 161: 231-241.

Lagerbäck, R., Sundh, M., 2008. Early Holocene faulting and paleoseismicity in northern Sweden. Geological Survey of Sweden, Research Paper C 836, 84 pp.

Le Roux, O., Schwartz, S., Gamond, J.F., Jongmans, D., Bourles, D., Braucher, R., Mahaney, W., Carcaillet, J., Leanni, L., 2009. CRE dating on the head scarp of a major landslide (Séchilienne, French Alps), age constraints on Holocene kinematics. Earth and Planetary Science Letters 280: 236-245.

Legros, F., 2002. The mobility of long-runout landslides. Engineering Geology 63: 301-331.

Leith, K., Amann, F., Moore, J.R., Kos, A., Loew, S., 2010a. Conceptual modelling of near-surface extensional fracture in the Matter and Saas Valleys, Switzerland. Geologically active : delegate papers 11th Congress of the International Association for Engineering Geology and the Environment, Auckland, Aotearoa, 5-10 September 2010. Auckland, New Zealand.pp. 363-371.

Leith, K., Moore, J., Amann, F., Loew, S., 2010b. Slope failure induced by post-glacial extensional fracturing in the Matter and Saas Valleys, Switzerland. Geophysical Research Abstracts 12

Lewis, W.V., 1954. Pressure release and glacial erosion. Journal of Glaciology 2: 417-422.

Lillie, A.R., Gunn, B.M., 1964. Steeply plunging folds in the Sealy Range, Southern Alps. New Zealand Journal of Geology & Geophysics 7: 403-423.

Lipovsky, P., Evans, S., Clague, J., Hopkinson, C., Couture, R., Bobrowsky, P., Ekström, G., Demuth, M., Delaney, K., Roberts, N., Clarke, G., Schaeffer, A., 2008a. The

July 2007 rock and ice avalanches at Mount Steele, St. Elias Mountains, Yukon, Canada. Landslides 5: 445-455.

Lipovsky, P.S., Evans, S.G., Clague, J.J., Hopkinson, C., Couture, R., Bobrowsky, P., Ekström, G., Demuth, M.N., Delaney, K.B., Roberts, N.J., Clarke, G., Schaeffer, A., 2008b. The July 2007 rock and ice avalanches at Mount Steele, St. Elias Mountains, Yukon, Canada. Landslides 5: 445-455.

Lo, K.Y., 1978. Regional distribution of in situ horizontal stresses in rocks of Southern Ontario. Canadian Geotechnical Journal 15: 371-381.

Luckman, B.H., 1988. Debris accumulation patterns on talus slopes in Surprise Valley, Alberta. Géographie Physique et Quaternaire 42: 247-278.

MacGregor, K.R., Anderson, R.S., Anderson, S.P., Waddington, E.D., 2000. Numerical simulations of glacial-valley longitudinal profile evolution. Geology 28: 1031-1034.

Malamud, B.D., Turcotte, D.L., Guzzetti, F., Reichenbach, P., 2004. Landslides, earthquakes, and erosion. Earth and Planetary Science Letters 229: 45-59.

Marshall, S.J., 2005. Recent advances in understanding ice sheet dynamics. Earth and Planetary Science Letters 240: 191-204.

Massey, C., McSaveney, M., Palmer, N., Manville, V., Hancox, G., 2008. The Young River Landslide. Poster, available online: http://www.geonet.org.nz/content/download/7518/43995/file/Young-River-poster-A3.pdf

Massey, C.I., 2010. The dynamics of reactivated landslides: Utiku and Taihape, North Island, New Zealand, Durham University. Available at Durham E-Theses Online: http://etheses.dur.ac.uk/587/

Mathews, W.H., McTaggart, K.C., 1978. Hope rockslides, British Columbia, Canada. In: Voight, B. (Ed.), Rockslides and Avalanches 1. Natural Phenomena. Elsevier, Amsterdam, pp. 259–275.

Matsuoka, N., Sakai, H., 1999. Rockfall activity from an alpine cliff during thawing periods. Geomorphology 28: 309–328.

Matsuoka, N., 2001. Direct observation of frost wedging in alpine bedrock. Earth Surface Processes and Landforms 26: 601-614.

Matsuoka, N., 2008. Frost weathering and rockwall erosion in the southeastern Swiss Alps: Long-term (1994-2006) observations. Geomorphology 99: 353-368.

Matsuoka, N., Murton, J., 2008. Frost weathering: Recent advances and future directions. Permafrost and Periglacial Processes 19: 195-210.

Matthes, F.E., 1936. Exfoliation of massive granite in the Sierra Nevada of California. Abstracts of the 36th annual meeting of the Geological Society of America.pp. 42-43.

Mattheson, D.S., Thomson, S., 1973. Geological implications of valley rebound. Canadian Journal of Earth Science 10: 961-978.

Matthews, J.A., Dahl, S., Berrisford, M.S., Nesje, A., Dresser, P.Q., Dumayne-Peaty, L., 1997. A preliminary history of Holocene colluvial (debris-flow) activity, Leirdalen, Jotunheimen, Norway. Journal of Quaternary Science 12: 117-129.

McColl, S.T., Davies, T.R.H., McSaveney, M.J., 2010. Glacier retreat and rock-slope stability: debunking debuttressing. Geologically active : delegate papers 11th Congress of the International Association for Engineering Geology and the Environment, Auckland, Aotearoa, 5-10 September 2010. Auckland, New Zealand.pp. 467-474.

McColl, S.T., Davies, T.R., 2011. Evidence for a rock-avalanche origin for `The Hillocks' "moraine", Otago, New Zealand. Geomorphology 127: 216-224.

McColl, S.T., 2012. Paraglacial rock-slope stability. Geomorphology 153-154: 1-16.

McGuire, B., 2010. Potential for a hazardous geospheric response to projected future climate changes. Philosophical Transactions of the Royal Society A: Mathematical, Physical and Engineering Sciences 368: 2317-2345.

McLean, J.D., 1976. Mount Cook National Park Ball Hut ground stability report on observations, May 1975-March 1976. Unpublished D.S.I.R. report EG 254, 10 pp.

McSaveney, M.J., Thomson, R., Turnbull, I.M., 1992. Timing of relief and landslides in Central Otago, New Zealand. 6th International Symposium on Landslides. Christchurch, New Zealand.1451-1456.

McSaveney, M.J., 2002. Recent rockfalls and rock avalanches in Mount Cook National Park, New Zealand. Reviews in Engineering Geology 15: 35-70.

McSaveney, M.J., Davies, T.R., Ashby, G.L., 2003. The fatal Ramsay Glacier rockfall of 9 November 2002. Institute of Geological and Nuclear Sciences, IGNS science report 2003/2, 17.

Meunier, P., Hovius, N., Haines, A.J., 2007. Regional patterns of earthquake-triggered landslides and their relation to ground motion. Geophys. Res. Lett. 34: L20408.

Meunier, P., Hovius, N., Haines, J.A., 2008. Topographic site effects and the location of earthquake induced landslides. Earth and Planetary Science Letters 275: 221-232.

Mitchell, W., McSaveney, M., Zondervan, A., Kim, K., Dunning, S., Taylor, P., 2007. The Keylong Serai rock avalanche, NW Indian Himalaya: geomorphology and palaeoseismic implications. Landslides 4: 245-254.

Molnar, P., 2004. Interactions among topographically induced elastic stress, static fatigue, and valley incision. J. Geophys. Res. 109: F02010.

Montgomery, D.R., 2002. Valley formation by fluvial and glacial erosion. Geology 30: 1047-1050.

Moore, J.R., Gischig, V., Amann, F., Hunziker, M., Burjanek, J., 2012. Earthquake-triggered rock slope failures: Damage and site effects. 11th International and Second North American Symposium on Landslides, 3rd-6th June 2012. Banff, Alberta, Canada. 6 p.

Mörner, N.-A., 1978. Faulting, fracturing, and seismicity as functions of glacio-isostasy in Fennoscandia. Geology 6: 41-45.

Mörner, N.-A., 1995. Paleoseismicity--The Swedish case. Quaternary International 25: 75-79.

Muir-Wood, R., 2000. Deglaciation seismotectonics: a principal influence on intraplate seismogenesis at high latitudes. Quaternary Science Reviews 19: 1399-1411.

Murphy, W., 2006. The role of topographic amplification on the initiation of rock slopes failures during earthquakes. In: Evans, S.G., Mugnozza, G.S., Strom, A., Hermanns, R.L. (Eds.), Landslides from Massive Rock Slope Failure. NATO Science Series. Springer Netherlands, pp. 139-154.

Newmark, N.M., Hall, W.J., 1982. Earthquake Spectra and Design. Earthquake Engineering Research Institute, Berkeley, California, 103 pp.

Nichols, T.C., Jr, 1980. Rebound, its nature and effect on engineering works. Quarterly Journal of Engineering Geology and Hydrogeology 13: 133-152.

Nicholson, D.T., 2009. Holocene microweathering rates and processes on ice-eroded bedrock, RÃ¸ldal area, Hardangervidda, southern Norway. Geological Society, London, Special Publications 320: 29-49.

Noetzli, J., Hoelzle, M., Haeberli, W., 2003. Mountain permafrost and recent Alpine rock-fall events: a GIS-based approach to determine critical factors. Proceedings of the 8th International Conference of Permafrost. Zurich, Switzerland.pp. 827-832.

Norris, R.J., Cooper, A.F., 2001. Late Quaternary slip rates and slip partitioning on the Alpine Fault, New Zealand. Journal of Structural Geology 23: 507-520.

O'Conner, J.E., Costa, J.E., 1993. Geologic and hydrologic hazards in glacierized basins in North America resulting from 19th and 20th century global warming. Natural Hazards 8: 121-140.

Orwin, J.F., Clague, J.J., Gerath, R.F., 2004. The Cheam rock avalanche, Fraser Valley, British Columbia, Canada. Landslides 1: 289-298.

Orwin, J.F., Guggenmos, M.R., Holland, P.G., 2010. Changes in suspended sediment to solute yield ratios from an alpine basin during the transition to winter, Southern Alps, New Zealand. Geografiska Annaler: Series A, Physical Geography 92: 247-261.

Owens, I.F., 1992. A note on the Mount Cook Rock Avalanche of 14 December 1991. New Zealand Geographer 48: 74-78.

Pánek, T., Hradecký, J., Minár, J., Hungr, O., Dusek, R., 2009. Late Holocene catastrophic slope collapse affected by deep-seated gravitational deformation in flysch: Ropice Mountain, Czech Republic. Geomorphology 103: 414-429.

Pánek, T., Táborík, P., Klimes, J., Komárková, V., Hradecký, J., Stastný, M., 2011. Deep-seated gravitational slope deformations in the highest parts of the Czech Flysch Carpathians: Evolutionary model based on kinematic analysis, electrical imaging and trenching. Geomorphology 129: 92-112.

Panizza, M., 1973. Glacio pressure implications in the production of landslides in the Dolomitic area. Geologia Applicata e Idrogeologia 8: 289-297.

Pascal, C., Roberts, D., Gabrielse, R.H., 2010. Tectonic significance of present-day stress relief phenomena in formerly glaciated regions. Journal of the Geological Society 167: 363-371.

Pere, V.H., 2009. Antiscarp initiation and evolution. Ph.D. Thesis, University of Canterbury, Christchurch, New Zealand, 203 pp.

Persaud, M., Pfiffner, O.A., 2004. Active deformation in the eastern Swiss Alps: post-glacial faults, seismicity and surface uplift. Tectonophysics 385: 59-84.

Petrovic, J.J., 2003. Review: Mechanical properties of ice and snow. Journal of Materials Science 38: 1-6.

Porter, S.C., Orombelli, G., 1981. Alpine rockfall hazards. American Scientist 69: 67-75.

Prager, C., Zangerl, C., Brandner, R., Patzelt, G., 2007. Increased rockslide activity in the middle Holocene? New evidence from the Tyrolean Alps (Austria). In: McInnes, R., Jakeways, J., Fairbank, H., Mathie, E. (Eds.), Landslides and climate change: Challenges and solutions: Proceedings of the international conference on landslides and climate change, Ventnor, Isle Of Wight, UK, 21-24 May 2007. Taylor & Francis Group, London, pp. 25-34.

Prager, C., Zangerl, C., Patzelt, G., Brandner, R., 2008. Age distribution of fossil landslides in the Tyrol (Austria) and its surrounding areas. Natural Hazards Earth System Science 8: 377-407.

Prager, C., Ivy-Ochs, S., Ostermann, M., Synal, H.A., Patzelt, G., 2009. Geology and radiometric 14C-, 36Cl- and Th-/U-dating of the Fernpass rockslide (Tyrol, Austria). Geomorphology 103: 93-103.

Rapp, A., 1960. Recent development of mountain slopes in Kärkevagge and surroundings, Northern Scandinavia. Geografiska Annaler 42: 65-200.

Ravanel, L., Allignol, F., Deline, P., Gruber, S., Ravello, M., 2010. Rock falls in the Mont Blanc Massif in 2007 and 2008. Landslides 7: 493-501.

Ravanel, L., Deline, P., 2011. Climate influence on rockfalls in high-Alpine steep rockwalls: The north side of the Aiguilles de Chamonix (Mont Blanc massif) since the end of the 'Little Ice Age'. The Holocene 21: 357-365.

Reid, E., Thomas, M.F., 2006. A chronostratigraphy of mid- and late-Holocene slope evolution: Creagan a' Chaorainn, Northern Highlands, Scotland. The Holocene 16: 429.

Reitner, J., Lang, M., van Husen, D., 1993. Deformation of high slopes in different rocks after Würmian deglaciation in the Gailtal (Austria). Quaternary International 18: 43-51.

Reneau, S.L., Dietrich, W.E., Dorn, R.I., Berger, C.R., Rubin, M., 1986. Geomorphic and paleoclimatic implications of latest Pleistocene radiocarbon dates from colluvium-mantled hollows, California. Geology 14: 655-658.

Reznichenko, N., Davies, T.R., Shulmeister, J., Larsen, S.H., 2012. A new technique for recognizing rock avalanche sourced deposits in moraines and some palaeoclimatic implications. Geology 40: 319-322.

Reznichenko, N.V., 2012. Rock avalanches on glaciers: processes and implications. Ph.D. Thesis, University of Canterbury, Christchurch, New Zealand, 400 pp.

Ryder, J.M., 1971. The stratigraphy and morphology of paraglacial alluvial fans in south-central British Columbia. Canadian Journal of Earth Sciences 8: 279-298.

Sanchez, G., Rolland, Y., Corsini, M., Braucher, R., Bourlès, D., Arnold, M., Aumaître, G., 2009. Relationships between tectonics, slope instability and climate change: Cosmic

ray exposure dating of active faults, landslides and glacial surfaces in the SW Alps. Geomorphology 117: 1-13.

Schulson, E.M., 1990. The brittle compressive fracture of ice. Acta Metall. Mater 38: 1963-1976.

Schulson, E.M., 1999. The structure and mechanical behaviour of ice. Journal of the Minerals, Metals, Materials Society 51: 21-27.

Selby, M.J., 1993. Hillslope Materials and Processes. Oxford University Press, New York, 480 pp.

Sepúlveda, S.A., Murphy, W., Jibson, R.W., Petley, D.N., 2005. Seismically induced rock slope failures resulting from topographic amplification of strong ground motions: The case of Pacoima Canyon, California. Engineering Geology 80: 336-348.

Shroder, J.F.J., Owen, L.A., Seong, Y.B., Bishop, M.P., Bush, A., Caffee, M.W., Copland, L., Finkel, R.C., Kamp, U., 2010. The role of mass movements on landscape evolution in the Central Karakoram: Discussion and speculation. Quaternary International 236: 34-47.

Sigurdsson, O., Williams, R.S., Jr., 1991. Rockslides on the terminus of 'Jokulargilsjokull', Southern Iceland. Geografiska Annaler. Series A, Physical Geography 73: 129-140.

Sissons, J.B., Cornish, R., 1982. Differential glacio-isostatic uplift of crustal blocks at Glen Roy, Scotland. Quaternary Research 18: 268-288.

Slaymaker, O., 2009. Proglacial, periglacial or paraglacial? In: Knight, J., Harrison, S. (Eds.), Periglacial and Paraglacial Processes and Environments. Geological Society Special Publication, pp. 71-84.

Smith, L.N., 2001. Columbia Mountain landslide: late-glacial emplacement and indications of future failure, Northwestern Montana, USA. Geomorphology 41: 309-322.

Soldati, M., Corsini, A., Pasuto, A., 2004. Landslides and climate change in the Italian Dolomites since the Late glacial. Catena 55: 141-161.

Spillmann, T., Maurer, H., Green, A.G., Heincke, B., Willenberg, H., Husen, S., 2007. Microseismic investigation of an unstable mountain slope in the Swiss Alps. J. Geophys. Res. 112: B07301.

Starkel, L., 1997. Mass movements during the Holocene: the Carpathian example and the European perspective. In: Matthews, J.A., Brunsden, D., Frenzel, B., Gläser, B., Weiß, M.M. (Eds.), Rapid Mass Movement as a Source of Climatic Evidence for Holocene. Gustav Fisher Verlag, Stuttgart, pp. 385-400.

Stewart, I.S., Sauber, J., Rose, J., 2000. Glacio-seismotectonics: ice sheets, crustal deformation and seismicity. Quaternary Science Reviews 19: 1367-1389.

Stewart, S., 1997. Rock Mass Strength And Deformability of unweathered closely jointed New Zealand Greywacke. Ph.D. Thesis, University of Canterbury, Christchurch

Strozzi, T., Farina, P., Corsini, A., Ambrosi, C., Thüring, M., Zilger, J., Wiesmann, A., Wegmüller, U., Werner, C., 2005. Survey and monitoring of landslide displacements by means of L-band satellite SAR interferometry. Landslides 2: 193-201.

Strozzi, T., Delaloye, R., Kääb, A., Ambrosi, C., Perruchoud, E., Wegmüller, U., 2010. Combined observations of rock mass movements using satellite SAR interferometry, differential GPS, airborne digital photogrammetry, and airborne photography interpretation. J. Geophys. Res. 115: F01014.

Terzaghi, K., 1962. Stability of steep slopes on hard unweathered rock. Geotechnique 12: 251–270.

Thomas, M.F., 2003. Extreme events in the context of late Quaternary environmental change. Geographia Polonica 76: 139-155.

Thorarinsson, S., Einarsson, T., Kjartansson, G., 1959. On the geology and geomorphology of Iceland. Geografiska Annaler 41: 135-169.

Tibaldi, A., Rovida, A., Corazzato, C., 2004. A giant deep-seated slope deformation in the Italian Alps studied by paleoseismological and morphometric techniques. Geomorphology 58: 27-47.

Tinner, W., Kaltenrieder, P., Soom, M., Zwahlen, P., Schmidhalter, M., Boschetti, A., Schlüchter, C., 2005. Der nacheiszeitliche Bergsturz im Kandertal (Schweiz): Alter und Auswirkungen auf die damalige Umwelt (Abstract only in English). Eclogae Geologicae Helvetiae 98: 83-95.

Turnbull, I.M. (compiler). 2000. Geology of the Wakatipu area. Institute of Geological and Nuclear Sciences 1:250 000 geological map 18. 1 sheet + 72 p. Lower Hutt, New Zealand. Institute of Geological and Nuclear Sciences limited.

Turnbull, I.M., Allibone, A.H., Jongens, R. (compilers). 2010. Geology of the Fiordland area. Institute of Geological and Nuclear Sciences 1:250 000 geological map 17. 97 pp.+1 folded map. Institute of Geological and Nuclear Sciences

Turpeinen, H., Hampel, A., Karow, T., Maniatis, G., 2008. Effect of ice sheet growth and melting on the slip evolution of thrust faults. Earth and Planetary Science Letters 269: 230-241.

Twidale, C.R., 1973. On the origin of sheet jointing. Rock Mechanics 5: 163-187.

Ustaszewski, M.E., Hampel, A., Pfiffner, O.A., 2008. Composite faults in the Swiss Alps formed by the interplay of tectonics, gravitation and postglacial rebound: an integrated field and modelling study. Swiss Journal of Geosciences 101: 223-235.

van Asch, T.W.J., 1997. The temporal activity of landslides and its climatological signals. In: Matthews, J.A., Brunsden, D., Frenzel, B., Gläser, B., Weiß, M.M. (Eds.), Rapid Mass Movement as a Source of Climatic Evidence for Holocene. Gustav Fisher Verlag, Stuttgart, pp. 7-16.

van Husen, D., Ivy-Ochs, S., Alfimov, V., 2007. Mechanism and age of Late Glacial landslides in the Calcareous Alps; The Almtal, Upper Austria. Austrian Journal of Earth Sciences 100: 114-126.

Varnes, D.J., 1978. Slope movement types and processes. In: Schuster, R.L., Krizek, R.J. (Eds.), Landslides Analysis and Control. Special Report 176. Transportation Research Board, National Academy of Sciences, Washington D.C., pp. 11-33.

Voight, B., 1989. A relation to describe rate-dependent material failure. Science 243: 200-203.

Watanabe, T., Dali, L., Shiraiwa, T., 1998. Slope denudation and the supply of debris to cones in Langtang Himal, Central Nepal Himalaya. Geomorphology 26: 185-197.

Watson, A.D., Moore, D.P., Stewart, T.W., Psutka, J.F., 2007. Investigations and monitoring of rock slopes at Checkerboard Creek and Little Chief Slide. Rock Mechanics: Meeting Society's Challanges and Demands, Proceedings of the 1st Canada-US Rock Mechanics Symposium. Vancouver, Canada.1015-1022.

Wegmann, M., Gudmundsson, G.H., Haeberli, W., 1998. Permafrost changes in rock walls and the retreat of alpine glaciers: a thermal modelling approach. Permafrost and Periglacial Processes 9: 23-33.

Whalley, W.B., Douglas, G.R., Jonsson, A., 1983. The magnitude and frequency of large rockslides in Iceland in the postglacial. Geografiska Annaler 65: 99-110.

Whitehouse, I.E., 1983. Distribution of large rock avalanche deposits in the central Southern Alps, New Zealand. New Zealand Journal of Geology and Geophysics 26: 271-279.

Wieczorek, G.F., Jäger, S., 1996. Triggering mechanisms and depositional rates of postglacial slope-movement processes in the Yosemite Valley, California. Geomorphology 15: 17-31.

Wieczorek, G.F., Snyder, J.B., 2009. Monitoring slope movements. In: Young, R., Norby, L. (Eds.), Geological Monitoring. Geological Society of America, Boulder, Colorado, pp. 245-271.

Wilson, P., Smith, A., 2006. Geomorphological characteristics and significance of late quaternary paraglacial rock-slope failures on Skiddaw Group terrain, Lake District, northwest England. Geografiska Annaler: Series A, Physical Geography 88: 237-252.

Winkler, S., 2009. First attempt to combine terrestrial cosmogenic nuclide (10Be) and Schmidt hammer relative-age dating: Strauchon Glacier, Southern Alps, New Zealand. Central European Journal of Geosciences 1: 274-290.

Wu, P., Johnston, P., 2000. Can deglaciation trigger earthquakes in N. America? Geophysical Research Letters 27: 1323-1326.

Wu, P., Mazzotti, S., 2007. Effects of a lithospheric weak zone on postglacial seismotectonics in eastern Canada and the northeastern United States. Geological Society of America Special Papers 425: 113-128.

Wu, X., Heflin, M.B., Schotman, H., Vermeersen, B.L.A., Dong, D., Gross, R.S., Ivins, E.R., Moore, A.W., Owen, S.E., 2010. Simultaneous estimation of global present-day water transport and glacial isostatic adjustment. Nature Geoscience 3: 642-646.

Wyllie, D.C., Mah, C.W., 2004. Rock Slope Engineering: Civil and Mining. Spon Press, Glasgow, 431 pp.

Wyrwoll, K., 1977. Causes of rock-slope failure in a cold area: Labrador-Ungava. Geological Society of America Reviews in Engineering Geology 3: 59-67.

Young, A., 1972. Slopes. Oliver and Boyd, Edinburgh, 288 pp.

Zoback, M.D., Grollimund, B., 2001. Impact of deglaciation on present-day intraplate seismicity in eastern North America and western Europe. Comptes Rendus de l'Académie des Sciences - Series IIA - Earth and Planetary Science 333: 23-33.

APPENDIX A:

In this thesis, it was recognised that any progress with linking rock slope failure activity to causative processes requires accurate landslide inventories. One of the challenges in achieving this is that rock slope failure deposits are often mistaken as glacial deposits because they can share similar morphology and sometimes similar sedimentary characteristics. The published manuscript 'Evidence for a rock-avalanche origin for 'The Hillocks' "moraine", Otago, New Zealand' was written by the PhD candidate during his degree and is presented below to provide an example of how rock avalanche deposits can be accurately identified in glaciated terrain.

Evidence for a rock-avalanche origin for `The Hillocks' "moraine", Otago, New Zealand.
McColl ST; Davies, T.R. *Geomorphology* 127: 216-224, Copyright © 2011 Elsevier B.V.
http://www.sciencedirect.com/science/article/pii/S0169555X10005489

Only formatting and pagination has been modified for production in the thesis

Abstract: A landform in Otago, New Zealand, previously interpreted as a glacial deposit, has been investigated, described and reinterpreted as a rock avalanche deposit. 'The Hillocks' is a conspicuous cluster of small conical hills on the Dart River floodplain. The landform is protected under a local bylaw because of its identification as an outstanding example of a glacial kame deposit. However, the geological and geomorphological setting, and the deposit morphology, sedimentology and lithology, suggest that it was formed by a large (c. 22.5×106 m3) rock avalanche subsequent to glacial retreat, and that the deposit temporarily dammed the Dart River valley. Relative age dating evidence suggests that it is at least several hundred years old but younger than ca 7500 B.P. This work highlights the

problem of paleoclimatic reconstructions using 'moraines' as indicators of regional climate events. Despite similarities in form and, in some cases, sedimentology, by applying an understanding of landslide initiation, runout and depositional process, we demonstrate that it is possible to distinguish the deposits produced by landslides from those produced by glacial deposition.

1. Landslides and glacial deposits

Misinterpretation of glacial landforms has recently been highlighted as a pertinent issue in glacial-geomorphology and for paleoclimate reconstructions (Larsen et al., 2005; Tovar et al., 2008; Deline, 2009; Deline and Kirkbride, 2009; Shulmeister et al., 2009; Winkler and Matthews, 2010). Misinterpreting depositional landforms is a particular problem because of the long-standing use of glacial deposits as indicators of past climate. The problem lies in distinguishing between glacier deposits that represent regional climatic events; those that represent localised (or regionalised) non-climatic events; and deposits of non-glacial origin (Orombelli and Porter, 1988; Hewitt, 1999; Tovar et al., 2008).

Landslide phenomena have been especially problematic for glacial-geomorphology and paleoclimate reconstructions. Erosional landforms created by landslides, such as cirque-like basins, have received conflicting interpretations (e.g. Shakesby and Matthews, 1996; Turnbull and Davies, 2006) but landslide deposits have been even more problematic; like glacial-deposits, landslide deposits often have hummocky morphology and occur in similar mountain valley locations. Supraglacial landslide debris that undergoes little glacial reworking before final deposition can exhibit similar sedimentary characteristics to that of the rock avalanche carapace material as well as similar morphology (Tovar et al., 2008; Vacco et al., 2010). Examples of landslides misinterpreted as having a glacial origin include numerous deposits in the Karakoram Himalaya (Hewitt, 1999), and several in the European Alps such as the famous Fernpass (Prager et al., 2009) and Flims rock avalanches (Ivy-Ochs et al., 2009). In New Zealand there have been similar misinterpretations (Thomson, 1994; Porter, 2000), and some remain controversial (Tovar et al., 2008; Vacco et al., 2010).

Glacial deposits have also been mistakenly identified as landslides, for example McSaveney and Whitehouse (1989) reinterpret a previously described landslide deposit as being moraine. It appears that although some criteria have been established for distinguishing between deposits of glacial and mass-movement origin (e.g. Hewitt, 1999), difficulties remain in distinguishing between the deposits produced by these very different processes.

'The Hillocks' in the Dart River valley, Queenstown Lakes District (Figure 1), is one such example of a landform of debatable origin. It is a collection of small, mostly conical, hills on the Dart River floodplain (Figure 2), formerly known as 'The Hillocks'. It is a protected landform under the Queenstown-Lakes District Council Plan due to its listing in the New Zealand Geopreservation Inventory, which describes it to be: "A kame field that formed when the Dart glacier extended this far..." and was classified therein as an "extremely well defined landform of scientific/education value" and given an importance status of Class B; "a site of national scientific, educational or aesthetic importance" (Kenny and Hayward, 1993). An expectation of glacier deposits in the glaciated valley and the hummocky nature of the deposit, appear to be the reasons it has received a glacial-origin interpretation. Following investigation of the deposit sedimentology, lithology, morphology and geographical setting, details of which follow, we interpret the deposit to be of rock avalanche origin.

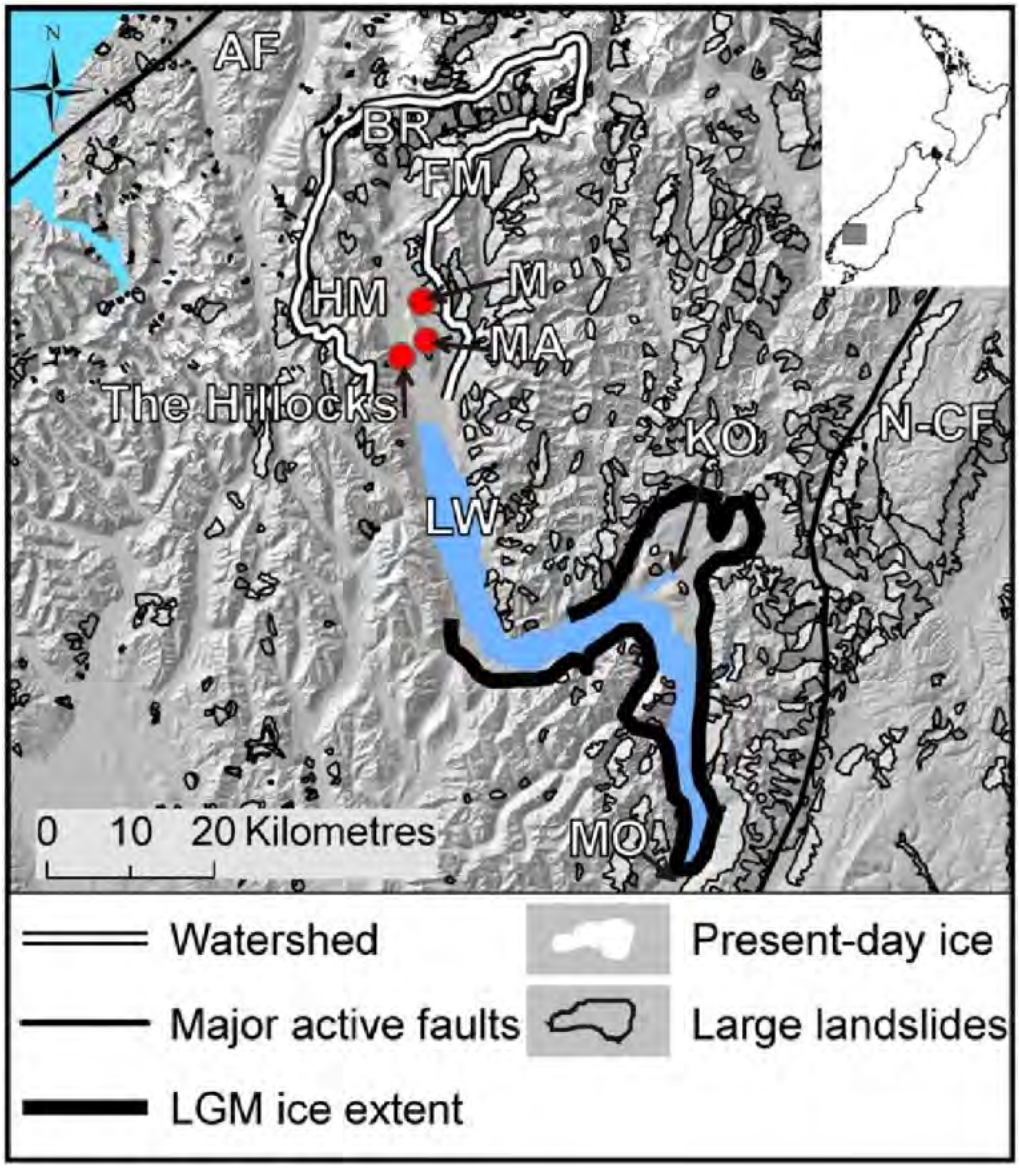

Figure 1. The Hillocks and Dart River Catchment. LGM=c. 20 ka. Present-day ice distribution sourced from the Land Information New Zealand. Landslide distribution sourced from Turnbull (2000) and GNS Science Large Landslide Database. DEM is 25 m cell size, from Landcare Research. AF = Alpine fault; N–CF = Nevis-Cardrona fault; BR = barrier range; FM = Forbes Mountains; HM = Humboldt Mountains; M = moraine near to The Hillocks; MA = Mt Alfred; LW = Lake Wakatipu; KO = Kawarau outlet; MO = Mataura outlet.

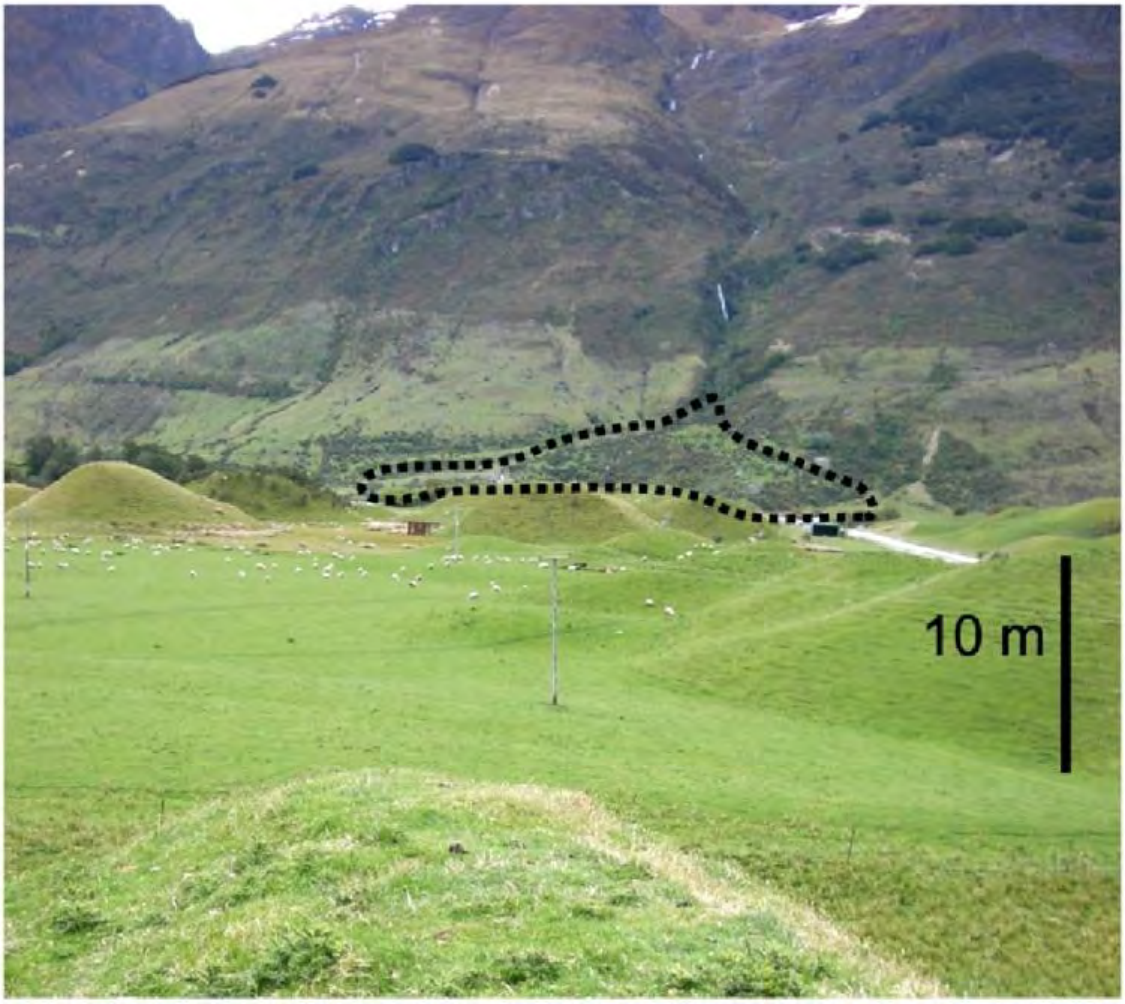

Figure 2. The Hillocks, looking west with debris fan (dotted outline) mapped by Turnbull (2000) visible in back-ground. Landslide source area is just out of the picture at top right.

2. Geology and geomorphology of the Dart Catchment

The Dart Catchment lies within the Mesozoic Haast Schist Group in the Southern Alps, a region of metamorphosed greywacke (Turnbull, 2000) (Figure 3). Weakly foliated volcaniclastic Caples terrane is predominant to the west in the Humboldt Mountains, while higher-grade schists (chlorite zone IIB and IV with well developed foliation and alteration) of the Caples and Rakaia terranes compose the Barrier Range and Forbes Mountains to the north and east, making up the greater part of the Dart Catchment. Elevations in the area range from c. 300–2300 m above sea level. Regional seismicity is high with the active Alpine and Nevis–Cardrona faults within 60 km of the study area (Figure 1) and with major earthquakes of up to Richter Magnitude 8 on the Alpine Fault every 250–500 years (Berryman et al., 1992; Sutherland et al., 2006). Based on a regional probabilistic hazard model, Stirling et al. (2002) estimate a peak ground acceleration of 0.7 g for a 475 year return time for the Hillocks area.

Landsliding is a dominant form of erosion in the Wakatipu region, and within a 50 km radius of The Hillocks ~700 landslide features – source areas, deposits, areas of gravitational deformation – have been identified and mapped (GNS Science and Turnbull, 2000) (Figure 1). Much of the landsliding occurs in the structurally weak schist but numerous landslides have been mapped in the less foliated rock.

Glaciations have helped to shape the landscape and form the characteristic large lakes in the region. The Dart glacier, the present day terminus of which lies some 50 km up-valley of the Hillocks, was once part of a much larger glacier that formed Lake Wakatipu (Figure 1). The glacial history of the Otiran and earlier glaciations is reasonably well known for the Wakatipu area (Barrell, 1994; Turnbull, 2000) but is poorly known for the late-Glacial and Holocene time. The Hillocks and a moraine 5–6 km up-valley (Figure 1) are speculated to be from an early Aranuian (present interglacial) advance (pers. comm. Royden Thompson) but there are no age-date data to support this. The level of Lake Wakatipu has fluctuated above and below its present level since its formation, in response to changes in drainage configuration (Barrell, 1994; Thomson, 1996).

3. Methodology

Topographic contours (20 m), Google Earth 3D, and the Wakatipu QMAP 1:250 k regional geology sheet and mapping by Kawachi (1974) were used for the identification and mapping of a likely source area for the landslide. Identifying the source areas in the field was not possible because of the difficult terrain.

A combination of satellite imagery (Google Earth), oblique photographs taken from Mt Alfred (1375 m.a.s.l.; Figure 1), and a Garmin GPSMAP 60CSx were used to map the location of the hillock features remotely and on foot. Where groupings of hillocks displayed a predominant orientation, or formed approximately linear groupings, lines were traced over them to indicate the orientation.

Deposit sedimentology and lithology were examined and described at outcrop and hand-specimen scale at several exposures cut by the Dart River and Stockyard Creek (Figure 4). Several large boulders exposed in the river and on the surfaces of some hillocks were examined.

4. Results

4.1. Landslide source area and locality

It is likely that a landslide large enough to form the Hillocks occurred in this locality. Other large rockslides and slope failures have been identified in the Humboldt Mountains (Figure 1). Landslide debris adjacent to The Hillocks (Figs. 2 and 4) was mapped by Turnbull (2000) but hitherto a source area for this deposit had not been identified. The upper part of the slope above the deposit has a conspicuous concave profile and bowl-shape (Figure 5). Such bowl-shaped depressions are often formed at the top of steep slopes by deep-seated coseismic rock slope failures (cf. Turnbull and Davies, 2006; Bazgard et al., 2009). We have mapped the extent of this source area and calculated a minimum volume of 22.5 million m^3, conservatively assuming a planar pre-failure surface.

The geology of the source area has been mapped as Bold Peak unit, a predominately weakly metamorphosed sandstone of the Caples terrane (Turnbull, 2000) (Figure 5). The degree of metamorphism probably ranges from weak to moderate foliation, within textural zones I to IIIa (Kawachi, 1974; Turnbull, 2000). We identify an unmapped structural lineation running through the proposed source area (Figure 5) and suggest that it is a zone of weak rock, possibly a fault, that may have contributed to the failure.

The elevation difference (H) between the top of the source area (2040 m.a.s.l.) and the Dart River floodplain (340 m.a.s.l.) is 1700 m. The horizontal distance (L) from the back of the source area to the distal down-valley hillock is 5300 m. This gives a travel angle of $\tan^{-1}$ (H/L)=18°, which is of the normal order of magnitude for a rock avalanche of this volume (e.g. Legros, 2002).

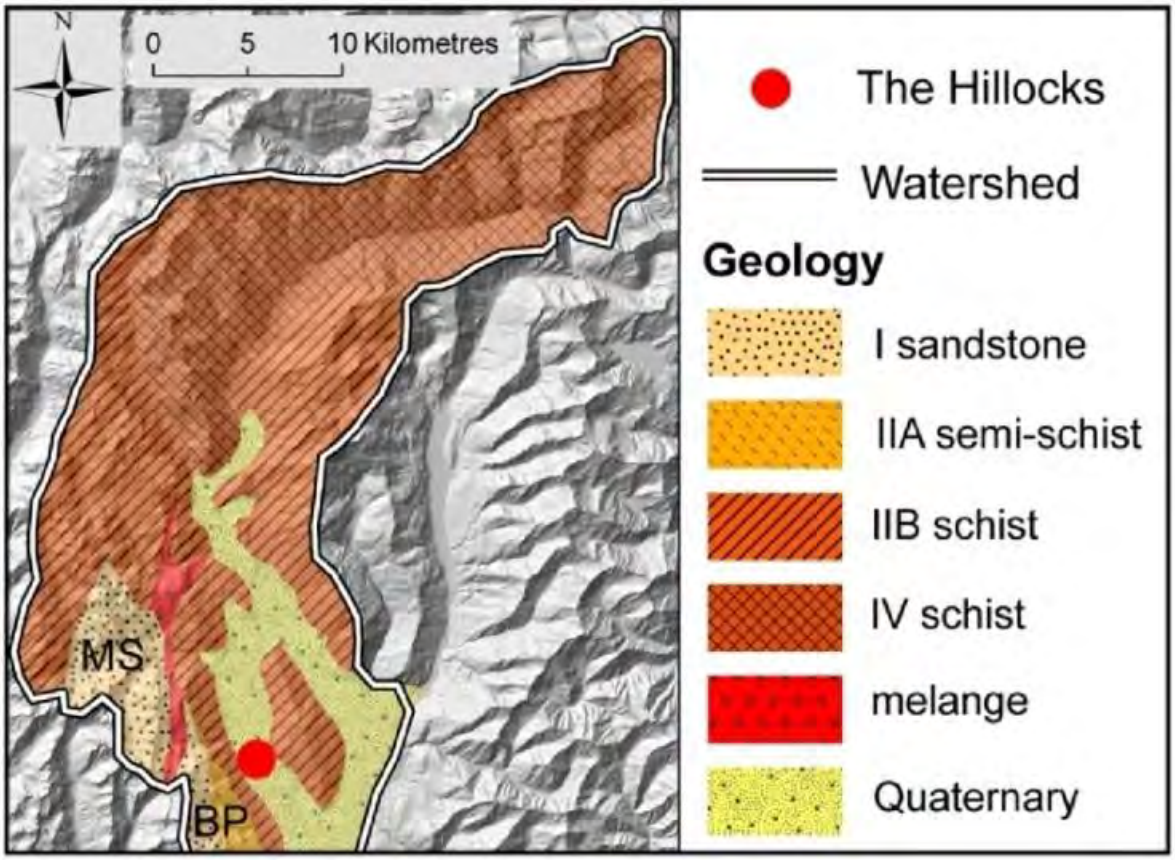

Figure 3. Geology of the Dart River catchment simplified from Turnbull (2000). The prefixes I, IIA, IIB and IV denote the textural zone of the schist. See Figure 1 for the geographic location of the catchment. DEM is 25 m cell size, from Landcare Research. BP = Bold Peak formation; MS = Momus Sandstone formation.

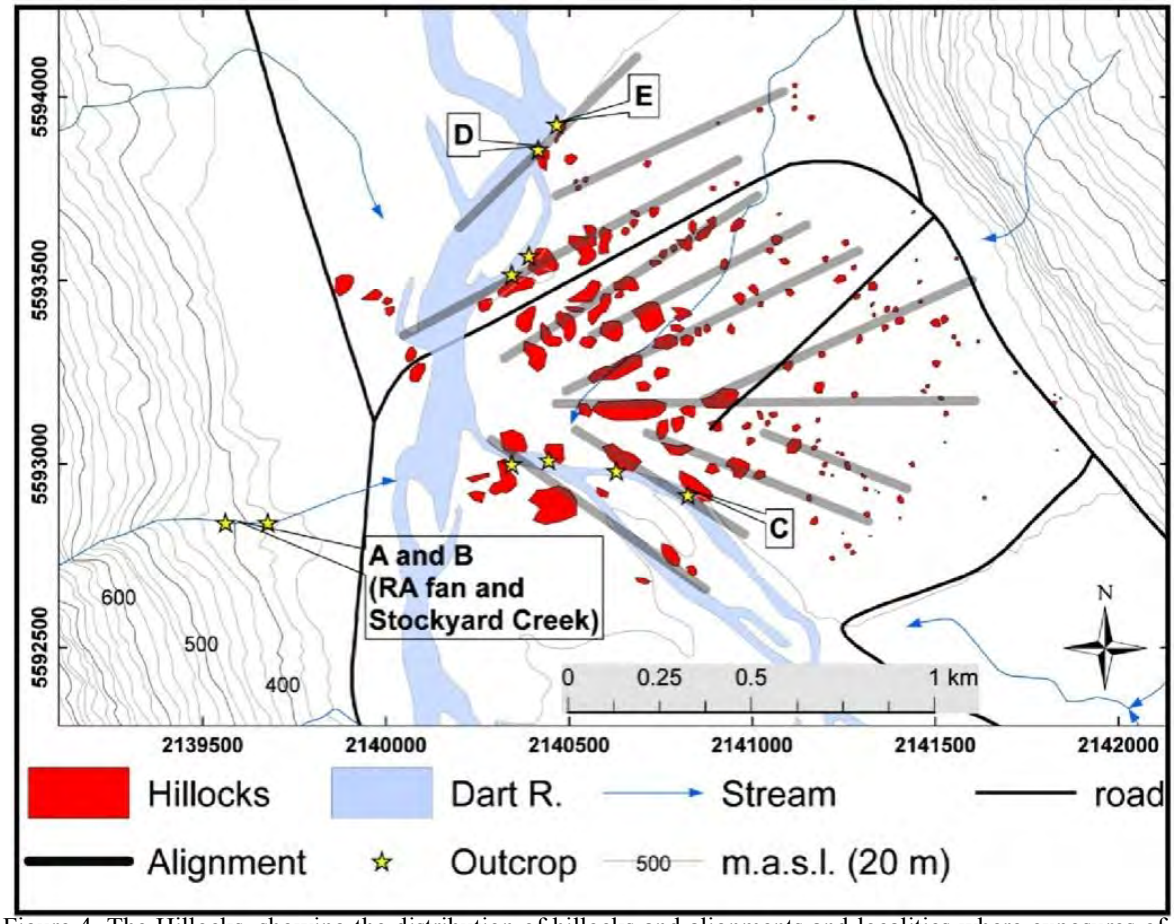

Figure 4. The Hillocks, showing the distribution of hillocks and alignments and localities where exposures of hillocks were observed. The rock avalanche (RA) fan is indicated by the widely spaced contours at the base of Stockyard Creek. Letters A–E relate to Figure 7 photograph locations. Contours (20 m) from Land Information New Zealand, data projected in Geodetic Datum 1949 with New Zealand Map Grid, 500 m grid spacing.

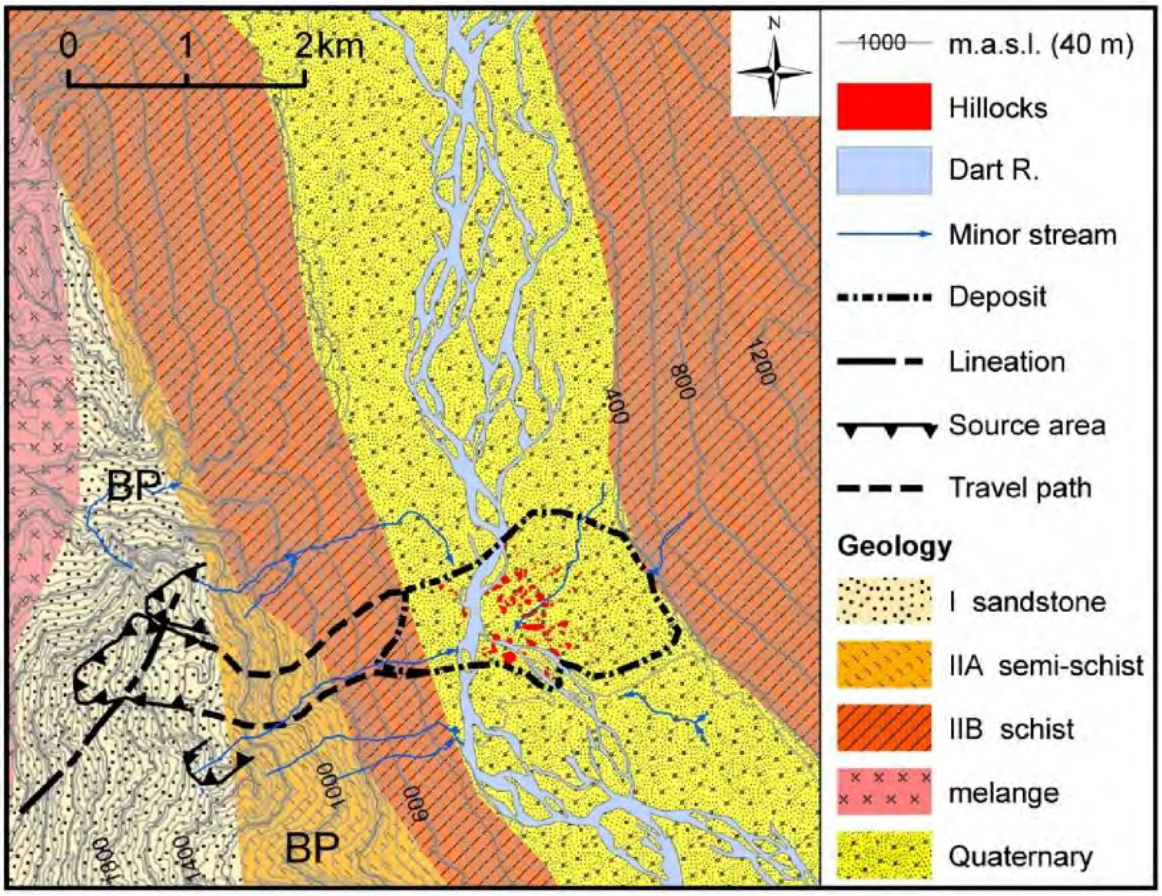

Figure 5. Geomorphology and geology[1] of the Dart Valley at The Hillocks, showing our preferred landslide source area, suggested runout path and deposit area. Contours (40 m) from Land Information New Zealand. BP = I and IIB textural zone Bold Peak Formation.

[1] Postscript: Since publication, the author has made revisions to the geological interpretations of the source area and hillocks lithology. Thin-section analysis has confirmed that the majority of debris in the hillocks (facies 1) is schist with a well developed foliation, not a low-grade metamorphic schist or sandstone as first identified. The author has walked up Stockyard Creek to the presumed source area and has found large angular boulder debris in the source area with the same lithology as found in the hillocks deposit. Therefore, the lithological boundaries presented in the geological maps are incorrect (at the scales presented). The source area for the hillocks, although now interpreted to be a different lithological unit, is still considered to be the same location (considering the original geomorphological evidence, the new lithological evidence, and the discovery of mass-movement debris in the source area and along the presumed transport path).

Figure 6. Panorama of The Hillocks from Mt Alfred (1375 m.a.s.l.) looking west. The b10 m wide semi-sinuous channel forms crossing the flat pasture are best observed right of the road. df = debris fan at Stockyard Creek. Black bar on road is 900 m long.

4.2. Deposit morphology

A prominent feature of the floodplain deposit is the numerous conical hills (Figs. 2, 4 and 6). We have mapped c. 160 individual hillocks, with planform areas between 6 m^2 and almost 10,000 m^2 and with heights ranging from about 1 to 15 m above the floodplain surface. While most of the hillocks are conical, several in the more proximal part of the deposit are elongate. These elongate hills, as well as alignments of the conical hills, form a quasi-radial distribution converging towards the western side of the valley (Figure 4). The course of the Dart River appears to be controlled by the distribution of the hillocks—the braided river is forced to narrow and travel westwards around the main cluster of the hillocks (Figure 4). The size of the hillocks (both area and height) decreases from west to east. The area between the hillocks is a flat surface of uniform elevation but with small (~10 m wide), shallow (~1 m) palaeo-channels etched onto it (Figure 6). The non-dendritic

channels are approximately aligned in the direction of the valley long axis and are slightly sinuous.

On the true-right of the Dart River, below our suggested source area, a fan builds out from Stockyard Creek gully towards the floodplain hillocks at a slope angle of about 16° (Figs. 2 and 4). It has been dissected by up to 5 m by Stockyard Creek. Turnbull (2000) mapped this fan as landslide debris.

4.3. Deposit sedimentology and lithology

Three distinctive sedimentary facies were observed (Figure 7). Facies 1 is most abundant and was identified in all of the exposures investigated, which included several locations where the Dart River has dissected hillocks, and the dissected fan at Stockyard Creek (Figure 4). Facies 1 consists of tightly interlocking angular to sub-angular clasts that range from fine gravel to boulder size, with some boulders ~4 m in diameter, and with fine-grain to coarse sand and silt matrix. The gross coarseness of the deposit is variable with the debris fan at Stockyard Creek being slightly finer than the other exposures in the hillocks. Facies 1 is homogenous without stratification. The rock type in each exposure is monolithic and across exposures it varies from non-metamorphosed to weakly foliated sandstone with thin black mudstone lenses. Higher-grade schist (above textural zone IIIa) was not identified but low-to medium-grade schists (textural zone IIa and IIb) were found occasionally. Facies 1 appeared to control the overall shape of the hillocks. A lower contact for facies 1 was not observed but the facies was observed to be at least 5 m thick.

Figure 7. Sedimentary facies of The Hillocks (see Figure 4 for photograph locations). A) and B) facies 1 in fan deposit showing coarse angular monolithic clast-supported material with matrix of fine gravels and sand. C) Coarser grained facies 1 in hillock exposure with extremely large boulder (10 m) overlaying (cf. Figure 9B) (hammer in centre is 325 mm long). D) Contacts between (a) angular greywacke of facies 1, (b) rounded mixed lithology river gravels of facies and (c) facies 3 loess. E) Rounded mixed lithology river gravels of facies 2 positioned in an exposure between two hillocks.

Facies 2 comprises well-sorted and well-rounded clasts of gravel to cobble size. It was found sometimes as a thin (~0.2 m) layer overlaying facies 1 on the lower parts of several hillocks (e.g. Figure 7D) and as a thicker (0.5 to 2 m) stratified deposit between individual hillocks (e.g. Figure 7 E). The gravels were a mix of lithology that included high-grade schists and quartz gravels, similar to the mixed gravels observed in the present-day Dart River channel.

A third facies identified was a soft well-sorted fine-grained (loess) deposit mantling many of the hillocks, up to several metres thick in places. It lacked obvious stratification; however, many of the exposures of this material had been affected by post-depositional reworking.

4.4. Deposit age

No quantitative age-dating has been done but several observations provide an indication of age. The source area does not appear fresh and substantial amounts of debris from rockfall and debris-flow processes have accumulated within the bowl-shaped source area. While the region was most likely deforested for farming by the 19th century, some trees remain on the slopes below the source area. These trees are in the path of the rock avalanche so they must post-date the avalanche, as would the few trees on and around some of the hillocks. The substantial mantling of the hillocks by fluvial and aeolian deposits, together with moderate soil development indicates that substantial time has passed since emplacement. Substantial time is also required for both the incision of the fan deposit by the small Stockyard Creek and the erosion of hillocks in the present Dart River channel, as indicated by clusters of well-rounded very-large boulders in the channel. It is also possible that a Maori Pa (village) was established here (pers. comm. Simon Cox, GNS Science, Dunedin), which would be consistent with Maori occupation of landslide generated hillock-features elsewhere in New Zealand (e.g. Mt Taranaki debris avalanche, Figure 8A).

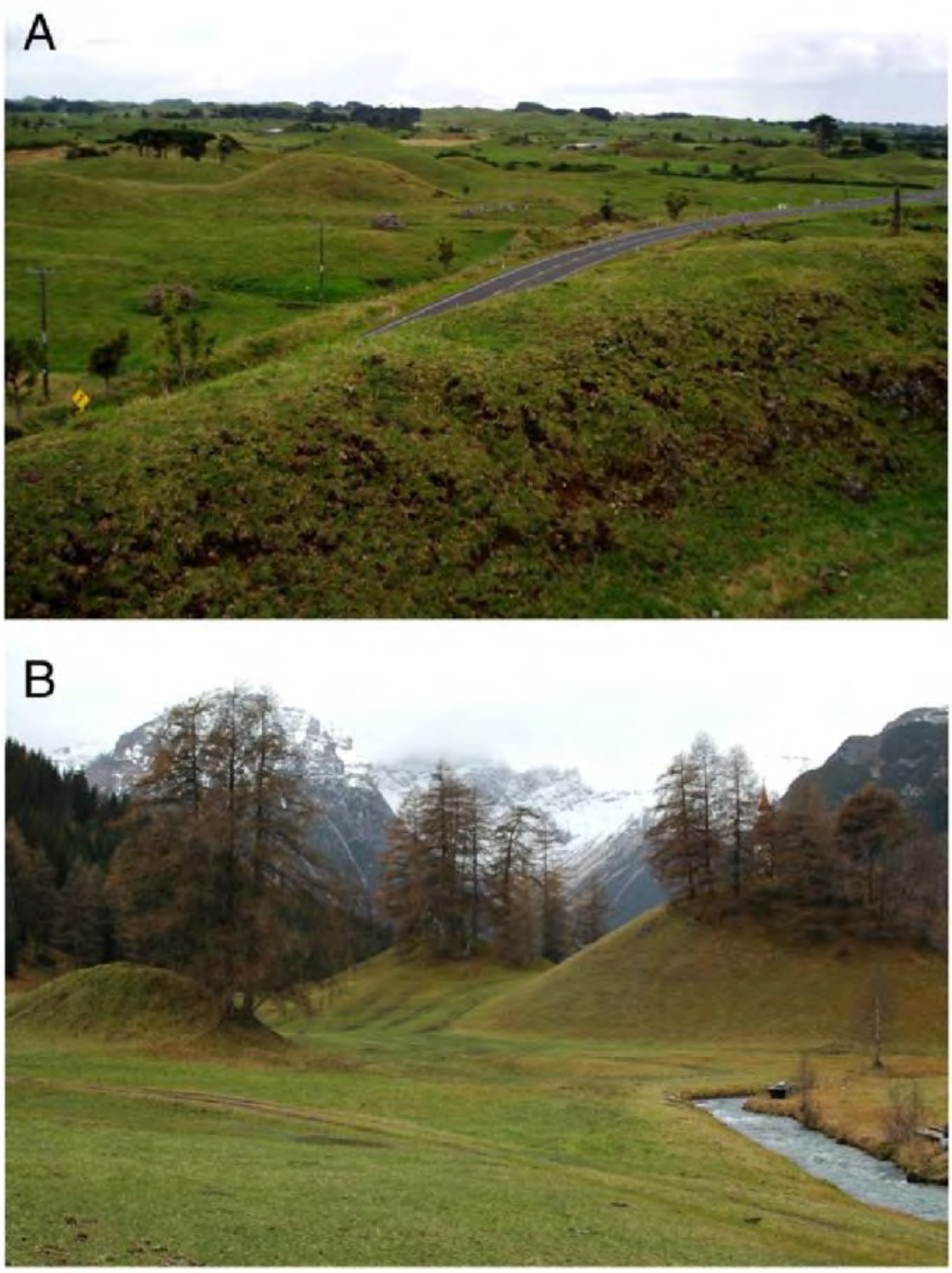

Figure 8. Hummocky morphology of other unequivocal rock avalanche. A) Mount Taranaki volcanic debris avalanche deposit, New Zealand. Photo is taken from the trench of an ancient fortified Maori Pa (village) atop one of the hillocks. 8 m high power-poles give scale. B) Obernberg rock avalanche deposit, Austrian Alps. Trees provide scale (photo courtesy of Marc Ostermann).

5. Discussion

5.1. Evidence for rejecting a glacial origin for The Hillocks

Before considering evidence that supports a landslide origin, we discuss evidence that we have used to reject a glacial origin for The Hillocks.

5.1.1. Glacial origin without landslide input

A dominance of coarse monolithic angular material precludes the possibility of a glacial origin not involving significant landslide input. Glacial till from basal and terminal ice melt, without a significant supraglacial landslide debris component, would be a matrix-supported diamicton accompanied by fluvially sorted and rounded outwash material. Further, it would have a mixing of different lithologies, including high-grade schist, sourced from the entire Dart River catchment. Glaciofluvial depositional processes, which would favour down-valley sorting and arrangement of sediments, seems unlikely to have formed either the quasi-radial alignment distribution of the hillock features or created the across-valley decrease in the hillock size. The localised extent of the hillock features, as opposed to their widespread occurrence throughout the catchment, is a further indicator that a purely glacial origin for The Hillocks is unlikely.

5.1.2. Supraglacial landslide origin

A supraglacial landslide farther up the catchment, with subsequent glacial transport to the present site, is a highly unlikely origin for The Hillocks. It would require a large landslide source area of weakly-metamorphosed rock, and a process of deposition from the glacier surface that can create or preserve the pattern of hillocks.

5.1.2.1 Source areas.

The only substantial sources of weakly-non metamorphosed rock in the Dart Catchment are the Bold Peak Formation and Momus Sandstone (Figure 3). There is no sufficiently

large landslide source area further up-valley in the Bold Peak unit. There is an apparent landslide scar immediately north-east of the source area we have identified that occurs in the Bold Peak unit (Figure 5), however we judge that its outline is too small and ambiguous to confidently assign it as a source area for The Hillocks rock avalanche. The Momus Sandstone occurs in tributary catchments 10–15 km up valley from The Hillocks. No landslide features have previously been mapped in the non-metamorphosed Momus Sandstone Formation further up valley within the Dart River catchment (GNS Science & Turnbull, 2000), and no new ones have been identified in this study.

5.1.2.2. Emplacement and reworking.

If the landslide from our suggested source area was emplaced onto the Dart Glacier, we would expect that the deposit would have been offset from the source area above Stockyard Creek by glacial transport, especially if the debris cover caused an advance (see McSaveney, 1978; Deline and Kirkbride, 2009; Shulmeister et al., 2009; Vacco et al., 2010). That the deposit was not transported by glacier flow suggests that, if emplacement was indeed onto the Dart Glacier, it must have been emplaced on to 'dead' ice being no longer capable of transporting it, which then melted to form the hillocks. It is unlikely that the distribution of the aligned and distally thinning hillocks would have been either formed by, or preserved during, this process. It is even less of the Dart River appears to be controlled by the distribution of the hillocks—the braided river is forced to narrow and travel westwards around the main cluster of the hillocks (Figure 4). The size of the hillocks (both area and height) decreases from west to east. The area between the hillocks is a flat surface of uniform elevation but with small (b10 m wide), shallow (b1 m) palaeo-channels etched onto it (Figure 6). The non-dendritic channels are approximately aligned in the direction of the valley long axis and are slightly sinuous.

On the true-right of the Dart River, below our suggested source area, a fan builds out from Stockyard Creek gully towards the floodplain hillocks at a slope angle of about 16° (Figs. 2 and 4). It has been dissected by up to 5 m by Stockyard Creek. Turnbull (2000) mapped this fan as landslide debris.

5.2. Evidence for a landslide origin for the Hillocks

5.2.1. Source area and failure mechanism

We propose that The Hillocks formed with the emplacement of a large rock avalanche sourced from the bowl-shaped depression identified in Figure 5. Given the deep-seated nature of the failure surface and its extension to the ridge-crest, a coseismic trigger is probable (Turnbull and Davies, 2006). Other triggering mechanisms, which may include rainfall, snowmelt, snow loading, or a critical reduction in strength are less likely to have developed a deep-seated concave source area shape. The three largest (N10 M m^3) historical aseismic rock avalanches in New Zealand have involved failure of a prominent spur or rock slab (Owens, 1992; Hancox et al., 2005; Massey et al., 2008). In contrast, the coseismic Falling Mountain Rock Avalanche of 1929 left a large hole in the mountain (McSaveney et al., 2000).

5.2.2. Runout

The Hillocks rock avalanche would have travelled rapidly down the steep (30°) valley-side slope before spreading out onto the flat floodplain below. The travel angle of 18° is in the upper range of typical values reported by others for rock avalanches of this size (McSaveney et al., 2000; Smith et al., 2006; Strom and Korup, 2006; Devoli et al., 2009). A longer runout distance may have been prevented by the opposite valley wall (Mt Alfred) but no evidence for brandung runup is observed. It is likely that the runout distance has been underestimated because of burial or erosion of the deposit.

5.2.3. Sedimentology

The sedimentology of The Hillocks corresponds clearly to that of unequivocal rock avalanche deposits elsewhere. A rock avalanche generally comprises a thoroughly fragmented mass of monolithic, fractally-graded, angular clasts from sub-micron to boulder sizes, with a carapace of less-fragmented coarser rocks (McSaveney and Davies, 2006)

(Figure 9). We suggest that the deposit exposed in the Stockyard Creek fan represents internal rock avalanche debris whereas the material exposed in the hillock features is coarser carapace overlaying buried internal and basal debris.

5.2.4. Depositional environment and post-depositional processes

It is probable that at the time of emplacement the floodplain surface was lower than today, as evidenced by the absence of an observable lower contact for facies 1. Further, for the estimated source area volume of 22.5 million m^3 to approximately equal the deposit volume, an average deposit thickness of 9.5 m is required. This is ignoring any bulking factor but it is also using a minimum areal deposit extent based on the present distribution of hillocks. In any case, the visible (unburied) volume of sediment contained within the hillocks (<1 million m^3) is considerably less than the source volume. The deposit must be substantially buried, which is consistent with our interpretation in 5.2.3 above.

We suggest that the deposit blocked the Dart River because the hillocks extend to the opposite valley wall (Mt Alfred). The breach of the landslide-dam is likely to have been non-catastrophic; fluvial deposits (facies 2) between the hillocks indicate that the river flowed through the entire width of the deposit for some time. The river cut its present course through the western side of the deposit and appears to remain confined there by the remaining deposit. That the river cut through the western (proximal) side of the deposit, is not unexpected.

Debris of primary rock avalanches, *sensu* Strom (1996), travel as a single mass, of which most arrests towards the distal end of the runout path. The Hillocks rock avalanche can therefore be classed as primary because of the absence of hillocks on the western side of the Dart River (see Figure 4) and the almost complete evacuation of debris from the source area. The Dart River would have cut through towards the western side of the valley because the deposit surface was most likely lower there. Subsequent progradation of the Dart River delta into Lake Wakatipu and the corresponding aggradation of the Dart River at The Hillocks is likely to be responsible for the partial burial of the deposit.

If the landslide occurred sufficiently early for Lake Wakatipu to have been at a higher level, it could have fallen into the lake water. Thomson (1996) suggests that prior to ca 7500 B.P. Lake Wakatipu drained into the Mataura River at the southern end of the lake (Figure 1), with a surface level at about 355 m.a.s.l. This is ~15 m above the present Dart River level at The Hillocks; since that time the drainage switched to the Kawarau River, which is inferred to have degraded gradually to its present level. There is no evidence to suggest that the rock avalanche fell into a lake; neither lacustrine deposits on top of the debris nor splash deposits have been observed.

5.2.5. Morphology

The radially-aligned and conical appearance of The Hillocks is a well-known form in landslide geomorphology. Indeed hummocky terrain is one of the diagnostic features of landslide deposits, including those from rock avalanche, volcanic debris avalanche, and debris flow (Figure 8) (Hewitt, 1999; Dufresne and Davies, 2009). Post-emplacement stream erosion or sediment mantling of a landslide deposit is more likely to produce channels and ridges that align down the valley axis rather than across the valley as observed here. Dufresne and Davies (2009), on the other hand, explain that rock avalanche flow dynamics can produce such features.

Dufresne and Davies (2009) explain that ridges develop from lateral instabilities in a granular flow (i.e. in a rock avalanche), especially one involving angular material travelling rapidly over an erodible substrate. These conditions are met by the suggestion that the Hillocks are a rock avalanche deposit emplaced onto river gravels. Dufresne and Davies (2009) also suggest that radially aligned hillocks are remnants of granular flow ridges that have begun to separate as the distal end of the ridge decelerates. Further, scattered hummocks may form when the lateral velocity of the flow is similar to the longitudinal velocity of the flow, as might happen when the flow becomes unconfined on a floodplain. We suggest that longitudinal ridges developed when the debris travelled onto the floodplain, and that lateral spreading as well as deceleration caused the breakup of ridges to create the

approximately aligned divergent distribution of hillocks that we record. Post-emplacement sedimentation has partly masked any ridge structures and enhanced the conical appearance of the hillocks. The maximum height of the hillocks, which appears as 15 m above the present surface, would be greater if not for post-emplacement burial. Hillock features in other unequivocal rock avalanche deposits have been observed to be of a similar height up to tens of metres high (e.g. Figure 8).

5.2.6. Hillocks age

The exact date of the event is yet to be determined but based on vegetative growth and possible Maori occupation, a minimum age of some 200–300 years can be assigned. Based on post-event modification of the source area and deposit the authors judge that the event may be closer to some thousands of years old. It must be considerably younger than the Last Glacial Maximum (~18–22 ka) when ice extended to the end of Lake Wakatipu some 90 km down valley (Barrell, 1994; Turnbull, 2000) (Figure 1) and is probably younger than the drainage capture by the Kawarau River, i.e. younger than c. 7500 B.P.

We note that in many parts of the world, clusters of large coseismic rock avalanches date to the late-Glacial to mid-Holocene (e.g. Hormes et al., 2008; Agliardi et al., 2009; Hancox and Perrin, 2009; Sanchez et al., 2010). The timing we suggest for The Hillocks rock avalanche in the late-Glacial to mid-Holocene would be compatible with this pattern.

5.3. Implications and further work

The misidentification of landslide deposits as glacial moraine has two serious implications. First, it omits events from landslide records, therefore concealing the real likelihood of future landslide hazards—because landslides are more likely to occur in areas where landslides have occurred in the past. Besides The Hillocks, there are probably other landslide deposits in New Zealand that may have been misinterpreted, as is the case elsewhere in the world. ‘Knobs Flat’ in the adjacent Eglinton valley, also recorded in the

New Zealand Landform Inventory as a glacial deposit, is one such example that requires further investigation. The perceived landslide risk at such sites may be dangerously low if the deposit has been misidentified.

Second, because of the longstanding practice of reconstructing past climates from glacial deposits, misinterpretation of origin leads to misinterpretation of past climate. The ongoing debate about inter-hemisphere climate synchroneity and the presence of a Younger Dryas event in New Zealand is complicated by such misinterpretations (Vacco et al., 2010; Ivy-Ochs et al., 1999; Schaefer et al., 2006; Tovar et al., 2008; Schaefer et al., 2009; Shulmeister et al., 2009; Winkler and Matthews 2010).

There is an urgent need for a systematic review of existing interpretations, and an improved methodology for distinguishing between the landforms and sedimentological characteristics that each process (landsliding and glacial sedimentation) produces.

Acknowledgements

We are grateful to the participants and leaders of the SIRG 2010 meeting and fieldtrip, and several other colleagues, especially M. McSaveney, for the useful discussions on the origin of The Hillocks. Thanks to M. Ostermann for supplying photographs of similar features in Austria. We are thankful to an anonymous reviewer and P. Deline for suggesting many improvements to the paper.

References

Agliardi, F., Crosta, G.B., Zanchi, A., Ravazzi, C., 2009. Onset and timing of deep-seated gravitational slope deformations in the eastern Alps, Italy. Geomorphology 103, 113–129.

Barrell, D.J.A., 1994. Surficial geology of the Wakatipu Basin, Central Otago, New Zealand. Institute of Geological and Nuclear Sciences science report. Lower Hutt. Institute of Geological and Nuclear Sciences report 94/39–94/39.

Bazgard, A., Buech, F., Davies, T.R., 2009. Coseismic Landslides: Factors Influencing Volume. American Geophysical Union, Fall Meeting 2009. Poster presentation, San Francisco.

Berryman, K.R., Beanland, S., Cooper, A.F., Cutten, H.N., Norris, R.J., Wood, P.R., 1992. The Alpine fault, New Zealand : variation in quaternary structural style and geomorphic expression. Annales tectonicae. Special issue supplement to 6, 126–163.

Deline, P., 2009. Interactions between rock avalanches and glaciers in the Mont Blanc massif during the late Holocene. Quaternary Science Reviews 28, 1070–1083.

Deline, P., Kirkbride, M.P., 2009. Rock avalanches on a glacier and morainic complex in Haut Val Ferret (Mont Blanc Massif, Italy). Geomorphology 103, 80–92.

Devoli, G., De Blasio, F., Elverhøi, A., Høeg, K., 2009. Statistical analysis of landslide events in Central America and their run-out distance. Geotechnical and Geological Engineering 27, 23–42.

Dufresne, A., Davies, T.R., 2009. Longitudinal ridges in mass movement deposits. Geomorphology 105, 171–181.

Hancox, G.T., McSaveney, M.J., Manville, V.R., Davies, T.R., 2005. The October 1999 Mt Adams rock avalanche and subsequent landslide dam-break flood and effects in Poerua River, Westland, New Zealand. New Zealand Journal of Geology and Geophysics 48, 683–705.

Hancox, G.T., Perrin, N.D., 2009. Green Lake Landslide and other giant and very large postglacial landslides in Fiordland, New Zealand. Quaternary Science Reviews 28, 1020–1036.

Hewitt, K., 1999. Quaternary moraines vs catastrophic rock avalanches in the Karakoram Himalaya, northern Pakistan. Quaternary Research 51, 220–237.

Hormes, A., Ivy-Ochs, S., Kubik, P.W., Ferreli, L., Maria Michetti, A., 2008. 10Be exposure ages of a rock avalanche and a late glacial moraine in Alta Valtellina, Italian Alps. Quaternary International 190, 136–145.

Ivy-Ochs, S., Schlüchter, C., Kubik, P.W., Denton, G.H., 1999. Moraine Exposure Dates Imply Synchronous Younger Dryas Glacier Advances in the European Alps and in the Southern Alps of New Zealand. Geografiska Annaler: Series A, Physical Geography 81 (2), 313–323.

Ivy-Ochs, S., Poschinger, A.v., Synal, H.-A., Maisch, M., 2009. Surface exposure dating of the Flims landslide, Graubünden, Switzerland. Geomorphology 103, 104–112.

Kawachi, Y., 1974. Geology and petrochemistry of weakly metamorphosed rocks in the upper Wakatipu District, Southern New Zealand. New Zealand Journal of Geology and Geophysics 17, 169–208.

Kenny, J.A., Hayward, B.W., 1993. Inventory of Important Geological Sites and Landforms in the Otago Region. Geological Society of New Zealand Miscellaneous Publication, 77.

Larsen, S.H., Davies, T.R.H., McSaveney, M.J., 2005. A possible coseismic landslide origin of the late Holocene moraines of the Southern Alps, New Zealand. New Zealand Journal of Geology and Geophysics 48, 311–314.

Legros, F., 2002. The mobility of long-runout landslides. Engineering Geology 63, 301–331. Massey, C., McSaveney, M., Palmer, N., Manville, V., Hancox, G., 2008. The Young River Landslide. GNS Science, Poster.

McSaveney, M.J., 1978. Sherman Glacier rock avalanche, Alaska, USA. In: Voight, B. (Ed.), Rockslides and Avalanches. Natural Phenomena, vol. 1. Elsevier, Amsterdam, pp. 197–258.

McSaveney, M.J., Whitehouse, I.E., 1989. An early Holocene glacial advance in the Macauley river valley, central Southern Alps, New Zealand. New Zealand Journal of Geology and Geophysics 32, 235–241.

McSaveney, M.J., Davies, T.R., Hodgson, K.A., 2000. A contrast in deposit style and process between large and small rock avalanches. In: Bromhead, E., Dixon, N., Ibsen, M.L. (Eds.), VIII ISL Cardiff, Landslides in Research. Theory and Practice. Thomas Telford, London, pp. 1053–1058.

McSaveney, M.J., Davies, T.R.H., 2006. Rapid rock mass flow with dynamic fragmentation: inferences from the morphology and internal structure of rockslides and rock avalanches. In: Evans, S.G., Mugnozza, G.S., Strom, A., Hermanns, R.L. (Eds.), Landslides from Massive Rock Slope Failure. Nato Science Series: IV: Earth and Environmental Sciences. Springer Netherlands, New York, pp. 285–304.

Orombelli, G., Porter, S.C., 1988. Boulder deposit of upper Val Ferret (Courmayeur, Aosta valley): deposit of a historic giant rockfall and debris avalanche or a late-glacial moraine? Eclogae Geologicae Helvetiae 81, 365–371.

Owens, I.F., 1992. A note on the Mount Cook rock avalanche of 14 December 1991. New Zealand Geographer 48 (2), 74–78.

Porter, S.C., 2000. Onset of neoglaciation in the southern hemisphere. Journal of Quaternary Science 15, 395–408.

Prager, C., Ivy-Ochs, S., Ostermann, M., Synal, H.A., Patzelt, G., 2009. Geology and radiometric 14 C-, 36Cl- and Th-/U-dating of the Fernpass rockslide (Tyrol, Austria). Geomorphology 103, 93–103.

Sanchez, G., Rolland, Y., Corsini, M., Braucher, R., Bourlès, D., Arnold, M., Aumaître, G., 2010. Relationships between tectonics, slope instability and climate change: cosmic ray exposure dating of active faults, landslides and glacial surfaces in the SW Alps. Geomorphology 117, 1–13.

Schaefer, J.M., Denton, G.H., Barrell, D.J.A., Ivy-Ochs, S., Kubik, P.W., Andersen, B.G., Phillips, F.M., Lowell, T.V., Schluchter, C., 2008. Near-Synchronous Interhemispheric Termination of the Last Glacial Maximum in Mid-Latitudes. Science 312 (5779), 1510–1513.

Shakesby, R.A., Matthews, J.A., 1996. Glacial activity and paraglacial landsliding in the Devensian late glacial: evidence from Craig Cerrygleisiad and Fan Dringarth, Fforest Fawr (Brecon Beacons), South Wales. Geological Journal 31, 82–93.

Shulmeister, J., Davies, T.R., Evans, D.J.A., Hyatt, O.M., Tovar, D.S., 2009. Catastrophic landslides, glacier behaviour and moraine formation—a view from an active plate margin. Quaternary Science Reviews 28, 1085–1096.

Smith, G., Davies, T., McSaveney, M., Bell, D., 2006. The Acheron rock avalanche, Canterbury, New Zealand—morphology and dynamics. Landslides 3, 62–72.

Stirling, M.W., Verry, G.H.M., Berryman, K.R., 2002. A new seismic hazard model for New Zealand. Bulletin. Seismological Society of America 92, 1878–1903.

Strom, A., Korup, O., 2006. Extremely large rockslides and rock avalanches in the Tien Shan Mountains, Kyrgyzstan. Landslides 3, 125–136.

Strom, A.L., 1996. Some morphological types of long-runout rockslides: effect of relief on their mechanism and on the rockslide deposits distribution. In: Senneset, K. (Ed.), Seventh International Symposium on Landslides. Rotterdam, Balkema, Trondheim, Norway, pp. 1977–1982.

Sutherland, R., Berryman, K., Norris, R., 2006. Quaternary slip rate and geomorphology of the Alpine fault: Implications for kinematics and seismic hazard in southwest New Zealand. Geological Society of America Bulletin 118, 464–474.

Thomson, R., 1994. Resta Road Slide: a re-evaluation of an area of hummocky terrain in the Gibbston Basin, Central Otago. Institute of Geological and Nuclear Sciences Science Report 94 (93), 29.

Thomson, R., 1996. Prehistoric changes in the level of Lake Wakatipu. An Outline Study Prepared for the Otago Regional Council.

Tovar, D.A., Shulmeister, J., Davies, T.R., 2008. Evidence for a landslide origin of New Zealand's Waiho Loop moraine. Nature Geoscience 1 (8), 524–526.

Turnbull, I.M., 2000. Geology of the Wakatipu area. Institute of Geological and Nuclear Sciences 1:250 000 geological map 18. 1 sheet + 72 p. Institute of Geological and Nuclear Sciences Limited, Lower Hutt, New Zealand.

Turnbull, J.M., Davies, T.R.H., 2006. A mass movement origin for cirques. Earth Surface Processes and Landforms 31, 1129–1148.

Vacco, D.A., Alley, R.B., Pollard, D., 2010. Glacial advance and stagnation caused by rock avalanches. Earth and Planetary Science Letters 294, 123–130.

Winkler, S., Matthews, J.A., 2010. Holocene Glacier Chronologies: Are 'High-resolution' Global and Inter-Hemispheric Comparisons Possible? Holocene, pp. 1–11.

APPENDIX B:

Engineering geological data for the Mueller Rockslide

Laboratory rock testing:

Intact rock strength and was assessed by point-load testing (ISRM, 1985) of saw-cut blocks of unweathered sandstone and mudstone/argillaceous samples collected from the rockslide surface. The samples were soaked in water for two weeks before testing. Low values, influenced by incipient fractures, were discarded and an average value was calculated from the remaining reliable values (Table 1). Densities for the sandstone and the mudstone were calculated by measuring the block volume with callipers for each point load sample and weighing as saturated and after 24 hours oven drying, and then averaging (Table 1).

Table 1: Point load strength, density, water content and porosity values for sandstone and interbedded fine sandstone/mudstone and argillite. Loading direction refers to orientation of bedding. Tests (n) = number tests done; s.d. is the standard deviation from the mean.

	Point load strength				Density				
	Loading Direction	Mean (MPa)	Tests (n)	s.d.	Wet (kg/m3)	Dry (kg/m3)	Water content (%)	Porosity (%)	Tests (n)
Sandstone (greywacke)	Parallel	5.84	5	0.78	2723	2710	0.5	1.35	15
	Perpendicular	6.93	6	1.26					
Mudstone (argillite)	Parallel	4.64	5	1.79	2770 (n =14)	2764	0.32	0.89	11
	Perpendicular	3.45	6	0.64					

Rock friction angles:

Sliding friction was assessed in the field by selecting approximately 15-25 cm^2 tabular blocks of rough and smooth unweathered sandstone and mudstone from the surface and measuring the angle at which one block resting on an underneath block began to slide upon tilting.

Table 2: Tilt-block test sliding angles for mudstone (argillaceous mudstone) and sandstone blocks with differing surface roughness. The angle measured was the inclination of the sliding surface as sliding started. Tests (n) = number tests done; s.d. is the standard deviation from the mean.

Sliding surface	Sliding block	Mean angle °	Tests (n)	s.d.
Mudstone	Mudstone	33	11	2.00
Smooth- sandstone	Mudstone	38	10	2.95
Smooth- sandstone	Smooth- sandstone	41	10	5.13
Rough- sandstone	Rough- sandstone	45	10	3.96

Rock mass properties:

Table 3: Rock mass classification and parameters for the greywacke sandstone, based on field and laboratory testing of samples collected from the rockslide. Rock mass parameters were calculated in the Rocscience program RocLab (version 1.032).

	Parameter	Value	Derivation
Hoek-Brown Classification	Intact uniaxial compressive strength, σ_{ci} (MPa)	150	25 times the average point load value from sandstone in Table 1
	Geological Strength Index, GSI	75	Field estimate
	Material constant, m_i	18	Program default value for greywacke
	Disturbance factor, D	0	Natural site – no blasting
	Intact elastic modulus, E_i	52500	(Hoek et al, 2002)
	Modulus Ratio, MR	350	Program default value for greywacke
Rock Mass Parameters	Tensile strength, σ_t (MPa)	-1.3	
	Uniaxial compressive strength, σ_c (MPa)	37	(Hoek et al., 2002)
	Global strength, σ_{cm} (MPa)	61	
	Elastic modulus, E_{rm} (MPa)	42858	

APPENDIX C:

FLAC code and output used in Section 4.3

Below are some representative examples of the command code used in the FLAC modelling from Section 4.3. The purpose of making this available is to make it simple for anyone wishing to replicate or modify the modelling. Command code is not provided for every model simulation because most of the time only simple differences between model runs were required, e.g. changing the input-wave frequency or material properties, but examples for each geometry used are included. A semi-colon at the start of a line indicates a comment (i.e. not a command). Text in bold format are headings (i.e. not command). User beware: some of the example commands provided below may contain errors.

At the end of the pages of command code, there are some examples of FLAC output for both the conceptual modelling and the 'realistic' modelling.

Conceptual modelling:

```
;Title:45 Degrees_no ice

;*** BRANCH: AVERAGE ****
new

;... STATE: NULL_EQUILB ....
config dynamic
grid 620, 120
model elastic
;creates a grid with element size of 10 m - this provides accurate wave propagation for any wave freq below 14 Hz for the GNSSandstone and less than 20 Hz for ice
gen 0,0 0,1200 6200,1200 6200,0 i=1,621 j=1,121
gen line 0.0,200.0 100.0,200.0
gen line 100.0,200.0 1100.0,1200.0
gen line 1100.0,1200.0 2100.0,200.0
gen line 2100.0,200.0 3100.0,1200.0
gen line 3100.0,1200.0 4100.0,200.0
gen line 4100.0,200.0 5100.0,1200.0
gen line 5100.0,1200.0 6100.0,200.0
gen line 6100.0,200.0 6200.0,200.0
; manual assign null around apex of slopes because of problems in null region command:
; to remove the sides of the grid. 'region' applies command to any zone containing the grid coords given e.g. i=1,j=50
model null region i 1 j 50
model null region i 210 j 50
model null region i 410 j 50
model null region i 610 j 50
; apply material to whole grid - 'GNSSandstone' is a material based on rock properties from GNS for greywacke
group 'User:GNSSandstone' region i 1 j 1
model elastic group 'User:GNSSandstone'
prop density=2680.0 bulk=3.807E10 shear=2.284E10 'User:GNSSandstone'
set grav 9.81
fix x i=1
fix x i=621
fix y j=1
set dyn off
hist unbal
hist ydis i 310 j 10
hist ydis i 310 j 50
hist ydis i 310 j 70
hist ydis i 310 j 120
solve elastic
save null_equilb.sav
;*** BRANCH: HRS.SAV ****
new

;... STATE: NULL_EQUILB_ALT_STRENGTH ....
config dynamic
grid 620, 120
model elastic
;creates a grid with element size of 10 m - this provides accurate wave propagation for any wave freq below 14 Hz for the GNSSandstone and less than 20 Hz for ice
gen 0,0 0,1200 6200,1200 6200,0 i=1,621 j=1,121
gen line 0.0,200.0 100.0,200.0
gen line 100.0,200.0 1100.0,1200.0
```

```
gen line 1100.0,1200.0 2100.0,200.0
gen line 2100.0,200.0 3100.0,1200.0
gen line 3100.0,1200.0 4100.0,200.0
gen line 4100.0,200.0 5100.0,1200.0
gen line 5100.0,1200.0 6100.0,200.0
gen line 6100.0,200.0 6200.0,200.0
; manual assign null around apex of slopes because of problems in null region command:
; to remove the sides of the grid. 'region' applies command to any zone containing the grid coords given e.g. i=1,j=50
model null region i 1 j 50
model null region i 210 j 50
model null region i 410 j 50
model null region i 610 j 50
; apply material to whole grid - 'GNSSandstone2' is a material based on rock properties from GNS for greywacke
group 'User:GNSSandstone2' region i 1 j 1
model elastic group 'User:GNSSandstone2'
prop density=2680.0 bulk=1.E10 shear=6E9 'User:GNSSandstone2'
set grav 9.81
fix x i=1
fix x i=621
fix y j=1
set dyn off
hist unbal
hist ydis i 310 j 10
hist ydis i 310 j 50
hist ydis i 310 j 70
hist ydis i 310 j 120
solve elastic
save null_equilb_Alt_strength.sav
;*** BRANCH: LRS.SAV ****
new

;... STATE: LRS_NULL_EQUILB_ALT_STRENGTH ....
config dynamic
grid 620, 120
model elastic
;creates a grid with element size of 10 m - this provides accurate wave propagation for any wave freq below 14 Hz for the GNSSandstone and less than 20 Hz for ice
gen 0,0 0,1200 6200,1200 6200,0 i=1,621 j=1,121
gen line 0.0,200.0 100.0,200.0
gen line 100.0,200.0 1100.0,1200.0
gen line 1100.0,1200.0 2100.0,200.0
gen line 2100.0,200.0 3100.0,1200.0
gen line 3100.0,1200.0 4100.0,200.0
gen line 4100.0,200.0 5100.0,1200.0
gen line 5100.0,1200.0 6100.0,200.0
gen line 6100.0,200.0 6200.0,200.0
; manual assign null around apex of slopes because of problems in null region command:
; to remove the sides of the grid. 'region' applies command to any zone containing the grid coords given e.g. i=1,j=50
model null region i 1 j 50
model null region i 210 j 50
model null region i 410 j 50
model null region i 610 j 50
group 'SandstoneLRS' region i 1 j 1
model elastic group 'SandstoneLRS'
prop density=2680.0 bulk=5.3E10 shear=32E9 group 'SandstoneLRS'
```

```
set grav 9.81
fix x i=1
fix x i=621
fix y j=1
set dyn off
hist unbal
hist ydis i 310 j 10
hist ydis i 310 j 50
hist ydis i 310 j 70
hist ydis i 310 j 120
solve elastic
save LRS_null_equilb_Alt_strength.sav



;Project Record Tree export
;Title:Ice 45 degrees 1000 m

;*** BRANCH: BRANCH FOR ICE_EQUILB.SAV ****
new

;... STATE: ICE_EQUILB ....
config dynamic
grid 620, 120
model elastic
;creates a grid with element size of 10 m - this provides accurate wave propagation for any wave freq below 14 Hz for the GNSSandstone and less than 20 Hz for ice
gen 0,0 0,1200 6200,1200 6200,0 i=1,621 j=1,121
gen line 0.0,200.0 100.0,200.0
gen line 100.0,200.0 1100.0,1200.0
gen line 1100.0,1200.0 2100.0,200.0
gen line 2100.0,200.0 3100.0,1200.0
gen line 3100.0,1200.0 4100.0,200.0
gen line 4100.0,200.0 5100.0,1200.0
gen line 5100.0,1200.0 6100.0,200.0
gen line 6100.0,200.0 6200.0,200.0
; manual assign null around apex of slopes because of problems in null region command:
; to remove the sides of the grid. 'region' applies command to any zone containing the grid coords given e.g. i=1,j=50
; apply material to whole grid - 'GNSSandstone' is a material based on rock properties from GNS for greywacke
group 'User:Sandstone' region i 1 j 1
model elastic group 'User:Sandstone'
prop density=2680.0 bulk=3.807E10 shear=2.284E10 'User:Sandstone'
group 'User:Ice' region i 1 j 50
group 'User:Ice' region i 210 j 50
group 'User:Ice' region i 410 j 50
group 'User:Ice' region i 610 j 50
model elastic group 'User:Ice'
prop density=916.0 bulk=8.7E9 shear=3.8E9 group 'User:Ice'
set grav 9.81
fix x i=1
fix x i=621
fix y j=1
set dyn off
hist unbal
hist ydis i 310 j 10
hist ydis i 310 j 50
hist ydis i 310 j 70
hist ydis i 310 j 120
solve elastic
save ice_equilb.sav
```

```
;Project Record Tree export
;Title:Half 45 degrees 1000 m

;*** BRANCH: BRANCH FOR HALF_EQUILB.SAV ****
new

;... STATE: HALF_EQUILB ....
config dynamic
grid 620, 120
model elastic
;creates a grid with element size of 10 m - this provides accurate wave propagation for any wave freq below 14 Hz for the GNSSandstone and less than 20 Hz for ice
gen 0,0 0,1200 6200,1200 6200,0 i=1,621 j=1,121
gen line 0.0,200.0 100.0,200.0
gen line 100.0,200.0 1100.0,1200.0
gen line 1100.0,1200.0 2100.0,200.0
gen line 2100.0,200.0 3100.0,1200.0
gen line 3100.0,1200.0 4100.0,200.0
gen line 4100.0,200.0 5100.0,1200.0
gen line 5100.0,1200.0 6100.0,200.0
gen line 6100.0,200.0 6200.0,200.0
gen line 0,700 600,700
gen line 1600,700 2600,700
gen line 3600,700 4600,700
gen line 5600,700 6200,700
; manual assign null around apex of slopes because of problems in null region command:
; to remove the sides of the grid. 'region' applies command to any zone containing the grid coords given e.g. i=1,j=50
; apply material to whole grid - 'GNSSandstone' is a material based on rock properties from GNS for greywacke
group 'User:Sandstone' region i 1 j 1
model elastic group 'User:Sandstone'
prop density=2680.0 bulk=3.807E10 shear=2.284E10 'User:Sandstone'
model null region i 1 j 90
model null region i 210 j 90
model null region i 410 j 90
model null region i 610 j 90
group 'User:Ice' region i 1 j 50
group 'User:Ice' region i 210 j 50
group 'User:Ice' region i 410 j 50
group 'User:Ice' region i 610 j 50
model elastic group 'User:Ice'
prop density=916.0 bulk=8.7E9 shear=3.8E9 group 'User:Ice'
set grav 9.81
fix x i=1
fix x i=621
fix y j=1
set dyn off
hist unbal
hist ydis i 310 j 10
hist ydis i 310 j 50
hist ydis i 310 j 70
hist ydis i 310 j 120
solve elastic
save half_equilb.sav

;Project Record Tree export
;Title:Null 45-65 degree slope
```

```
;*** BRANCH: BRANCH FOR 45-65_NULL_EQUILB.SAV ****
new

;... STATE: 45-65_NULL_EQUILB ....
config dynamic
grid 620, 120
model elastic
;creates a grid with element size of 10 m - this provides accurate wave propagation for any wave freq below 14 Hz for the GNSSandstone and less than 20 Hz for ice
gen 0,0 0,1200 6200,1200 6200,0 i=1,621 j=1,121
gen line 0.0,200.0 370.0,200.0
gen line 370.0,200.0 600,700
gen line 600,700 1100.0,1200.0
gen line 1100, 1200 1600,700
gen line 1600.0,700.0 1830.0,200.0
gen line 1830, 200 2370,200
gen line 2370,200 2600,700
gen line 2600,700 3100,1200
gen line 3100.0,1200.0 3600.0,700.0
gen line 3600,700 3830,200
gen line 3830,200 4370,200
gen line 4370,200 4600,700
gen line 4600,700 5100,1200
gen line 5100.0,1200.0 5600.0,700.0
gen line 5600,700 5830,200
gen line 5830.0,200.0 6200.0,200.0
; manual assign null around apex of slopes because of problems in null region command:
; to remove the sides of the grid. 'region' applies command to any zone containing the grid coords given e.g. i=1,j=50
model null region i 1 j 50
model null region i 210 j 50
model null region i 410 j 50
model null region i 610 j 50
; apply material to whole grid - 'GNSSandstone' is a material based on rock properties from GNS for greywacke
group 'User:GNSSandstone' region i 1 j 1
model elastic group 'User:GNSSandstone'
prop density=2680.0 bulk=3.807E10 shear=2.284E10 'User:GNSSandstone'
set grav 9.81
fix x i=1
fix x i=621
fix y j=1
set dyn off
hist unbal
hist ydis i 310 j 10
hist ydis i 310 j 50
hist ydis i 310 j 70
hist ydis i 310 j 120
solve elastic
save 45-65_null_equilb.sav

;Project Record Tree export
;Title:Ice Cap 45-65 degrees

;*** BRANCH: BRANCH FOR 65-45ICECAP_EQUILB.SAV ****
new

;... STATE: 65-45ICECAP_EQUILB ....
config dynamic
grid 620, 120
model elastic
```

```
;creates a grid with element size of 10 m - this provides accurate wave propagation for any wave freq below 14 Hz for the GNSSandstone and less than 20 Hz for ice
gen 0,0 0,1200 6200,1200 6200,0 i=1,621 j=1,121
gen line 0.0,200.0 370.0,200.0
gen line 370.0,200.0 600,700
gen line 600,700 1100.0,1200.0
gen line 1100, 1200 1600,700
gen line 1600.0,700.0 1830.0,200.0
gen line 1830, 200 2370,200
gen line 2370,200 2600,700
gen line 2600,700 3100,1200
gen line 3100.0,1200.0 3600.0,700.0
gen line 3600,700 3830,200
gen line 3830,200 4370,200
gen line 4370,200 4600,700
gen line 4600,700 5100,1200
gen line 5100.0,1200.0 5600.0,700.0
gen line 5600,700 5830,200
gen line 5830.0,200.0 6200.0,200.0
; manual assign null around apex of slopes because of problems in null region command:
; to remove the sides of the grid. 'region' applies command to any zone containing the grid coords given e.g. i=1,j=50
; apply material to whole grid - 'GNSSandstone' is a material based on rock properties from GNS for greywacke
group 'User:Sandstone' region i 1 j 1
model elastic group 'User:Sandstone'
prop density=2680.0 bulk=3.807E10 shear=2.284E10 'User:Sandstone'
group 'User:Ice' region i 1 j 50
group 'User:Ice' region i 210 j 50
group 'User:Ice' region i 410 j 50
group 'User:Ice' region i 610 j 50
model elastic group 'User:Ice'
prop density=916.0 bulk=8.7E9 shear=3.8E9 group 'User:Ice'
set grav 9.81
fix x i=1
fix x i=621
fix y j=1
set dyn off
hist unbal
hist ydis i 310 j 10
hist ydis i 310 j 50
hist ydis i 310 j 70
hist ydis i 310 j 120
solve elastic
save 65-45icecap_equilb.sav

;Project Record Tree export
;Title:45-65 slope 1000 m high half filled with ice

;*** BRANCH: BRANCH FOR 45-65_HALF_EQUILB.SAV ****
new

;... STATE: 45-65_HALF_EQUILB ....
config dynamic
grid 620, 120
model elastic
;creates a grid with element size of 10 m - this provides accurate wave propagation for any wave freq below 14 Hz for the GNSSandstone and less than 20 Hz for ice
```

```
gen 0,0 0,1200 6200,1200 6200,0 i=1,621 j=1,121
gen line 0.0,200.0 370.0,200.0
gen line 370.0,200.0 600,700
gen line 600,700 1100.0,1200.0
gen line 1100, 1200 1600,700
gen line 1600.0,700.0 1830.0,200.0
gen line 1830, 200 2370,200
gen line 2370,200 2600,700
gen line 2600,700 3100,1200
gen line 3100.0,1200.0 3600.0,700.0
gen line 3600,700 3830,200
gen line 3830,200 4370,200
gen line 4370,200 4600,700
gen line 4600,700 5100,1200
gen line 5100.0,1200.0 5600.0,700.0
gen line 5600,700 5830,200
gen line 5830.0,200.0 6200.0,200.0
gen line 0,700 600,700
gen line 1600,700 2600,700
gen line 3600,700 4600,700
gen line 5600,700 6200,700
; manual assign null around apex of slopes because of problems in null region command:
; to remove the sides of the grid. 'region' applies command to any zone containing the grid coords given e.g. i=1,j=50
; apply material to whole grid - 'GNSSandstone' is a material based on rock properties from GNS for greywacke
group 'User:Ice' region i 1 j 50
group 'User:Ice' region i 210 j 50
group 'User:Ice' region i 410 j 50
group 'User:Ice' region i 610 j 50
model elastic group 'User:Ice'
prop density=916.0 bulk=8.7E9 shear=3.8E9 group 'User:Ice'
group 'User:Sandstone' region i 1 j 1
model elastic group 'User:Sandstone'
prop density=2680.0 bulk=3.807E10 shear=2.284E10 'User:Sandstone'
model null region i 1 j 90
model null region i 210 j 90
model null region i 410 j 90
model null region i 610 j 90
set grav 9.81
fix x i=1
fix x i=621
fix y j=1
set dyn off
hist unbal
hist ydis i 310 j 10
hist ydis i 310 j 50
hist ydis i 310 j 70
hist ydis i 310 j 120
solve elastic
save 45-65_half_equilb.sav

;Project Record Tree export

;*** BRANCH: BRANCH FOR NULL65_EQUILB.SAV ****
new

;... STATE: NULL65_EQUILB ....
config dynamic
grid 320, 128
model elastic
;creates a grid with element size of 10 m - this provides accurate wave propagation for any
```

wave freq below 14 Hz for the GNSSandstone and less than 20 Hz for ice

gen 0,0 0,1280 3200,1280 3200,0 i=1,321 j=1,129

gen line 0.0,200.0 100.0,200.0

gen line 100.0,200.0 600.0,1280.0

gen line 600.0,1280.0 1100.0,200.0

gen line 1100.0,200.0 1600.0,1280.0

gen line 1600.0,1280.0 2100.0,200.0

gen line 2100.0,200.0 2600.0,1280.0

gen line 2600.0,1280.0 3100.0,200.0

gen line 3100.0,200.0 3200.0,200.0

; manual assign null around apex of slopes because of problems in null region command:

; to remove the sides of the grid. 'region' applies command to any zone containing the grid coords given e.g. i=1,j=50

; manual assign null around apex of slopes because of problems in null region command:

; to remove the sides of the grid. 'region' applies command to any zone containing the grid coords given e.g. i=1,j=50

model null region i 1 j 60

model null region i 110 j 60

model null region i 210 j 60

model null region i 310 j 60

; apply material to whole grid - 'GNSSandstone' is a material based on rock properties from GNS for greywacke

group 'User:GNSSandstone' region i 1 j 1

model elastic group 'User:GNSSandstone'

prop density=2680.0 bulk=3.807E10 shear=2.284E10 'User:GNSSandstone'

set grav 9.81

fix x i=1

fix x i=321

fix y j=1

set dyn off

hist unbal

hist ydis i 160 j 10

hist ydis i 160 j 50

hist ydis i 160 j 70

hist ydis i 160 j 128

solve elastic

save null65_equilb.sav

;Project Record Tree export

;Title:Ice 65

;*** BRANCH: BRANCH FOR ICE65_EQUILB.SAV ****

new

;... STATE: ICE65_EQUILB ....

config dynamic

grid 320, 128

model elastic

;creates a grid with element size of 10 m - this provides accurate wave propagation for any wave freq below 14 Hz for the GNSSandstone and less than 20 Hz for ice

gen 0,0 0,1280 3200,1280 3200,0 i=1,321 j=1,129

gen line 0.0,200.0 100.0,200.0

gen line 100.0,200.0 600.0,1280.0

gen line 600.0,1280.0 1100.0,200.0

gen line 1100.0,200.0 1600.0,1280.0

gen line 1600.0,1280.0 2100.0,200.0

gen line 2100.0,200.0 2600.0,1280.0

gen line 2600.0,1280.0 3100.0,200.0

```
gen line 3100.0,200.0 3200.0,200.0
; apply material to whole grid - 'GNSSandstone' is a material based on rock properties from GNS for greywacke
group 'User:GNSSandstone' region i 1 j 1
model elastic group 'User:GNSSandstone'
prop density=2680.0 bulk=3.807E10 shear=2.284E10 'User:GNSSandstone'
group 'User:Ice' region i 1 j 90
group 'User:Ice' region i 100 j 90
group 'User:Ice' region i 200 j 90
group 'User:Ice' region i 310 j 90
model elastic group 'User:Ice'
prop density=916.0 bulk=8.7E9 shear=3.8E9 group 'User:Ice'
set grav 9.81
fix x i=1
fix x i=321
fix y j=1
set dyn off
hist unbal
hist ydis i 160 j 10
hist ydis i 160 j 50
hist ydis i 160 j 70
hist ydis i 160 j 128
solve elastic
save ice65_equilb.sav
;Project Record Tree export
;Title:Half Ice

;*** BRANCH: BRANCH FOR HALF65_EQUILB.SAV ****
new

;... STATE: HALF65_EQUILB ....
config dynamic
grid 320, 128
model elastic
;creates a grid with element size of 10 m - this provides accurate wave propagation for any wave freq below 14 Hz for the GNSSandstone and less than 20 Hz for ice
gen 0,0 0,1280 3200,1280 3200,0 i=1,321 j=1,129
gen line 0.0,200.0 100.0,200.0
gen line 100.0,200.0 600.0,1280.0
gen line 600.0,1280.0 1100.0,200.0
gen line 1100.0,200.0 1600.0,1280.0
gen line 1600.0,1280.0 2100.0,200.0
gen line 2100.0,200.0 2600.0,1280.0
gen line 2600.0,1280.0 3100.0,200.0
gen line 3100.0,200.0 3200.0,200.0
gen line 0,740 350,740
gen line 850,740 1350,740
gen line 1850,740 2350,740
gen line 2850,740 3200,740
; apply material to whole grid - 'GNSSandstone' is a material based on rock properties from GNS for greywacke
group 'User:GNSSandstone' region i 1 j 1
model elastic group 'User:GNSSandstone'
prop density=2680.0 bulk=3.807E10 shear=2.284E10 'User:GNSSandstone'
group 'User:Ice' region i 1 j 70
group 'User:Ice' region i 100 j 70
group 'User:Ice' region i 200 j 70
group 'User:Ice' region i 310 j 70
model elastic group 'User:Ice'
prop density=916.0 bulk=8.7E9 shear=3.8E9 group 'User:Ice'
```

```
model null region i 1 j 90
model null region i 100 j 90
model null region i 200 j 90
model null region i 310 j 90
set grav 9.81
fix x i=1
fix x i=321
fix y j=1
set dyn off
hist unbal
hist ydis i 160 j 10
hist ydis i 160 j 50
hist ydis i 160 j 70
hist ydis i 160 j 128
solve elastic
save half65_equilb.sav
```

Example of dynamic input for conceptual model

```
;*** BRANCH: 0.5 ****

;... STATE: NULL_0 ....
set dyn on
apply ff
apply xquiet j=1
apply yquiet j=1
; apply seismic input - need to apply input as a stress instead of a velocity or acceleration because of quiet boundary condition. shear stress = 2*(material density*shear wave velocity)*shear particle velocity (multiplier (hist wave) to get time-dependent variation of stress.
def wave
; period of wave = 1/freq  Freq = 0.5 Hz
period = 2
wave = 0.5 * (1.0 - cos(2*pi*dytime/period))
if dytime > 2 then
wave = 0
end_if
end
apply sxy -15647517.37 hist wave j 1
set dytime 0
hist reset
hist dytime
hist xvel i 211 j 1
hist xvel i 211 j 21
hist xvel i 261 j 71
hist xvel i 286 j 96
hist xvel i 311 j 120
hist wave
solve dytime 3.5
save null_0.5.sav

;*** BRANCH: 1 ****
restore null_equilb.sav

;... STATE: NULL_1 ....
set dyn on
apply ff
apply xquiet j=1
apply yquiet j=1
def wave
; period of wave = 1/freq  Freq = 1 Hz
period = 1
wave = 0.5 * (1.0 - cos(2*pi*dytime/period))
if dytime > 1 then
wave = 0
end_if
end
```

```
apply sxy -15647517.37 hist wave j 1
set dytime 0
hist reset
hist dytime
hist xvel i 211 j 1
hist xvel i 211 j 21
hist xvel i 261 j 71
hist xvel i 286 j 96
hist xvel i 311 j 120
hist wave
solve dytime 4
save null_1.sav
```

Modelling command for ALFRED and CIRQUE (including dynamic command)

```
;Project Record Tree export

;*** BRANCH: HALF ICE ****
new

;... STATE: ALFRED_HALFICE_SE ....
; Mt Alfred Half Ice
config dynamic
grid 550,140
gen 0.0,0.0 0.0,1400.0 5500.0,1400.0 5500.0,0.0 i=1,551 j=1,141
model elastic i=1,550 j=1,140
table 101 delete
table 101 0 150 400 200 600 275 1000 400 1200 600 1800 800 1850 870 2050 &
 900 2600 1150 2720 1230 2750 1250 2800 1315 2820 1320 2850 1315 2950 1265 &
 3000 1240 3100 1175
 table 101 3370 1060 3550 940 3800 800 4000 690 4250 600 4695 335 5050 280 &
 5300 250 5450 200 5500 200
 table 102 delete
 table 102 0 800 1800 800
 table 103 delete
 table 103 3800 800 5500 800
 gen table 101
 gen table 102
 gen table 103
 group 'User:Schist' region i 50 j 1
 model elastic group 'User:Schist'
 prop density=2800.0 bulk=2.13063E10 shear=2.09292E10 group 'User:Schist'
 group 'User:Ice' region i 40 j 40
 group 'User:Ice' region i 450 j 50
 model elastic group 'User:Ice'
 prop density=916.0 bulk=8.7E9 shear=3.8E9 group 'User:Ice'
 model null region i 40 j 120
 set grav 9.81
 fix x i=1
 fix x i=551
 fix y j=1
 set dyn off
 hist unbal
 hist ydis i 282 j 133
 hist ydis i 282 j 76
 hist ydis i 282 j 1
 solve elastic
 save Alfred_halfice_se.sav

 ;*** BRANCH: HALFICE_LOMAPRIETA_PARALLEL ****
```

```
;...                                    STATE:
ALFRED_HALFICE_LOMAPRIETA_PARAL
....
;LomaPrieta Fault Parallel, velocity m/s, time
interval 0.01 seconds
set dyn on
apply ff
apply xquiet j=1
apply yquiet j=1
call 22.dat
apply sxy -1.5310400E7 hist table 22 j 1
set dytime 0
hist reset
hist dytime
hist xvel i 282 j 133
hist xvel i 282 j 76
hist xvel i 338 j 107
hist xvel i 282 j 1
hist xacc i 282 j 133
hist xacc i 282 j 76
hist xacc i 338 j 107
hist xacc i 282 j 1
hist yvel i 282 j 133
hist yvel i 282 j 76
hist yvel i 338 j 107
hist yvel i 282 j 1
hist yacc i 282 j 133
hist yacc i 282 j 76
hist yacc i 338 j 107
hist yacc i 282 j 1
solve dytime 25
history write 2 vs 1 tab 2
history write 4 vs 1 tab 4
history write 6 vs 1 tab 6
history write 8 vs 1 tab 8
save Alfred_halfice_LomaPrieta_paral.sav

;*** BRANCH: HALFICE_CHCH_N ****
restore Alfred_halfice_se.sav

;... STATE: ALFRED_HALFICE_CHCH_N
....
;Christchurch February quake McQueens
Valley, velocity m/s, time interval 0.02 seconds
set dyn on
apply ff
apply xquiet j=1
apply yquiet j=1
call 333.dat
apply sxy -1.5310400E7 hist table 333 j 1
set dytime 0
hist reset
hist dytime
hist xvel i 282 j 133
hist xvel i 282 j 76
hist xvel i 338 j 107
hist xvel i 282 j 1
hist xacc i 282 j 133
hist xacc i 282 j 76
hist xacc i 338 j 107
hist xacc i 282 j 1
hist yvel i 282 j 133
hist yvel i 282 j 76
hist yvel i 338 j 107
hist yvel i 282 j 1
hist yacc i 282 j 133
hist yacc i 282 j 76
hist yacc i 338 j 107
hist yacc i 282 j 1
solve dytime 20
```

```
save Alfred_halfice_Chch_N.sav

;*** BRANCH: HALFICE_CHCH_N_DAMPED ****
restore Alfred_halfice_se.sav

;... STATE: ALFRED_HALFICE_CHCH_N_DAMPED ....
;Christchurch February quake McQueens Valley, velocity m/s, time interval 0.02 seconds
set dyn on
apply ff
apply xquiet j=1
apply yquiet j=1
call 333.dat
set dy_damp=rayleigh 0.06 4.0 mass
apply sxy -1.5310400E7 hist table 333 j 1
set dytime 0
hist reset
hist dytime
hist xvel i 282 j 133
hist xvel i 282 j 76
hist xvel i 338 j 107
hist xvel i 282 j 1
hist xacc i 282 j 133
hist xacc i 282 j 76
hist xacc i 338 j 107
hist xacc i 282 j 1
hist yvel i 282 j 133
hist yvel i 282 j 76
hist yvel i 338 j 107
hist yvel i 282 j 1
hist yacc i 282 j 133
hist yacc i 282 j 76
hist yacc i 338 j 107
hist yacc i 282 j 1
solve dytime 20
history write 2 vs 1 tab 2
history write 4 vs 1 tab 4
history write 6 vs 1 tab 6
history write 8 vs 1 tab 8
save Alfred_halfice_Chch_N_damped.sav

;*** BRANCH: HALFICE_MORGAN_PARAL ****
restore Alfred_halfice_se.sav

;... STATE: ALFRED_HALFICE_MORGAN_PARAL ....
;Morgan Hill fault parallel, velocity m/s, time interval 0.005 seconds;
set dyn on
apply ff
apply xquiet j=1
apply yquiet j=1
call 222.dat
apply sxy -1.5310400E7 hist table 222 j 1
set dytime 0
hist reset
hist dytime
hist xvel i 282 j 133
hist xvel i 282 j 76
hist xvel i 338 j 107
hist xvel i 282 j 1
hist xacc i 282 j 133
hist xacc i 282 j 76
hist xacc i 338 j 107
hist xacc i 282 j 1
hist yvel i 282 j 133
hist yvel i 282 j 76
```

```
hist yvel i 338 j 107
hist yvel i 282 j 1
hist yacc i 282 j 133
hist yacc i 282 j 76
hist yacc i 338 j 107
hist yacc i 282 j 1
solve dytime 18
history write 2 vs 1 tab 2
history write 4 vs 1 tab 4
history write 6 vs 1 tab 6
history write 8 vs 1 tab 8
save Alfred_halfice_Morgan_paral.sav

;*** BRANCH: HALFICE_MORGAN_PARAL_DAMPED ****
restore Alfred_halfice_se.sav

;... STATE: ALFRED_HALFICE_MORGAN_PARAL_DAMPED ....
;Morgan Hill fault parallel, velocity m/s, time interval 0.005 seconds;
set dyn on
apply ff
apply xquiet j=1
apply yquiet j=1
call 222.dat
set dy_damp=rayleigh 0.06 5.0 mass
apply sxy -1.5310400E7 hist table 222 j 1
set dytime 0
hist reset
hist dytime
hist xvel i 282 j 133
hist xvel i 282 j 76
hist xvel i 338 j 107
hist xvel i 282 j 1
hist xacc i 282 j 133
hist xacc i 282 j 76
hist xacc i 338 j 107
hist xacc i 282 j 1
hist yvel i 282 j 133
hist yvel i 282 j 76
hist yvel i 338 j 107
hist yvel i 282 j 1
hist yacc i 282 j 133
hist yacc i 282 j 76
hist yacc i 338 j 107
hist yacc i 282 j 1
solve dytime 18
history write 2 vs 1 tab 2
history write 4 vs 1 tab 4
history write 6 vs 1 tab 6
history write 8 vs 1 tab 8
save Alfred_halfice_Morgan_paral_damped.sav

;*** BRANCH: HALFICE_LOMAPRIETA_PARALLEL_DAMPED ****
restore Alfred_halfice_se.sav

;... STATE: ALFRED_HALFICE_LOMAPRIETA_PARAL_DAMPED ....
;LomaPrieta Fault Parallel, velocity m/s, time interval 0.01 seconds; damped 3%
set dyn on
apply ff
apply xquiet j=1
apply yquiet j=1
```

```
set dy_damp=rayleigh 0.06 5.0 mass
call 22.dat
apply sxy -1.5310400E7 hist table 22 j 1
set dytime 0
hist reset
hist dytime
hist xvel i 282 j 133
hist xvel i 282 j 76
hist xvel i 338 j 107
hist xvel i 282 j 1
hist xacc i 282 j 133
hist xacc i 282 j 76
hist xacc i 338 j 107
hist xacc i 282 j 1
hist yvel i 282 j 133
hist yvel i 282 j 76
hist yvel i 338 j 107
hist yvel i 282 j 1
hist yacc i 282 j 133
hist yacc i 282 j 76
hist yacc i 338 j 107
hist yacc i 282 j 1
solve dytime 25
history write 2 vs 1 tab 1102
history write 4 vs 1 tab 1104
history write 6 vs 1 tab 1106
history write 8 vs 1 tab 1108
save
Alfred_halfice_LomaPrieta_paral_damped.sav

;*** BRANCH: 0.5 ****
restore Alfred_halfice_se.sav

;... STATE: ALFRED_HALFICE_05HZ ....
set dyn on
apply ff
apply xquiet j=1
apply yquiet j=1
; apply seismic input - need to apply input as a stress instead of a velocity or acceleration because of quiet boundary condition. shear stress = 2*(material density*shear wave velocity)*shear particle velocity (multiplier (hist wave) to get time-dependent variation of stress.
def wave
; period of wave = 1/freq  Freq = 0.5 Hz
period = 2
wave = 0.5 * (1.0 - cos(2*pi*dytime/period))
if dytime > 2 then
wave = 0
end_if
end
apply sxy -1.5310400E7 hist wave j 1
set dytime 0
hist reset
hist dytime
hist xvel i 282 j 133
hist xvel i 282 j 76
hist xvel i 338 j 107
hist xvel i 282 j 1
hist xacc i 282 j 133
hist xacc i 282 j 76
hist xacc i 338 j 107
hist xacc i 282 j 1
hist yvel i 282 j 133
hist yvel i 282 j 76
hist yvel i 338 j 107
hist yvel i 282 j 1
hist yacc i 282 j 133
hist yacc i 282 j 76
```

```
hist yacc i 338 j 107
hist yacc i 282 j 1
hist wave
solve dytime 8
save Alfred_halfice_05hz.sav

;Project Record Tree export

;*** BRANCH: CIRQUE_NOICE ****
new

;... STATE: CIRQUE_NOICE_SE ....
config dynamic
grid 190,70
gen 0.0,0.0 0.0,700.0 1900.0,700.0 1900.0,0.0 i=1,191 j=1,71
model elastic i=1,190 j=1,70
table 101 0,460 500,560 800,620 1400,660 1700,680 1900,700
table 102 0,350 25,350 50,300 75,270 100,250 125,220 150,200 175,180 &
 225,150 275,140 425,140 475,150
table 102 525,155 575,180 625,220 675,300 720,390 745,430 770,470 795,500 &
 820,540 845,570 890,530 940,420
table 102 965,380 990,340 1015,320 1075,290 1125,280 1175,275 1225,270 &
 1325,270 1375,275 1425,275 1475,290
table 102 1525,300 1575,340 1635,390 1685,430 1725,480 1785,590 1815,660 &
 1835,685 1855,695 1875,700 1900,700
table 103 0,350 25,350 50,345 75,315 100,290 125,275 150,260 175,255 &
 200,250 500,275 600,300 660,355 730,435
table 103 780,480
table 104 890,520 965,435 990,415 1015,395 1065,370 1090,365
table 104 1250,360 1510,420 1585,450 1660,480 1685,490 1735,525 1790,590
;gen table 101
gen table 102
;gen table 103
;gen table 104
group 'User:Rock' region i 1 j 1
model elastic group 'User:Rock'
prop density=2680.0 bulk=3.807E10 shear=2.284E10 group 'User:Rock'
group 'User:Ice' region i 36 j 20
group 'User:Ice' region i 130 j 32
group 'User:Ice' region i 40 j 40
model elastic group 'User:Ice'
prop density=916.0 bulk=8.7E9 shear=3.8E9 group 'User:Ice'
model null region i 40 j 65
set grav 9.81
fix x i=1
fix x i=191
fix y j=1
set dyn off
hist unbal
hist ydis i 86 j 57
hist ydis i 86 j 30
hist ydis i 86 j 1
solve elastic
save Cirque_noice_se.sav

;*** BRANCH: 0.5 ****

;... STATE: CIRQUE_NOICE_05HZ ....
set dyn on
```

```
apply ff
apply xquiet j=1
apply yquiet j=1
def wave
; period of wave = 1/freq  Freq = 0.5 Hz
period = 2
wave = 0.5 * (1.0 - cos(2*pi*dytime/period))
if dytime > 2 then
wave = 0
end_if
end
apply sxy -15647517.37 hist wave j 1
set dytime 0
hist reset
hist dytime
hist xvel i 86 j 57
hist xvel i 86 j 30
hist xvel i 74 j 41
hist xvel i 86 j 1
hist xacc i 86 j 57
hist xacc i 86 j 30
hist xacc i 74 j 41
hist xacc i 86 j 1
hist yvel i 86 j 57
hist yvel i 86 j 30
hist yvel i 74 j 41
hist yvel i 86 j 1
hist yacc i 86 j 57
hist yacc i 86 j 30
hist yacc i 74 j 41
hist yacc i 86 j 1
hist wave
solve dytime 8
save Cirque_noice_05hz.sav
```

```
;*** BRANCH: CIRQUE_ICECAP ****
new

;... STATE: CIRQUE_ICECAP_SE ....
config dynamic
grid 190,70
gen 0.0,0.0 0.0,700.0 1900.0,700.0 1900.0,0.0 i=1,191 j=1,71
model elastic i=1,190 j=1,70
table 101 0,460 500,560 800,620 1400,660 1700,680 1900,700
table 102 0,350 25,350 50,300 75,270 100,250 125,220 150,200 175,180 &
 225,150 275,140 425,140 475,150
table 102 525,155 575,180 625,220 675,300 720,390 745,430 770,470 795,500 &
 820,540 845,570 890,530 940,420
table 102 965,380 990,340 1015,320 1075,290 1125,280 1175,275 1225,270 &
 1325,270 1375,275 1425,275 1475,290
table 102 1525,300 1575,340 1635,390 1685,430 1725,480 1785,590 1815,660 &
 1835,685 1855,695 1875,700 1900,700
table 103 0,350 25,350 50,345 75,315 100,290 125,275 150,260 175,255 &
 200,250 500,275 600,300 660,355 730,435
table 103 780,480
table 104 890,520 965,435 990,415 1015,395 1065,370 1090,365
table 104 1250,360 1510,420 1585,450 1660,480 1685,490 1735,525 1790,590
gen table 101
gen table 102
;gen table 103
;gen table 104
```

```
group 'User:Rock' region i 1 j 1
model elastic group 'User:Rock'
prop density=2680.0 bulk=3.807E10 shear=2.284E10 group 'User:Rock'
;group 'User:Ice' region i 36 j 20
;group 'User:Ice' region i 130 j 32
group 'User:Ice' region i 40 j 40
model elastic group 'User:Ice'
prop density=916.0 bulk=8.7E9 shear=3.8E9 group 'User:Ice'
model null region i 40 j 65
set grav 9.81
fix x i=1
fix x i=191
fix y j=1
set dyn off
hist unbal
hist ydis i 86 j 57
hist ydis i 86 j 30
hist ydis i 86 j 1
solve elastic
save Cirque_Icecap_se.sav

;*** BRANCH: CIRQUE_HALFICE ****
new

;... STATE: CIRQUE_HALFICE_SE ....
config dynamic
grid 190,70
gen 0.0,0.0 0.0,700.0 1900.0,700.0 1900.0,0.0 i=1,191 j=1,71
model elastic i=1,190 j=1,70
table 101 0,460 500,560 800,620 1400,660 1700,680 1900,700
table 102 0,350 25,350 50,300 75,270 100,250 125,220 150,200 175,180 &
 225,150 275,140 425,140 475,150
table 102 525,155 575,180 625,220 675,300 720,390 745,430 770,470 795,500 &
 820,540 845,570 890,530 940,420
table 102 965,380 990,340 1015,320 1075,290 1125,280 1175,275 1225,270 &
 1325,270 1375,275 1425,275 1475,290
table 102 1525,300 1575,340 1635,390 1685,430 1725,480 1785,590 1815,660 &
 1835,685 1855,695 1875,700 1900,700
table 103 0,350 25,350 50,345 75,315 100,290 125,275 150,260 175,255 &
 200,250 500,275 600,300 660,355 730,435
table 103 780,480
table 104 890,520 965,435 990,415 1015,395 1065,370 1090,365
table 104 1250,360 1510,420 1585,450 1660,480 1685,490 1735,525 1790,590
;gen table 101
gen table 102
gen table 103
gen table 104
group 'User:Rock' region i 1 j 1
model elastic group 'User:Rock'
prop density=2680.0 bulk=3.807E10 shear=2.284E10 group 'User:Rock'
group 'User:Ice' region i 36 j 20
group 'User:Ice' region i 130 j 32
;group 'User:Ice' region i 40 j 40
model elastic group 'User:Ice'
prop density=916.0 bulk=8.7E9 shear=3.8E9 group 'User:Ice'
model null region i 40 j 65
```

```
set grav 9.81
fix x i=1
fix x i=191
fix y j=1
set dyn off
hist unbal
hist ydis i 86 j 57
hist ydis i 86 j 30
hist ydis i 86 j 1
solve elastic
save Cirque_HalfIce_se.sav
```

Command for Little Red Hill

```
;Project Record Tree export
;Title:Little Red Hill

;*** BRANCH: BRANCH A ****
new

;... STATE: LRHSE ....
config dynamic
grid 73, 38
model elastic
gen 0,0 0,380 730,380 730,0 i=1,74 j=1,39
call table1.dat
gen table 1
group 'rock:gw' region 36 17
model elastic group 'rock:gw'
prop density=2500.0 bulk=3.33333E10 shear=2E10 group 'rock:gw'
model null region 60 33
group 'null' region 60 33
group delete 'null'
model null region 19 34
group 'null' region 19 34
group delete 'null'
set gravity=9.81
fix x i=1
fix x i=74
fix y j=1
set dyn off
hist unbal
hist ydis i 39 j 39
hist ydis i 39 j 20
solve elastic
save LRHse.sav

;*** BRANCH: BRANCH FOR LRH_1.SAV ****

;... STATE: LRH_1 ....
set dyn on
apply ff
apply xquiet j=1
apply yquiet j=1
def wave
; period of wave = 1/freq  Freq = 1 Hz
period = 1
wave = 0.5 * (1.0 - cos(2*pi*dytime/period))
if dytime > 1 then
wave = 0
end_if
end
apply sxy -14140000 hist wave j 1
set dytime 0
hist reset
hist dytime
hist xvel i 39 j 39
hist xvel i 39 j 1
```

```
hist wave
solve dytime 3
save LRH_1.sav
```

Examples of FLAC modelling output: The first graph shows the velocity as measured at the crest of the 45 degree model with an ice-cap. The velocity is shown on the y-axis and time is along the x-axis. The second graph shows the measured velocities at the crest (green), centre (blue) and base (red) for the Mount Alfred model for the Morgan Hill earthquake input. Peak velocities were used in the analysis in Section 4.3.